LOCAL DELIVERY OF ANTIMICROBIAL PEPTIDES FROM TITANIUM SURFACE FOR THE PREVENTION OF IMPLANT-ASSOCIATED INFECTIONS

by

Mehdi Kazemzadeh-Narbat

A THESIS SUBMITTED IN PARTIAL FULFILLMENT OF
THE REQUIREMENTS FOR THE DEGREE OF

DOCTOR OF PHILOSOPHY

in

The Faculty of Graduate Studies
(Biomedical Engineering)

THE UNIVERSITY OF BRITISH COLUMBIA
(Vancouver)

March 2013

ABSTRACT

Titanium (Ti) is a key biomedical material extensively used in orthopaedic implants. Prevention of implant-associated infections has been one of the main challenges in orthopaedic surgery. This challenge is further complicated by the concern over the development of antibiotic resistance as a result of using traditional antibiotics for infection prophylaxis. One of the promising alternatives is the family of antimicrobial peptides (AMPs). The present dissertation develops progressive approaches that enable the loading and local delivery of a unique group of cationic antimicrobial peptides through titanium implant surfaces.

In the first technique, a thin layer of micro-porous calcium phosphate (CaP) coating was processed by electrolytic deposition onto the surface of titanium as the drug carrier. The AMP-loaded CaP coating was not cytotoxic for MG-63 osteoblast-like cells, and the implants showed high antimicrobial activity against *Staphylococcus aureus* (as a representative of Gram-positive strain) and *Pseudomonas aeruginosa* (as a representative of Gram-negative strain) bacteria with 10^6-fold reductions of both bacterial strains within 30 min and ~92% and ~77% inhibition of luminescence at 4 h and 24 h, respectively.

Second study investigated the *in vitro* AMP release, antimicrobial performance, and cytotoxicity of a modified Tet213 (HHC36), as well as the *in vivo* bone growth of AMP loaded into calcium phosphate coated Ti implants in a rabbit model. Burst release during the first few hours followed by a slow and steady release for 7 days was observed. *In vivo* bone growth study showed that loading of AMP did not impair bone growth onto the implants.

In the last study multilayer thin films of titania nanotubes (NT) and CaP coatings were formulated with AMP and were topped with a thin phospholipid film similar to cell membrane.

The films were shown to be non-cytotoxic, hydrophilic, with the potential of tuning loading and release kinetics of AMP. The best model describing the AMP release was first-order model.

The first two approaches demonstrated a promising method for an early stage peri-implant infection prevention. The last study proposed a technique to improve the kinetics of AMP release and total loaded AMP quantity, and to increase the Ti interfacial strength while maintain the osteoconductivity by applying CaP coating.

PREFACE

A version of Chapter 4 has been published. **Mehdi Kazemzadeh-Narbat**, Jason Kindrachuk, Ke Duan, Håvard Jenssen, Robert E W Hancock, Rizhi Wang. Antimicrobial peptides on calcium phosphate-coated titanium for the prevention of implant-associated infections. Biomaterials, 2010. MK conducted all the experiments and wrote the manuscript. Note that part of the Introduction in the original publication has been moved to the literature review (Chapter 2).

A version of Chapter 5 has been published. **Kazemzadeh-Narbat M**, Noordin S, Masri BA, Garbuz DS, Duncan CP, Hancock REW. Drug release and bone growth studies of antimicrobial peptide-loaded calcium phosphate coating on titanium. Journal of Biomedical Materials Research Part B: Applied Biomaterials, 2012. With the exception of the surgery done by NS, MK conducted all the experiments and wrote the manuscript. Note that part of the Introduction in the original publication has been moved to the literature review (Chapter 2). The animal study protocol was approved by the Animal Care Committee of the University of British Columbia (ethic approval # C04-0030).

A version of Chapter 6 is under submission for publication. **Mehdi Kazemzadeh-Narbat**, Benjamin Lai, J N Kizhakkedathu, Robert E W Hancock, Rizhi Wang. Multilayered coated titanium for controlled release of antimicrobial peptides for the prevention of implant-associated infections. With the exception of the blood tests done by BL (technician at the Centre for Blood Research), MK conducted all the experiments and wrote the manuscript. Note that part of the Introduction in the original publication has been moved to the literature review (Chapter 2). The study was approved by the Clinical Research Ethics Review Board at the UBC (ethic approval # H07-01076).

Some data in appendix A has been published. Gao, Guangzheng; Lange, Dirk; Hilpert, Kai; Kindrachuk, Jason; Zou, Yuquan; Cheng, John T. J.; **Kazemzadeh-Narbat, Mehdi**; Yu, Kai; Wang, Rizhi; Straus, Suzana K.; Brooks, Donald E.; Chew, Ben H.; Hancock, Robert E. W.; Kizhakkedathu, Jayachandran N. The biocompatibility and biofilm resistance of implant coatings based on hydrophilic polymer brushes conjugated with antimicrobial peptides. Biomaterials, 2011. MK conducted the cell study and cytotoxicity assays.

Some data in appendix C has been published. Ma, Menghan; **Kazemzadeh-Narbat, Mehdi**; Hui, Yu; Lu, Shanshan; Ding, Chuanfan; Chen, David D. Y.; Hancock, Robert E. W.; Wang, Rizhi. Local delivery of antimicrobial peptides using self-organized TiO2 nanotube arrays for peri-implant infections. Journal of Biomedical Materials Research Part A, 2012. MK conducted the antimicrobial tests, imaging, cell study and cytotoxicity assays.

TABLE OF CONTENTS

LIST OF TABLES

LIST OF FIGURES

LIST OF ABBREVIATIONS

ACP	Amorphous Calcium Phosphate
AMP	Antimicrobial Peptide
ANOVA	Analysis Of Variance
ATR-FTIR	Attenuated Total Reflectance-Fourier Transform Infrared
BSE	Backscattered Electron Microscope
CaP	Calcium Phosphate
CFU	Colony-Forming Unit
DCPA	Dicalcium Phosphate Anhydrous
DCPD	Dicalcium Phosphate Dehydrate
d-HA	Calcium-Deficient Hydroxyapatite
DMEM	Dulbecco's Modified Eagle Medium
DMSO	Dimethylsulfoxide
DNA	Deoxyribonucleic Acid
ECM	Extracellular Matrix
EDTA	Ethylenediaminetetraacetic Acid
EDS	Energy Dispersive X-ray
ELD	Electrolytic Deposition
ELIZA	Enzyme-Linked Immunosorbent Assay
FA	Focal Adhesion
FBS	Fetal Bovine Serum
FESEM	Field Emission Scanning Electron Microscopy
Fg	Fibrinogen
Fn	Fibronectin
GEPIs	Genetically Engineered Peptides for Inorganic Solids
HA	Hydroxyapatite
HEPES	4-(2-hydroxyethyl)-1-piperazineethanesulfonic acid
hMSCs	Human Mesenchymal Stem Cells
IC	Inhibitory Concentration
MDR	Multidrug Resistant

MHA	Mueller-Hinton Agar
MHB	Mueller Hinton Broth
MIC	Minimal Inhibitory Concentration
MRSA	Methicillin-Resistant *S. Aureus*
MTT	3-(4,5-dimetyl-2-tiazolyl)-2,5-diphenyl-2H-tetrazolium bromide
NT	Nanotubes
OCP	Octacalcium Phosphate
OD	Optical Density
PBS	Phosphate-Buffered Saline solution
PI	Isoelectric Point
Pt	Platelet
PMMA	Poly(methyl methacrylate)
POPC	Palmitoyl-Oleoyl Phosphatidyl-Choline
PRP	Platelet Rich Plasma
PZC	Point of Zero Charge
QSAR	Quantitative Structure–Activity Relationship
RBC	Red Blood Cell
SBF	Simulated Body Fluid
SEM	Scanning Electron Microscopy
s-HA	Stoichiometric Hydroxyapatite
ss-NMR	Solid-State Nuclear Magnetic Resonance
THR	Total Hip Arthroplasty
Ti	Titanium
TKR	Total Knee Arthroplasty
TNT	Titania Nanotube
SSCP	Supersaturated Calcium Phosphate
UV/Vis	Ultraviolet–Visible
vWF	Willebrand factor

ACKNOWLEDGEMENTS

I would like to show my greatest appreciation to my supervisor Prof. Dr. Rizhi Wang, for providing me an opportunity to accomplish this project. Without his encouragement and guidance the ideas in this dissertation would not have materialized. I feel motivated and inspired every time I attend his meeting.

I wish to express my sincere gratitude to Prof. Dr. R.E.W. Hancock for his kind support, and generous offer for providing the laboratory facilities. Deepest gratitude is also due to the members of my supervising committee, Dr. Jayachandran N Kizhakkedathu, Dr. Frank Ko. I would like to gratefully acknowledge Dr. Jason Kindrachuk, Dr. Håvard Jenssen, Mr. Reza Falsafi, Ms. Jelena Pistolic and Dr. Shaan Gellatly, for kindly assisting in cell and bacteria study. Special thanks also to Dr. Danmei Liu for sharing the histology protocols and invaluable assistance. I would also like to convey thanks to Dr. Shahryar Noordin, and Ms. Stephanie Smith for assisting in surgery, and Mr. Benjamin Lai for blood tests. I also wish to gratefully thank the UBC Orthopaedic, Dr. Donald S. Garbuz, and Dr. Clive P. Duncan. I take immense pleasure in thanking my colleague, Dr. Ke Duan, for his help with experimental setup and general advice, and many appreciations also go to my dear lab colleagues Dr. Vincent Ebacher, Shanshan Lu, Millie Kwan, Dr. Felipe Eltit Guersetti, Tony Tang, Chia-Jade Lee, Youxin Hu , Allen Tang and special thanks to Menghan Ma for assisting me on nanotubes experiments. This work was supported by the Natural Sciences and Engineering Research Council of Canada and the Canadian Institutes of Health Research. I am also grateful for the University Graduate Fellowship from UBC, and the Cy and Emerald Keyes Fellowship from Materials Engineering.

Finally, I would like to express my heartfelt gratitude to my beloved parents for their blessings, and encouragement which help me in completion of this work.

CHAPTER 1 INTRODUCTION

Titanium and titanium alloys are frequently used as orthopaedic implants because of their good biocompatibility, chemical stability and mechanical properties [1, 2]. However, formation of a surface biofilm, and compromised immune ability at the implant/tissue interface may cause infection on and around titanium implants. This infection is usually difficult to treat and in most cases, replacement of a prosthesis is the only remedy [3-5]. Most implants are vulnerable to bacterial contamination [6].

In orthopaedic surgery, pathogens such as the *Staphylococcus* species, *S. aureus, S. epidermidis,* and *Pseudomonas aeruginosa*, are thought to be mainly responsible for implant-associated infections. These bacteria can be attached shortly after the installation of implants or at a later stage (via a haematogenous route) [7-9]. Moreover, the emergence of multi-drug resistant bacteria like Methicillin-resistant *S. aureus* (MRSA) has critically challenged current therapies, such as prophylaxis with broad spectrum antibiotics and systemic administration of antimicrobial agents [10-12]. These therapies involve several drawbacks such as relatively low drug concentration at the target site and potential toxicity [11].

Hence, localized delivery of antimicrobial agents with time-effective handling of infection, while potentially eliminating problems associated with systemic administration is highly desirable [13, 14]. An ideal local antibiotic release profiles should exhibit a high initial release rate within 6 h post implantation in which implant is particularly susceptible to surface colonization, followed by a sustained 'prophylactic' slow release within the therapeutically efficacious dosing zone to hinder latent infection [15, 16]. Antibacterial agents for local delivery should have high antimicrobial activity against broad spectrum of bacteria, and the released agent concentration should exceed several times (~10 times) the minimal inhibitory

concentration (MIC) of the pathogens [17-19]. In addition, the antibacterial agent should not inhibit osteointegration, be stable at body temperature, and preferably be water soluble [19]. Conventional antibiotics like vancomycin, tobramycin, cefamandol, cephalothin, carbenicillin, amoxicillin and gentamicin have already been incorporated in controlled-release devices [16]. A serious concern regarding the use of these antibiotics is that their release at levels below the MIC may evoke bacterial resistance [20, 21]. Moreover, high doses of antibiotics often harm cell viability and osteogenic activity and may impair osteointegration [22, 23].

A promising alternative for conventional antibiotics is the antimicrobial peptides which are short amino acid sequences, amphipathic, cationic charge and small enough to allow them to interact with bacteria membrane bilayers. Different models have been proposed for antimicrobial activity of AMPs, including formation of pores on bacteria membrane and/or displacement of high density of polycationic charges into polyanionic outer layer of microbes leading to membrane disruption [24-27]. This complex mechanism kills bacteria more rapidly than conventional antibiotics and makes it extremely difficult for AMP to develop resistant phenotypes [24, 28, 29]. AMPs possess broad-spectrum antimicrobial activity against Gram-positive, Gram-negative, and multi-drug resistant bacteria, and are also known to be antifungal and antiviral [30, 31].

Considering the unique properties of AMPs, local delivery of AMP from coated orthopaedic implants can be a potential technique to reduce the systemic administration of antibiotics, risk of bacteria resistance while maintaining the biocompatibility and osteointegration.

CHAPTER 2 LITERATURE REVIEW

2.1 BONE

Bone refers to a family of materials which own a common basic building block, the mineralized collagen fibril. This fibril is composed of fibrous protein collagen. The collagen constitutes the main component of a three-dimensional matrix acts as a framework in which plate-shaped crystals of carbonated apatite (also known as dahllite) form. The third major component of bone is water. Whereas the only mineral type in mature bone is dahllite, there are two hundred or more so-called non-collagenous proteins present beside the type I collagen protein. However the non-collagenous proteins generally comprise less than 10% of the total protein content [32, 33].

Bone tissue is usually categorized into two types. The first type is trabecular or cancellous bone with 50–95% porosity and the second type is cortical or compact bone with 5–10% porosity. Cortical bone is usually found in the shafts of long bones and surrounding the trabecular bone forming the external shell (Fig. 2.1) [34].

Bone cells are divided into five types, osteoblasts, osteoclasts, osteocytes, osteoprogenitor cells and bone-lining cells [35]. Osteoblast cells arise from osteoprogenitor cells under the influence of growth factors. Osteoprogenitors located in the periosteum and bone marrow. Osteoblasts synthesize the bone tissue and this process is maintained by the osteocytes and bone-lining cells. Bone-lining cells cover most bone surfaces and are essentially inactive osteoblasts that differentiate into synthetic osteoblasts within 48 h after a mechanical stimulus [36]. Osteoclasts' function is resorption and degradation of bone. The osteocytes are former osteoblasts that are buried in the bone matrix. They are strain-sensitive cells and can transduce

mechanical signals derived from mechanical loading into signals that ultimately result in bone reduction or formation [34, 36-38].

Bones undergo an internal process called “remodelling”. In remodelling, large tunnels are excavated out in the bone by osteoclast cells. These tunnels are then refilled by deposition of a thin layer of cement followed by layers of lamellar bone by osteoblasts until the tunnel is almost completely filled. However, a narrow channel (Haversian canal) at the center of the tunnels will be remained that act as a blood vessel. This structure in cortical bones is called osteon or Haversian system (Fig. 2.1) [32-34].

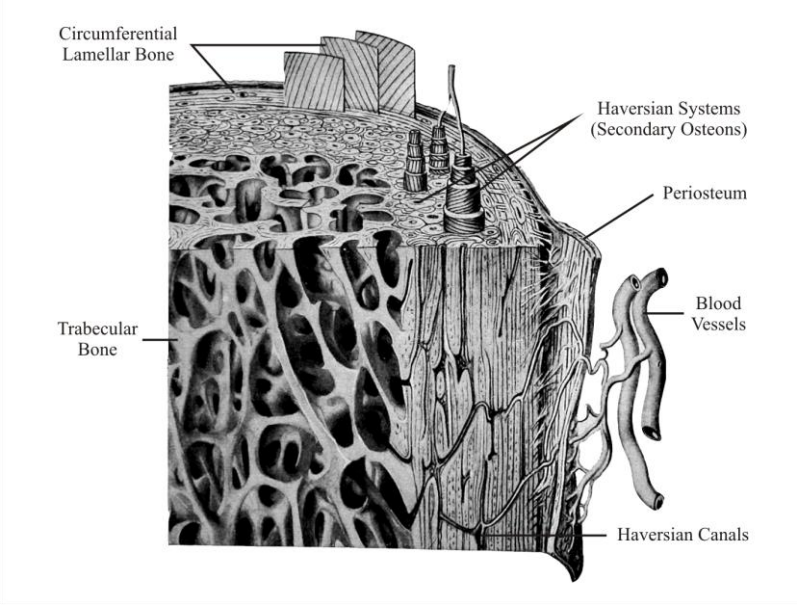

Figure 2.1. Cortex of human long bone. Reprinted from [39] with permission from Elsevier.

The bones of the hip are the *femur* and the *pelvis*. The top end of the femur is shaped like a ball, called the *femoral head*. The femoral head fits into a round socket on the side of the pelvis, called the *acetabulum*. The femoral head is attached to the rest of the femur by a short section of bone called the *femoral neck*. The surfaces of both the head of the femur and the acetabulum are covered with a thin layer of hyaline cartilage which allows smooth movement of

the joint. The hip joint, scientifically referred to as the acetabulofemoral joint, is the joint between the femur and acetabulum of the pelvis and its primary function is to support the weight of the body in both static (e.g. standing) and dynamic (e.g. walking or running) postures (Fig. 2.2) [40].

Usually severe bone diseases of the hip and knee, femoral neck fractures, and pathologic conditions affecting proximal and distal femur and the proximal tibia lead to joint replacement surgery (Fig 2.2). Among the bone injuries, severe progressive osteoarthritis (OA) of the hip and knee accounts for approximately 40% to 60% of musculoskeletal complaints in the elderly. OA is a mechanical abnormality involving chronic degradation of joints, including cartilage and the bone next to it [41, 42]. Osteoporosis is another major health problem characterized by compromised bone strength that predisposes patients, resulting in bone fragility and an increase in susceptibility to fracture. In osteoporosis, bone resorption (i.e. osteoclastic activity) exceeds bone formation (i.e. osteoblastic activity), this leads to net loss of bone mass and bone becomes increasingly porous. This is a devastating disease that affects more than ten million people in the United States. Worldwide, 100−200 million people are at risk of an osteoporotic fracture each year. Another example of severe bone disease is a tumor metastasis to proximal and distal femur or proximal tibia [43].

2.2 ORTHOPAEDIC IMPLANTS

In total hip arthroplasty (THR) the surgical excision is performed on the head and proximal neck of the femur and removal of the acetabular cartilage and subchondral bone. Afterward, a metal femoral prosthesis, composed of a stem and small-diameter head, is inserted into the femoral medullary canal created in the proximal medullary region of the femur. An acetabular component (cup) is inserted proximally into the enlarged acetabular space. The total

hip arthroplasty components is fixed firmly to the bone, either with bone cement or, in uncemented designs, by bony ingrowth into the implant surface, resulting in "biologic" fixation (Fig 2.2) [44].

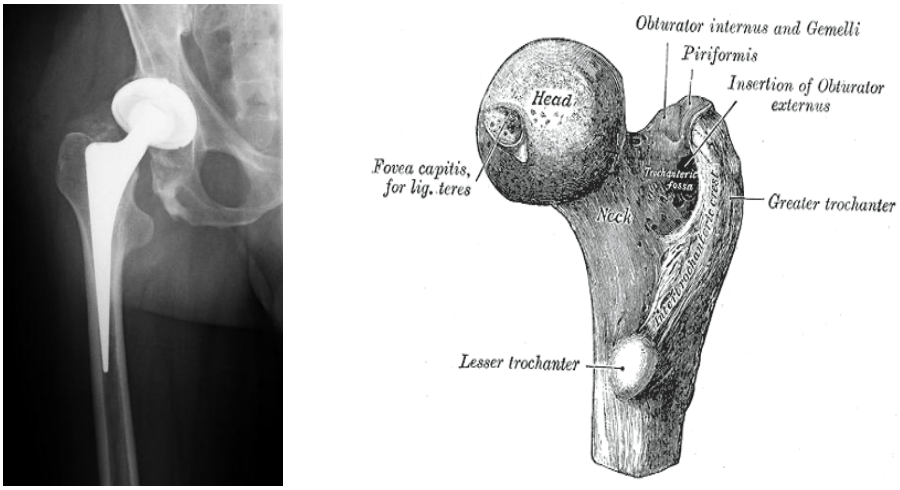

Figure 2.2. Hip joint image and radiographic image of a hip joint replaced with artificial hip implant. In total hip arthroplasty all or part of the hip joint is replaced with an implant to restore joint movement. First, the head of the femur and a layer of the hip socket are removed and replaced with a prosthetic implant, then a metal ball and stem are inserted in the femur and the prosthetic socket is placed in the enlarged pelvis cup. Reprinted from [45, 46] with permission.

2.3 BONE-IMPLANT INTERACTION

The first environment the implant is exposed is the blood, mostly consisting of red blood cells, plasma protein and platelets. Immediately after implantation the wound site is occupied by a blood clot and series of adhesive proteins like fibrinogen, fibronectin and Von Willebrand factor etc. which promote platelets activation [47]. Degree of platelet activation deponds on implant surface micro-topography. Attached platelets secret cytokines and other growth factors that cause activation of other platelets in fluid. Increase in the concentration of cytokines and growth factors is detected by Mesenchymal cells or potentially osteogenic cells in the healing compartment [48, 49]. As a result osteogenic cells start to migrate through the 3D fibrin and

other structural proteins matrix of the blood clot, which creates tension in the matrix (fibrin retention). During migration, the osteogenic cells differentiate and when they arrive at the implant surface they stop, become polarized and adhere and interact with the implant through focal adhesions (FAs) (Fig. 2.3) [48, 50].

During interaction with implant, the cell changes its shape and dynamically develops FA which are dynamic macromolecular clusters, 15–30 nm in dimension containing over 100 different proteins that serve as transmitter of regulatory signals and mechanical linkages of the cell cytoskeleton (F-actin) to the extracellular matrix (ECM) [51]. Connection between focal adhesions and proteins of the ECM generally involves integrins [52, 53]. FAs are associated with "focal contacts" which is referred to extensions called *lamellipodia* (membrane veils rich in actin) and *filopodia* (finger-like protrusions) that act as sensing and traction elements to allow cells to crawl and perceive topographical cues (Fig 2.3) [54, 55].

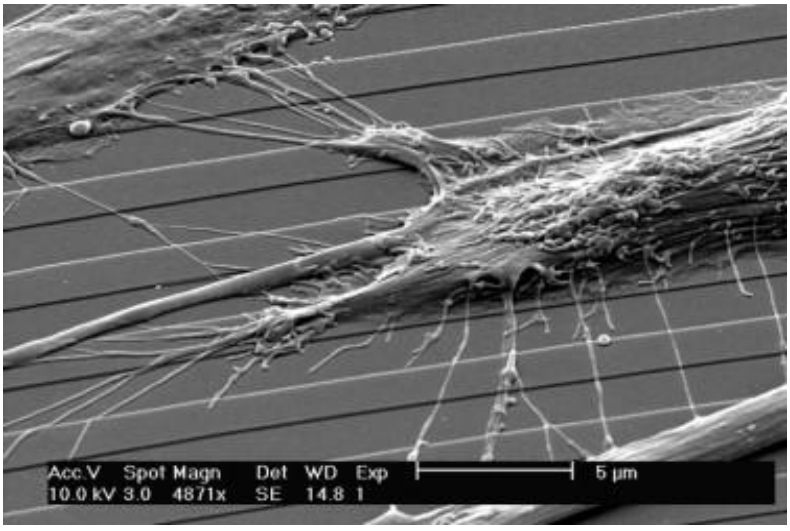

Figure 2.3. SEM micrographs displaying SaOs-2 cells adhering to 200 nm deep round concentric grooves and ridges in quartz, from [56] with permission from Elsevier.

Dynamic sequence of cell–substrate attachment may initiate the cell migration. For a cell to migrate, it must initially sense, and respond to, a stimulus. This will be done by developing and orienting filopodia and lamellipodia structures at the leading edge in the direction of movement. The formation of FA through the anchorage of lamellipodia and pseudopodia to the underlying substrate provides the necessary traction that is required to move the cell body forward. By FA disassembly and cell–substrate detachment at the rear of the cell, forward movement of a cell is performed during an active migration (Fig 2.4) [54, 55, 57-59].

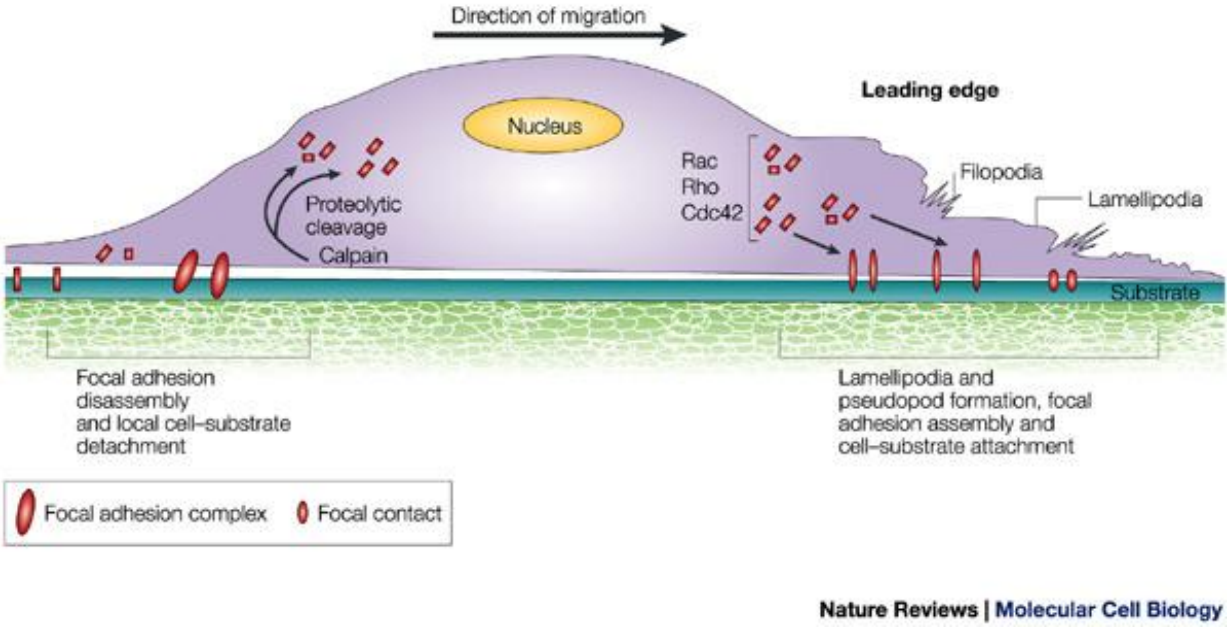

Figure 2.4. Schematic drawing of cell attachment and migration, from [57] with permission from Elsevier.

The first attached osteoblast cells secret calcified collagen free bone cement on implant substrate, the later attached cells create a bone matrix on top of this cement line, and buried osteoblasts in the bone matrix turn to osteocytes. The recruitment and migration of osteogenic cells to the implant is defined as osteoconduction. Both formation and osteoconduction

phenomenon constitute contact osteogenesis [48, 50]. Bone growth at early stage of implantation is a critical parameter in intimate apposition of bone to implant i.e. osteointegration. This intimate contact requires a reasonable gap between bone and implant. Dalton *et al.* reported that when the gap between the implant and bone is 1.0 mm or less, mechanical attachment strength and bone ingrowth increase significantly [60]. At this stage any unfavorable conditions, like premature loading results in micromotion and will disrupt the newly forming tissue, leading to formation of a fibrous capsule. The speed of bone growth can be influenced by various factors such as surface hydrophilicity, surface chemistry and topography [61, 62].

The complex osteointegration process can be summarized in four phases; hemostasis, inflammatory phase, proliferative phase and remodeling phase. Hemostasis includes protein adsorption on implant surface followed by platelets aggregation and forming thrombus. The inflammatory phase begins about 10 min after surgery and lasts for the first day. At this time macrophages attach to injured bone surfaces and clean it from tissue debris and bacteria. To limit the inflammatory phase, super clean surgical environment and antibacterial measures are essential. The duration of proliferative phase ranges from a few days to a few weeks. At early stage of this phase, the fibroblast cells drill tunnels through the provisional extracellular matrix of the fibrin clot. They attach via integrins to the RGD peptides of fibronectin and crawl forward into the wound [63, 64]. Subsequently they form granulation tissue by synthesizing new collagen. In the late phase of proliferation, osteoblasts sense the implant surface with pseudopodia. They attach via integrins to proteins e.g. insoluble fibronectin, which is bound to the implant surface. After attachment, they start to form bone extracellular matrix. As early as one week after implantation the new bone formation in the form of woven bone with randomly oriented collagen fibers starts [64, 65]. Remodeling phase begins with the appearance of

osteoclasts. Lamellar bone formation starts during this process and may last several years until most woven bone is replaced by newly formed and load oriented bone (Fig. 2.5) [64].

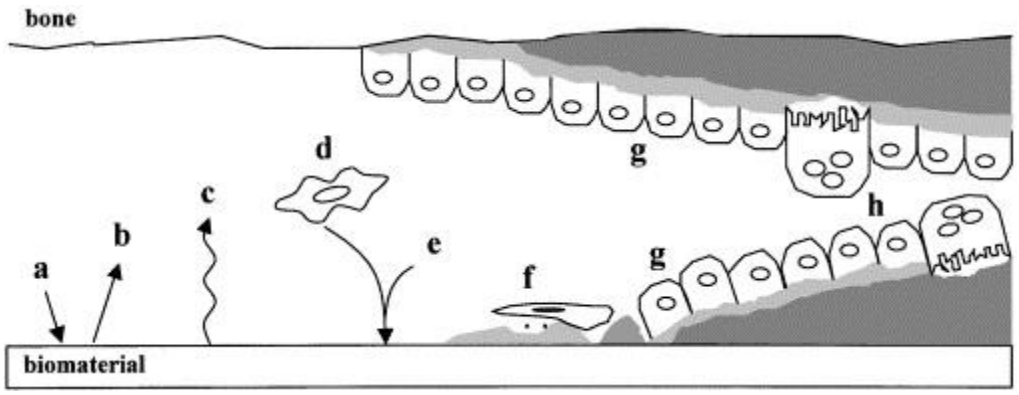

Figure 2.5. Bone–implant interaction (a) protein adsorption and platelets aggregation in haemostasis phase (b) protein desorption, (c) surface changes and material release, (d) inflammatory phase (e) release of matrix proteins (f) proliferative phase including formation of cement *line* and adhesion of osteogenic cells, (g) bone deposition on both the exposed bone and implant surfaces, (h) remodeling of newly formed bone, from [62] with permission from Elsevier.

Release of metal ions into the surrounding tissues is one of the most significant complications regarding the loosening of prosthesis [66, 67]. According to the literature the level of these corrosion byproducts can be up to 21 ppm Ti, 10.5 ppm Al, and 1 ppm V around Ti–6Al–4V in the fibrous membrane encapsulating implants [68-70]. In vitro studies have revealed that trace metal ions, even at sublethal doses can be toxic or cause hypersensitivity reactions, and may interfere with differentiation of osteoblasts and osteoclasts [70-72].

2.4 OSTEOINTEGRATION TO METAL IMPLANTS

Metals have been used successfully in fracture fixation and joint replacement. For a successful joint replacement, achievement and maintaining of mechanical interlock between rigid implant and host bone (osteointegration) is a necessary requirement on both macroscopic and microscopic levels. The factors recognized as affecting the rate of osteointegration include

the type of metal, implant topography, surface chemistry, nature of the host site (vascularity, osteogenic potential), and the mechanical properties within the implant-bone interface zone [73-76]. Currently, stainless steel, cobalt, titanium, and their alloys (e.g. 316L, Co-Cr-Mo and Ti-6Al-4V) are widely used and they are expected to be inert when implanted into the human bone. A layer of fibrous tissue encapsulates the metal implant right after implantation. The thickness of this tissue is proportional to the biocompatibility of implant, and to the amount of motion between the implant and the adjacent tissues. Studies report that pure Ti elicits a minimal fibrous encapsulation compared to stainless steel implants which may cause the creation of fibrous layer as much as 2 mm thick [77]. Titanium is a reactive metal, the surface of which quickly oxidizes on exposure to air, creating a stable oxide surface which is incorrodible after implantation. This provides a surface onto which bone can grow and adhere. Titanium has advantages over cobalt alloys such as lower modulus of elasticity and higher biocompatibility [78]. Jinno *et al.* showed that both titanium and cobalt alloys demonstrate good biocompatibility but less osteointegration was observed on cobalt alloy surfaces. However in general all metal implants are suffering from low osteoconductivity [79].

Surface properties of titanium oxide layer (naturally about 3–8 nm in thickness) e.t. composition, roughness, hydrophilicity, texture, and morphology significantly affect the adhesion, morphologic change, functional alteration, proliferation and differentiation of osteoblast cells [80, 81]. Among Ti surface properties, surface roughness and composition have been reported to be the most important parameters for altering osteoblast cell activity [82, 83]. Increasing the rate of bone growth along implant surfaces is an important issue. In this regard, surface topography/chemical treatments or use of coatings on metal implants are usually applied to improve the osteointegration [84, 85]. Brunette *et al.* showed that Ti surface topography plays

a primary role in regulating cell behaviour, e.g. the shape, orientation and adhesion of cells [86]. Osteoblast-like cells exhibit roughness-dependent phenotypic characteristics and tend to attach more readily to surfaces with a rougher microtopography [87-90]. Lincks *et al.* suggest that best design for an orthopaedic implant is a pure titanium surface with a rough microtopography [82]. An investigation by Boyan *et al.* demonstrated that surface roughness affect differentiation and local factor production of MG-63 osteoblast like cells and tougher surfaces cause a significant increase in alkaline phosphatase activity [91]. You *et al.* showed that a periodic pattern of 400 nm dots enhances osteoblast differentiation of human mesenchymal stem cells (hMSCs), but not when cultured on 150 and 600 nm dot patterns [92].

Since water molecules first reach the implant, surface wettability plays a major role in protein adsorption and subsequent cell adhesion. Therefore, hydrophilic surfaces initiate better cell attachment [93, 94]. Lang *et al.* showed clinically that the more hydrophilic surfaces result in faster osteointegration [61, 62]. On the other hand hydrophilicity of biomaterial surface is important for bacteria attachment, hydrophobic bacterial cell surfaces adhere better to hydrophobic biomaterial surfaces due to a reduction in free surface energy [6]. Nano structures influence the wettability. Webster *et al.* demonstrated that aqueous contact angles reduced three-times when alumina grain size was decreased from 167 to 24 nm [95]. It has also been reported that osteoblasts deposited more calcium on hydrophilic Ti surface composed separately of nanophase compared with conventional Ti, however further tests concerning the cytotoxicity of nanophase materials must be performed [96].

Another parameter affecting the osteointegration is the Ti surface chemistry which plays an important role in protein adsorption following cell adhesion [97]. Kennedy *et al.* demonstrated that surface chemistry using self-assembled monolayers can modulate cell

adhesion and spreading to influence tissue regeneration [98]. Some of chemical modifications of titanium surfaces which have been reported to affect cellular responses to the implant are treatment in simulated body fluid, covalent attachment of biological molecules, changes in the surface ion content and alkali treatment [99, 100]. An electrochemical method, known as anodization of Ti surface have been also shown to have positive biological responses [101]. *In vivo* records show that implant surfaces containing both Ca and P enhance bone growth on the implant surface [102]. Calcium phosphate (CaP) coatings are a proven method that improves the implants' mechanical bonding and biocompatibility [103]. Although CaP coatings are highly osteoconductive, they increase susceptibility to contamination of bacteria as well [104].

2.5 PROSTHETIC-ASSOCIATED INFECTIONS

Infection is described as the invasion and multiplication of disease-causing microorganisms such as bacteria, viruses, and parasites within the host's body tissues [105]. Arthroplasty-associated infections are one of the most serious complications in orthopedic surgery [106]. Peri-prosthetic infection is a severe problem with 0.5-2% infection rates after primary THR [107]. Recent articles described the total knee arthroplasty (TKR) infection range between 1 and 2% [108]. It has been reported that at least 14% of the total hip and knee revisions were done due to infection [10, 109-114]. The economic burden to treat such an infection is estimated to be least $50,000 per patient and $250 million per year in the USA [115]. Currently more than one million hip implants is used per year worldwide and by considering the increasing use of orthopaedic devices, the number of infected implants will continue to rise [116]. Systemic administration of antibiotics involves many drawbacks such as relatively low drug concentration at the target site and potential toxicity [11]. Despite these problems, solutions to prevent implant-

associated infections, beyond the use of ultra-clean surgical technique and prophylactic antibiotics have been very limited [10, 107-114].

Implant surfaces serve as ideal substrates for bacterial colonization, a condition that leads to destruction of local tissues, patient disability and morbidity, and on occasion, death following infection [113, 117]. The early postoperative infection occurs within four postoperative weeks when the local defense system is severely disturbed by the surgical trauma, and so it is the most dangerous time for infection. [118]. Currently, the only treatment for patients with periprosthetic deep infection in total joint arthroplasty is two-stage surgery. This revision operation requires removal of the contaminated implant coupled with extensive bone debridement, excision of infected tissues and bone. Moreover it is followed with a prolonged antimicrobial treatment. The current local antibiotic delivery systems face a major problem of emergence of resistant organisms. This bacteria resistance results from antibiotics elution which causes the antibiotic to fall below the minimal inhibitory concentration for a longer period [119-121]. Common pathogens such as *Staphylococcus aureus, S. epidermidis,* and *Pseudomonas aeruginosa* (Fig. 2.6), can be acquired at the time of surgery or at a later stage and preferentially attach to the surfaces of the implants [122, 123].

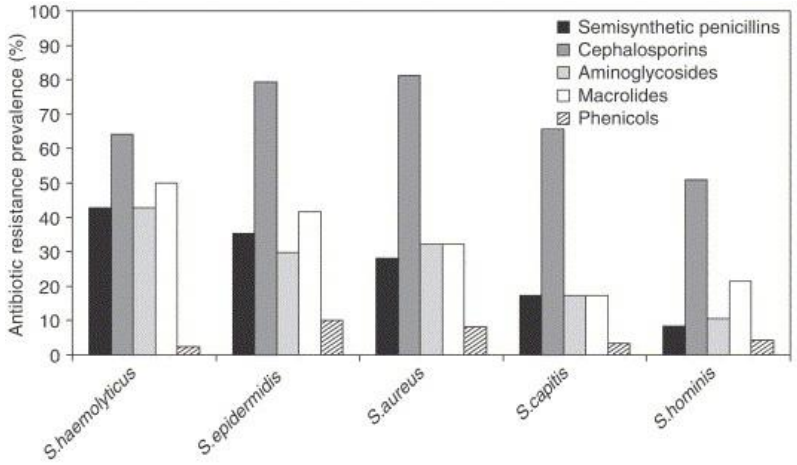

(a)

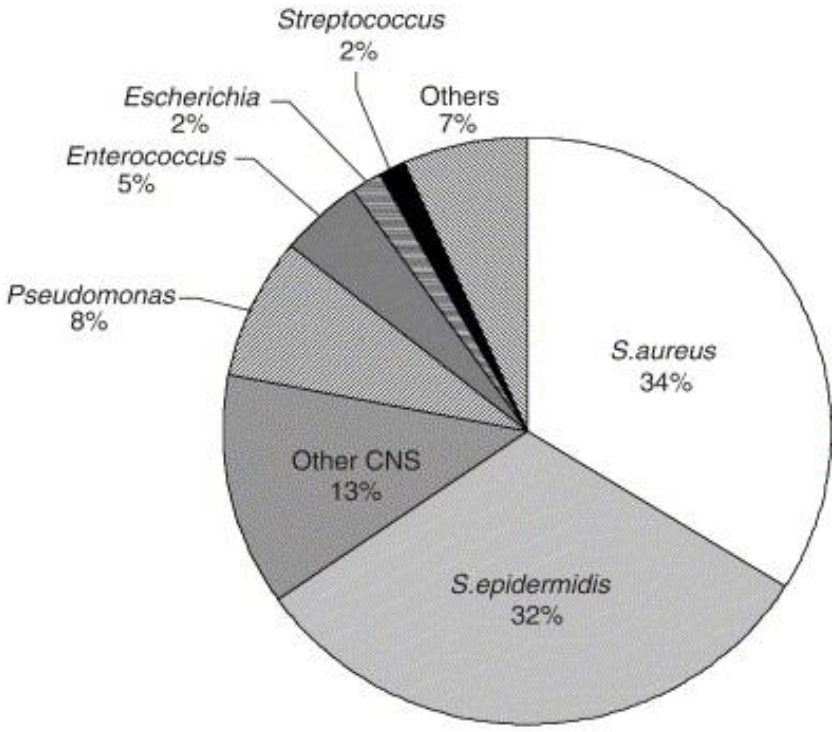

(b)

Figure 2.6. (a) Frequency of main pathogenic species among orthopaedic implant-associated infections, and (b) prevalence of antibiotic-resistant strains isolated from orthopaedic implant-related infections. Reprinted from [122] with permission from Elsevier.

The microorganisms then grow in the form of a biofilm which can result in up to 1000-fold decrease in susceptibility to antimicrobial agents, largely due to poor antibiotic penetration into the biofilm and the stationary phase of growth of the bacteria underlying the surface layer [7, 124-126]. Biofilms are aggregate of microorganisms characterized by cells irreversibly attached to a substratum, interface or to each other, embedded in a matrix of extracellular polymeric substance (EPS) that they have produced, and exhibiting an altered phenotype with respect to growth rate and gene transcription [5, 7, 11]. The presence of biofilms which protects

adherent bacteria in the company of poor vascularization of the bone/implant interface, make prosthetic joint infections extremely difficult to treat (Fig. 2.7) [119-121, 125, 127].

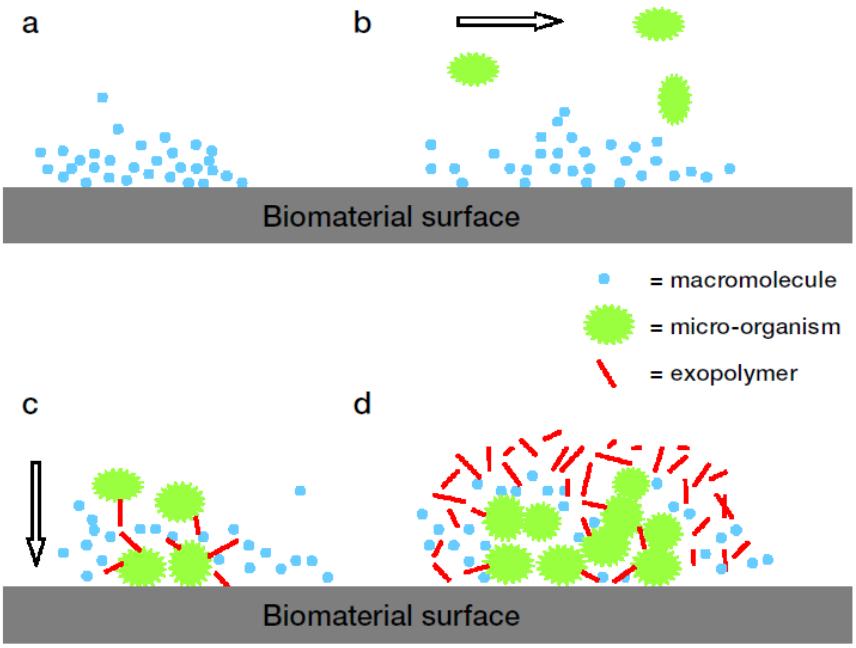

Figure 2.7. Sequential steps in the formation of biofilms on a biomaterial surface, including (a) Formation of a conditioning film. (b) Microbial mass transport. (c) Initial microbial adhesion and anchoring through exopolymer production. (d) Growth of adhering microorganisms. Reprinted from [126] with permission from Elsevier.

2.6 PREVENTION OF INFECTIONS THROUGH LOCAL DELIVERY OF ANTIBIOTICS

To prevent the infections and to improve the operating standards a few strategies have been employed. Preventive strategies involve minimizing the risk of contamination during surgery, reducing the possibility of the infection establishment by peri-operative administration of antibiotics, and isolating the patients in order to confine pathogenic strains [122, 123]. Antibiotics are administrated in two ways, systemic peri-operative antibiotic prophylaxis and local application of antimicrobial agents (antibiotics or antiseptics). The advantage of local

applications of antimicrobial agents over systemic administrations of antibiotics is the higher drug levels on the surface of the device and/or in its immediate vicinity without exceeding the systemic toxicity level of the drug and risking. The aims of local antimicrobial prophylaxis are to prevent implant-associated infections by impeding bacterial adherence to the implant surface and/or reducing the concentration of bacteria in the immediate vicinity of the implant [122, 128]. Various methods have been developed for this purpose. A commonly used technique is to load antibiotics into the bone cement. It has been reported that this technique results in significantly lower infection rates [129, 130]. However, there are a few limitations to mixing antibiotics with cements, like chemical stability with the monomers, sterility, solubility in water, thermo-stability, negative influence on the mechanical strength etc. [131]. Moreover this technique cannot be applied to the cementless implants that are being increasingly used. Therefore, local delivery of antibiotics through implant surface has attracted considerable attention recently particularly with reference to difficulties in controlling dosage, time, and effectiveness without systemic side effects [15].

2.6.1 Strategies for delivery of antimicrobial agents from orthopaedic implants

Three approaches have been researched toward delivery of antimicrobial agents from orthopaedic implants; coating the drug on implant surface, incorporating the drug in biomaterials/cement scaffold and including the drugs into the beads [132]. In another classification, antibacterial coatings have been categorized as passive or active. Passive coatings just inhibit bacterial adhesion and/or kill bacteria upon contact and do not release bactericidal agents. These coatings can be achieved through physiochemical modification of the surface properties such as the surface hydrophilicity and crystal structure. On the other hand, active coatings release preloaded bactericidal agents such as antibiotics, antiseptics, silver etc [11, 16].

In this attempt, beside antibacterial agents, growth factors (e.g bone morphogenetic protein-2) have been also successfully investigated [133].

Combination of bone cements and antibiotics is considered as a precursor approach in drug delivery systems [132]. Resorbable calcium phosphate ceramics [134], and polymers such as poly methyl methacrylate (PMMA) as beads for the treatment of osteomyelitis [135] or as cement have been developed as antibiotics (mostly vancomycin and gentamicin) carriers [136]. Use of PMMA as a drug delivery system has a drawback which is the need for a second operation to remove the non-absorbable cement in the setting of osteomyelitis. Moreover, the possibility of thermal damage to the antibiotics caused by the exothermic polymerization reaction of the cement is its disadvantage [19].

Another antibiotic carrier is biodegradable composites such as poly(lactide/glycolide) copolymers and poly(propylene glycol-fumerate)/methyl methacrylate composites [137]. Lucke *et al.* reported titanium implants coated with a 10 μm thin biodegradable poly(D,L−Lactide) coating that incorporated gentamicin. However, the antibiotic was released with an initial burst from the coating [136]. Chlorhexidine [138] is an antiseptic that has been impregnated into polylactide coating on anodized Ti surface by spraying deposition [139]. Zhang *et al.* produced an antiseptic coating on functionalized Ti by atom transfer radical polymerization of Poly(methacrylic acid) and silk sericin and calcium phosphate coatings impregnated with chlorhexidine , however surface showed cytotoxicity to fibroblasts [140]. Immersion of RGD into PLL-*g*-PEG/PEG coating has been reported to be able to decrease bacterial adhesion by 69% [141]. Polyelectrolyte multilayers of hyaluronic acid/chitosan functionalized Ti substrates immobilized with RGD through dipping technique showed high antibacterial efficacy with increased osteoblast functions by 100–200% [142]. Gao *et al.* developed AMP conjugated

polymer coatings using polymer brush approach which significantly decreased the number of bacteria adherent to the Ti implants [143]

Considerable attention has been paid on the silver compounds like silver-containing hydroxyapatite (HA) coating [109], and silver nanoparticles as an antibacterial agent [112, 144]. Zhao *et al.* reported that the titania nanotubes (NT) incrorporated with silver nanoparticles was able to kill all the planktonic bacteria in the suspension during the first several days. The NT-Ag structure resisted bacterial adhesion for 30 days, but showed cytotoxicity [145]. Silver ions are clearly effective against various bacteria *in vitro* [110], however there are evidences of antibacterial ineffectiveness *in vivo* [146, 147]. In many cases most of the loaded silver is released very quickly from the coating, and there are questions of clinical effectiveness and damage to human cells. In addition, complex of silver and proteins which may alter protein functions is another concern [148, 149].

The antibacterial compounds containing chemically reactive groups such as hydroxyl, carboxyl or amino groups, can be covalently grafted to a wide variety of surfaces as coatings [15]. These include covalently bonding vancomycin to titanium beads surface to kill staphylococci [119, 150-152], and loading antibiotics into biodegradable coatings [153] or CaP bioceramic coatings [154, 155]. Radin *et al.* studied the vancomycin-loaded calcium phosphate coatings using dipping method against *S. aureus* [134]. However, it has been reported that loading CaP by a dipping method leads to burst release of the antibiotics, that is, more than 80–90% of the antibiotics released from the calcium phosphates coating within the first 60 min [135, 156]. Antibiotics incorporated carbonated hydroxyapatite coatings fabricated by biomimetic coprecipitation method has been reported to be able to inhibit *S. aureus* growth [22, 157]. Hiroyuki *et al.* fabricated an iodine-supported titanium that suppressed the microbial activities,

he coated the Ti with adhesive anodic oxide films through anodization [158]. Statz *et al.* reported antimicrobial peptide oligomers (ampetoids) with an adhesive peptide moiety anchoring onto TiO_2 surface [159].

In a few studies titania nanotubes have been used and filled by antibiotics via a simplified lyophilization method [160]. Implanting the Ti surface with ions [161, 162] is another method for creating antimicrobial surface. Finke *et al.* implanted the Ti surface with Cu ions by means of plasma immersion ion implantation, the obtained antimicrobial surface however showed cytotoxicity [163]. Yoshinari *et al.* could inhibit the bacteria growth by implanting F^+ ions on Ti surface [164]. In another method, UV treated Ti surface by irradiating reduced bacterial adhesion without altering cell adhesion [165].

The development of delivery systems combining osteoconductive materials which can maintain and release antimicrobial agents takes advantage of a two-fold beneficial effect [134, 166]. Thus, attention has focused on the use of well-known bone grafting materials such as calcium phosphate. The unique ability of calcium phosphate based materials to adsorb different chemical species on their surfaces is an added value [134, 166]. As an example, Denissen *et al.* showed that bisphosphonated-complexed CaP orthopaedic implants can be beneficial on alveolar bone destruction disease [167]. Garbuz *et al.* demonstrated a significant bone growth into the porous tantalum implant coated with CaP-alendronate [168].

Fast release delivery systems provide rather high doses (may reach toxic level) during short-term action. On the other hand, required therapeutic level may not be reached by slow release delivery system. This phenomenon may result in bacterial resistance due to survival of strains. The released antibiotics must act immediately post-surgery before the formation of a biofilm. Bacteria protected by a biofilm require 1000-times more antibiotic dose necessary to

combat than the bacteria in suspension. Therefore, local antibiotic release profiles should ideally exhibit fast initial release in the first 6 h after intervention to protect the site while the immune system is weakened, as well as continuous 'prophylactic' slow release within the therapeutical zone to hinder the latent infection [15, 16]. Current antimicrobial implants do not satisfy all of these properties, primarily due to poor design, biomaterial selection, drug release mechanism, drug selections, matrix/device fabrication methods, and manufacturing specific to the environmental characteristics of host site. In addition, bacterial resistance is still an issue due to use of conventional antibiotics in most of the techniques [169].

Table 2-1. Representative antibacterial coatings on titanium implants, (based on [11])

Type of Coating	**Fabrication Method**	**Test**	**Effect**	**Experimental Model**
Vancomycin-loaded calcium phosphate coatings [134]	Immersion	*In vitro*	Effective bacterial inhibition up to 72 h	*Staphylococcus aureus*
Antibiotics incorporated carbonated hydroxyapatite coatings [22, 157]	Biomimetic coprecipitation	*In vitro*	Inhibit bacterial growth and the release rate of antibiotics is related to the structure of the antibiotics	*Staphylococcus aureus*
Gentamicin-loaded titania nanotubes [160]	The nanotubes were filled via a simplified lyophilization method	*In vitro*	Reduce bacterial adhesion and enhance osteoblast differentiation	*Staphylococcus epidermis* and MC3T3-E1
Gentamicin-loaded poly(D,L-lactide) coating [137]		*In vitro*	Reduce implant-related infection	Rat acute osteomyelitis model induced by *Staphylococcus aureus* inoculation
Vancomycin-loaded sol–gel films [170]	Dipping	*In vitro*	Zero-order release of vancomycin up to 2 wk	
Vancomycin-bonded surfaces [119, 151, 152]	Covalent Bonding	*In vitro*	Reduce bacterial colonization even upon repeated challenge	*Staphylococcus aureus* and *Staphylococcus epidermidis*

Type of Coating	Fabrication Method	Test	Effect	Experimental Model
Chlorhexidine-containing Polylactide coating on anodized surface [139]	Spraying deposition	*In vitro*	Large inhibition zone	*Staphylococcus aureus*
Polymer and calcium phosphate coatings with chlorhexidine [138]	Impregnation	*In vitro*	Inhibit the growth and viability of bacteria tested, show cytotoxicity to fibroblasts	*Staphylococcus aureus*, *Staphylococcus epidermidis* and hTERT human fibroblasts
Coatings with the antiseptic combination of chlorhexidine and chloroxylenol [171]	Unclear	*In vitro*	Produce zones of inhibition against bacteria tested	*Staphylococcus epidermidis*, *Staphylococcus aureus*, *Pseudomonasaerugi nosa*, *Escherichia coli* and *Candida albicans*
Silver coating [147]	Unclear	*In vivo*	Show no local or systemic side-effect	Human
Titanium/silver hard coating [112]	Physical vapor deposition	*In vitro*	Reduce bacterial adhesion; show no cytotoxic effect	*Staphylococcus epidermis, Klebsiella pneumoniae*, Epithelial cells 16HBE and osteoblasts hFOB1.19
Silver-containing hydroxyapatite coating [110]	Magnetron sputtering	*In vitro*	Reduce bacterial number on specimen surface and show no cytotoxicity compared with HA surface	*Staphylococcus aureus*, *Staphylococcus epidermidis* and human embryonic palatal mesenchyme cells
Silver or copper doping [161, 162]	Ion implantation	*In vitro*	Improve the antibacterial rate	*Staphylococcus aureus*
F^+-implanted surfaces [164]	Ion implantation	*In vitro*	Inhibited the growth of bacteria tested	*Porphyromonas gingivalis* and *Actinobacillus actinomycetemcomit ans*
UV treated surface [165]	UV irradiation	*In vitro*	Reduce bacterial adhesion without altering cell	*Staph., epidermidis* and Saos-2 cells

Type of Coating	Fabrication Method	Test	Effect	Experimental Model
PLL-*g*-PEG/PEG-RGD coating [141]	Immersion	*In vitro*	Decrease bacterial adhesion by 69%	*Staphylococcus aureus*
Polyelectrolyte multilayers of hyaluronic acid/ chitosan functionalized Ti substrates immobilized with RGD [142]	Dipping	*In vitro*	Show high antibacterial efficacy with increased osteoblast functions by 100–200%	*Staphylococcus aureus* and MC3T3-E1

2.6.2 Antimicrobial peptides (AMPs)

Resistance to antibiotics dates back to the introduction of the first antibiotic (penicillin) into clinical usage. Today, many significant pathogens are resistant to various clinically useable antimicrobial agents, so-called multidrug resistant (MDR) organisms. Infections caused by MDR are costly to treat due to high risk of treatment failure [172]. With the increasing of MDR against most antimicrobial agents, there is an urgent need to discover novel classes of antibiotics. Therefore, cationic peptides have been developed as antimicrobial agents [173]. AMPs are amongst the most potent therapeutic agents produced against microbial infections. Not only it is possible for peptides to kill different kinds of bacteria and viruses, but they have also been shown to have the capability of wound healing and killing transformed cells (e.g. cancerous cells) [174-177]. AMPs are also recognized as a possible alternative for the treatment of antibiotic-resistant bacterial infections or septic shock [27, 174-177]. Some examples of commercially available AMP are MX226 (ILRWPWWPWRRK) and hLF1-11 (GRRRRSVQWCA). There are also other potent clinically developed AMPs like HHC10 (KRWWKWIRW), HHC36 (KRWWKWWRR), Tet213 (KRWWKWWRRC), Bac2A (RLARIVVIRVAR), etc. [27, 178, 179]. AMPs are generally defined as having less than 50

amino acids with 2–9 positively charged lysine or arginine residues and up to 50% hydrophobic amino acids [27, 174-176, 180]. In other words, all natural cationic AMPs share common features, including cationicity (with an overall charge ranging from +2 to +9) and amphiphilic with a large proportion (>50%) of hydrophobic residues [175]. Many have very broad bactericidal activity spectra against both Gram- negative and Gram-positive bacteria including most clinically antibiotic-resistant bacteria. They kill these organisms within minutes of contact [173, 181, 182]. The available evidence regarding AMP antimicrobial mechanism indicates that cationic AMPs interact with bacterial surfaces to either permeabilize them or to translocate across the cytoplasmic membrane to attack cytoplasmic targets. The initial step in this mechanism is the occurrence of an electrostatic interaction between the negatively charged outer layer of the bacterium and the positively charged AMP. This attraction would cause the microbes to more strongly associate with these surfaces leading to enhanced killing. Subsequently, the high local concentration of the AMP would result in the displacement of positively charged counterions attached to the outer surface layers, and could thus induce a dramatic change in bacterial surface electrostatics which results in lysis (Fig. 2.8) [27, 174, 175]. The ability of AMPs to selectively interact with the bacterial cells rather than the mammalian cells makes them highly antimicrobial with low toxicity for host cells. The major factor that contributes to the selectivity property of AMPs is the cationic property. The surface of the bacterial membranes is more negatively charged than mammalian cells. This will initiate higher affinity between AMPs and bacterial membrane [183, 184]. Moreover, mammalian cell membranes contain high amount of cholesterol as a membrane stabilizing agents which is absent in bacteria cells. It's well understood that the interaction between cholesterol and AMP will decrease the AMP activities,

and protect host cells from AMP (Fig. 2.9). However, the cytotoxicity concentration level of different AMPs for host cells is diverse and should be measured [183, 184].

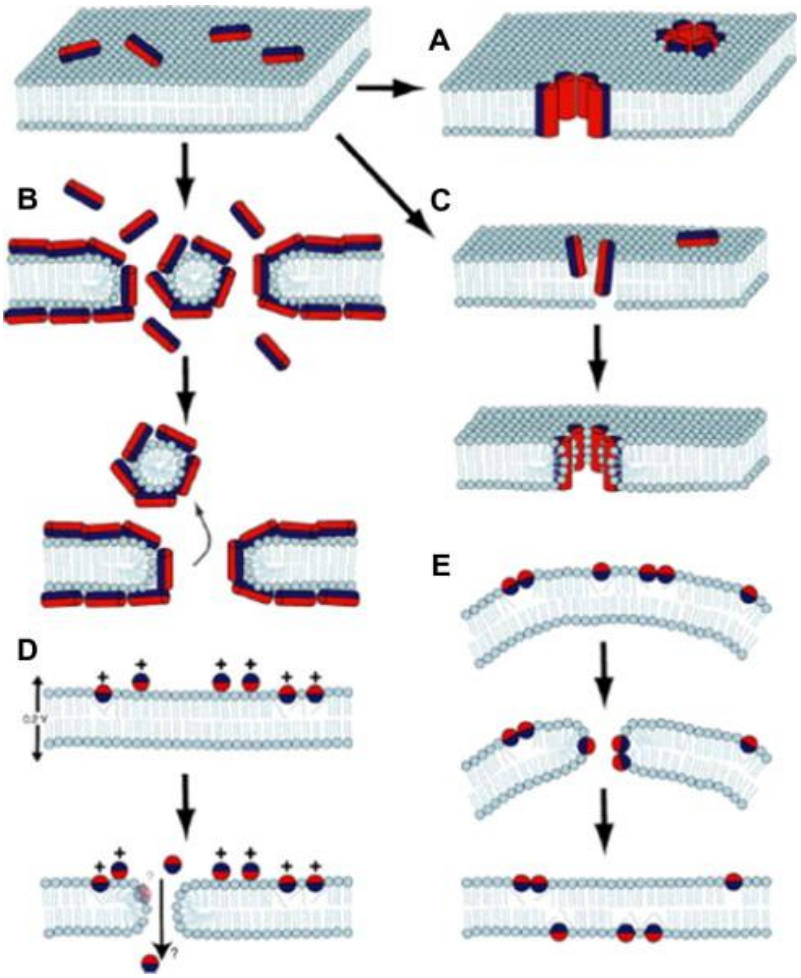

Figure 2.8. Proposed models for antimicrobial peptide mechanisms of action. (A) The Barrel-stave model: the peptides span the membrane and form a pore with the hydrophilic portion lining the pore. (B) The carpet model: the peptides span the membrane by a detergent-like action that disrupts the membrane structure. (C) The toroidal model: the hydrophilic portion of the peptide is associated with the lipid head group. (D) The molecular electroporation model: the interaction of the cationic peptide with the pathogen membrane promotes an electrical potential difference across the membrane. When this potential reaches 0.2 V, a pore is believed to be created by molecular electroporation. (E) The sinking raft mechanism proposes a mass imbalance between the two leaflets of the membrane induced by the peptide. By creating a curvature gradient along the membrane and by self-association, peptides sink into the membrane and form transient pores that are thought to promote a transitory increase on membrane's permeability and leakage of intracellular contents. Reprinted from [185] with permission from Elsevier.

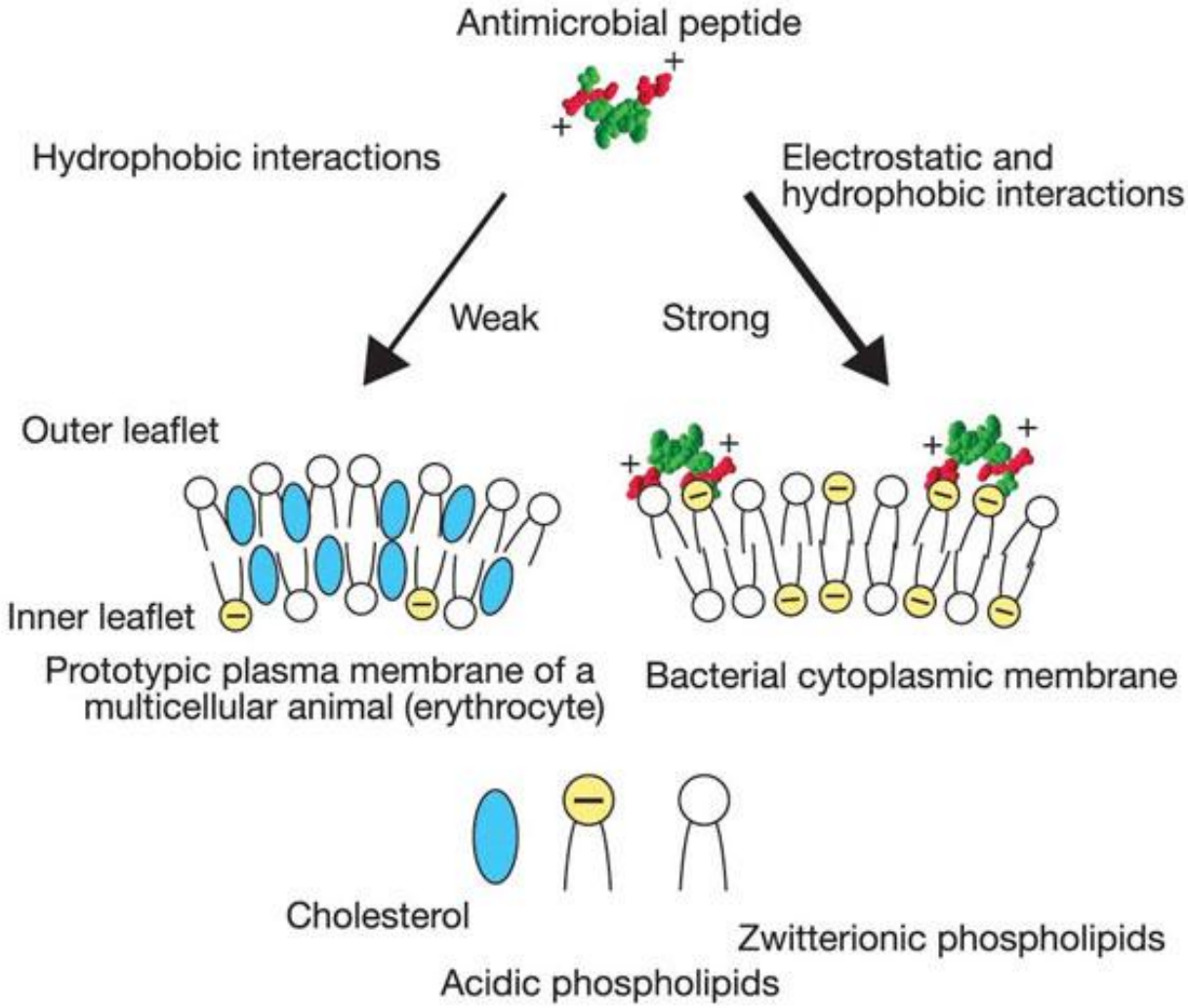

Figure 2.9. Cell selectivity of antimicrobial peptide. Reprinted from [186] with permission from Elsevier.

2.7 CALCIUM PHOSPHATE COATINGS

Hydroxyapatite is a major mineral component of bone with a typical formula of $Ca_{10-x}(HPO_4)_x(PO_4)_{6-x}(OH)_{2-x}$, where x ranges from 0-2, giving a Ca/P atomic ratio of between 1.67 and 1.33 [187]. It is claimed that calcium-deficient HA (d-HA, 1.33<Ca/P<1.67), is of greater biological interest than stoichiometric HA (s-HA, Ca/P=1.67) because the Ca/P ratio in bone

apatite is between 1.67 and 1.5 [187]. Osteoconductivity and biocompatibility of HA with various tissues have made this bioceramic an important material for bone regeneration. Figure 2.10 proposes a mechanism by which hydroxyapatite surfaces are recognized after implantation. However, inherent mechanical properties of ceramics, i.e. brittleness, and poor impact resistance limit the HA applications particularly in load-bearing parts. One of the solutions to overcome these problems is applying the CaP in form of coatings on the metallic implants. The calcium phosphate coated metallic implants will therefore inherit both high tensile strength and ductility of the metal and bioactivity of hydroxyapatite. Various methods have been used to prepare HA coatings, such as thermal spraying, sputter coating, electron beam deposition, dip coating, electrophoretic deposition, hot isostatic pressing, biomimetic coating, etc. These methods are summarized in table 2-2 [188, 189].

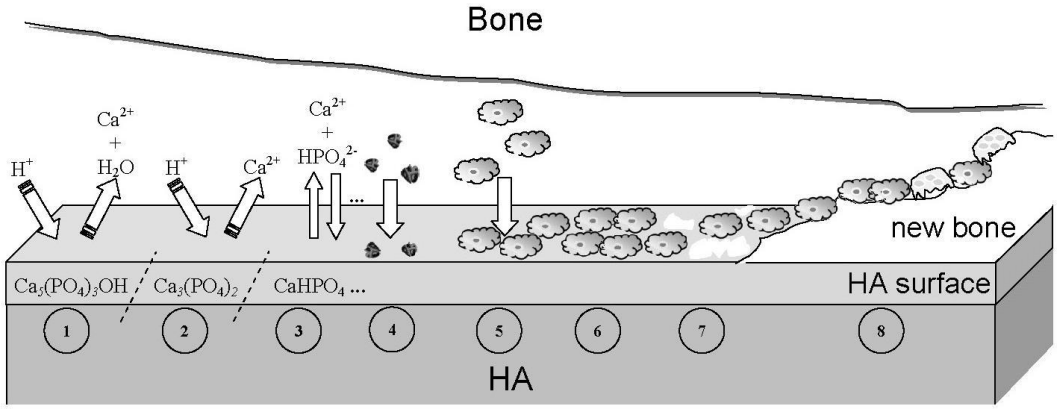

Figure 2.10. A schematic diagram showing the phenomena that takes place on HA surface after implantation: (1) the solubilization of the HA surface starts; (2) continuation of the solubilization of the HA surface; (3) the equilibrium between the physiological solutions and the modified surface of HA has been achieved; (4) adsorption of proteins and/or other bioorganic compounds; (5) cell adhesion; (6) cell proliferation; (7) beginning of a new bone formation; (8) new bone has been formed, from [190] with permission from Elsevier.

Table 2-2. CaP coating produced using various deposition technologies, (based on [188, 191])

Techniqe	Thickness	Advantages	Disadvantages
Plasma spraying	30–200 µm	High deposition rates; low cost	Line of sight technique; high Temperatures induce decomposition; rapid cooling produces amorphous coatings
Sputter coating	0.5–3.0 µm	Uniform coating thickness on flat substrates; dense coating	Line of sight technique; expensive, time-consuming; produces amorphous coating
Pulsed-laser deposition	0.05–5.00 µm	Coating with crystalline and amorphous; coating with dense and porous	Line of sight technique
Ion-beam method	0.05–1.30 µm	High adhesive strength	Line of sight technique; expensive; produces amorphous coating
Dip coating	0.05–0.50 mm	Inexpensive; coating applied quickly; can coat complex substrates	Requires high sintering temperatures; thermal expansion mismatch
Sol-gel	< 1 µm	Can coat complex shapes; low processing temperatures; relatively inexpensive as coating is very thin	Some processes require controlled atmosphere processing; expensive raw materials
Electrophoretic deposition	0.1–2.0 mm	Uniform coating thickness; rapid deposition rates; can coat complex substrates	Difficult to produce crack-free coatings; requires high sintering temperatures
Biomimetic coating	< 30 µm	Low processing temperatures; can form bone-like apatite; can coat complex shapes; can incorporate bone growth stimulating actors	Time-consuming; requires replenishment and constant pH of simulated body fluid
Hot-isostatic pressing	0.2–2.0 mm	Produces dense coatings	Cannot coat complex substrates; high temperature required; thermal expansion mismatch; elastic property differences; expensive; removal/ interaction of encapsulation material

2.7.1 Electrolytical deposition (ELD)

Electrolytical deposition process of calcium phosphate phases takes place with electrically conductive substrates in calcium and phosphate containing electrolytes. In this process, when a current passes through an electrolytic cell, electrons are injected into the solution through cathodic reactions, and drawn out through anodic reactions which results in the formation of OH ions on cathode. Subsequently, local increase in pH near the substrate surface happens due to either consumption of acid (H^+) or generation of base (OH^-) (Fig 2.11) [192-194]. Since the solubility of CaP phase is pH-dependent, this rise in pH leads to an increase in the relative supersaturation (σ) of CaP, leading to their subsequent precipitation onto the cathode, thereby forming a desired coating with respect to CaP phase (e.g. σ varies from 1.90 to 2.41 for octacalcium phosphate (OCP) and 15.40 to 18.50 for HA [195]). Considering the substrate as inert, in air-saturated solutions the two following overall reactions take place (Fig. 2.11) [196, 197].

$$2H_2O + 2e^- \rightarrow H_2 + 2OH^- , \quad (1)$$

$$O_2 + 2H_2O + 4e^- \rightarrow 4OH^- \quad (2)$$

OH generation at the cathode induces acid–base reactions to form PO_4^{-3} and HPO_4^{-2}:

$$OH^- + H_2PO_4^- \rightarrow HPO_4^{2-} + H_2O, \quad (3)$$

$$OH^- + HPO_4^{2-} \rightarrow PO_4^{3-} + H_2O \quad (4)$$

Furthermore, the following precipitation reactions have to be taken into consideration:

$$10Ca^{+2} + 6PO_4^{3-} + 2OH^- \rightarrow Ca_{10}(PO_4)_6(OH)_2 \quad (5) \quad \text{(HA formation)}$$

$$8\ Ca^{+2} + 6HPO_4^{2-} + 5H_2O \rightarrow Ca_8H_2(PO_4)_6 \,.\, 5\ H_2O + 4\ H^+ \quad (6) \quad \text{(OCP formation)}$$

$$Ca^{+2} + HPO_4^{2-} + 2H_2O \rightarrow CaHPO_4 + 2H_2O \quad (7) \quad \text{(DCPD formation)}$$

In which DCPD stands for dicalcium phosphate dehydrate. These well-known reactions lead to the generation of a CaP precipitate and to the formation of a thin coating on the cathode (Fig. 2.12). The thermodynamics and kinetics analysis of CaP precipitation indicates that there are two primary factors controlling CaP phases: supersaturation of Ca^{2+}, PO_4^{-3} and HPO_4^{2-} ; and the pH value in the supersaturated solution. In electrochemical deposition, current density controls the rate of OH^- formation and consequently the pH value of the electrolyte. Also, the formation rates of PO_4^{-3} and HPO_4^{2-} are controlled by the current density [197-201].

In the electrolyte containing nitrate there is a special case, as the reduction of this ion creates an additional cathodic process which contributes to the total current, but since low nitrate concentrations (millimolar) is used, similar to the reduction of oxygen this contribution is negligible. It has been reported that the CaP phase coating thickness increases linearly with the square root of deposition time [202].

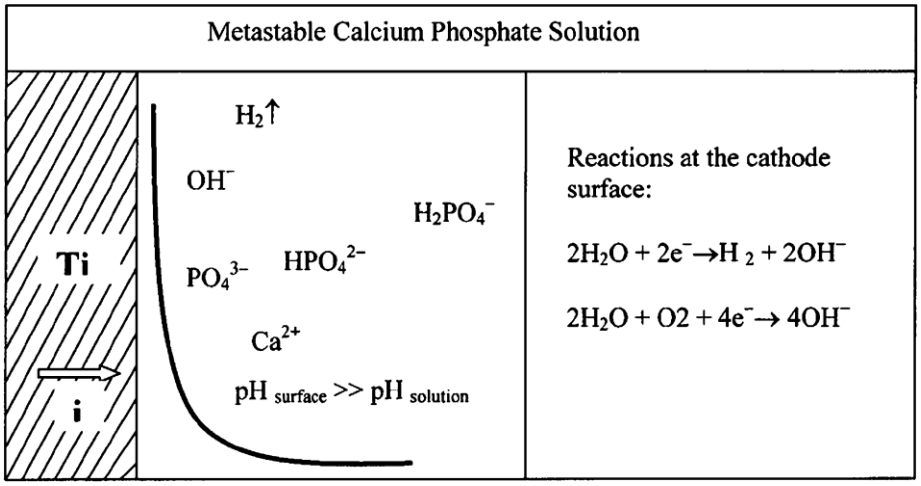

Figure 2.11. Reactions during electrochemically assisted deposition (ELD) of CaP phase (CPP) coatings. Reprinted from [196] with permission from Elsevier.

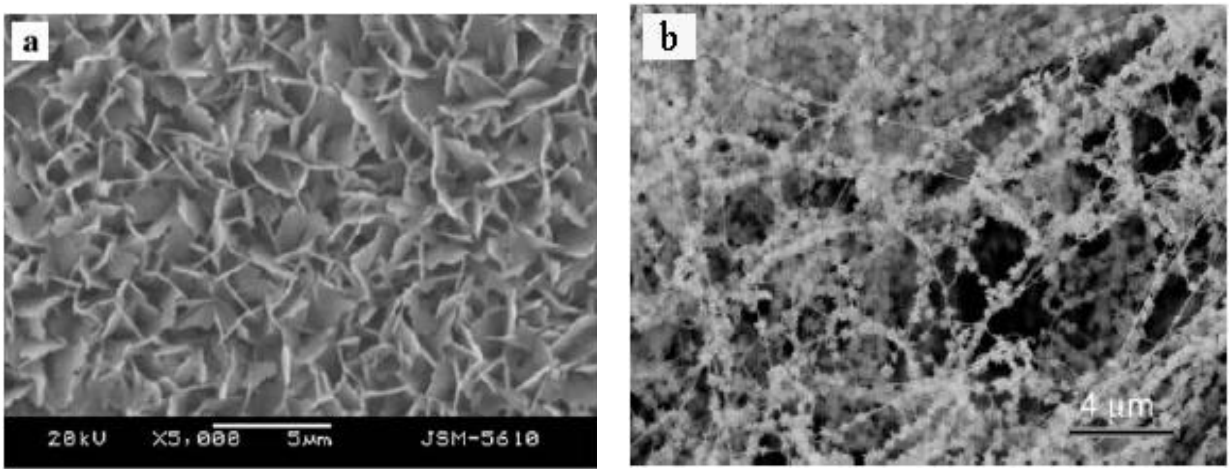

Figure 2.12. Scanning electron micrographs of (a) the electrolytic deposition of octacalcium phosphate coating on titanium alloy. Reprinted from [203] with permission from Elsevier (b) collagen/OCP composite coating. Reprinted from [194] with permission from Elsevier.

Below are some advantages of the ELD method:

- The coatings have excellent homogeneity on flat, irregular or porous surfaces as it is a non-line-of-sight process.
- The deposition of controlled thin layers (down to the sub-micrometer level) with a composition, crystal size, and chemical close to that of bone mineral is possible.
- In comparison to the biomimetic technique (incubation in simulated body fluid (SBF)), ELD produces more defined, higher relative supersaturation at the interface, resulting in shorter processing times.
- High specific surface area coatings can be achieved.
- Possible physiological processing parameters (pH, temperature, aqueous solution), permits the deposition of CaP phase combined with the immobilization/incorporation of organic components such as peptides (Fig. 2.12b).
- There is no adverse effect of heat on the substrate.

- It is a low energy process in compare to typical deposition techniques e.t. plasma spraying.
- It is a low cost process [188, 204-209].

Below are some disadvantages of the ELD method:

- There is potentially low interfacial strength of the coatings [210].
- An electrically conductive substrate or substrate top layer is essential.
- Extreme electrochemical conditions (high current densities, long duration polarization) may cause hydrogen embrittlement for metallic substrates [188, 204-209].

2.7.2 Types of calcium phosphates coatings generated by ELD

Four types of CaP phases have been achieved with the ELD method: brushite or dicalcium phosphate dehydrate (DCPD, $CaHPO_4 . 2H_2O$), monetite or dicalcium phosphate anhydrous (DCPA, $CaHPO_4$), octacalcium phosphate (OCP, $Ca_8(HPO_4)_2(PO_4)_4 . 5H_2O$), and HA ($Ca_{10}(OH)_2(PO_4)_6$). DCPD and DCPA phases, have generally been used as precursors to HA coatings. In a physiological condition the solubility of these calcium phosphates follows the order from highest to lowest: DCPD>OCP>HA, however the pH of the solution also affected the solubility of these calcium phosphates. In general, as the pH increases from 3 to 9, the solubility of all four forms of calcium phosphates decreases (table 2-3) [197, 211]. In diluted aqueous solution based on the solution pH, phosphate transforms into several forms such as PO_4^{3-}, HPO_4^{2-} and $H_2PO_4^-$. In strongly basic solution, the phosphate mainly exists as phosphate ions (PO_4^{3-}); when the solution is mildly basic, the phosphate is mostly hydrogen phosphate ions (HPO_4^{2-}); and in the mildly acidic solution, the phosphate is comprised of dihydrogen phosphate ions ($H_2PO_4^-$) [212, 213].

Table 2-3. CaP phase specifications in aqueous solutions at room temperature (based on [214-217]).

CaP phase	Formula	Log K_{SP}	Ca/P ratio	pH range
DCPD	$CaHPO_4$	-6.6	1.0	2-6
OCP	$Ca_8(HPO_4)_2(PO_4)_4 \cdot 5H_2O$	-72.5	1.33	5.5-7
HA	$Ca_{10}(OH)_2(PO_4)_6$	-117.1	1.67	9.5-12

Recent studies on OCP have shown that since this CaP phase is more resorbable and it enhances more bone formation than HA does, it has a positive role in osteoconduction and osteoinduction [197-200]. As a type of ceramic, HA is brittle. Its fracture toughness (K_{IC}) is less than 0.9 $MPa \cdot m^{1/2}$, and its compressive and tensile strengths are less than 300 MPa and 50 MPa respectively [212, 213].

2.8 PROTEIN-CALCIUM PHOSPHATE INTERACTION

Solid-state NMR (ss-NMR) techniques have been utilized to determine the molecular structure of proteins and peptides on calcium phosphate surfaces. Using the ss-NMR it has been found out that HA crystals has a surface area of about 80 m^2/g. HA unit cell dimensions are $a = b$ = 9.432 A°, and c = 6.881 A°. There are two different binding sites positively cooperative, called the P and C sites, in the crystal surface of the primitive unit cell (see Fig. 2.13) [218-220].

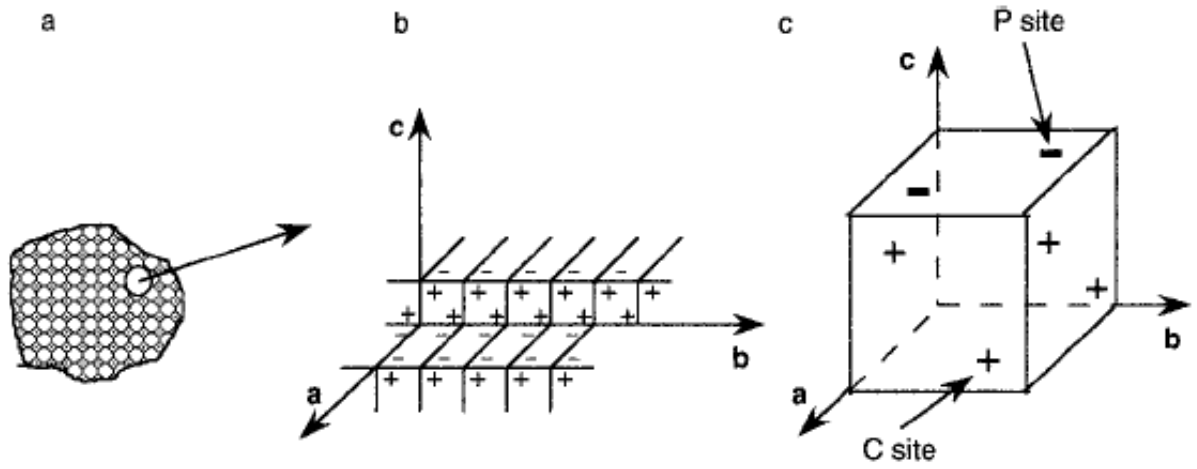

Figure 2.13. Illustraion of HA surface charge in crystal state: (a) Hydroxyapatite particle; (b) expanded area of hydroxyapatite; (c) crystal unit cell of hydroxyapatite from [219] with permission from Elsevier.

Proteins are made of chains of amino acids, containing side-chain of carboxyl or amino groups. These groups may dissociate in aqueous solution at a suitable pH, resulting in COO^- and NH_3^+ ions covalently attached to the protein molecule. The carboxyl group tends to ionize at pH values over about 4 and the amino group at below about 12. Accordingly, in acid solution, the presence of NH_3^+ and COOH groups makes a typical protein positively charged, and in basic solution it is charged negatively because of NH_2 and COO^- groups. When pH equals to isoelectric point (pI), the net charge is zero, indicating the presence of equal numbers of oppositely charged groups on the protein or so-called dipolar ion. At pHs near the pI, both NH_3^+ and COO^- groups are present, so that the net charge is small (Fig. 2.14) [219, 221, 222].

In crystalline state of hydroxyapatite P sites include six oxygen ions belonging to three crystal phosphates. They have hexagonal arrangement on the (*a*, *b*) crystal face of HA with a minimal distance of 9.432 A°. C sites are arranged in a rectangular manner with the inter-distance in the *a* or *b* direction equal to 9.432A° and the inter-distance in the *c* direction, equal to 3.441 A° (*c*/2). P sites lack calcium ions or positive charge, and therefore bind basic groups in

proteins, but C sites are rich in calcium ions or positive charge, and thus bind with acidic groups in proteins (Fig. 2.13) [219, 221, 222].

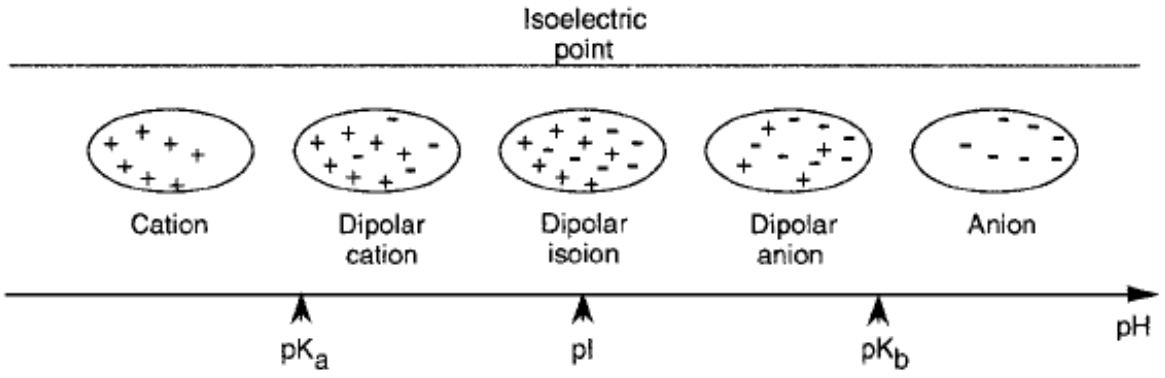

Figure 2.14. Schematic representation of the variation of charge with pH for a protein, from [219] with permission from Elsevier.

The surface properties of HA in aqueous solution are dramatically changed because the ions are hydrated. The surface charges on HA in aqueous solution depend upon various dissolution and hydrolytic reactions and relate to the pH of the suspension solution. In this situation, the pH determines the ζ potential of HA particles when the ratio of Ca/P is fixed without any other determinant ions in suspension. Figure 2.15 shows the relation of the ζ potential to the pH of the suspension solution [217, 219, 220]. The point of zero charge (pzc) of HA is dependent upon the Ca/P ratio and the physical state. When pH > pzc, the negative charge on the HA surface will dominate; when pH < pzc, HA accumulates positive charge more readily [221, 222]. The affinity of Ca^{2+} on the C site in HA with COO^- in protein is larger than the affinity of the negative charge in the P site for NH_3^+ in proteins, because both the surface of HA and proteins are heterogeneous, with both negative and positive charges in the suspension

solution. There is also affinity between HA and proteins due to hydrophobic (*a*, *c*) or (*b*, *c*) crystal face in HA, and hydrophobic patches in proteins [217, 219, 220].

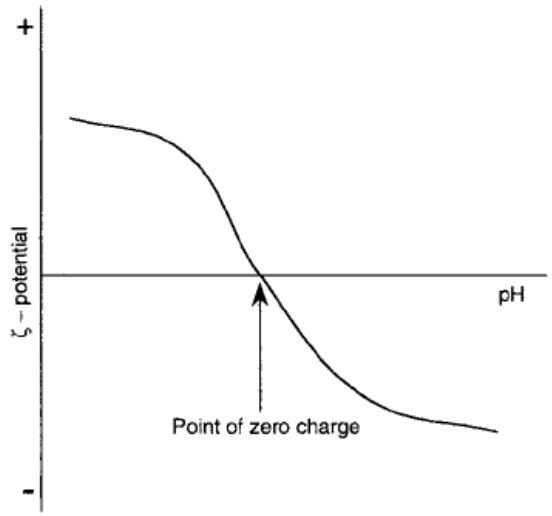

Figure 2.15. typical relation of zeta potential to pH for CaP suspension solution, from [219]

A substrate with multiple binding site like CaP can result in a cooperative adsorption with proteins containing multiple groups with affinity for the CaP sites (see Fig. 2.16) [219].

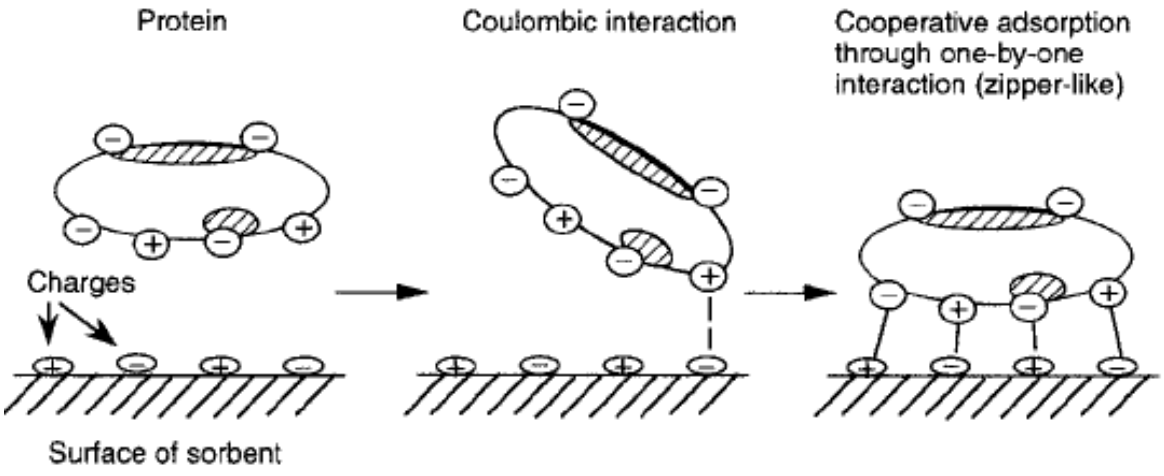

Figure 2.16. Schematic presentation of protein-CaP surface cooperative adsorption, from [219] with permission from Elsevier.

Stayton *et al.* reported that, the strong interaction of statherin with HA is mediated by the acidic N-terminus, where two phosphoserines and three carboxylate-containing side-chains are located [218]. Lee *et al.* demonstrated that proteins have a greater tendency to bind onto amorphous calcium phosphate (ACP) than crystalline HA. He observed high release rate of 74% from ACP and 15% from highly crystalline HA [225]. Weiger *et al.* identified a short peptide that binds to crystalline HA and to HA-containing domains of human teeth. They found the peptide (SVSVGMKPSPRPGGGK) binds with relatively high affinity (K_D = 14.1 µM ± 3.8 µM) to HA [226]. Sarikaya *et al.* identified the high affinity sequence (CMLPHHGAC) out of more than 50 sequences of peptide-phage library. They flanked the sequences by a pair of cysteine (Cys) residues to mimic the native peptides with random sequences in the library that were Cys-Cys constrained and displayed on the pIII coat protein of M13 bacteriophage. The binding strength of this peptide to HA was reported as 75 + 5% binding [227]. Sarikaya *et al.* also showed that in the non-metal peptide binding sequences (metal oxides and zeolites), the basic amino acids (arginine and lysine) and hydroxyl-containing residues were common [227-231].

2.9 TiO_2 NANOTUBES

Different techniques have been developed to modify the surface properties of metal implants. Modifying surface features can effectively enhance *in vitro* and *in vivo* biological events [52, 232-234]. About 40 % of today's biomedical implant materials are based on titanium or titanium alloys [235]. The main reason why TiO_2 have attracted such a high interest is because some of the intrinsic properties of TiO_2 such as high biocompatibility, acceptable mechanical properties, and chemical inertness [235, 236]. The titanium dioxide layer would enable titanium implants to bind with bone while pure titanium metal lacks osteoconductivity [237].

Various methods have been used for preparation of titanium oxide nanotubes, such as sol–gel method [238], electrophoretic deposition [239], and anodization [240]. Among these methods anodization is preferred as it provides strongly adherent TiO_2 layer as compared to the other two approaches. The adhesion and mechanical integrity of the TiO_2 layer is very important for bio-implant applications [240]. Anodization of titanium in fluoride-based electrolyte is a controllable, reproducible and simple process which provides an aligned TiO_2 nanotube structure with very high specific surface area [241, 242]. In TiO_2 nanotubes coating, not only can the diameter of the tube surfaces be accurately adjusted to virtually any value between 10–250 nm [243], but owing to the anodization nature, entire, even complex shaped surfaces (such as dental-implant screws or hip implants) can be coated easily with such nanotube layers (Fig. 2.17) [244].

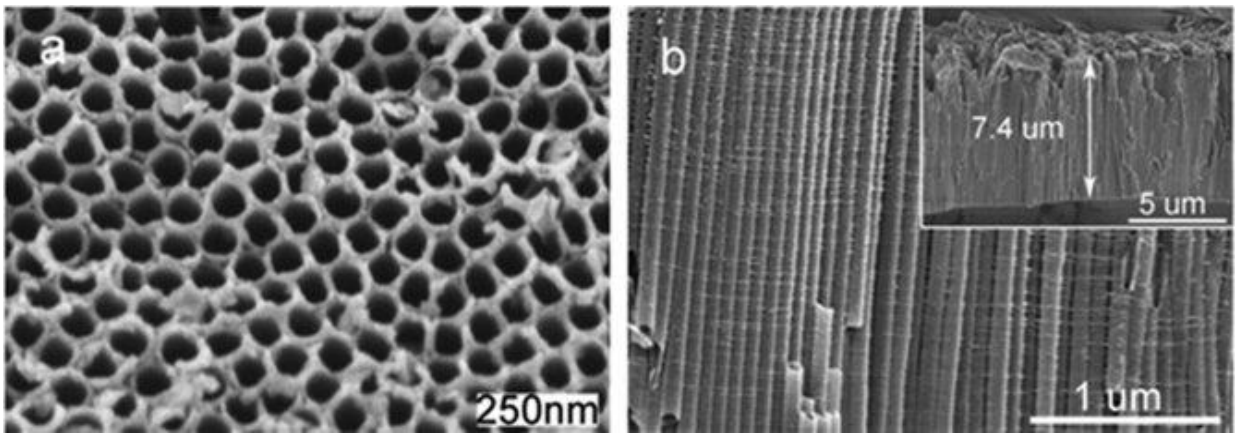

Figure 2.17. SEM micrographs of TiO_2 nanotubes. (a) Top view, (b) cross-sectional view, from [236] with permission from Elsevier.

TiO_2 exists naturally mainly in three crystalline phases: anatase, rutile, and brookite. The as-prepared TiO_2 nanotubes are amorphous in nature but can be annealed (under oxidizing conditions in air or O_2) to anatase or rutile. Annealing can also affect the nanotube morphology.

Usually, for extended annealing, nanotubes are stable up to 650 °C, but at higher temperatures the tubes start collapsing [245].

It is generally accepted that TiO_2 nanotubes form in F^- containing electrolytes by two competing electric field-assisted processes. The water was electrolyzed at the Ti anode, and a layer of compact anodic oxide resulted: In the first process water is electrolyzed at the Ti anode to form a passive uniform TiO_2 layer across the surface. The overall reactions for anodic oxidation of titanium can be represented as

$$Ti + 2H_2O \rightarrow TiO_2 + 4H^+ + 4e^- \quad (1)$$

The second process is related to the field-assisted dissolution of the oxide at the oxide/electrolyte interface followed by chemical dissolution of newly formed oxide at the oxide/electrolyte interface. In field-assisted dissolution Ti cations migrate from the metal/oxide interface towards the oxide/electrolyte interface and dissolved into the electrolyte while the free anions (O^{2-}) migrate towards the Ti/oxide interface to interact with the Ti by the following reactions [246-248].

$$Ti^{4+} + 6F^- \rightarrow [TiF_6]^{2-} \quad (2) \quad \text{(Field –assisted dissolution)}$$

$$TiO_2 + 6F^- + 4H^+ \rightarrow [TiF_6]^{2-} + 2H_2O \quad (3) \quad \text{(Chemical dissolution)}$$

Field-assisted dissolution dominates chemical dissolution in the initial stage of anodization due to the relatively large electric field across the thin oxide layer. Localized dissolution of the oxide results in the formation of small pits on Ti surface. The pits then, convert to larger pores and spread uniformly over the surface. The inward movement of the oxide layer at the pore bottom leads to the pore growth. The thickness of the tubular structure ceases to increase when the rate of oxide growth at the metal/oxide interface becomes equal to the rate of oxide dissolution at the pore-bottom/electrolyte interface [249]. Increasing the anodization

voltages increase the field-assisted dissolution and therefore a greater nanotube layer thickness is achieved before equilibrating with the chemical dissolution (Fig. 2.18) [248].

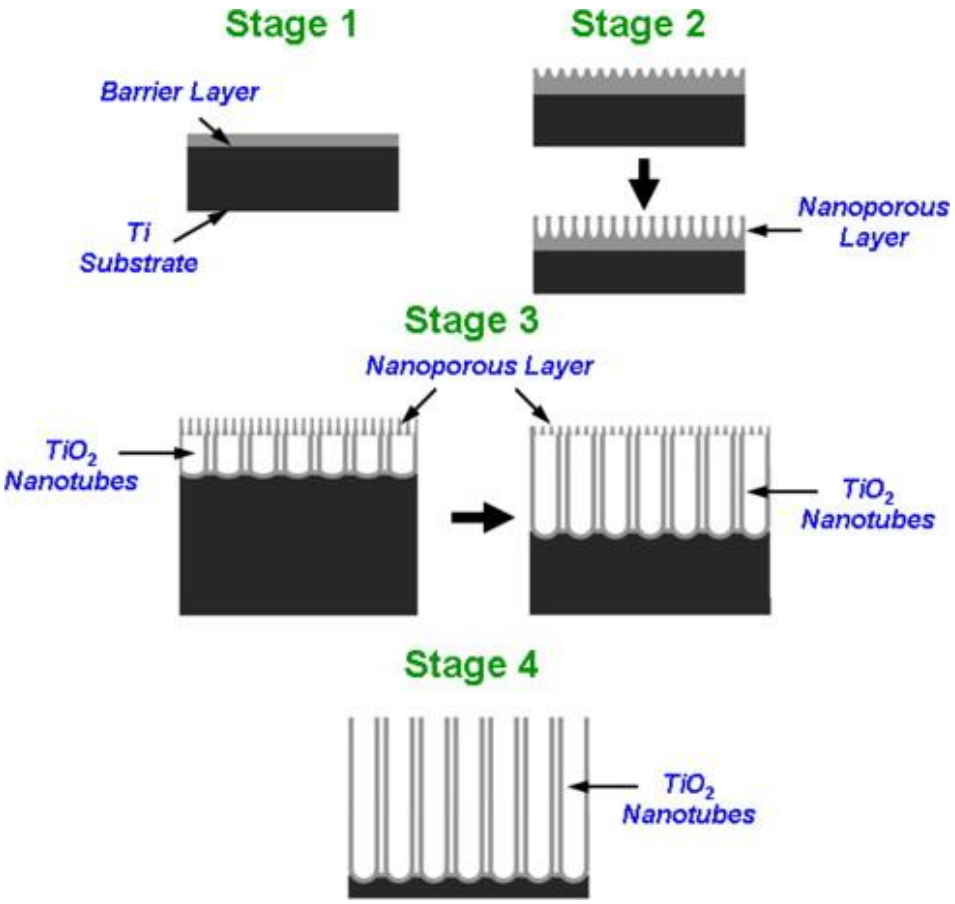

Figure 2.18. Schematic showing the mechanism for TiO_2 nanotube formation at constant anodization voltage. Stage 1: the formation of a dense oxide layer by the dissolution of Ti until the current density and thickness stabilize at a constant value. Stage 2: local dissolution of TiO_2 reduces the film thickness, locally, and increases the electric field intensity leads to the formation of nanopores across the surface of the TiO_2 layer. Stage 3: nano pores turn to nanotubes growing deeper into the substrate due to the competition of oxide growth (Eq. (1)) and dissolution (Eq. (2,3)) at the bottom of the nanotube. Stage 4: nanotubes continue to grow in length, and the current density gradually drops, until the so-called "equilibrium thickness" is established, from [247] with permission from Elsevier.

The geometry of the TiO_2 nanotube arrays suggests that the material may be used as a drug-eluding coating on implants [250, 251]. Loading techniques into titania nanotubes usually follow either the physical adsorption or chemical immobilization method [252]. It has been

reported that the surface of antibiotic-loaded TiO_2 nanotubes is capable of reducing bacterial adhesion whilst retaining the normal osteoblast adhesion and differentiation [160, 252-254]. Shrestha *et al.* showed that TiO_2 nanotubes can be filled with magnetic Fe_3O_4 particles and thus be magnetically guided to desired locations, for example for the site-selective killing of cancer cells [255]. Bae *et al.* reported that the TiO_2 nanotubular structure is a promising configuration for sustained rhBMP-2 delivery [256]. Ketul *et al.* filled the nanotubes with gentamicin and reported significantly reduction in bacterial adhesion on the surface [160].

Even when the drug is simply filled into nanotubes, a main problem is the uncontrolled release of drugs. In this regard, hydrophobic surface modification (caps) on hydrophilic TiO2 nanotubes have been investigated to control the release profile, the achieved release however was in the order of hours [252, 257].

2.10 SUMMARY OF CURRENT CHALLENGES

Biofilm-associated implant infections are still very difficult to treat. The only remedy for patients with peri-prosthetic deep infection is two-stage surgery which requires removal of the contaminated implant. Moreover, the creation of biofilm and sub-exposure to antibiotics will drive the emergence of multi-drug resistant bacteria which is known as a global problem. Treatment options such as prophylaxis with broad spectrum antibiotics and systemic administration of antimicrobial agents are usually ineffective against these pathogens. Serious concern regarding local delivery of conventional antibiotics is that the release of them at levels below the minimal inhibitory concentration may evoke bacterial resistance. Conversely, high release dose of these antibiotics often harm cell viability and osteogenic activity and may impair osteointegration. Therefore local administration of novel class of broad spectrum antimicrobial is necessary.

Another challenge concerning releasing devices (orthopaedic implants) is developing a drug delivery system with a controlled kinetics of release. In other words, loading and controlling antimicrobial compound release over prolonged periods is complicated. What is learned from literature is that the implant-antibiotic binding obtained from the developed techniques still does not satisfy the ideal releasing profile. This ideal profile should exhibit fast initial release of antimicrobial agent during the peri-implant infection phase (~6 hr) which is critical time for initial elevated infection risk, followed by a long period of drug release. Most of the suggested approaches release the significant amount of the drug in very short time (cytotoxicicity risk). This kind of burst release demands large amount of drug loading to keep the antibiotic level above the minimal inhibitory concentration for a longer period, otherwise it may result in emergence of resistant organisms. Hence, there is a need to either formulate a proper

antimicrobial compound which wouldn't cause the bacteria resistance or to develop a device with capability to load and release the antimicrobial agent in a controlled manner. Of course, the antimicrobial activity of the drug should not impair the osteointegration or biocompatibility of the implant.

An ideal antimicrobial orthopaedic implant should meet the following characteristics at the same time:

- It should be effective against broad spectrum of bacteria (both Gram-positive and Gram-negative).
- It should not develop bacteria resistance even when the concentration falls below MIC.
- It should carry enough drug required for initial burst release (within the first 6 hr after implantation), following long period of therapeutic release in a controlled manner.
- It should not impair bone growth.
- It should not cause cytotoxicity for the host cells (biocompatible, hemocompatible).
- The coating's interface with titanium surface should have robust mechanical properties.

CHAPTER 3 SCOPE AND OBJECTIVES

An ideal strategy to combat implant-associated infections is prevention of infection at the site of implant. Despite recent progresses, developing an antimicrobial delivery system which would be able to avoid antibiotic resistance, and satisfy antimicrobial release kinetics without impairing bone growth is still a challenge.

The scope of this dissertation is to develop antimicrobial coatings for local delivery of a new class of antimicrobial agent from orthopaedic implant surface. There are a few factors involving the designs of antimicrobial coatings that should be considered such as, the development of a new antimicrobial agent, the release kinetics profile, antimicrobial activity while maintaining the osteointegration, and biocompatibility. Due to the multi drug resistance of many important pathogens, the novel therapeutic agents "antimicrobial peptides" have been proposed in our study because of their outstanding features such as killing different strains of bacteria without developing multidrug resistant organisms. In this regard, different approaches were developed to deliver AMPs from Ti implant surface. The surface of Ti implant has been modified in various ways to load and release AMP without impairing the biocompatibility, and osteointegration properties.

Osteoconductivity and biocompatibility of calcium phosphate material and its affinity with proteins have made this bioceramic an attractive material for orthopaedic implant coatings with a drug-delivery capability. We developed a thin layer of microporous osteoconductive calcium phosphate coating on Ti implant as an AMP carrier through simple soaking adsorption technique. The antimicrobial activity and biocompatibility of this coating were studied *in vitro* while a comprehensive animal study was performed for bone growth and osteointegration.

Titania nanotubes are another interesting platform for drug delivery due to their very high specific surface area, and their chemical inertness. High biocompatibility, better mechanical properties in compared to calcium phosphate, and the advantage of titanium dioxide over pure titanium in terms of interaction with bone are some of the features of this coatings. Hence, titania nanotubes coatings on titanium were fabricated using anodization technique. This coating was loaded with AMP via vacuum-assisted physical adsorption method.

The burst release of the antimicrobial compound is a complex issue. To control both the quantity of loaded AMP, and keep the release profile in therapeutic level for longer period, while keeping the osteoconductivity, and biocompatibility we developed a new technique. To achieve this purpose, a combination of different coatings including nanotubes, CaP and phospholipid layers were utilized.

The purpose of these studies is to develop more robust and flexible antimicrobial coatings on Ti that won't impair bone growth. Detailed objectives of this study are as follows:

- To develop an efficient technique to load AMP into the thin layer of microporous CaP coating on Ti implant fabricated by ELD technique.
- To choose a proper AMP-CaP combination amongst proposed antimicrobial agents including, Tet213, Tet1010, Tet20, HHC36, hlF1-11, Mx226 and Tobramycin, in terms of cytotoxicity and antimicrobial activity.
- To develop techniques for measuring loaded AMP and release properties.
- To evaluate *in vitro* biocompatibility of AMP loaded CaP coating on implants.
- To evaluate *in vivo* effect of AMP containing CaP coating implants on bone growth and osteointegration in femur of rabbit.
- To evaluate *in vitro* effect of AMP containing nanotube coatings on Ti implants.

- To develop multi layered coatings including nanotubes, calcium phosphate and phospholipids with the purpose of controlling the release of loaded AMP and release rate.
- To evaluate *in vitro* biocompatibility, and hemocompatibility of multi layered coatings.

The research chapters (Chapters 4-5-6) are organized as follows. Chapter 4 focuses on the fabrication and delivery of antimicrobial peptides on calcium phosphate-coated titanium. This chapter investigates the characteristics of the CaP coatings, AMP loading technique, antimicrobial activity, detection of AMP and cytotoxicity tests. Chapter 5 applies a modified AMP and studies the effect of CaP-AMP on bone growth *in vivo*. This chapter develops an improved AMP detection, and studies the antimicrobial activity and biocompatibility *in vitro.* Chapter 6 develops a progressive multi-layer assembly coating with the advantage of the previous studies plus the capability of controlling the AMP release kinetics. Biocompatibility and hemocompatibility of the coatings were also conducted in this chapter.

CHAPTER 4 ANTIMICROBIAL PEPTIDES ON CALCIUM PHOSPHATE-COATED TITANIUM FOR THE PREVENTION OF IMPLANT-ASSOCIATED INFECTIONS[1]

Implant-associated infections are one of the most serious complications in orthopaedic surgery. This challenge is further complicated by the concern over the development of antibiotic resistance as a result of using traditional antibiotics for infection prophylaxis [258]. The objective of this chapter is to develop a technique that enables the loading and local delivery of a unique group of antimicrobial peptide (AMP) through implant surfaces, using a simple soaking technique. A thin layer of micro-porous calcium phosphate (CaP) coating was processed by electrolytic deposition (ELD) onto the surface of titanium as the drug carrier. Various surface analysis techniques were performed to study the coating properties. The biocompatibility of the AMP loaded CaP was investigated against osteoblast-like cells, and the antimicrobial activity of the coating was evaluated against *S. aureus* (as a representative of Gram-positive) and *P. aeruginosa* (as a representative of Gram-negative) bacteria. The total amount of loaded AMP was measured using a fluorometry technique.

4.1 MATERIALS AND METHODS

4.1.1 Processing of CaP coating on titanium surface

Calcium phosphate coating onto Ti surfaces was performed using the electrolytic deposition technique reported earlier [259, 260]. Commercially pure titanium plates (Goodfellow, USA) of $10 \times 10 \times 0.5$ mm dimensions were used as the working electrode

[1] A version of Chapter 4 has been published. **Mehdi Kazemzadeh-Narbat**, Jason Kindrachuk,

(cathode), while a platinum plate served as the anode. The distance between the working electrode and the anode was set to 3 cm. The electrolyte solution used for the ELD consisted of 5.25 mM of $Ca(NO_3)_2$ (Sigma Aldrich), 10.5 mM of $NH_4H_2PO_4$ (Fisher Scientific), and 150 mM of NaCl (Fisher Scientific). The pH of the solution was adjusted to 5.30 by adding the NaOH (Fisher Scientific) and the coating process was conducted with a DC power source operated at 2.5 V at room temperature for 3 h. Before ELD processing, the Ti specimens were ground with 320 grit sandpaper and cleaned with alkaline detergent (Fisher Scientific SF105), acetone, 70% ethanol and distilled water. The specimens were then etched in 2% HF (Fisher Scientific) for 1 min at room temperature. They were ultrasonically cleaned in distilled water and air-dried (Fig. 4.1).

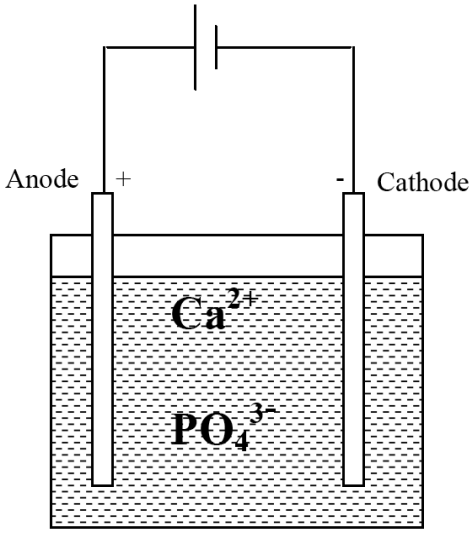

Figure 4.1. Schematic of the electrolytic deposition setup. Ti plate was used as the working electrode (cathode), while a platinum plate served as the anode.

Surface morphology and thickness of the CaP coating were analyzed by a scanning electron microscope (SEM Hitachi S3000N) after being sputter-coated with a thin layer of Au–Pd. For coating thickness measurement, three samples were embedded into the epoxy resin

(Buehler 208130), mechanically ground using sandpapers and polished using diamond suspensions and silica colloidal suspension (0.05 μm). Chemical compositions were also analyzed with the Energy Dispersive Spectrometer (EDS) equipped in the SEM. To examine the crystal structure, CaP coating was scratched off the Ti plates, and analyzed with Fourier transform infrared spectroscopy (FTIR Nexus 870) and powder X-ray diffraction (XRD Bruker D8, Cu Kα, 40 kV and 40 mA, step scanning).

4.1.2 AMP loading on titanium

One of the most potent short (9 amino acids), broad spectrum AMPs identified in a recent large QSAR study was HHC36 [27, 261]. Further testing with surface-immobilized HHC36 (C-terminally modified and renamed Tet213) demonstrated that it retained antimicrobial activity [27, 262]. Tet213 with a C-terminal Cys residue (KRWWKWWRRC) was therefore selected for the current study. To load Tet213 onto the titanium samples, a buffer solution of 50 mM of Na_2HPO_4 (Calbiochem) in distilled water was prepared, and the pH was adjusted to 7.4 by dropping 0.1 M NaOH. 1 mL of this buffer was transferred into a vial containing 1 mg of peptide. The Ti sample was immersed into the vial and kept for 1 h at room temperature under constant, gentle shaking. The plate was then rinsed with distilled water for 10 times, 1 min each, and kept in a vial after being dried in slow air stream.

4.1.3 Detection of loaded AMP

The amount of AMP immobilized on the Ti surface was determined by fluorometry technique [262]. After dissolving the coating in 1 mL of 0.1 M HCl (Fisher Scientific) for 1 h in ultrasound bath, 3 mL of 3.23 mM PHQ (9,10- Phenanthrenequinone) solution (Fluka Chemika)

was added into the vial. Subsequently, 0.5 mL of 2 M NaOH solution was added. The vial was then placed in 30 °C water bath for 3 h to allow the reagent PHQ react with Arg residues within the AMP. The reaction product was a compound with fluorescence that could be used to quantify sub-μg amounts of Arg (Fig. 4.2). To stop the reaction, acidification was performed by adding 2.25 mL of 2.4 M HCl into the vial. The amount of AMP, based on arginine concentration, was measured using a Luminometer (Perkin Elmer Ltd UK LS-50B) [263], calibrated with six standard solutions of known AMP concentrations. Four groups of samples, six in each group, were tested to study the efficiency of AMP loading onto the CaP coating. Group one (CaP) was the CaP-coated Ti without AMP as a control. Group two (CaP-AMP) was the CaP-coated Ti, immobilized with AMP and rinsed with distilled water ten times. Group three (CaP-AMP-PBS) was the coated Ti, immobilized with AMP. Instead of using water, this group was rinsed with PBS and immersed in PBS for 30 min before the test. Group four (Ti–AMP) was Ti without CaP coating, but loaded with AMP in the same way as Group two.

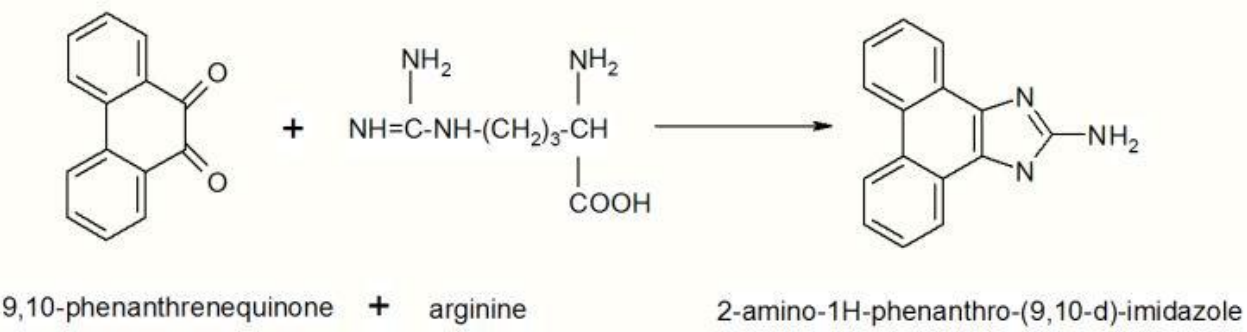

Figure 4.2. Fluorescent compound from PHQ and arginine reaction.

4.1.4 Antimicrobial activity testing

Antimicrobial activity of the specimens was tested against *S.s aureus* and *P. aeruginosa* bacteria. Both bacteria strains were cultured overnight. One hundred μL of each solution was transferred into sterile tubes containing 5 mL of Mueller Hinton Broth (MHB) and incubated at 37 °C for 1 h to obtain bacteria in the mid logarithmic phase of growth. *P. aeruginosa* and *S. aureus* bacterial suspensions were then re-suspended using Basal Medium 2 (BM2) or MHB, respectively, to dilute the solution and provide a final density of $\sim 10^6$ cells/mL. To study the capability of specimens in killing bacteria, a survival assay was performed. Four hundred μL of the *P. aeruginosa* or *S. aureus* bacterial suspensions were separately dripped onto groups of three bare Ti plates and three CaP-coated Ti plates, which had been treated with AMP and rinsed with distilled water, as described above. After 30, 90, 150 and 270 min incubation with *P. aeruginosa* (H1001: *luxCDABE*) or *S. aureus* (ATCC 25293) bacterial suspensions the residual bacteria were plated on nutrient agar and incubated overnight at 37 °C and bacterial survival assessed by counting the number of colony-forming units (CFU). The susceptibility of bacteria to the peptide from six CaP-AMP specimens was also evaluated by the inhibition of *P. aeruginosa* that constitutively expresses a luciferase gene cassette. Samples were incubated at 37 °C for 4 h and 24 h and the inhibition of *P. aeruginosa* was measured by the decrease in bacterial luminescence (which is dependent on bacterial energization). The result was reported as percent inhibition relative to average luminescence value of the untreated *P. aeruginosa* H1001.

Since the direct measurement of peptide release from CaP-AMP samples over time was a substantial challenge, the antimicrobial test was used to indirectly study the release of AMP and to evaluate the antibacterial efficacy after different antimicrobial test cycles. Six CaP-AMP

samples were incubated with *P. aeruginosa*. After 30 min, the bacteria solution was pipetted and the samples were rinsed three times with PBS. The samples were then air-dried, and treated with equal amounts of bacteria for another 30 min after which remaining CFU were determined as above. This antimicrobial activity cycle was performed four times consecutively.

To compare the efficacy of AMPs with conventional antibiotics on CaP coating, CaP samples, were incubated with equimolar concentrations of (0.63 mM) Tet213, two commercially developed antimicrobial peptides MX226, and hLF1-11 or Tobramycin (potent antibiotic against Gram-negative bacteria especially *P. aeruginosa).* The specimens were rinsed with distilled water and air-dried. The prepared CaP-Tet213, CaP-MX226, CaP-hLF1-11 and CaP-Tobramycin plates were incubated with *P. aeruginosa* solution for 1 h before measuring bacterial survival.

4.1.5 Cytotoxicity assay

MG-63 osteoblast-like cells from human osteosarcoma (ATCC® CRL-1427™, USA), were cultured in standard culture medium Dulbecco's Modified Eagle Medium (DMEM, GIBCO), which consisted of a minimal essential medium, supplemented with 10% fetal bovine serum, and 1% non-essential amino acids (GIBCO). The medium was renewed every 2 days. Cultures were maintained in a humidified atmosphere with 5% CO_2, at 37 °C. The confluent osteoblast cultures (passage nine) were detached from the culture flask by incubation with 0.1% trypsin and 0.1% ethylenediaminetetraacetic acid (EDTA) for 5 min. The Osteoblast solution was centrifuged at 400 g for 10 min, and re-suspended in the medium. The growth and viability of cells colonizing the samples were evaluated by measuring the mitochondrial dehydrogenase activity using a modified MTT (3-(4,5-dimetyl-2-tiazolyl)-2,5-diphenyl-2H-tetrazolium bromide) (Biotium Inc., USA) reduction assay. To determine the cytotoxicity of CaP-AMP samples, MG-

63 cells were seeded in 12-well plates at 10^4 cells/mL in a humidified 5% CO_2 atmosphere. Three types of samples were studied in triplicate: (1) bare titanium (as control) (2) CaP-coated Ti (3) CaP-coated Ti soaked with Tet213. Negative controls in this experiment were cells cultured under normal conditions without AMP. After 24 h of incubation, MTT solution in 1 mL serum free medium was added and the plate was incubated for 4 h at 37 °C in a humidified 5% CO_2 atmosphere. The solution was then removed, dimethyl sulfoxide (DMSO) added, and the plate was shaken for 15 min before measuring adsorbance at 570 nm (the reference value was 690 nm) on an ELISA microplate reader (Bio-Tek Instruments). The MTT assay was performed after 1, 2, 3, 7 and 10 days (see appendix A).

4.1.6 Statistical analyses

The differences between all values were analyzed using an independent *t*-test, and a *p* value of less than 0.05 was considered statistically significant.

4.2 RESULTS

4.2.1 Calcium phosphate coating on titanium surface

The CaP coating on Ti was microporous and consisted of plate-like crystals (Fig. 4.3a). The cross-sectional image of the coating showed an average thickness of ~7μm, with increased pore and crystal sizes from the bottom to the surface (Fig. 4.3b). The coating adhered to the Ti substrate without cracks.

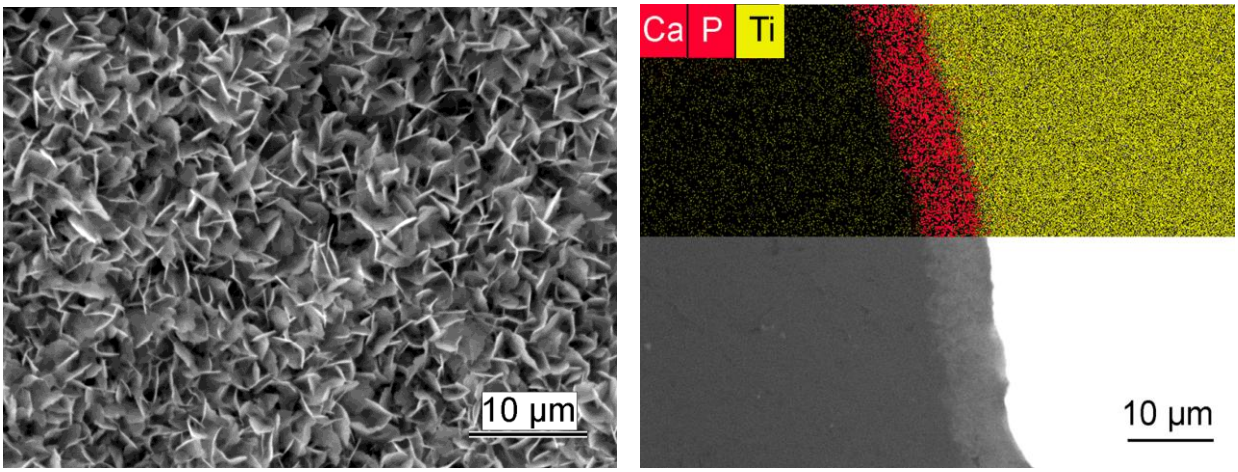

(a) (b)

Figure 4.3. Calcium phosphate (CaP) coating on Ti surfaces (a) SEM image showing micro-porous plate-like CaP crystals, (b) A back scattered electron image (lower half) and EDS mapping of the CaP coating cross-section showing an average thickness of ~7 µm.

The XRD spectrum of the CaP coating matched that of octacalcium phosphate (OCP). The 2θ at 4.722° in Figure 5.2a is the characteristic peak of OCP (010) plane. However, due to the peak overlapping between HA and OCP, the presence of small amount of HA could not be excluded [186, 261, 262]. Electron Dispersive Spectroscopy under the SEM measured the average Ca/P ratio of the CaP coating to be 1.3, which is close to OCP (Fig. 4.4a).

FTIR spectroscopy (Fig. 4.4b) was used to compare the CaP coating with HA (Acros Organics). A clear distinction could be observed between HA and the ELD CaP coating in the phosphate ν4 vibration mode in the 500–650 cm^{-1} range. The wave numbers attributed to HA were 566 cm^{-1}, 603 cm^{-1} and a shoulder at 630 cm^{-1} from the OH group. In contrast, the two peaks for the CaP coating were at 601 cm^{-1} and 561 cm^{-1}, which could be attributed to typical OCP absorption. Both spectra exhibited obvious strong bands attributed to PO_4^{3-} groups. The bands at about 1100 cm^{-1} and about 1040 cm^{-1} are assigned to the components of the triply

degenerated ν3 antisymmetric P–O stretching mode. The ~962 cm^{-1} band is assigned to νl, the non-degenerate P–O symmetric stretching mode [207, 259, 266].

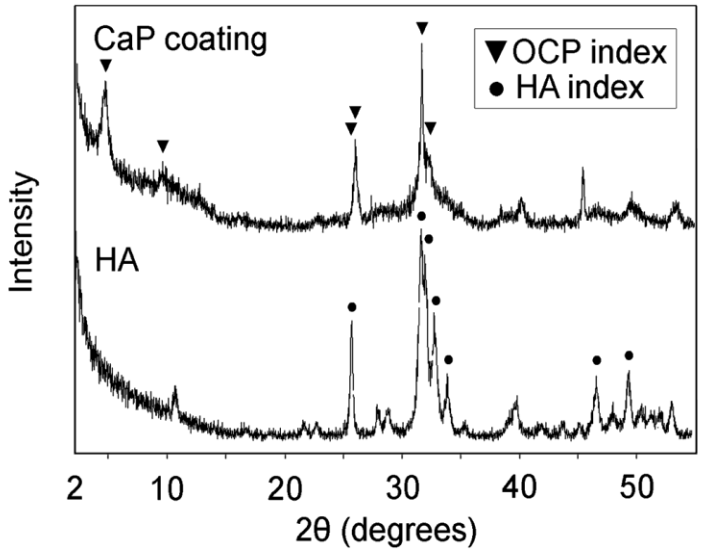

(a)

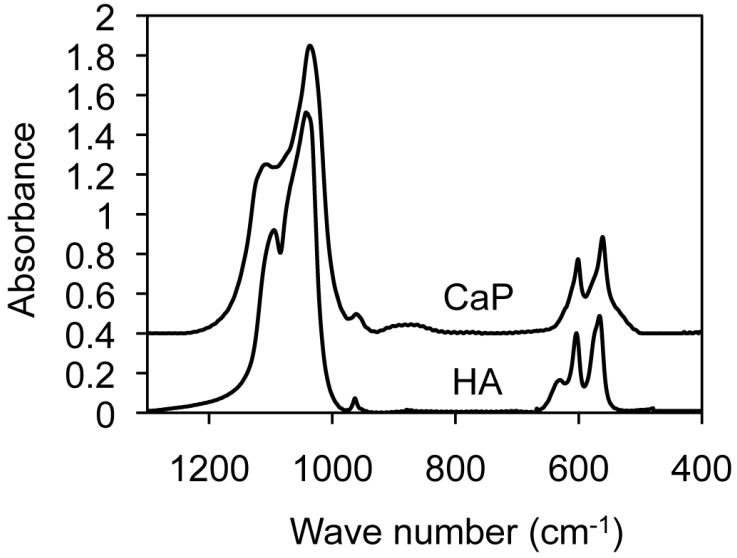

(b)

Figure 4.4. (a) X-ray diffraction patterns of the HA powder and CaP from the coating. The 2θ at 4.722° is the characteristic peak of OCP. (b) FTIR spectra of HA and CaP coating. The two peaks for the CaP coating at 601 cm^{-1} and 561 cm^{-1} could be attributed to OCP absorption.

4.2.2 Antimicrobial peptide loading onto CaP coatings

The amount of AMP Tet213 absorbed to the CaP surface in the four sample groups is shown in figure 4.5. The CaP group that was not treated with peptide served as a negative control. Among the three other groups that were treated with peptide, the CaP-Tet213 group, i.e. CaP coating loaded with peptide and rinsed in water, had the highest peptide concentration of ~9 μg/cm^2. Interestingly, the CaP-Tet213-PBS group, which was soaked in the PBS for 30 min after peptide loading, still showed an average peptide concentration of ~8.5 μg/cm^2. No statistical difference was found between the two groups. The Ti-Tet213 samples that had no CaP coatings, showed no significant AMP loading (less than 0.1 μg/cm^2).

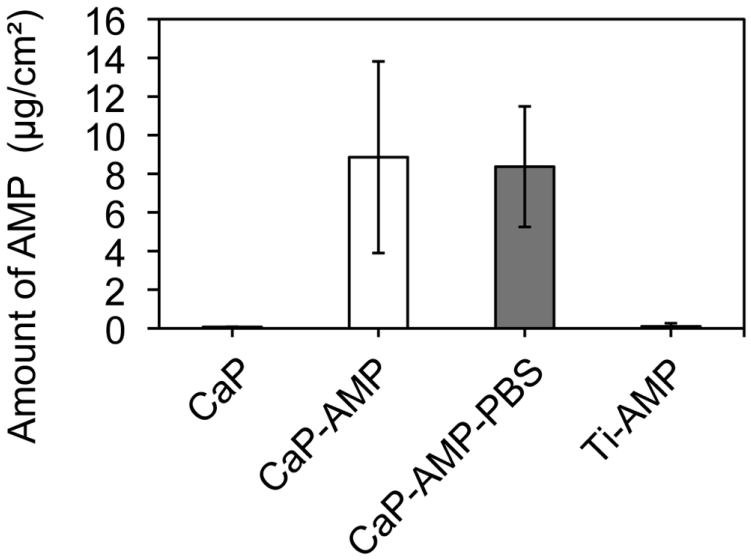

Figure 4.5. The amount of peptide immobilized on sample surfaces. CaP: CaP-coated Ti without AMP, CaP-AMP: CaP-coated Ti immobilized with Tet213 and rinsed with distilled water, CaP-AMP-PBS: CaP-coated Ti immobilized with Tet213 rinsed and preserved in PBS for 30 min, Ti-AMP: Ti without CaPbcoating immobilized with Tet213. The Ca-AMP and Ca-AMP-PBS groups (six samples each) showed an average peptide concentration of ~9 and ~8.5 μg/cm^2, respectively.

4.2.3 Antimicrobial activity

In assessing the antimicrobial effect against *P. aeruginosa* (Fig. 4.6a), the Ti-Tet213 group showed no antibacterial activity and there was no change in bacterial growth compared to the negative control group. The CaP-Tet213 group killed all bacteria within 30 min. The same results were observed for the antimicrobial effects against *S. aureus* (Fig. 4.6b), demonstrating the ability of CaP-coated Ti to deliver active antimicrobial peptides with bactericidal effectiveness vs. a Gram-positive pathogen strain. When examined over longer periods (4 and 24 h), using the *lux* assay *P. aeruginosa* bacteria were still efficiently inhibited by CaP-Tet213 by 92% and 77% respectively (Fig. 4.6c).

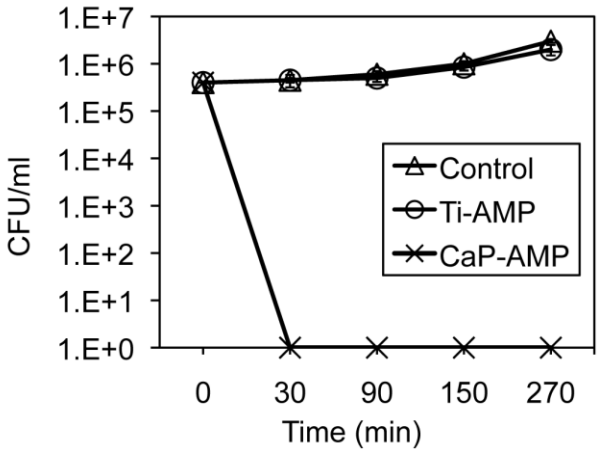

(a)

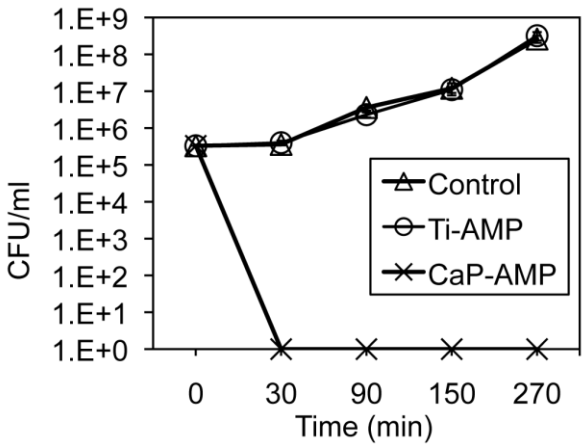

(b)

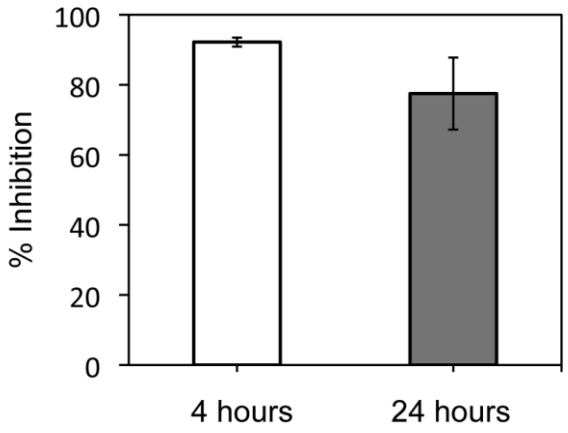

(c)

Figure 4.6. (a) Antimicrobial activity of Ti-Tet213 and CaP-Tet213 specimens (three samples each) against *P. aeruginosa.* (b) Antimicrobial activity of Ti-Tet213 and CaP-Tet213 samples against *S. aureus*. The CaP-Tet213 group killed all bacteria of both strains within 30 min, while the Ti-Tet213 group showed no antibacterial activity. (c) *lux* assay showing *P. aeruginosa* bacteria efficiently inhibited by CaP-Tet213 (three samples) by 92 and 77% at 4 and 24 h.

To examine if the Tet213 loaded CaP surface was able to repetitively kill bacteria when challenged, four consecutive killing assays were performed in which the *P. aeruginosa* was added to the surface for 30 min, bacterial killing assessed and then the surface washed before a second, third and fourth addition of bacteria. In the first round 100% of bacteria were killed. In subsequent rounds killing was somewhat diminished but efficiently inhibited the bacteria growth relative to control bacteria incubated with negative control CaP surfaces (Fig. 4.7).

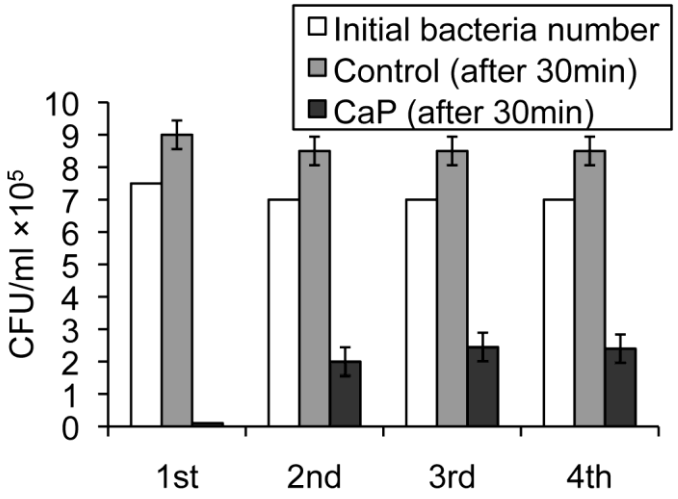

Figure 4.7. Antimicrobial activity of CaP-Tet213 specimens (six samples) against *P. aeruginosa* for four 30 min cycles. After each 30 min, the samples were rinsed with PBS and treated with equal amounts of bacteria for another 30 min after which remaining CFU were determined. In the first cycle (1st) 100% of bacteria were killed. In subsequent cycles killing was diminished but efficiently inhibited the bacteria growth.

To compare the activity of the CaP-Tet213 samples with CaP surfaces coated with a potent conventional antibiotic, CaP surfaces were incubated with equimolar concentrations of MX226, hLF1-11, Tobramycin or Tet213. The CaP-Tet213 samples clearly demonstrated more effective antimicrobial activity against *P. aeruginosa* than did CaP-MX226, CaP-hLF1-11 and CaP–Tobramycin (Fig. 4.8). The CaP–Tobramycin samples reduced the total bacterial inoculum by 3 log orders over 4 h while 100% (6 log orders) of the inoculum was killed by CaP-Tet213 (Fig. 4.8b). Moreover, as shown in figure 4.8a the CaP-Tet213 was capable of killing 100% of the same number of bacteria in less than 30 min.

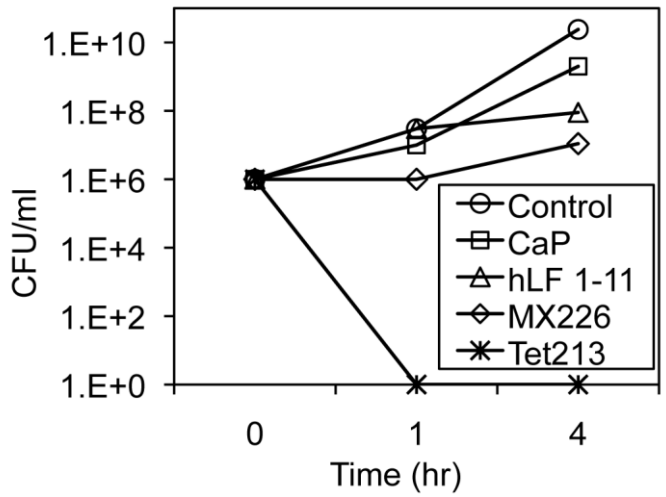

(a)

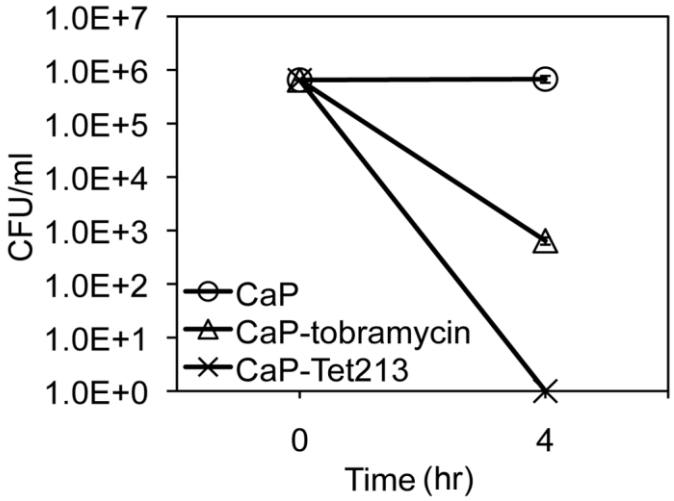

(b)

Figure 4.8. (a) Antimicrobial activity of the CaP-Tet213 sample as compared with CaP-MX226 and CaP-hLF1-11 AMPs. CaP-Tet213 clearly demonstrated more effective antimicrobial activity against *P. aeruginosa*. (b) Antimicrobial activity of the CaP-Tet213 as compared with CaP–Tobramycin. The CaP–Tobramycin specimens (three samples) reduced the total bacterial inoculum by 3 log orders over 4 h while 100% (6 log orders) of the inoculum was killed by CaP-Tet213.

4.2.4 Cytotoxicity on osteoblast-like cells

The peptide-loaded samples (soaking the samples in 1 mg/mL Tet213 buffer solution), (Fig. 4.9) showed no statistical difference in cell activity compared to the CaP-coated and non-coated Ti controls ($P > 0.05$). After 7 days in culture the cells stopped growing as judged in the MTT assay but there was no difference in any treatment condition. Thus, the amount of peptide loaded on the CaP-coated Ti surface is thus not toxic to the osteoblast-like cells.

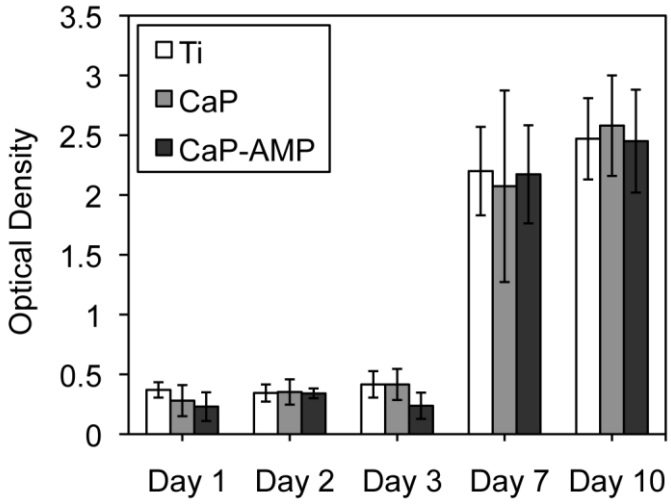

Figure 4.9. MTT assay performed to evaluate the cytotoxicity of CaP-Tet213 with MG-63 osteoblast-like cell in the solution. No statistical difference ($p > 0.05$) in cell activity between the peptide-loaded (CaP-AMP) and the two controls (CaP coating and Ti) after 10 days incubation.

4.3 DISCUSSION

We have demonstrated that cationic antimicrobial peptides can be successfully loaded to the CaP-coated Ti substrates. The peptide-loaded titanium samples had strong bactericidal effect against *S.s aureus* and *P. aeruginosa* bacteria and were also biocompatible with osteoblast-like cells. A combinational device based on this system could be a potential solution for the peri-

implant infection in orthopaedic surgery. In the current study, we used simple soaking technique to achieve efficient peptide loading and effective antimicrobial activity. The advantage of this technique is its clinical feasibility. Both the implants and the drugs can be developed and packed independently. The drug loading can be done in the operating room. This will simplify the regulation process and prolong the shelf-time.

4.3.1 Cationic antimicrobial peptides

AMPs have been actively researched in the past three decades, mainly due to their potent bactericidal capability and the low risk of developing antibiotic-resistant pathogens. It has been previously demonstrated that AMPs have an increased affinity for the negatively charged membranes of bacteria and act through either permeabilization of the bacterial membrane or translocate across the bacterial membrane to attack cytoplasmic targets [27]. The initial step of this mechanism is the affinity of AMPs for the bacterial membrane as a result of the electrostatic interaction between the negatively charged outer layer of the bacterium and the positively charged AMP. This attraction would cause the microbes to more strongly associate with these surfaces leading to enhanced killing. Subsequently, the high local concentration of the AMP would result in the displacement of positively charged counterions attached to the outer surface layers, and could thus induce a dramatic change in bacterial surface electrostatics which results in lysis [27, 174, 175]. Recently, AMPs have also been shown to have immunomodulatory activities that include angiogenesis, modulation of cytokine/chemokine expression, wound healing, and reduction of LPS-mediated pro-inflammatory responses [175, 267]. These unique properties make cationic antimicrobial peptides ideal candidates for the local delivery of novel anti-infective therapeutics on orthopaedic implants. The drug-loaded implants will protect the

surfaces from colonization by microbes without incurring the problem of resistance against common antibiotics.

The antimicrobial peptide used in this study is a cysteinylated version of HHC36, one of the most potent peptides identified by the high-throughput peptide synthesis (peptide arrays on cellulose and rapid screening technologies) in combination with quantitative structure activity relationship (QSAR) modeling [179]. It was effective against a broad array of multi-drug resistant "Superbugs" including MRSA. It has also been shown that this peptide caused minimal red blood cell lysis for concentrations up to 251 μM [179]. In the current study the results confirmed that the peptide has low cytotoxicity and is pathogen-specific. The selection of carriers for local delivery of antibiotics through orthopaedic implants has to meet two goals. The carrier should be able to deliver adequate amount of antibiotics to achieve the antimicrobial activity. At the same time, it should not impair peri-implant bone growth. Ideally, the carrier should also enhance bone growth onto the implants. For these reasons, we chose a calcium phosphate coating as the delivery carrier in this study since calcium phosphates are known for their osteoconductivity [198]. With a simple soaking technique, we demonstrated that high amount of peptide (9 μg/cm^2 on the 7 μm coating) can be loaded onto the CaP coating. The peptide-loaded samples did not have significant effect on the activity of the osteoblast-like cells (Fig. 4.9), but could effectively kill both *S. aureus* and *P. aeruginosa* within 30 min (Fig. 4.6). Interestingly, the antimicrobial activity of CaP-Tet213 was maintained following extended incubation (24 h) with *P. aeruginosa*. Since MX226 peptide has been reported as the most advanced AMP to show statistically significant clinical effects to date [267] and due to a few study performed on delivery of hLF1-11 AMP from CaP coatings [268-270], these two AMPs were selected to be compared with Tet213. In this study we also demonstrated that this CaP

coating was a better carrier for the Tet213 antimicrobial peptide than for MX226, hLF1-11 or tobramycin in terms of bactericidal efficiency (Fig. 4.8). One limitation of current study was the relatively short term *in vitro* tests. Longer duration of *in vitro* tests and especially *in vivo* animal study would be needed to verify such an antimicrobial effect.

Calcium phosphates have been extensively studied for delivering growth factors and drugs for the purpose of enhancing bone growth [166, 260, 271]. Delivering traditional antibiotics through calcium phosphate-coated implants has also been actively studied [134, 157, 166]. However, there are few reports if any on the delivery of cationic antimicrobial peptides through calcium phosphate coatings. Relevant studies were done by Stallmann *et al.*, who loaded the 11-mer antimicrobial peptide hLF1-11 (GRRRRSVQWCA, which consists of N-terminal amino acids 1–11 of human lactoferrin) onto calcium phosphate bone cements for potential application in osteomyelitis [267-269]. When mixed into the calcium cements, the peptide showed slow release both *in vitro* and *in vivo* [268, 270]. When loaded onto CaP granules through soaking, it was commented that the peptide had burst release only [269], indicating a weak interaction between the peptide and the CaP granules. In our current study, the high amount of peptide was measured after 10 min of water rinse. The samples killed all the *P. aeruginosa* in 30 min. Subsequent wash and repeated testing of the same samples showed mild bactericidal properties (Fig. 4.7). Our results indicated a relatively strong interaction between the studied peptide (Tet213) and CaP coating. Both the morphological factor and the chemical factor of the coating could contribute to the efficient loading of the peptide. Firstly, the CaP coating processed by the electrolytic deposition technique is microscopically porous (Fig. 4.3). This created large surface area for peptide-CaP interaction. Secondly, the antimicrobial peptide (Tet213) has an isoelectric point of 11.72 with five positively charged residues (Arg and Lys),

which makes it a highly positive peptide at working pH (7.4). The positively charged side groups in the cationic antimicrobial peptide may electrostatically interact with the negatively charged phosphate group in the CaP crystals. The AMP in this study has two adjacent Arg residues in its sequence. This may further enhance the electrostatic interaction. In protein–protein interaction, it has been reported that the electrostatic interactions between the guanidinium groups in a basic epitope containing adjacent Arg residues and the phosphate groups in acidic epitopes can possess "covalent-like" stability [272]. It has also been well known that some short peptides could selectively bind to solid surfaces [229]. One of the identified short peptide sequence (SVSVGMKPSPRPGGGK) reported by Weiger *et al.* for HA is also cationic [226]. It is not clear whether similar interaction mechanisms are also involved in our systems.

4.4 CONCLUSIONS

Calcium phosphate coating was successfully formed on titanium substrate by electrolytic deposition. The as-processed CaP coating was mainly octacalcium phosphate. This micro-porous CaP coating has high drug loading efficiency for the antimicrobial peptide, with 9 μg/cm^2 of peptide on a 7 μm thick coating. The peptide-loaded CaP coating on titanium surface has no cytotoxicity with osteoblast-like cells. It could kill both Gram-positive (*S. aureus*) and Gram-negative (*P. aeruginosa*) bacteria within 30 min *in vitro*. The local delivery of antimicrobial peptides through implant surfaces could be a potential solution for early stage peri-implant infection.

CHAPTER 5 DRUG RELEASE AND BONE GROWTH STUDIES OF ANTIMICROBIAL PEPTIDE-LOADED CALCIUM PHOSPHATE COATING ON TITANIUM[2]

The demand for artificial joints is constantly rising due to the increasing age of our populations with increasing prevalence of osteoarthritis, failure of previously implanted components and the steady increase of trauma patients requiring joint replacement surgery [128, 273]. Implant-associated infection as the major cause of implant revision has been a serious challenge to joint arthroplasty [5, 7]. Antibacterial coatings have attracted wide attention as a technique of preventing implant-associated infections at the site of implant. In chapter four, an antimicrobial coating was developed by loading a novel antimicrobial agent (AMP) onto calcium phosphate coating. One challenge facing the antibacterial coatings is to inhibit bacteria growth on the implant surface without impairing osteointegration. [26, 172, 274]. The purpose of this chapter is to investigate the *in vitro* drug release, antimicrobial performance, and cytotoxicity, as well as the *in vivo* bone growth of an antimicrobial peptide loaded into calcium phosphate coated Ti implants in a rabbit model. In this study, we first compared two antimicrobial peptides, HHC36 (KRWWKWWRR) (Fig. 5.1) and its cysteinylated form Tet213, in terms of their *in vitro* biocompatibility, cytotoxicity, and bactericidal activity. In the second stage, we studied the effect of AMP on bone growth in a rabbit model using CaP coated-Ti implants.

[2] A version of Chapter 5 has been published. **Kazemzadeh-Narbat M**, Noordin S, Masri BA, Garbuz DS, Duncan CP, Hancock REW. Drug release and bone growth studies of antimicrobial peptide-loaded calcium phosphate coating on titanium. Journal of Biomedical Materials Research Part B: Applied Biomaterials, 2012.

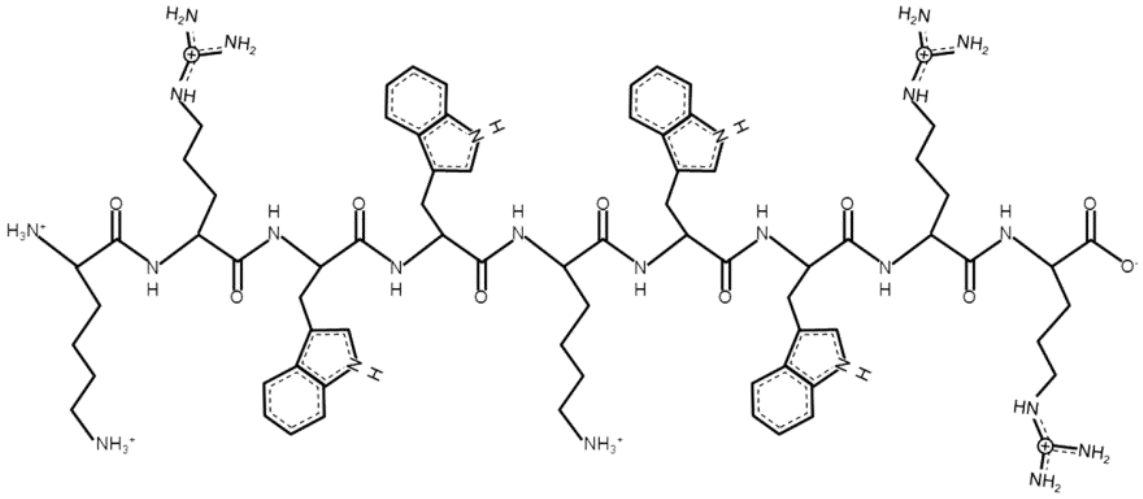

Figure 5.1. Molecular structure of HHC36 based on ExPASy portal (http://www.expasy.org).

5.1 MATERIALS AND METHODS

5.1.1 Implants and CaP coating deposition

Commercially pure titanium plates (Goodfellow, USA) of dimensions 10 × 10 × 0.5 mm^3 were prepared for *in vitro* tests. All Ti specimens were ground using a 320 grit sandpaper followed by thorough cleaning with alkaline detergent (Fisher Scientific SF105), ultrasonically washing with acetone, 70% ethanol, and distilled water for 10 min, respectively, to remove any residuals, and grease. The cleaned samples were then chemically etched by 2% hydrofluoric acid (Fisher Scientific) for 1 min and ultrasonically washed in distilled water followed by air-drying at room temperature. The calcium phosphate coating applied onto Ti surfaces was applied using our previously reported electrolyte deposition (ELD) technique [259, 260, 275]. Briefly, a two-electrode base ELD (Ti as cathode and platinum as anode) with electrode working distance of 3 cm was employed for CaP deposition. The electrolyte composed of 5.25 mM of $Ca(NO_3)_2$ (Sigma Aldrich), 10.5 mM of $NH_4H_2PO_4$ (Fisher Scientific), and 150 mM of NaCl (Fisher

Scientific). After increasing the pH of electrolyte to 5.30 ± 0.05 by adding drop wise NaOH (Fisher Scientific) solution, a DC voltage of 2.5 V was conducted between the electrodes for 3 h at room temperature. Based on our previous study the CaP coating thus processed was a uniform micro-porous plate-like CaP with increased pore and crystal sizes from the bottom to the surface. The coating consisted of octacalcium phosphate (OCP) with a thickness of about 7 μm, and adhered to the Ti substrate without cracks (Fig. 5.2) [275].

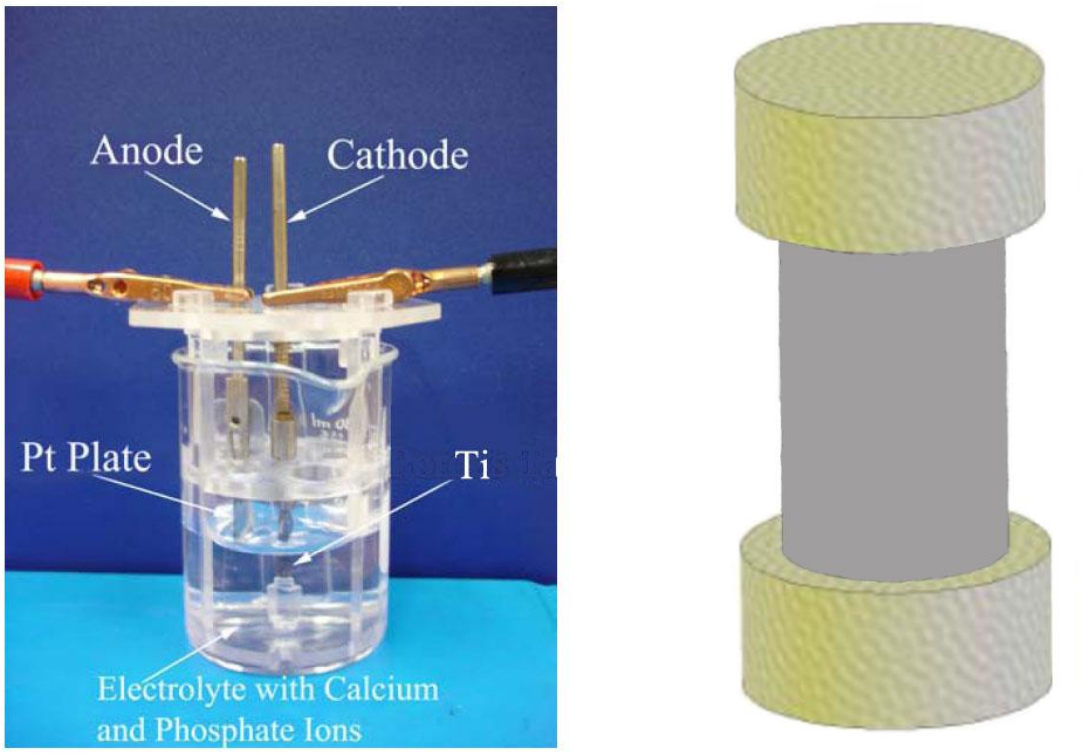

Figure 5.2. Schematic of a two-electrode base ELD (Ti as cathode and platinum as anode) (left), a gap model was designed by capping both ends of implant cylinders coated with CaP with polymethylmethacrylate (PMMA) bone cement (right).

For the *in vivo* bone growth study, commercially pure titanium rods (Goodfellow, USA) were machined into cylindrical implants, each 3.18 mm in diameter and 8 mm long. Three groups of cylindrical implants were used in the animal experiment, etched Ti, CaP-coated Ti (CaP), and CaP-coated Ti loaded with AMP (CaP-AMP). To investigate bone growth, a gap model was designed by capping both ends of implant cylinders with polymethylmethacrylate (PMMA) bone cement. Each cap had an outer diameter of 4.37 mm, height of 2 mm, which made the total length of implant including caps 9 mm. This model provided a gap space of 0.6 mm and a gap volume of 35.3 mm^3 (Fig. 5.3) [260]. The introduction of a gap was based on an animal model previously developed in the lab [260]. The idea was to simulate a real situation in implant surgery. Such a model also made it easier to characterize new bone growth.

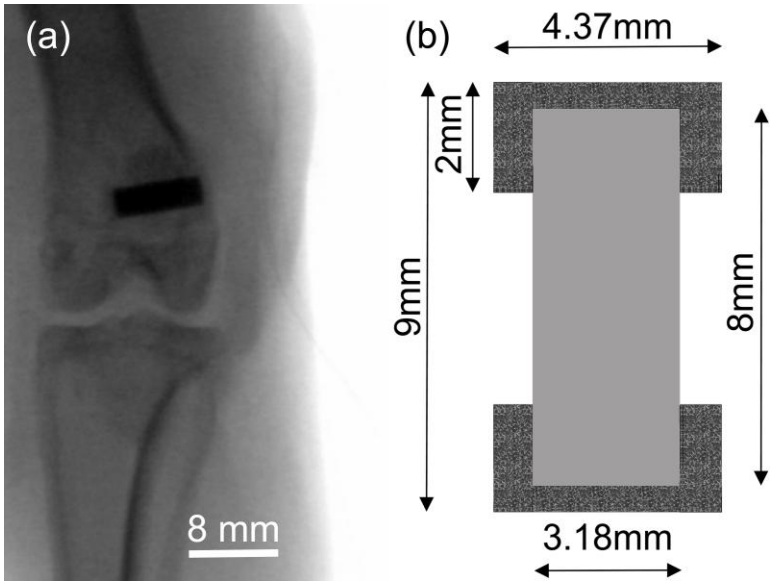

Figure 5.3. (a) X-ray image showing implant position on lateral aspect of the distal portion of the rabbit femur. (b) A schematic diagram of gap model designed for bone growth study. The Ti rod is capped by PMMA bone cement creating a 0.6 mm gap distance between the Ti implant and the host bone.

5.1.2 AMP loading on CaP

On the basis of the most recent quantitative structure-activity relationships (QSAR) analysis, short cationic AMPs with high antimicrobial activity, namely HHC36 (KRWWKWWRR) and its cysteinylated derivative Tet213 (KRWWKWWRRC), were screened [179, 261]. To select the best AMP for bone growth investigation, antimicrobial testing, and the MTT cytotoxicity assay using MG-63 osteoblast-like were performed.

To load the HHC36 into CaP coating, a peptide solution with a concentration of 1 mg/mL was prepared by dissolving 1 mg of HHC36 in 1 mL of simple phosphate solution containing 50 mM of NaH_2PO_4 (Calbiochem) in distilled water. The buffer pH was adjusted to 7.5 by adding 0.1M NaOH prior to addition of AMP. The CaP-coated Ti specimens were immersed into peptide solution separately for 1 h and slowly shaken at room temperature. To remove the residual peptide samples were then washed three times for 1 min with phosphate buffer. The implants were then gently air-dried and stored in safe dry containers.

5.1.3 AMP detection and release experiment

The total AMP concentration loaded on CaP was measured by UV/Vis spectroscopy by recording the absorption peak at 280 nm, which is the characteristic excitation wavelength for tryptophan [275, 276]. The AMP was removed from the CaP coating by ultrasonically dissolving six independent AMP-CaP plate samples with HCl (0.1N) at room temperature for 30 min. A series of standards in the concentration range 2–100 μg/mL of HHC36 in 0.1N HCl were prepared in triplicate to calibrate the system. AMP quantification was then calculated based on the external standard method.

To determine the release profile of AMP from the CaP coating, three CaP-AMP specimens were immersed in 1 mL of PBS (pH 7.4) in a glass vial while gently rotating at 37°C. After 30 min, 90 min, 150 min, 270 min, 1 day, 3 day, and 7 day, 500 μL of PBS was sampled and fresh PBS was replenished to each sample. Each release test was done in triplicate. The samples were stored at -20°C and the AMP cumulative release ratio was calculated by using UV/Vis spectroscopy.

5.1.4 Antimicrobial activity

The antimicrobial effect of CaP-AMP was tested by a survival assay by counting the residual number of colony-forming units (CFU) in triplicate experiments. The specimens were evaluated against *S. aureus* (ATCC 25293) as well as *P. aeruginosa* (H1001:*lux*CDABE) strains. The bacteria strains were grown in Mueller-Hinton agar (MHA; Difco) and subcultured overnight at 37°C incubator under aerobic conditions. After the appearance of colonies, two colonies were harvested from the MHA agar and suspended in Mueller Hinton Broth (MHB; Difco) overnight while shaking in the incubator. The bacteria status in the mid logarithmic phase of grow was determined by suspending 100 μL of each bacteria solution into 5 mL of MHB following incubation at 37°C for 1 h. *P. aeruginosa*, and *S. aureus* bacterial suspensions were diluted by MHB, and adjusted to the final concentration of 10^6 CFU/mL using spectrophotometer. Six CaP-AMP specimens (10 × 10 × 0.5 mm^3) were rinsed with phosphate buffer saline (PBS) three times, then 400 μL of each bacterial suspension was pipette onto two different groups of samples. The bacterial suspension alone was considered as a negative control group. After incubating the samples for 30, 90, 150, and 270 min, the residual bacteria in 10 μL

were spotted on nutrient MHA agar. Corresponding agar plates were incubated at 37°C overnight, and bacterial survival was evaluated by CFU measurement.

5.1.5 Cell viability

The viability of MG-63 osteoblast-like cells derived from human osteosarcoma (ATCC CRL-1427, USA) was studied by measuring the mitochondrial dehydrogenase activity using a modified MTT (3-(4,5-dimetyl-2-tiazolyl)-2,5-diphenyl-2H-tetrazolium bromide) (Biotium) reduction assay. The cells were cultured in a medium consisting of Dulbecco's Modified Eagle Medium (DMEM, GIBCO), including a minimal essential medium, 10% fetal bovine serum (FBS), and 1% nonessential amino acids (GIBCO). The culture medium was refreshed at 2-day interval and the incubator ambience was maintained at 37°C under 95% humidified atmosphere with 5% CO_2. To evaluate the cytotoxicity level of HHC36 and Tet213, 10^4 cells per sample were cultured with both AMPs. Cells were incubated with different concentrations of AMPs/medium at 37°C and humidified 5% CO_2 in triplicate. Negative controls were assigned to cells cultured in fresh medium and normal conditions with no AMP. After 16 h, 100 µL MTT was dissolved in 1 mL serum free medium, and was added to each well, and were incubated for 4 h. Then the solution was removed and was replaced with 200 µL DMSO (dimethylsulfoxide). After shaking the plates for 15 min, the absorbance was measured at 570 nm, and the reference wavelength of 690 nm on an ELISA microplate reader (Bio-Tek Instruments).

To assess the cytotoxicity of HHC36 on CaP, three groups of samples, Ti, CaP, and CaP-AMP, were investigated in triplicate by the same MTT assay procedure. 10^4 of cell dispersion were seeded on each sample and the cells were allowed to attach to each sample for 2 h before

adding the culture medium. Fresh medium was replaced every 2 days and MTT assay was carried out after 1, 2, and 5 days.

5.1.6 Cell attachment and morphology

The morphology and adherence of cells were investigated by culturing the MG-63 cells on specimens. By incubating the confluent cells with 0.25% trypsin-0.1% ethylenediaminetetraacetic acid (trypsin/EDTA) solution for 5 min, adequate number of cells was detached from culture flask, and centrifuged at 400*g* for 10 min to be used for each experiment.

For cell adhesion experiments, samples were first washed with 70% ethanol, and PBS, respectively, three times each. Then, MG-63 cells were seeded on Ti, CaP, and CaP-AMP six samples of each at a density of 5×10^5 cells per sample. After 4 h the specimens were rinsed with PBS to remove nonadherent cells and samples were digested with 0.5 mL of trypsin/EDTA for 10 min in incubator. Subsequently, a 0.5 mL culture medium was added to each sample to stop the trypsinization, and the cell quantity was counted by hematocytometer using a microscope. Cell attachment efficiency was presented by the percentage of number of attached cells divided by number of seeded cells.

To study the cell morphology and proliferation, specimens were sterilized and MG-63 cells were cultured identical as described. Then, 10^4 cells per sample was used after 4 h and 1-day incubation for fluorescence analysis. The specimens were washed with PBS, and fixed using 4% paraformaldehyde. The fixed cells were rinsed with PBS, and soaked into permeabilization buffer for 20 min at room temperature. Subsequently, the cytoskeletal filaments of cells were

stained using rhodamine-phalloidin F-actin (Invitrogen), and DNA staining was performed by 4′,6-diamidino-2-phenylindole (Invitrogen). The samples were then mounted on μ-slides (ibidi) and analyzed with confocal laser scanning microscopy (FV1000 Olympus).

5.1.7 Surgery and implantation procedure

For *in vivo* rabbit study, a total of 25 adult New Zealand white female rabbits weighting 3.5 to 5 kg were randomly distributed to three groups of implants, Ti (5 rabbits), CaP (10 rabbits), and CaP-AMP (10 rabbits). All rabbits were weighed at regular intervals but no attempt was made to standardize weights. The animals were fed with standard diet and observed on daily basis for signs of pain, infection, weight loss, and wound healing. Fifty cylindrical implants, etched Ti (n = 10), CaP (n = 20), and CaP-AMP (n = 20) were seal-packed and beta-ray sterilized (25 to 27 kGy; Iotron Technologies, Port Coquitlam, British Columbia, Canada). Surgery was performed under sterile conditions and general anesthesia. The animals were positioned supine with their legs shaved and decontaminated with a povidine and 70% alcohol. For implantation, an incision of 3 cm was made using a scalpel blade on the lateral aspect of the distal portion of the femur. The bone was exposed by splitting vastus lateralis. To avoid thermal damage to bone, a 4.37-mm hole was created perpendicular to the distal femoral condyle bilaterally using sequential low speed drilling of growing diameter (1.95, 3.18, and 4.37 mm) with saline irrigation. After verifying the depth of the hole with a gauge, the implants were press-fitted into the hole. The wound was closed in layers using standard techniques. Each rabbit received two identical implants, one on each femur. After six weeks all rabbits were euthanized with intravenous injection of Pentobarbital (2 mg/kg), and the femura were harvested. The

implants' positions in the femurs were examined with a fluoroscope (Fig 5.3a). The animal study protocol was approved by the Animal Care Committee of the University of British Columbia.

5.1.8 Histological processing and evaluation

The harvested femora were cleaned and the implants and the surrounding tissues were fixed and stored in 10% formalin solution before histological processing. All specimens were then dehydrated in a graded series of ethanol washings (70–100%), infiltrated, and embedded in epoxy resin (Spurr; Canemco, Canton de Gore, Quebec, Canada) according to standard histological procedure [278]. After polymerization the samples were sectioned longitudinally in three parallel course slices, 200, 850, and 1500 μm deep from implant surface, with each slice roughly perpendicular to the long axis of the femur. Each section was ground, polished, and sputtered with gold-palladium alloy, and examined with backscattered electron microscope (BSE) at 20 kV, 25 times magnification, and 27 mm of working distance, (S3000N; Hitachi, Tokyo, Japan). To create the final image, three images taken from each sample were merged together (see appendix B).

Bone growth in the gap region and on the implant surface was quantified by analyzing the BSE images using image analysis software (Clemex Vision PE 3.5; Clemex Technologies, Longueuil, Quebec, Canada). Four distinct materials in each image (titanium, bone cement caps, new grown bone, and epoxy) were discriminated in grayscale spectrum. The analysis provided quantitative data on the total gap and, total area of bone-gap filling (new bone formation in the gap created by caps) and bone on-growth (new bone formation in direct contact on the implant surface) (see appendix B).

5.1.9 Statistics

"Primer of Biostatistics" software was used to assess the difference between the testing groups using one-way ANOVA (analysis of variance). A significant difference was considered when *p*-value was 0.05 or less, indicating 95% confidence limit.

5.2 RESULTS

5.2.1 Cytotoxicity

The MTT absorbance values reporting on the cytotoxicity of different concentrations of HHC36 and Tet213 AMPs revealed that there was a significant difference between two peptides in terms of retention of cell metabolic activity. While HHC36 showed cytotoxicity at concentrations greater than 200 μg/mL ($p = 0.08$ at 200 μg/mL, and $p = 0.01$ at 300 μg/mL), Tet213 exhibited higher cytotoxicity with significant effects at concentrations greater than 50 μg/mL ($p = 0.06$ at 50 μg/mL, and $p < 0.01$ at 75 μg/mL) compared with the negative control (Fig. 5.4a). Therefore subsequent experiments employed HHC36 as the coating AMP.

In another MTT assay carried out on CaP-HHC36 using Ti and CaP (with no AMP loaded) as negative controls, it was observed that the cytocompatibility of HHC36 loaded specimens didn't show any significant difference compared to controls ($p > 0.05$) (Fig. 5.4b).

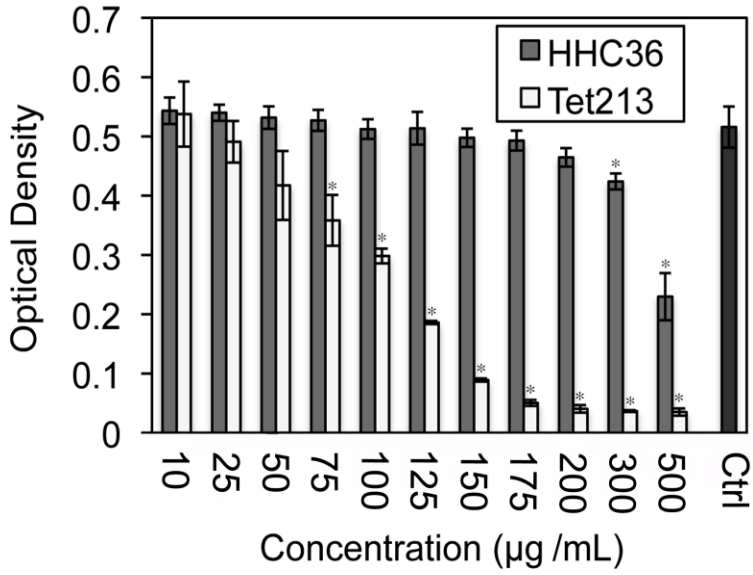

(a)

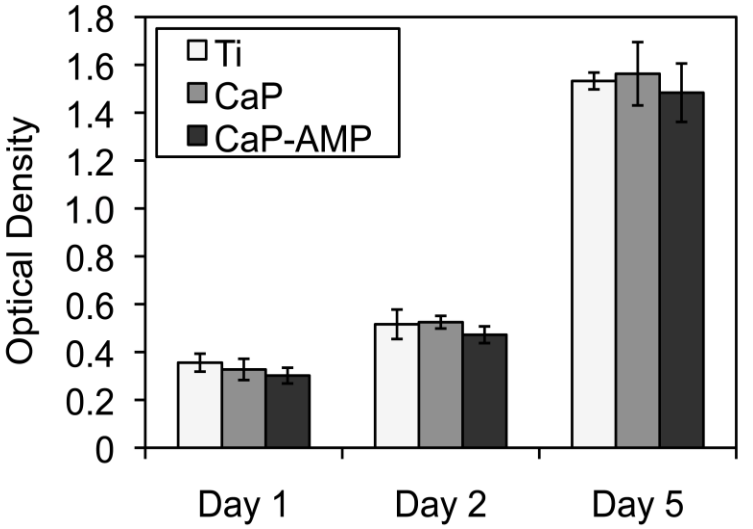

(b)

Figure 5.4. (a) The MTT assay of MG-63 cells cultured with various concentrations of HHC36 and Tet213 alone. Significant differences were observed in the cytotoxicity of the two AMPs. While HHC36 showed cytotoxicity at concentrations of 300 µg/mL and above (p = 0.01 at 300 µg/mL), the Tet213 exhibited cytotoxicity at relatively lower concentrations µg/mL ($p < 0.01$ at 75 µg/mL) compared with the negative control. (b) No increased cytotoxicity was observed on CaP-HHC36 samples compared to controls ($p > 0.05$). The higher level at day 5 was due to increased growth of cells after 5 days.

5.2.2 AMP loading and release

The tryptophan absorbance peak at 280 nm in the UV/Vis spectra was used for AMP quantification. Tests on standard solutions showed excellent linear relationships between peak intensity and AMP concentration in the ranges of 2–100 μg/mL (R^2 =0.999) (see appendix C). Based on this calibration, the amount of AMP loaded on CaP samples was 34.7 ± 4.2 μg/cm^2.

Fig. 5.5 shows the amount of AMP eluted from CaP-coated Ti samples over a 7-day period. The results indicate that 71.2% of AMP was eluted in the first 30 min; the number reached 84.3% in 150 min and 90.8% after 1-day release. This high release rate at the early time points was followed by a slow and steady release for days (Fig. 5.5). After 7 days of this experiment, intact coatings were still observed on the Ti surfaces.

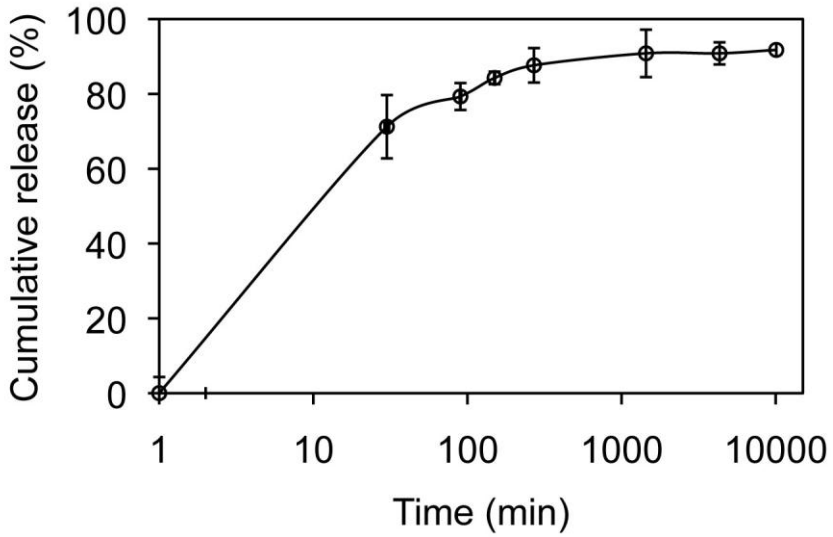

Figure 5.5. The cumulative in vitro release of HHC36 from CaP coating in PBS after 30 min, 90 min, 150 min, 270 min, 1 day, 3 day, and 7 day (n = 3). Error bars represent the means ± standard deviation. Quantification of total AMP concentration loaded on CaP showed (34.7 ± 4.2 μg/cm^2) using UV/Vis spectroscopy at 280 nm based on the use of external standards (n = 6)

5.2.3 Antimicrobial activity

The antimicrobial activities of CaP-AMP against *S. aureus* and *P. aeruginosa* are shown in Fig. 5.6. The negative controls in the assay contained the same quantity of bacteria incubated in fresh MHB under the same condition without AMPs. The results illustrated that CaP-AMP was able to kill 100% bacteria of both strains in less than 150 min, while bacteria colonies in controls grew by more than a hundred fold. If we assume 100% release of peptide in the antimicrobial assay, the maximum concentration of AMP in 400 μL of bacterial suspension would be ~174 μg/mL.

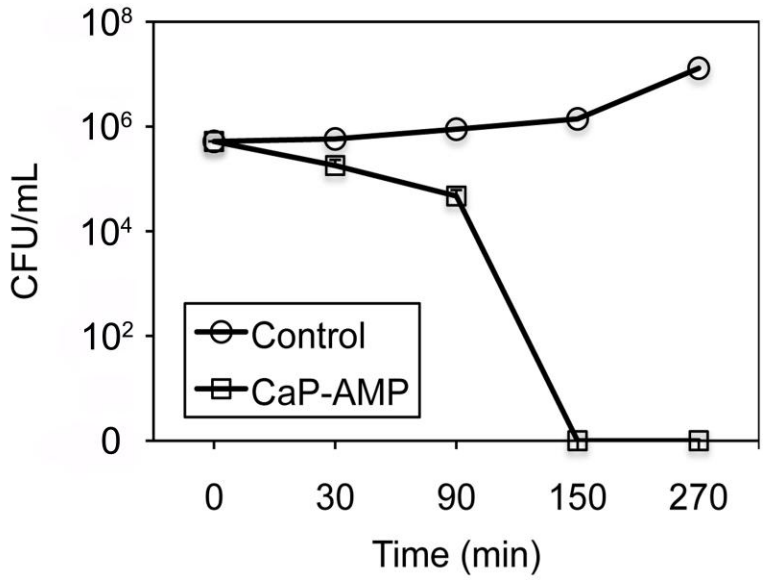

(a)

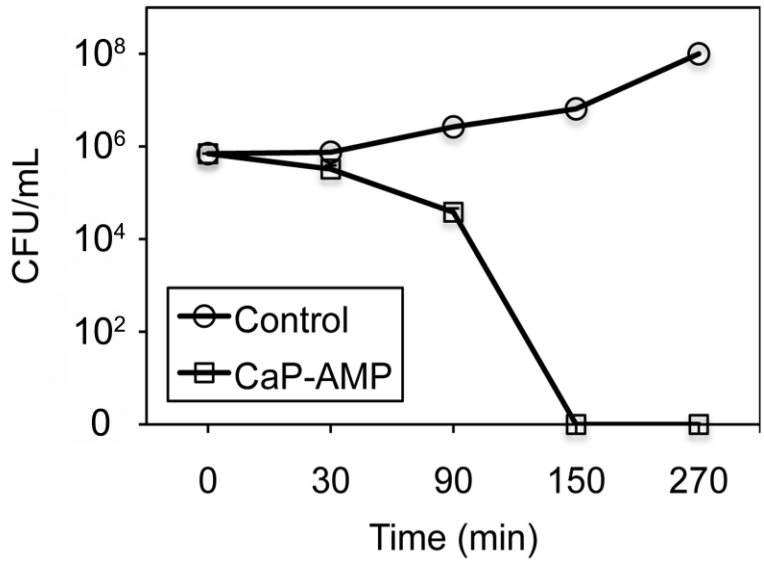

(b)

Figure 5.6. Antimicrobial activity of the CaP-AMP (HHC36) samples against (a) *S. aureus*, (b) *P. aeruginosa*. The specimens CaP-AMP were able to entirely kill both strains in less than 150 min.

5.2.4 MG-63 osteoblast-like cell attachment and morphology

The number of attached MG-63 cells on Ti, CaP, and CaP-AMP were measured after 4 h of culturing (Fig. 5.7). The efficiency of adhered cells on Ti, CaP, and CaP-AMP were calculated to be 55.8, 73.3, and 77.6%, respectively, indicating a significant increase ($p < 0.01$) of cell attachment on CaP and CaP-AMP.

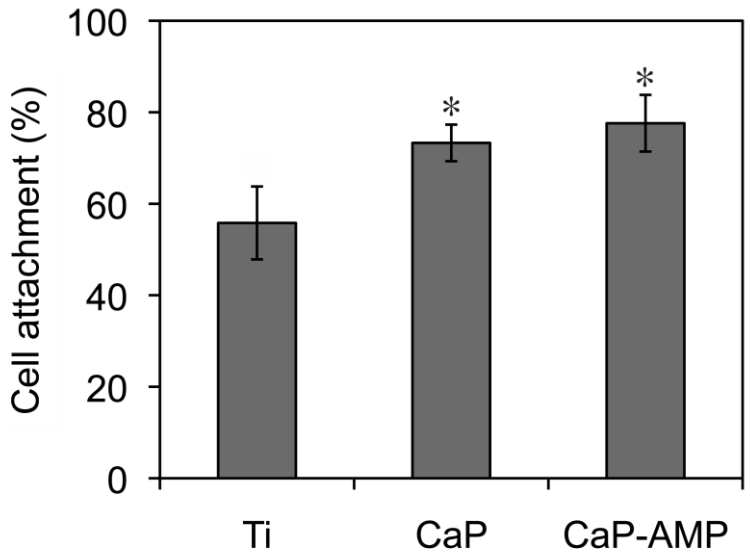

Figure 5.7. Cell attachment efficiency of specimens after seeding 5×10^5 MG-63/sample (n = 6) after 4 h. The efficiency of adhered cells on Ti, CaP, and CaP-AMP (HHC-36) were calculated to be 55.8, 73.3, and 77.6%, respectively. Asterisk indicates significant difference between cell attachment efficiency on Ti and other groups ($p < 0.01$).

The morphology of MG-63 cells was evaluated by confocal laser scanning microscopy. During the first 4 h, active cells spread on all substrates (Fig. 5.8a–c). After 1 day, cells spread and extensively covered the surface of the CaP and CaP-AMP samples, while fewer cells were observed on Ti samples (Fig. 5.8d–f). The stretching of cells on the CaP-AMP samples indicated proliferation of cells (Fig. 5.8e,f).

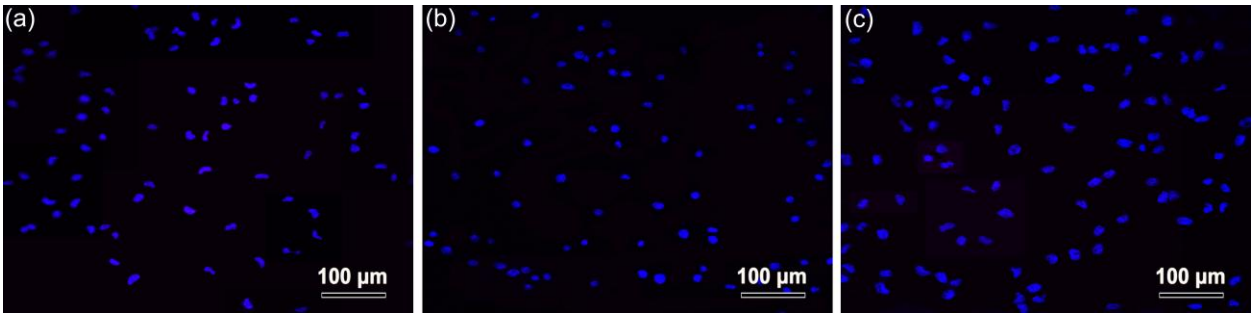

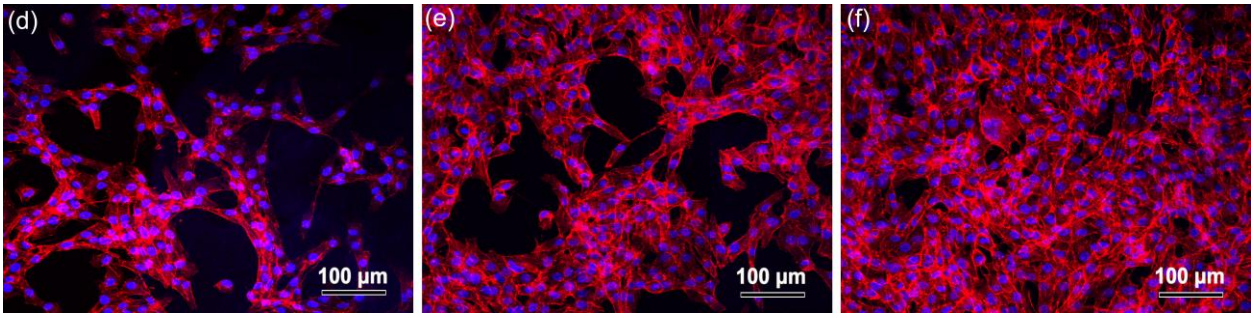

Figure 5.8. (a) Confocal laser scanning of cells cultured on (a) Ti, (b) CaP-Tet213, and (c) CaP-HHC36 after 4 h, showing the distribution and adherence of MG-63 cells. Confocal laser scanning of cells cultured on (d) Ti, (e) CaP-Tet213, and (f) CaP-HHC36 after 1 day, well-defined presence of stress fibers implies the firm attachment of cells, sheet-like proliferation of cells, and distribution of focal contacts on the coating and between cells on CaP-AMP coating. Blue and red colors represent DNA and F-actin staining.

5.2.5 Bone growth analysis

After surgery, one rabbit from each group was excluded from the histological study due to either improper implantation or weight loss exceeding 20%. The remaining rabbits had no signs of severe reaction, infection or other abnormalities determined by clinical signs such as persisting local pain, erythema, edema, wound healing disturbance, large hematoma and fever. Backscattered electron microscopy confirmed that newly formed bone had grown into the gap region in all three groups of implants (Fig. 5.9). The bone growth results are summarized in Table 5-1 and Fig. 5.10. The average bone growth slightly increased from Ti, CaP-coated Ti (CaP), to AMP-loaded CaP (CaP-AMP), but no significant differences ($p > 0.05$) were observed among the groups. However, the contact length between bone and the implant showed a significant difference ($p = 0.01$) between the uncoated Ti and the other two coated surfaces, indicating considerable bone on-growth on CaP (~54%) and, CaP-AMP (~60%) compared with Ti (~ 36%) surfaces. Compared with the CaP group, the group treated with the AMP had a slight increase in the percentage of bone contact length (by ~6%). However this increase was not significant ($p = 0.13$) (Fig. 5.10).

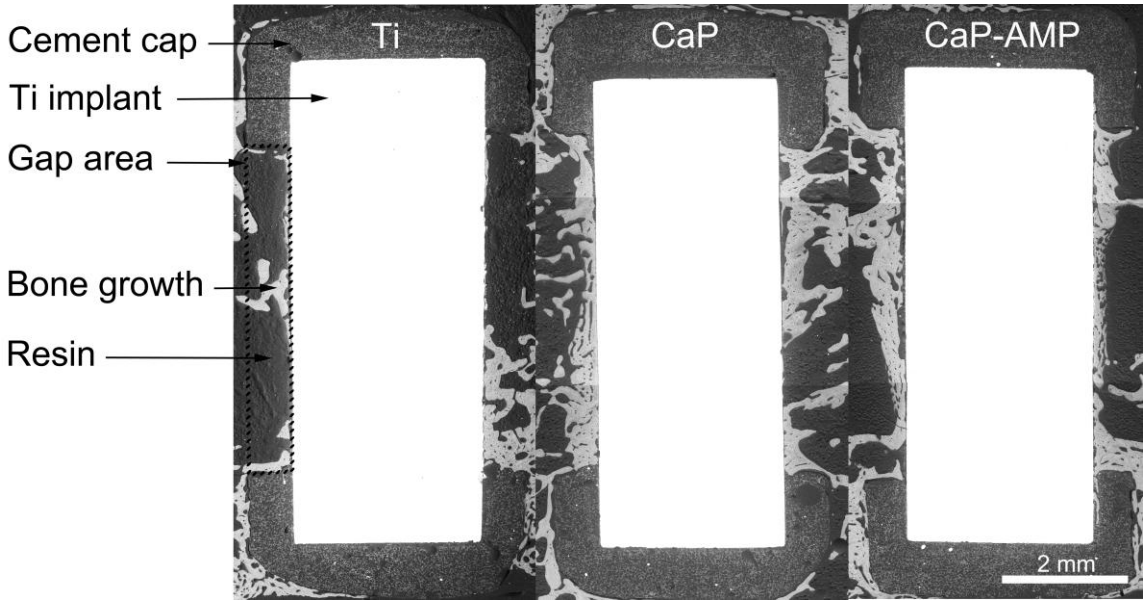

Figure 5.9. Representative BSE images of the implant surfaces of each group displaying bone growth expanding into gap. Dotted line shows the bone growth region and magnified images exhibit random bone on-growth on each interface.

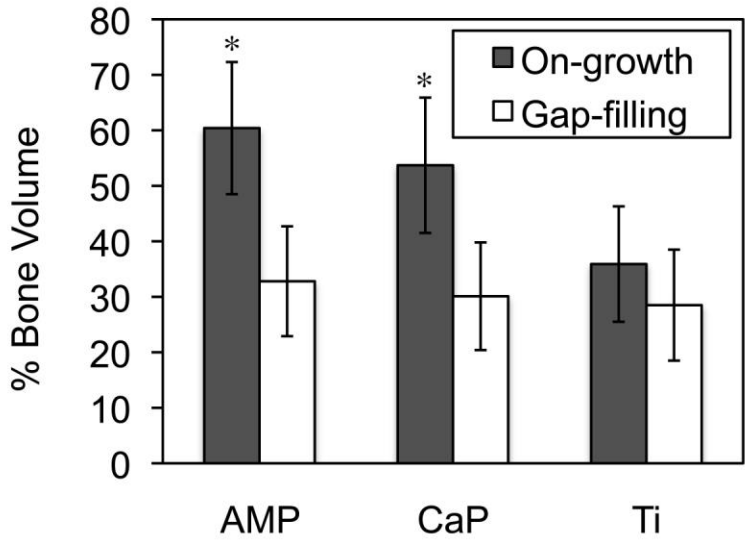

Figure 5.10. Total gap filling and bone on-growth (mean values and standard deviations) of three sections. No significant statistical difference was observed in terms of gap-filling between three groups. Bone on-growth values however revealed different results. Asterisk indicates a significant difference (p = 0.01) between Ti and other groups, indicating considerable contact bone growth on CaP and, CaP-AMP (HHC36) versus Ti samples. Compared with the CaP group, the group treated with the AMP had a relative increase in the percentage of the length of the implant that was in contact with new bone. However this increase was not significant (p = 0.13).

Table 5-1. Histomorphometric Bone (a) Gap Filling, and (b) Bone On-Growth data are expressed as Mean ± Standard Deviation. Sections 1, 2 and 3 were in three parallel course slices, with 200, 850 and 1500 μm deep from the tangent surface of implants, respectively.

Implant	**Bone Gap Filling (%)**	**Section 1**	**Section 2**	**Section 3**
Ti (*n*=8)	28.5 ± 10.0	28.7 ± 11.8	29.1 ± 10.1	27.7 ± 11.0
CaP (*n*=18)	30.1 ± 9.7	28.1 ± 8.5	30.8 ± 10.1	31.3 ± 11.0
CaP-HHC36 (*n*=18)	32.8 ± 9.9	33.3 ± 11.6	32.6 ± 9.2	32.3 ± 10.1

(a)

Implant	**Bone Gap Filling (%)**	**Section 1**	**Section 2**	**Section 3**
Ti (*n*=8)	35.9 ± 10.4	32.5 ± 14.9	42.6 ± 8.8	32.7 ± 8.8
CaP (*n*=18)	53.7 ± 12.2	54.5 ± 12.9	55.5 ± 13.0	51.0 ± 13.2
CaP-HHC36 (*n*=18)	60.4 ± 11.9	60.7 ± 14.7	63.8 ± 9.4	56.6 ± 14.6

(b)

5.3 DISCUSSION

One concern regarding the local delivery of antibiotics in orthopedics is the relative inhibition of osteointegration [22]. High doses of antibiotics often impair cell viability and osteogenic activity [23]. Therefore, the development and selection of antimicrobial agents for local delivery onto orthopedic implants should consider osteoconductivity. Results from the current study demonstrate that locally delivering antimicrobial peptides using calcium phosphate coatings can effectively kill bacteria *in vitro*, but does not impair bone growth. In fact, local delivery of HHC36 led to a moderate enhancement in bone growth, although the increase was

not significant. In our study, the *in vivo* test has been used to investigate the bone growth in the presence of AMP coating and does not involve infection study.

Extensive effort has been made to identify the AMPs' antimicrobial mechanisms of surface associated AMPs [27, 169, 173, 183, 184, 268, 279-286]. Recent studies indicated that the killing mechanism of AMPs is based on the high density of polycationic charges in vicinity of the surface, which would initiate an electrostatic interaction with polyanionic outer layer of microbes. The high local concentration of AMPs would then displace positively charged ions, leading to membrane disruption [27, 287]. The ability of AMPs to selectively interact with the bacterial cells rather than the mammalian cells makes them highly antimicrobial with low toxicity for host cells. The major factor that contributes to the selectivity property of AMPs is the cationic property. The surface of the bacterial membranes is more negatively charged than mammalian cells. This will lead to higher affinity of AMPs for bacterial surfaces. Moreover, mammalian cell membranes contain high amounts of cholesterol, which is absent in bacteria cells, as membrane stabilizing agents and inhibitor of AMP activites [183, 184]. Nevertheless, different AMPs vary in their cytotoxicity towards host cells [183, 184]. For the two potent antimicrobial peptides compared in this study, HHC36 and Tet213, despite their shared peptide sequence, the addition of one cysteine in Tet213 substantially lowered the minimal osteoblast toxicity concentrations from 300 to 75 μg/mL (Fig. 5.4a).

In this work, the substantial amount of HHC36 (34.7± 4.2 $\mu g/cm^2$) loaded on CaP coating can be attributed to the affinity between the positively charged side groups of HHC36 and negatively charged phosphate groups in the CaP and the porous structure of the coating. HHC36 with the sequence of KRWWKWWRR-NH_2 has a cationic charge of +5, and a theoretical

isoelectric point of 12.31. Such a high IE point makes HHC36 highly positive at working pH (7.4), and provides numerous opportunities for positively charged Arg and Lys residues to interact with CaP. According to Amina *et al.*, the presence of two adjacent basic residues (Arg-Arg, in our case) might create a "covalent-like" stability with phosphate under the right electrostatic conditions [272]. This explanation however is not entirely compatible with the rapid initial release kinetics of the peptide from CaP surfaces although it may help to explain the subsequent slow release.

An ideal implant related infection treating method would locally release high concentration of antibiotic initially followed by an effective long-term release, while maintaining osteointegration at the same time [169]. In this study, following the initial burst stage, the coating released 71% of AMP in the first 30 min and 90% within 24 h (Fig. 5.5). HHC36 has a very low minimal inhibitory concentration (MIC) of 1.4 to 2.9 μM against *S. aureus* (MDR) and 0.7 to 5.7 μM against *P. aeruginosa* (MDR), with the half maximal inhibitory concentration (IC_{50}) value of 0.13 [179, 261]. The total AMP loaded on to each implant is calculated to be ~28 μg. If we assume the entire AMP is released to the trabecular bone region that is 5–100 times of the gap volume, the concentration of AMP would be 106.6–5.3 μM. Therefore, the local AMP release, even though relatively quick, should enable elimination of a significant number of bacteria introduced to the surgical site in the first day. Since current animal study did not involve an infection model, the *in vivo* efficacy of the AMP loaded implants is to be confirmed.

To date there have been few reports on *in vivo* bone growth onto antimicrobial peptide loaded orthopedic implants. Most of studies on implant associated antimicrobial agents have focused on conventional antibiotic delivery systems especially through bone cement [280-282].

A relevant report investigated the *in vivo* release of the antimicrobial peptide hLF1-11 from calcium phosphate cement [268]. Despite the initial burst release of this AMP, it was concluded that hLF1-11 could be considered as a prophylactic agent for osteomyelitis treatment. No inflammation or necrosis signs were observed in bone grown into the cement [268, 283]. In our study, the backscattered electron microscopy study of the new bone grown on the CaP-AMP implants showed normal bone structure with no distinguishable differences between CaP-AMP and CaP controls. Assuming 100% release of the AMP into the gap region only (35.3 $mm^3$of volume), the local peptide concentration would be 793 μg/mL, which is higher than the cytotoxicity concentration (200 μg/mL). Nevertheless, *in vivo* bone growth study demonstrated the calculated high AMP concentration does not lead to impaired osteoconductivity. One possible explanation is the dynamic fluid flow in and out of the gap region. The observed slightly higher total new bone formation on CaP-AMP than CaP implants in Table 5-1 may imply a potential role of AMP (HHC36) in stimulating bone growth *in vivo*. In this regard synthetic cationic peptides including many AMPs have the ability to modulate innate immunity in host cells including stimulation of wound healing, and neutralization of some characteristics of inflammation such as endotoxemia [173, 284].

It is well understood that OCP plate-like coating improves osteoblast adhesion, spreading and proliferation by enhancing the focal contacts or selectively adsorption of proteins [285, 286]. Our *in vitro* cell attachment and proliferation test showed that the integration of HHC36 into the OCP coating did not inhibit the cell attachment and proliferation. The extensive bone on-growth on CaP-AMP and CaP surfaces in the animal experiment also confirmed a positive bone response to the combination of AMP and CaP coating (Fig. 5.9). This is consistent with the observation that the AMP concentration on the CaP coating (~70 μg per sample/1 mL culture

media), was lower than the minimal cytotoxic concentration of HHC36 (<200 μg/mL) (Fig. 5.4a). The observation of adhering MG-63 cells by fluorescent microscopy after 4 h of incubation (Fig. 8a–c), showed that cells attached, and strongly bonded to the substrate on coating. The even distribution of stress fibers after 1 day implied firm attachment and might be an evidence for lower motility of cells (Fig. 8e,f). It could be seen in figure. 8e,f that in contrast to uncoated Ti surface, the cells in mitosis state reached confluency covering almost all the surface on both samples treated with AMP, indicating cell proliferation.

5.4 CONCLUSIONS

This study shows that osteoconductive OCP coating loaded with HHC36 AMP has the potential to serve as an antimicrobial coating while maintaining osteointegration. *In vitro* tests concluded that this AMP-CaP coating can effectively kill *S. aureus,* and *P. aeruginosa* bacteria without negatively affecting MG-63 osteoblast like cells. Loading of AMP HHC36 did not impair *in vivo* bone growth onto the implants. There was *a s*ignificant bone on-growth on CaP-AMP as compared with the negative control. The ELD calcium phosphate coating, and the simplicity of AMP loading provide substantial advantages for this antimicrobial coating.

CHAPTER 6 MULTILAYERED COATED TITANIUM FOR CONTROLLED RELEASE OF ANTIMICROBIAL PEPTIDES [3]

6.1 INTRODUCTION

As discussed in previous chapters, the formation of a bacterial surface biofilm and compromised immunity at the implant/tissue interface may lead to persistent infections on and around titanium implants. This infection is usually difficult to treat and in most cases, replacement of a prosthesis is the only remedy [3-5]. The suggested therapy is localized delivery of antimicrobial agents with time-effective handling of infection, while potentially eliminating problems associated with systemic administration [13, 14]. In chapters four and five, we examined *in vitro* and *in vivo* feasibility of using micro-porous calcium phosphate [275, 288] on Ti surfaces as carriers to deliver HHC36, one of the most potent broad-spectrum antimicrobial peptides (AMP).This strategy offered high initial release of HHC36 for early stage peri-implant infection, and loaded HHC36 on CaP coated Ti didn't impair bone growth [236, 275, 288]. The main objective of this chapter was to develop multilayer thin films on Ti implant in order to control the prolonged AMP release.

Extensive research has been explored in modification of Ti surfaces by coating, chemical modification and nano-structuring to improve bone integration, and antibacterial activities on Ti implants [164, 289-291]. Calcium phosphate coatings have been broadly used as a carrier for delivering growth factors and drugs for orthopaedic implants due to their high osteoconductivity [188, 292]. Vertically aligned titania nanotube (NT) arrays generated on a Ti surface is another

[3] A version of Chapter 6 is under submission for publication. **Mehdi Kazemzadeh-Narbat**, Benjamin Lai, J N Kizhakkedathu, Robert E W Hancock, Rizhi Wang. Multilayered coated titanium for controlled release of antimicrobial peptides for the prevention of implant-associated infections.

investigated platforms for local drug delivery applications [252, 293-295]. Titania nanotubes with excellent biocompatibility, high surface-to-volume ratio, controllable dimensions, adjustable wettability, and simple processing procedures, are able to carry substantial amount of drugs. Moseke *et al.* showed that the NT samples could be loaded with up to 450% more active agent than the untreated Ti surfaces [296]. TiO_2 nanotubes have been reported to exhibit higher Young's modulus (roughly 4 to 30 GPa in the first 30 nm of indentation) [297], and can accommodate and release more drug [296] than conventional CaP coatings, however on the other hand CaP coatings can enhance bone growth [188, 241, 297]. A recent experiments on antimicrobial coating fabricated via a simple vacuum-assisted physical adsorption of AMP into self-organized TiO_2 nanotube arrays could slightly improve the burst release and provided better mechanical properties [236]. Studies have reported that the annealed titanium nanotubes can load large amount of therapeutic in compare to bare Ti due to high surface-to-volume ratio while maintaining acceptable interfacial mechanical strengths [298]. However, the release profile still could not be adjusted. In short, it was shown that both CaP and NT coatings are promising carriers for HHC36 as an early stage peri-implant infection prevention, however, both suffer from quick release of AMP in limited time.

Although several studies have reported the controlled release of antibiotics [145, 299, 300], very few offered osteoconductive, mechanically robust antimicrobial surface with controlled release. In this study, in order to create a coating that has dual beneficial effects, thin layers of titania NT and CaP coatings were impregnated with AMP. To load the HHC36 into NT, the AMP was dissolved in a low surface tension solvent (ethanol), and forced into NT using vacuum-assisted physical adsorption method. These films were topped with a thin phospholipid film to control the release of AMP based on a bio-mimetic cell membrane. Lipids offer a variety

of applications such as supported membranes like liposomes [301], or non-adhesive coatings for materials with blood contact (Fig. 6.1) [302]. Phospholipid coatings on Ti were reported to exhibit good cytocompatibility, cell adherence and proliferation [303-308]. The variety of the phospholipids in membranes is high and variable from species to species (Table 6-1). Willumeit *et al.* investigated different kinds of phospholipids to facilitate cell-metal interaction, and proposed POPC (palmitoyl-oleoylphosphatidyl-choline), which is naturally present in eukaryotic cell membranes as the least bacteria growth support (81% reduction), and the most suitable platform for bone cell attachment (Fig. 6.1) [309]. POPC has also shown to exhibit clinically acceptable osteointegration [310]. Figure 6.2 introduces various models for lipid biological membranes.

Table 6-1.The phospholipid composition of bacteria and eukaryotic cells (based on [301, 311]).

	PG	PE	CL	PC	SM	PS	Others
Gram negarive E. coli IM	6	82	12	0	0	0	0
Gram positive S. aureus	57	0	43	0	0	0	0
Erythrocyte	0	18	0	20	18	7	37
Mitochondria	0	29	14	38	0	0	19
Cartilage (resting)*	1	15	0	61	6	4	13
Bone (cancellous)*	1	18	0	52	11	6	13

IM = Inner Membrane; PG = Phosphatidyl-glycerole, PE =Phosphatidyl ethanolamine,CL=Cardiolipin, PC=Phosphatidylcholine,SM=Sphingomyelin, PS=Phosphatidyl-serine, *Isolated from tissue [299].

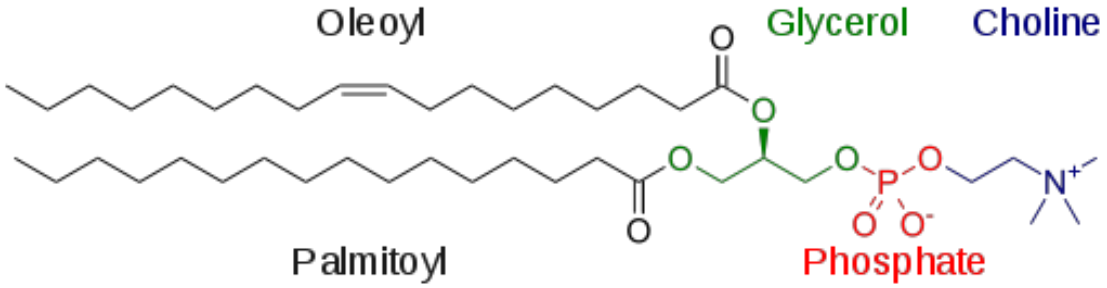

Figure 6.1. Molecular structure of POPC (palmitoyl-oleoylphosphatidyl-choline) with molecular formula $C_{42}H_{82}NO_8P$, percent composition C, 66.37; H, 10.87; N, 1.84; O, 16.84; P, 4.08, and Molar mass of 760.08 g mol^{-1}.

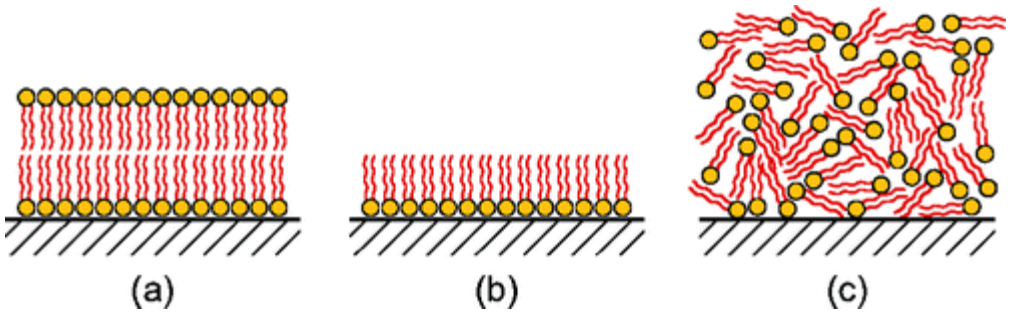

Figure 6.2. different lipid overlayer structures: (a) bilayer, (b) Langmuir−Blodgett monolayer, (c) disordered layer. Reprinted from [311] with permission from Elsevier.

Biocompatibility of coatings has generally been performed through *in vitro* assessment of the interaction of the coatings with recognized cell culture lines. However, they do not adequately address the acceptability of these materials in blood interfacing (composed of a fibrin film containing platelets and red blood cells) which plays a significant role in osteogenesis [50, 313]. Immediately after implantation, the wound site is first occupied by a blood clot. The connective tissue cells, including osteogenic cells, which are not interacting with the implant surface, migrate through the remnants of the clot still attached to the implant surface. In this regard, platelet attachment and degree of activation on implant surface and surrounding fluid are critical steps in initiating osteoconduction. Adhered platelets release multiplicity of growth

factors and cytokines which promote migration of osteogenic cells to implant surface [47, 314, 315]. Therefore, it is also the purpose of this chapter to address the hemocompatibility of the Ti-NT-CaP-POPC20 multilayer coating system, using platelet attachment, activation, and hemolysis studies.

6.2 MATERIALS AND METHODS

6.2.1 Fabrication of TiO_2 nanotubes on titanium surface

The commercially pure Ti foils (0.1 mm, 99.6% purity, Goodfellow) were sonicated with acetone, ethanol, distilled water and air dried. Titania nanotubes were prepared using anodization technique, in which Ti was used as the working electrode (anode), and platinum as the cathode. The TiO_2 nanotubes were prepared in 75% glycerol ($C_3H_8O_3$, Fisher Scientific, Canada) solution containing 0.27M ammonium fluoride (NH_4F, Fisher Scientific, Canada) at 30 V (DC power supply, Matsusada R4K-80 Series) for 6 h at room temperature (Fig. 6.3). After anodizing, the samples were rinsed with water, and sequentially soaked in absolute ethanol and distilled water over night and air dried. The nanotube samples were then annealed at 400 °C (5°C/min) for 3 h and cooled down in the furnace to crystallize the amorphous TiO_2 nanotubes into the anatase structure, following the protocol of Macak *et al.* [316].

The antimicrobial peptide HHC36 (KRWWKWWRR) (CPC Scientific, Sunnyvale, CA), was used in our study [27, 258]. The NT specimens (1 × 1 cm) were filled with HHC36 using a simplified lyophilization technique. Fifty micro-litre of 672 µM HHC36 solution (1 mg/mL in ethanol) was pipetted onto the nanotube surfaces, gently spread, and allowed to dry under vacuum desiccator at room temperature for 30 min. The loading process repeated three times.

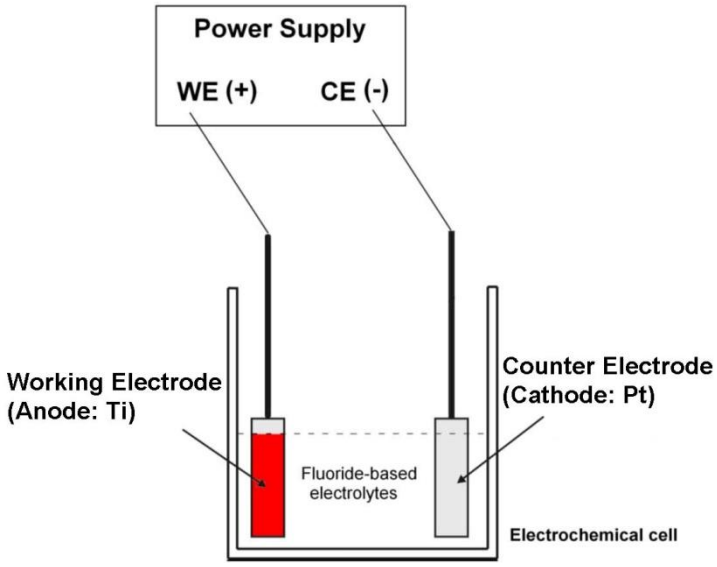

Figure 6.3. Schematic diagram of anodization setup

6.2.2 Processing of CaP on TiO_2 nanotubes

Since titania NT reduces the conductivity of the titanium surface, the electrolytic deposition technique used in chapter four is no longer feasible. In this study, calcium phosphate coating was prepared on titania nanotubes using drop-and-dry technique, a modified approach of the dip-and-dry method developed by Duan *et al.* [317]. The supersaturated calcium phosphate (SSCP) containing 2.32 mM $NH_4H_2PO_4$ (Fluka), 3.87 mM $CaCl_2$ (Fluka), 150 mM NaCl (Fluka), 40 mM HCl (Fisher), and 50 mM tri(hydroxymethyl)aminomethane (Tris) (Fluka) was adjusted to pH 7.30 ± 0.05 at room temperature by NaOH (Fisher). Fifty micro litres of SSCP solution was pipetted onto the specimen surfaces, gently spread, and dried in air at room temperature for 3 h. After the drop-and-dry treatment for four times, the samples were each rinsed with PBS and allowed to dry in air. The CaP coated specimens were loaded with AMP by pipetting fifty micro litre of 672 µM HHC36 solution (1 mg/mL in ethanol) onto the CaP surfaces, and air dried. The loading process repeated three times.

6.2.3 Phospholipid coating on CaP

POPC (1-Palmitoyl-2-oleoyl-sn-glycero-3-phosphocholine) (genzyme Pharmaceuticals) and AMP were dissolved in an appropriate volume of ethanol by sonication to give final concentrations of 26 mM (20 mg/mL) POPC, including 672 µM (1 mg/mL) HHC36. Fifty micro litre of this solution (POPC-20) pipetted onto the specimen surfaces, and dried in air at room temperature. The samples were kept in fridge for future experiments. Figure 6.4 shows a cartoon of multilayered coatings.

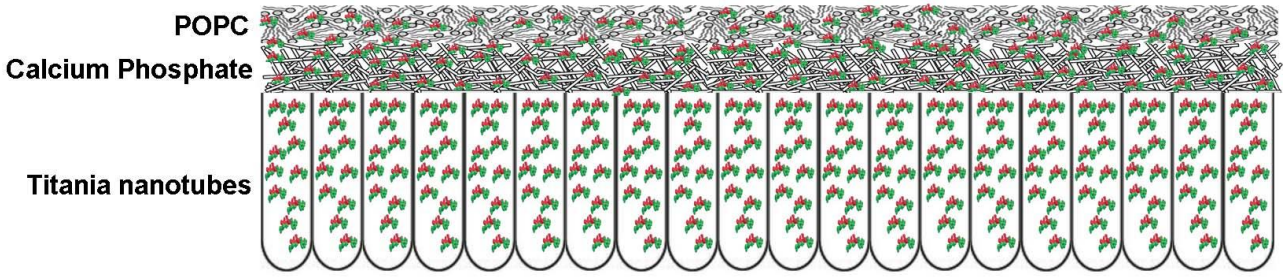

Figure 6.4. Cartoon of multilayered coated Ti. Each layer was impregnated with AMP.

6.2.4 Surface characterization

Surface morphologies, and coating microstructure were studied with a field emission scanning electron microscope (FE-SEM Zeis Sigma) equipped with energy dispersive X-ray analysis (EDS), after being sputter-coated with a thin layer of gold. A focused ion beam (FIB-SEM) analysis was performed using a FEI Helios 650 dual beam microscope to investigate the cross section of specimens. The analysis was carried out at low beam current 0.20 nA, while the energy of ions was 3 kV. Chemical compositions of coatings were evaluated using EDS, and attenuated total reflectance-Fourier transform infrared spectroscopy (ATR-FTIR Perkin Elmer Spectrum 100) in the range from 4000 to 400 cm^{-1}. Chemical binding identification of POPC-20

solution was investigated using liquid chromatography-mass spectrometry (BrukerEsquire-LC/MS). The ten times diluted solution of POPC-20 (HHC36/POPC=67 μM/2.6 mM in ethanol) was injected at 10 μL/min infusion rate and the accurate *m*/*z* values were obtained from a mass spectrum average. The mass spectrometer was calibrated using pure POPC and HHC36 standards.

The wettability of surfaces was characterized by contact angles measurements using 1 μL distilled water by sessile drop method at room temperature. Images were captured and analyzed using Northern Eclipse software at 10x magnification.

6.2.5 Release profile of AMP

The *in vitro* AMP release kinetics of the samples were measured using ultraviolet–visible spectroscopy (UV/Vis) by recording the absorption peak at 280 nm, which is the characteristic excitation wavelength for tryptophan [318]. Three specimens, nanotube coated Ti loaded with AMP (NT), CaP coated nanotubes loaded with AMP (CaP), and POPC-20 were gently rinsed with PBS and dried at room temperature. The specimens in triplicate were then immersed in 1 mL of PBS (pH 7.4) in a glass vial while rotating at 37°C. All samples were rinsed with PBS. After 30 min, 90 min, 150 min, 270 min, 1 day, 2 day, 3 day, 5 day and 7 day, 500 μL of solution was sampled and fresh PBS was replenished every time the samples were taken. The samples were stored at -20°C, and the AMP cumulative release ratio was analyzed for AMP content using a UV/Vis. A series of standards in the concentration range 2-100 μg/mL of HHC36 in PBS were prepared in triplicate to calibrate the system. AMP quantification was then calculated based on the external standard method. Degradation of POPC-20 samples in 1 mL of PBS (pH 7.4) in a glass vial while rotating at 37 °C in triplicate were studied up to 7 days. After each day, the

samples were fixed in 2.5% glutaraldehyde in PBS for 2 h at 4°C, dehydrated with graded ethanol (50, 70, 80, 90, 95, and 100%, 15 min each), and examined using a FE-SEM.

6.2.6 Antimicrobial activity

Assessment of antibacterial activity against both Gram-positive (*S. aureus*) and Gram-negative (*P. aeruginosa*) bacteria were tested using the disk-diffusion test (Kirby-Bauer). To obtain bacteria in the mid logarithmic phase of growth, 100μL of bacteria solution was cultured overnight and was transferred into sterile tubes containing 5 mL of MHB and incubated at 37 °C for 1 h. *P. aeruginosa* and *S. aureus* bacterial suspensions were then re-suspended with MHB, to dilute the solution and provide a final density of ~10^6 CFU mL^{-1}. The bacterial suspension (1 mL) was applied uniformly on the surface of a nutrient MH agar plate before placing the disks on the plate. The inoculated agar plates were allowed to dry for 5 to10 min, and then the round disks (1 cm in diameter) POPC-20, POPC-10 (the same samples treated with half concentration of POPC), and Ti as negative control were placed on the inoculated agar, with the coated side touching the inoculated agar. The agar plates were then incubated at 37 °C for twenty four hours.

The antimicrobial activity of POPC samples were also confirmed by SEM imaging of incubated ~10^6 CFU mL^{-1} of the *S. aureus*, and *P. aeruginosa* bacteria strains on samples over night. The nanotube sample without AMP treatment was used as control.

6.2.7 Cell study

Commercially available MG-63 human osteoblast-like cells (ATCC CRL-1427, USA) were cultured in a medium consisting of Dulbecco's Modified Eagle Medium (DMEM, GIBCO), including a minimal essential medium supplemented with 10% fetal bovine serum (FBS), and 1% nonessential amino acids (GIBCO). The culture medium was refreshed at 2-day interval and

the incubator ambience was maintained at 37°C under 95% humidified atmosphere with 5% CO_2. Cells were washed with 0.1 M PBS and isolated from culture dishes by trypsinization, and cell number were checked with trypan blue dye exclusion test.

Cytocompatibility level of cells cultured on specimens were evaluated by measuring the mitochondrial dehydrogenase activity using a modified MTT (3-(4,5-dimetyl-2-tiazolyl)-2,5-diphenyl-2H-tetrazolium bromide) (Biotium) reduction assay. To assess the cytotoxicity of specimens, 10^4 of cell dispersion were seeded on nanotube coated Ti without AMP (NT) and POPC-20 in triplicate. Negative controls were assigned to cells cultured in fresh medium, and normal conditions with no AMP. The cells were allowed to attach for 2 h before adding 1 mL culture medium. Fresh medium was replaced every 2 days and MTT assay was carried out after 1, 2, and 5 days. After each time point, the media was removed, 100 μL MTT was dissolved in 1 mL serum free medium, and was added to each well, and were incubated for 4 h. Subsequently, the solution was removed and was replaced with 200 μL DMSO (dimethylsulfoxide). After shaking the plates for 15 min, the absorbance was measured at 570 nm, and the reference wavelength of 690 nm on an ELISA microplate reader (Bio-Tek Instruments).

To study the cell attachment, 10^4 of MG-63 cell dispersion were cultured on each sample, and incubated for 4 h. The samples were then washed with 0.1 M PBS for three times and incubated in 2.5% glutaraldehyde in PBS for 2 h at 4°C. After washing the samples for 3 times with 0.1 M PBS, specimens were dehydrated using graded ethanol (50, 70, 80, 90, 95, and 100%, 15 min each), and critically point dried (Autosamdri®-815B, Series A). The samples were Au sputter coated (Moorestown, NJ), and viewed using a FE-SEM.

6.2.8 Platelet activation and attachment analysis

The blood experiment protocols were approved by the clinical ethics committee of university of British Columbia. Blood from two healthy consented donors was collected into 3.8% sodium citrated tube with a blood/anticoagulant ratio of 9:1 at Centre for Blood Research, University of British Columbia. Platelet-rich plasma (PRP) was prepared by centrifuging citrated whole blood samples at 900 rpm for 10 min in an Allegra X-22R Centrifuge (Beckman Coulter, Canada). Ten percent hematocrit was prepared first by removing plasma via centrifuging citrated whole blood samples at 3000 rpm for 15 min and then the red blood cell were subjected to cleaning by PBS for three times at 1000 x g for 4 minutes.

The level of platelet activation upon interaction with implants was quantified by flow cytometry. Different samples including NT, CaP coated NT, POPC-20 which had already been treated with AMP, and pure Ti and POPC coated Ti without AMP as controls, were soaked and incubated with 740 μL of PRP at 37°C. After 2 h, aliquots of the incubation mixtures were removed for assessment of the platelet activation state. Five microlitre of post-incubation platelet rich plasma, diluted in 45 μL of HEPES (4-(2-hydroxyethyl)-1-piperazineethanesulfonic acid) buffer, was incubated for 20 minutes in the dark with 5 μL of monoclonal anti-CD62P-PE (Immunotech). The samples were then stopped with 0.3 mL of phosphate-buffered saline solution. The level of platelet activation was analyzed in a BD FACSCanto II flow cytometer (Becton Dickinson) by gating platelets specific events based on their light scattering profile. Activation of platelets was expressed as the percentage of platelet activation marker CD62P-PE fluorescence detected in the 10,000 total events counted. Duplicate measurements were done, and the mean of which was reported. Controls were done for the flow cytometric analysis. One U/mL of bovine thrombin (Sigma) was used as a positive control, and HEPES buffer was used as

a negative control. The samples were also washed with PBS and fixed with 2.5% glutaraldehyde in PBS. After washing the samples with PBS, specimens were dehydrated using graded ethanol (50, 70, 80, 90, 95 and 100%, 15 min each). The samples were Au sputter coated (Moorestown, NJ), and studied using a FE-SEM for platelet adhesion on each sample surface.

6.2.9 Red blood cell hemolysis assay

In RBC hemolysis study, the same groups of samples as platelet activation analysis were soaked and incubated with 740 μL of 10% hematocrit RBC suspension for 1 h at 37 °C. The 100% lysis of RBCs incubated with distilled H_2O was used as positive control. The percent of RBC lysis was measured by the Drabkin method. Twenty microlitres of the 10% hematocrit RBC suspension mixture was added to 1 mL of Drabkin's solution. The RBC suspension was then centrifuged at 8000 rpm for 3 minutes, and two hundred microlitres of supernatant solution was also subjected to 1 mL of Drabkin's solution dilution. The difference in optical density (OD) was measured using the spectrophotometer at 540 nm. The percentage of red blood cell lysis (hemolysis degree) in each sample is measured from the OD of supernatant divided the OD of suspension solution.

6.2.10 Statistical analyses

"Primer of Biostatistics" software was used to calculate the difference between sets of data based on analysis of variance (ANOVA). The *p* value of less than 0.05 was considered statistically significant.

6.3 RESULTS

6.3.1 Characteristics of TiO_2 nanotubes

The morphology of titania nanotubes after annealing has been shown in figure 6.5. The FE-SEM images show that titania nanotubes were about 2 μm long with pore size of approximately 120 nm in diameter; they are oriented vertically to the sample surface. The nanotube array was uniformly distributed over the substrate (Fig. 6.5a). There were ripples observed on the side wall of nanotubes due to thickness fluctuations along the nanotubes (Fig. 6.5b). This phenomenon can be explained by periodic oscillations of the current during anodization [313, 316, 317].

6.3.2 Calcium phosphate coating on titania nanotubes surface

Figure 6.6 shows the titania nanotube surface treated by the drop-and-dry technique. After four times of super saturated calcium phosphate (SSCP) treatment, the nanotubes were completely covered with CaP flakes that are about 1 μm long and less than 100 nm thick (Fig. 6.6). The CaP coating morphology was examined by FE-SEM and the presence of CaP coating was confirmed by detection of corresponding peaks of calcium and phosphorus using EDS. The calcium:phosphorus atomic ratios was calculated to be 1.31 ± 0.04 ($n = 3$), which is close to that of octacalcium phosphate (Ca/P = 1.33) and CaP coating produced using ELD technique in chapter four. Too thin layer of CaP didn't permit further analysis with FTIR or XRD.

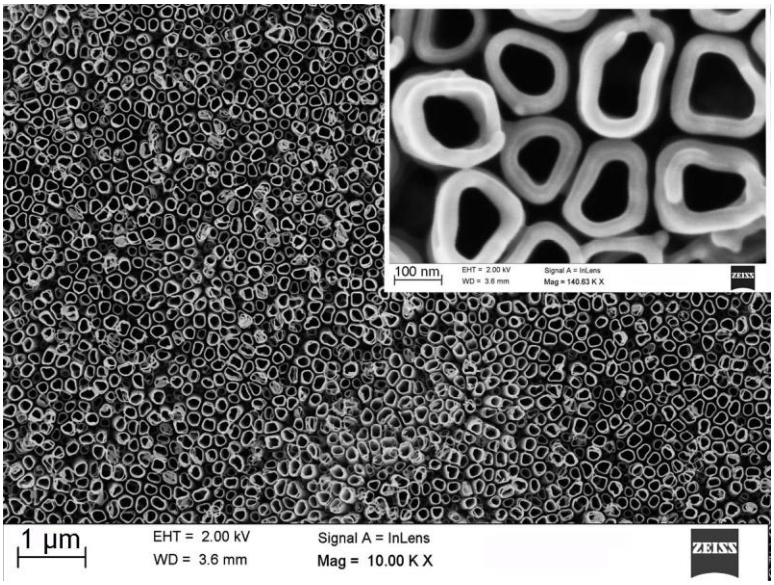

(a)

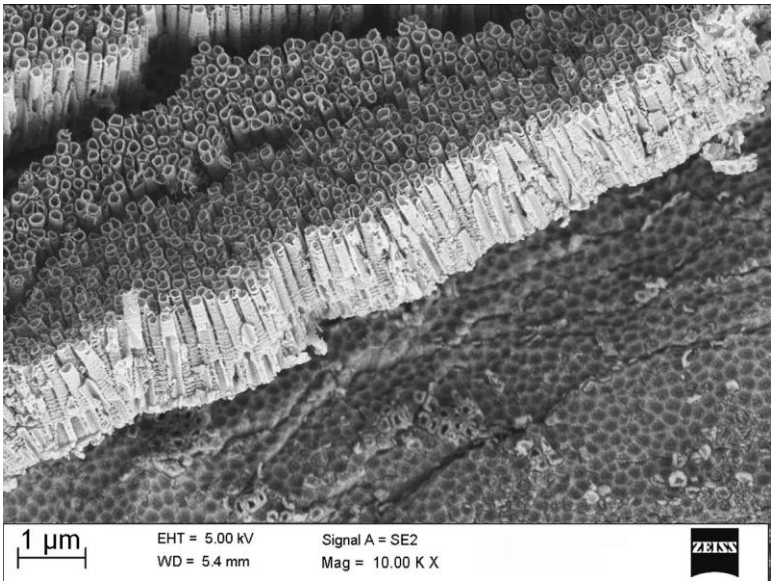

(b)

Figure 6.5. SEM micrographs of TiO_2nanotubes, (a) Top view, with high magnification showing a close packed structure, anodized in 75% glycerol solution containing 0.27M ammonium fluoride at 30 V for 6 h at room temperature, (b) Side view of mechanically fractured sample.

Figure 6.7 represents the FIB-SEM analysis of multilayer coated NT. The results indicate a very thin coating of 200-300 nm thick.

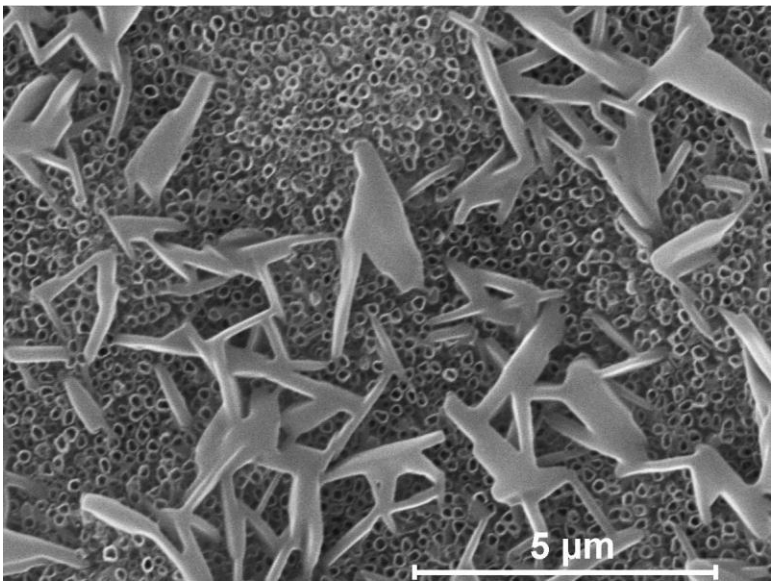

(a)

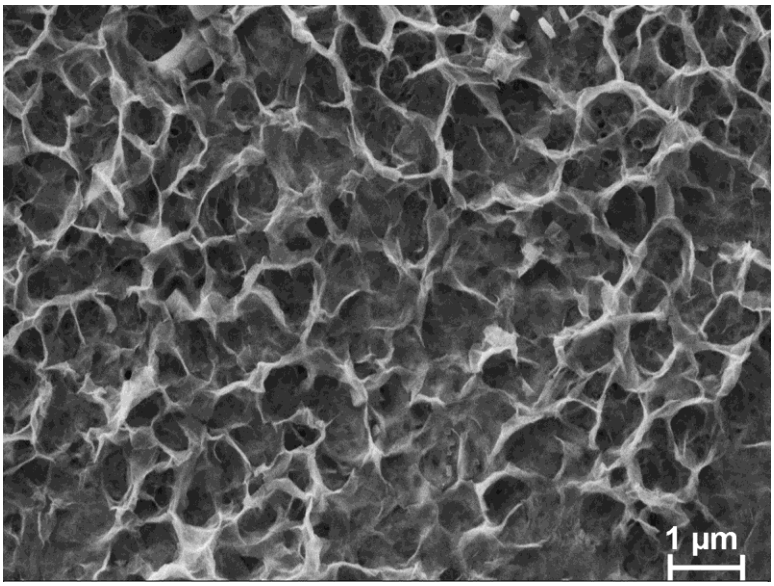

(b)

Figure 6.6. SEM micrographs of CaP coating on TiO_2 nanotubes,(a) initial stage, (b) after four times of drop-and-dry treatment, showing the coverage of NT by CaP crystal flakes.

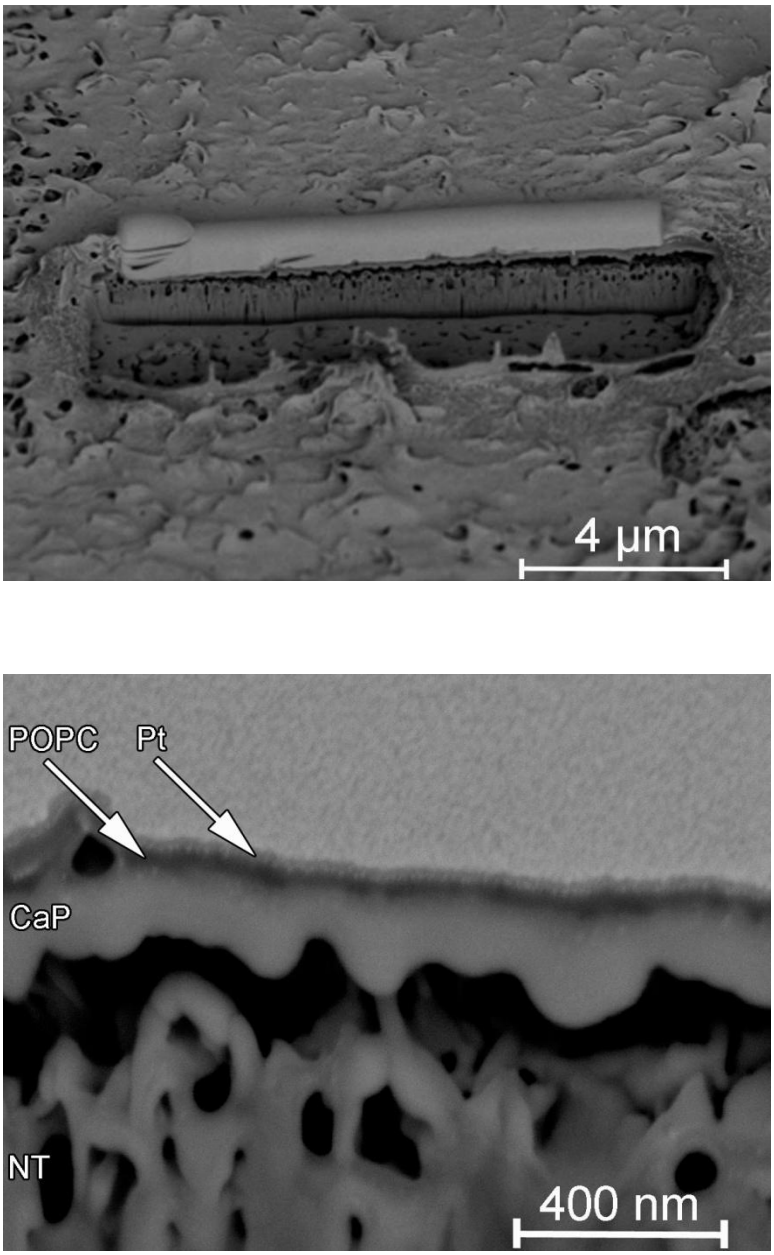

Figure 6.7. FIB micrographs of POPC-20 specimen after Pt deposition. Image of coatings at low and high magnifications showing that the total thickness of multilayers measured between 200-300 nm.

6.3.3 Phospholipid coating

As expected, the FE-SEM analysis of POPC coated samples showed that CaP coating has been embedded uniformly with POPC all over the sample. The POPC filled up the CaP pores but

did not completely cover up the CaP coating, so the underneath CaP layer can still be seen (Fig. 6.8). FTIR spectroscopy (Fig. 6.9) was used to investigate and compare the chemical characteristics of pure POPC and POPC-20 treated with AMP. According to the observed infrared absorption frequencies, the corresponding assignments of POPC are CH_2 antisymmetric stretch, and CH_2 symmetric stretch at 2923, and 2853 cm^{-1} respectively. The C=O stretching vibration band of POPC is depicted at about 1735 cm^{-1}. The wave numbers 1463, and 1231 cm^{-1} are attributed to CH_2 scissoring, and PO_2^- antisymmetric stretch. The 1030-1090 cm^{-1} range includes PO_2^- symmetric stretch, and CO-O-CH_2 symmetric stretch [321].

Identification of the individual molecular species in POPC-20 solution was based on the *m/z* value of their monoisotopic H^+ adducts, as detected by MS. Range of fragments detected by MS at 760.8 *m/z* corresponds to the molecular mass of POPC (760.8 g mol^{-1}), and the dimer peak at 1521 *m/z* depicts the characteristic ions generated from dimer molecules of POPC (760.8+760.8). A small peak at 1125.1 *m/z* matches the corresponding molecular mass of POPC and HHC36 (1488 g mol^{-1}) with two positive ions H^+ adducts [(1488+760+2)/2][312, 322] (Fig. 6.10).

Figure 6.11 shows the degradation of POPC-20 coatings after three and seven days in PBS. Nanotubes were observable after three days incubation, however degradation was heterogeneous and different levels of degradation were detected on random spots.

The hydrophilicity of the surfaces has been shown in figure 6.12. Cleaned Ti surface was used as a control with the contact angle of about 67°. The other samples exhibited a decrease in contact angle in compare to Ti. The obtained contact angles for CaP, and NT were about 14°, 10° respectively, and for the POPC, and POPC-20 the calculated contact angles were in the range of 7 ± 1°.

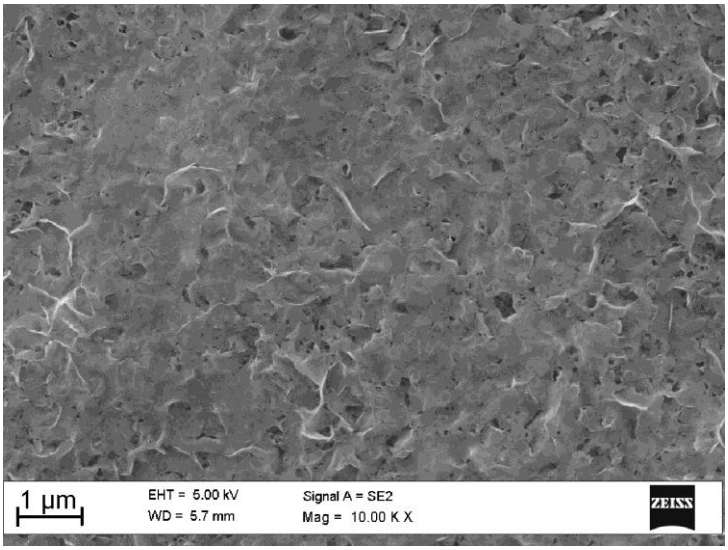

Figure 6.8. SEM micrographs of POPC-20 coating on CaP

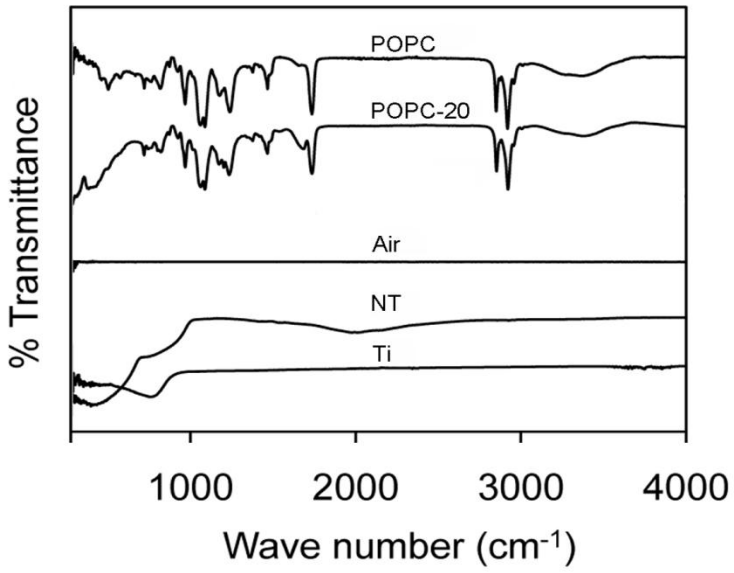

Figure 6.9. ATR-FTIR spectra of pure Ti, NT, POPC-20 in compare to POPC alone coatings. The inclusion of AMP does not change the chemical characteristics of POPC.

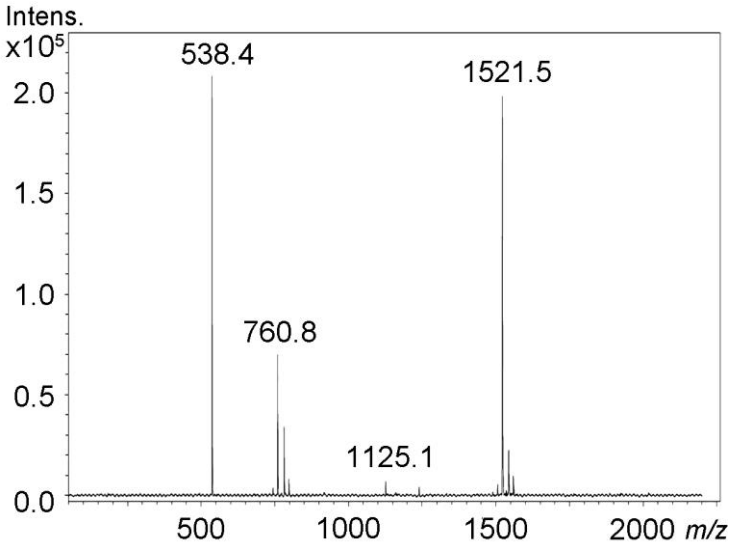

Figure 6.10. Mass spectrum of ten times diluted solution of POPC-20 (HHC36/POPC : 67μM/2.6mM in ethanol).

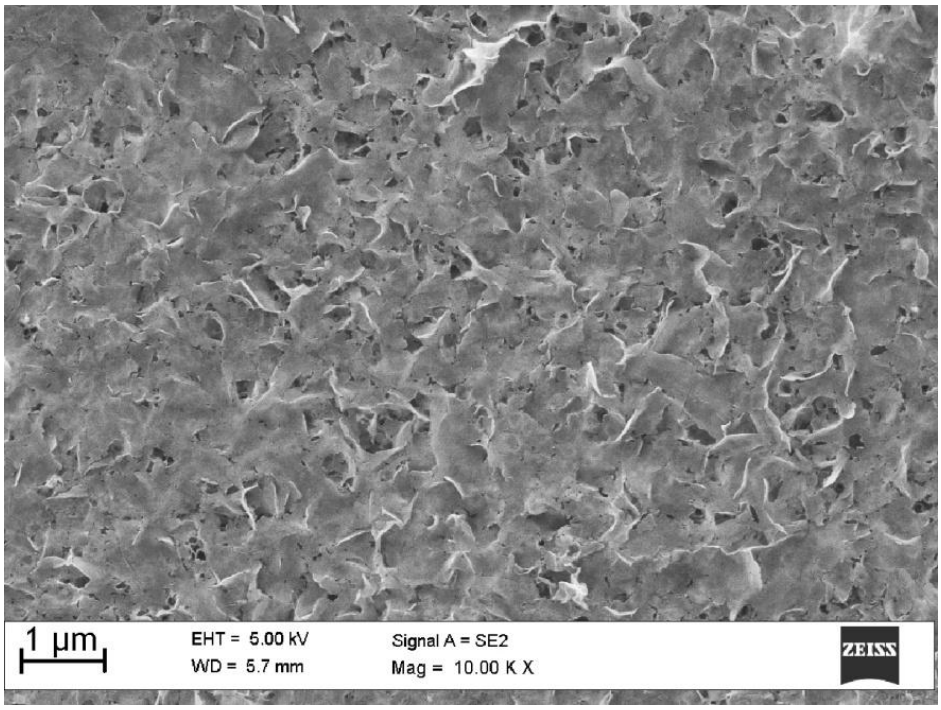

(a)

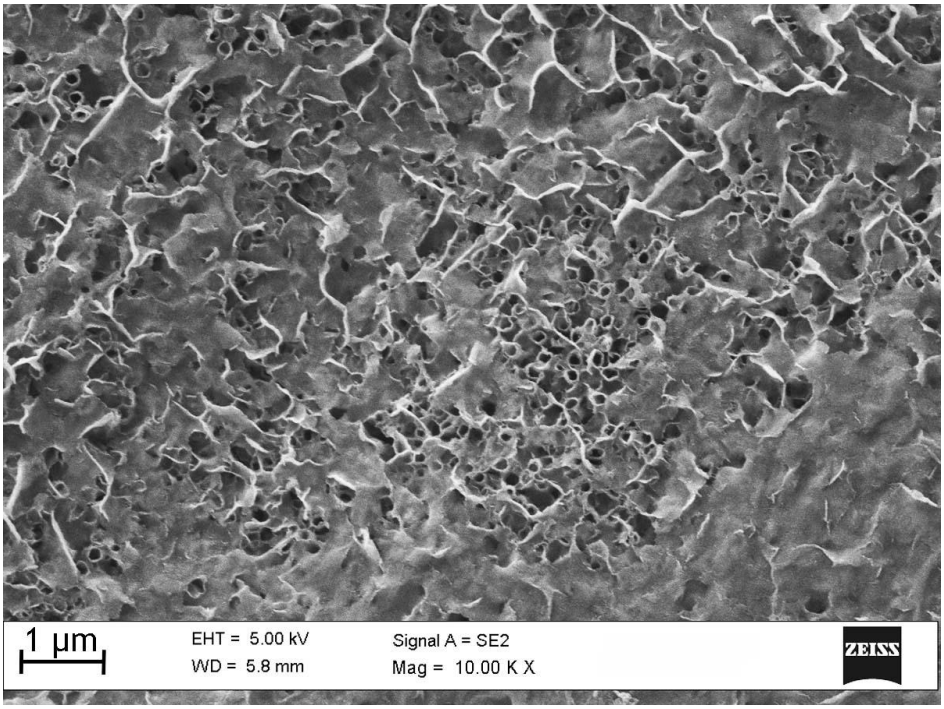

(b)

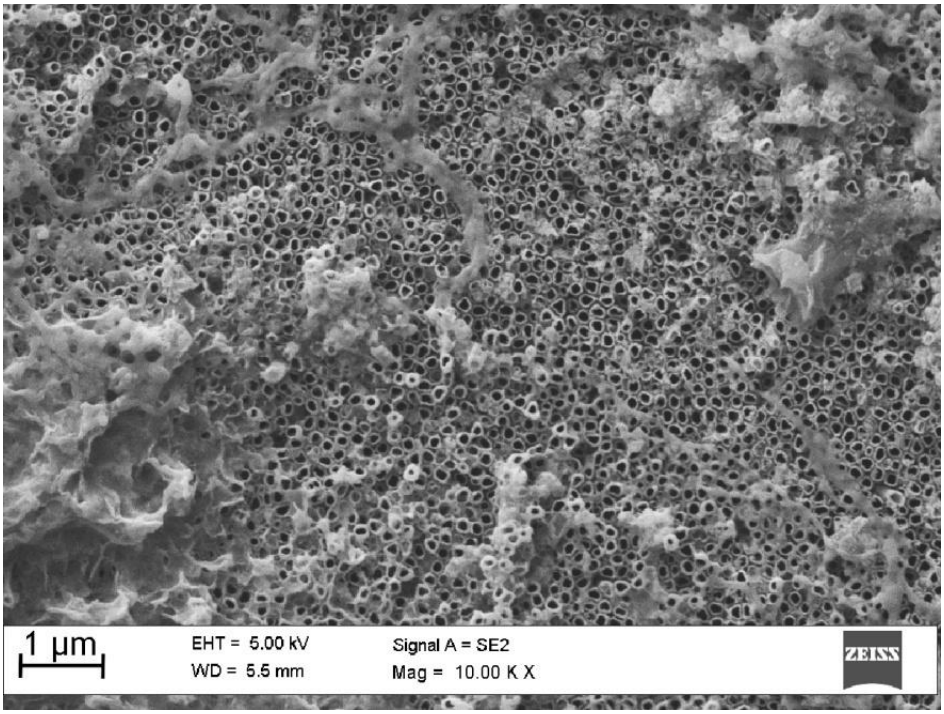

(c)

Figure 6.11. Degradation of POPC-20 after (a) as prepared, (b) 3 day, and (c) 7 day incubation in PBS at 37 °C while gently shaking.

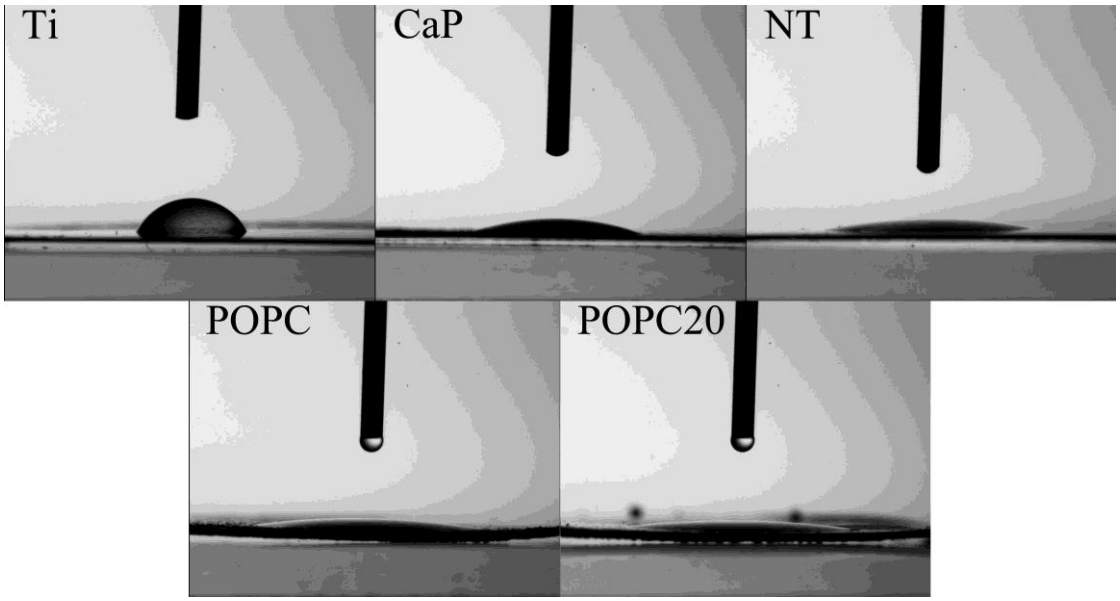

Figure 6.12. Images collected during contact angle measurements indicating the extensive spreading of water drop on different coatings in comparison to the Ti substrate.

6.3.4 Release kinetics

Figure 6.13 shows the AMP release profiles of POPC-20, and two controls. As expected burst release of total loaded AMP was observed from both controls during the first few hours after incubation. However AMP was successfully incorporated, and steady and slow release was observed from POPC-20 samples.

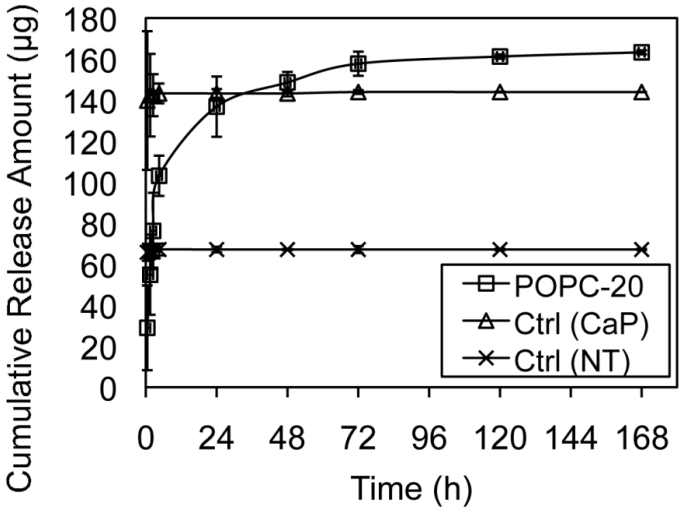

(a)

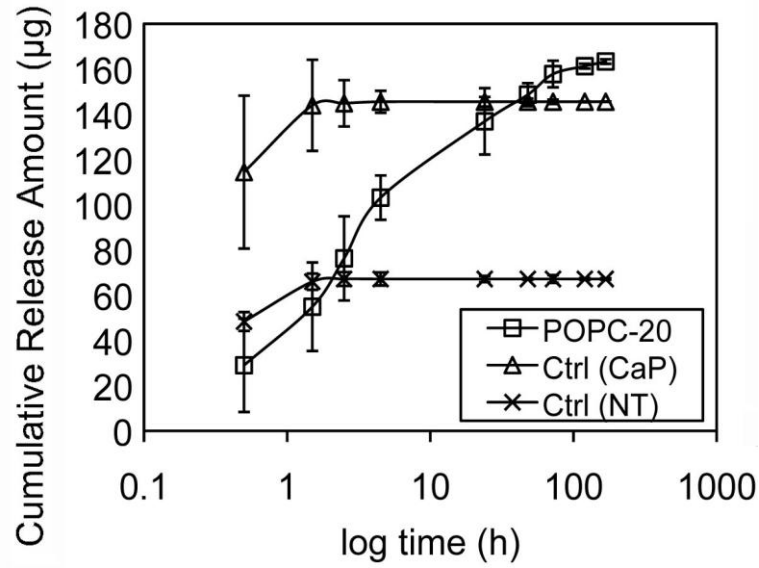

(b)

Figure 6.13. *In vitro* release of AMP from POPC-20, and NT, CaP controls, (a) time, (b) log time. Error bars indicate standard deviation (n = 4).

6.3.5 Cell attachment and cytotoxicity

Analysis of variance showed no statistically significant difference ($p > 0.05$) between samples (POPC-20), and controls (cells cultured in fresh medium, and normal conditions with no AMP, and NT coated Ti without AMP treatment) after 1 day ($p = 0.13$), 2 days ($p = 0.37$), and 5 days ($p = 0.24$) with regard to MTT (Fig. 6.14). This means that the layer modification of the Ti does not affect the viability and the cell function.

After 4 h incubation with 10^4 of MG-63 cells, NT, and POPC-20 samples were examined with FE-SEM. Figures 6.15 represent typical cell morphologies. MG-63 osteoblast-like cells had spread extensively after 4 h. The cells were polygonal in shape with high extent of filopodia. However, some thicker cells with elongated appearance were also detected occasionally in

random area of samples. In general the cells with branched look have scattered all over the specimens in all directions with no regular orientation. All cells exhibited dorsal ruffles representing filopodia promoting activity [323, 324].

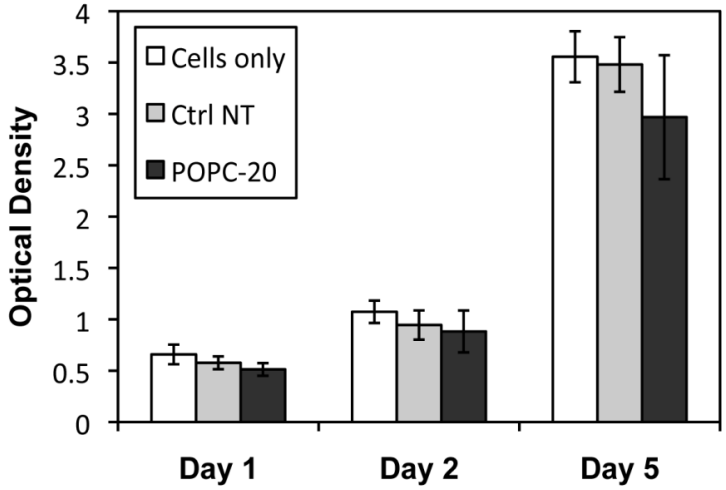

Figure 6.14. MTT assay performed to evaluate the cytotoxicity of POPC-20 with MG-63 osteoblast-like cell in the solution. Analysis of variance showed no statistically significant difference ($p > 0.05$) in cell activity between the POPC-20, and two controls (cells only, and NT) after 1 day ($p = 0.13$), 2 days ($p = 0.37$), and 5 days ($p = 0.24$) incubation.

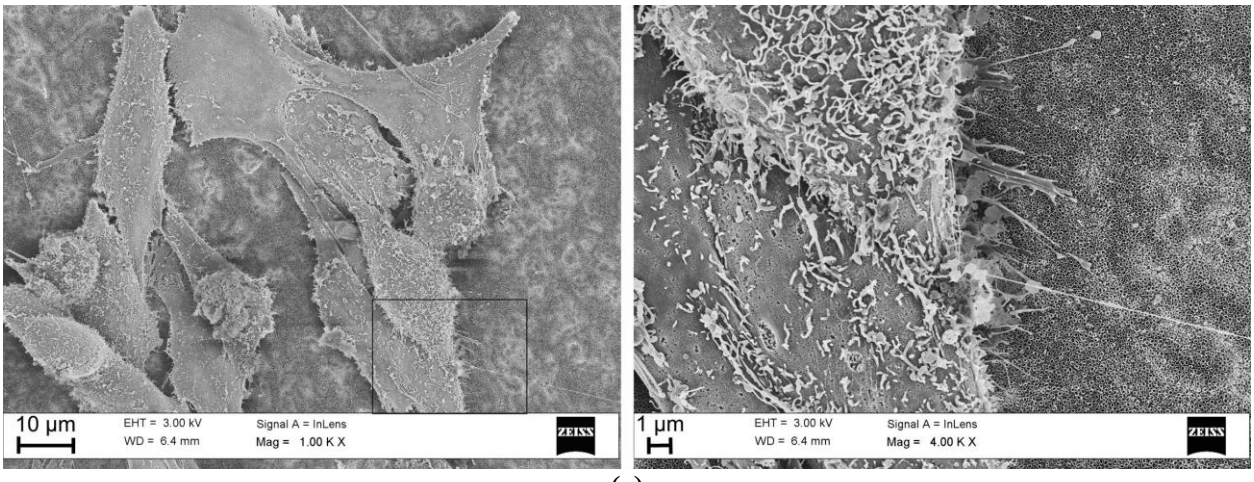

(a)

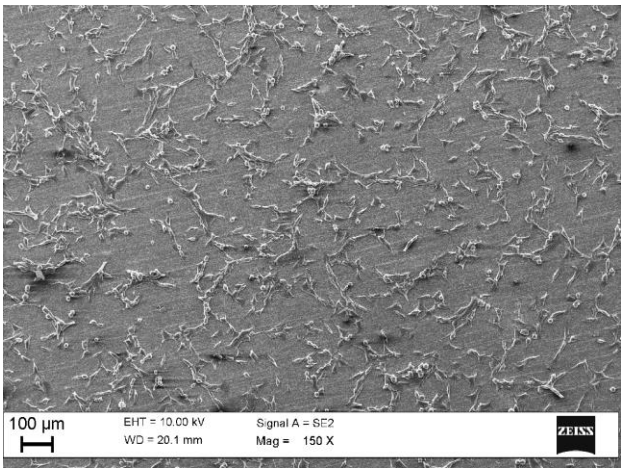

(b)

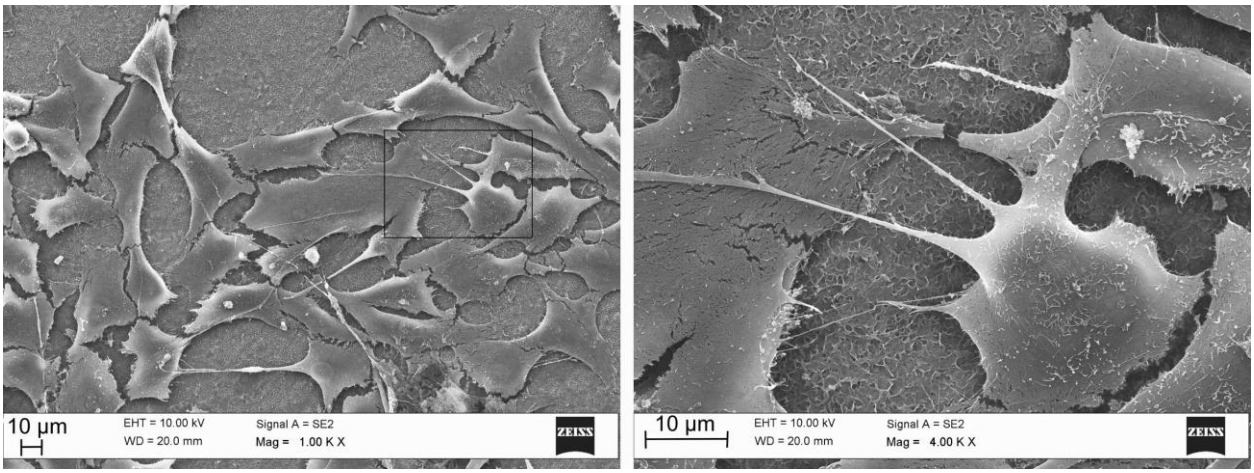

(c)

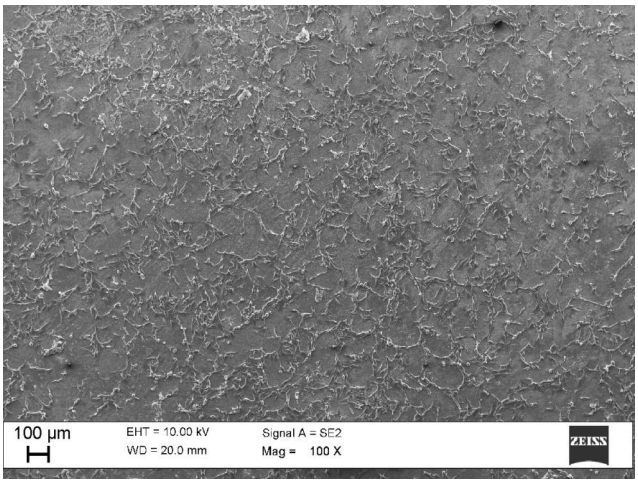

(d)

Figure 6.15. SEM photomicrographs of MG-63 osteoblast-like cells on, (a,b) NT after 4 h incubation, (c,d) POPC-20 after 4 h incubation.

6.3.6 Antimicrobial activity

Diffusion of AMP from POPC-20 could inhibit both *S. aureus*, and *P. aeruginosa* bacteria strains. Distinct area of clearing around the implants (zone of inhibition) was observed for POPC-20, and POPC-10. Slightly larger zone of inhibition was observed for POPC-10 (Fig. 6.16).

Figure 6.17 shows the qualitative SEM assessment of incubated bacteria on NT controls, and POPC-20 overnight. As expected, extensive bacteria covered NT surface. A self-produced matrix of extracellular polymeric substance from *P. aeruginosa* can be observed in different areas in figure 6.16b of control NT sample. Very few bacteria were detected on POPC-20 samples which supports the disk-diffusion test results in figure 6.17, and can be explained by the elution of AMP from the AMP-loaded POPC-20, and subsequent bactericidal activity (Fig. 6.17c,d).

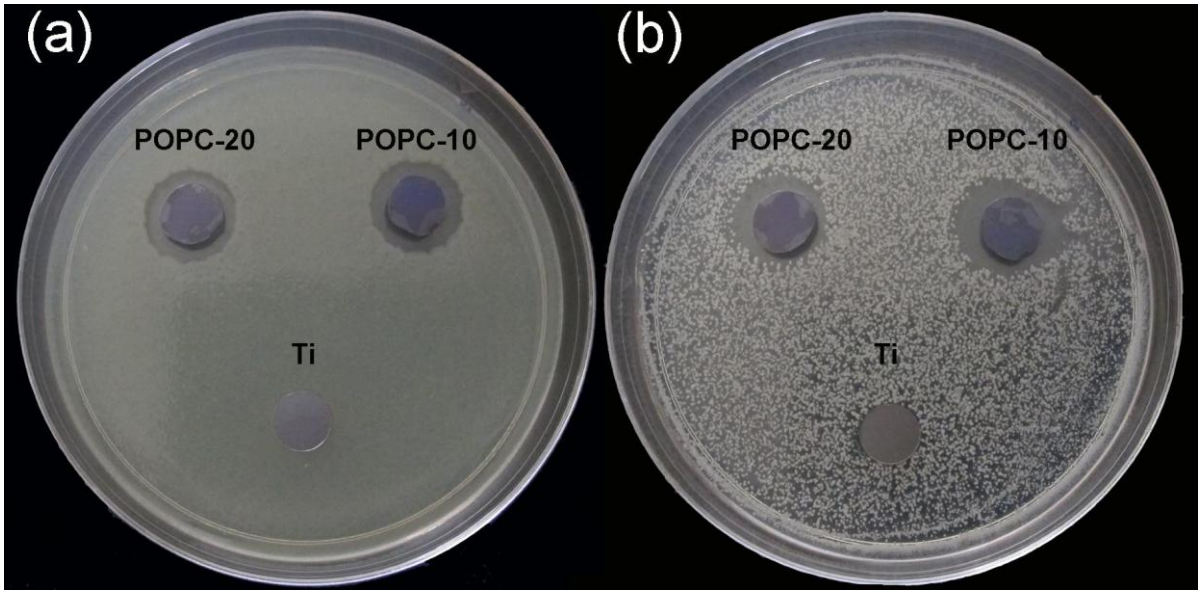

Figure 6.16. Evaluation of antimicrobial effects by the disk-diffusion method including confluent (a) *P. aeruginosa*, and (b) *Staphylococcus aureus* bacteria. Titanium was used as control versus POPC-10 and POPC-20 disks.

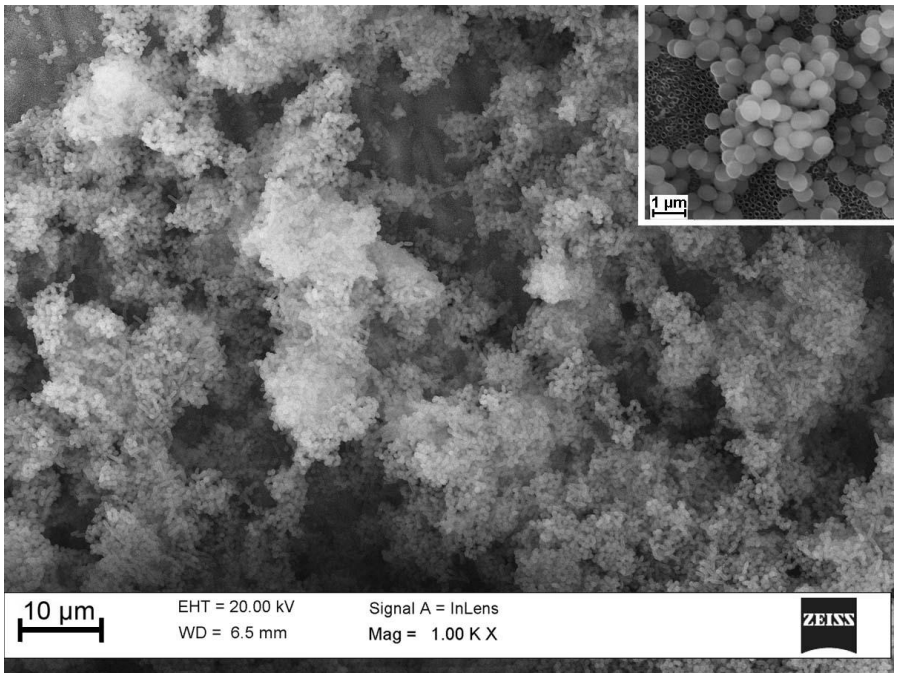
1 µm
10 µm
EHT = 20.00 kV
WD = 6.5 mm
Signal A = InLens
Mag = 1.00 K X
ZEISS

(a)

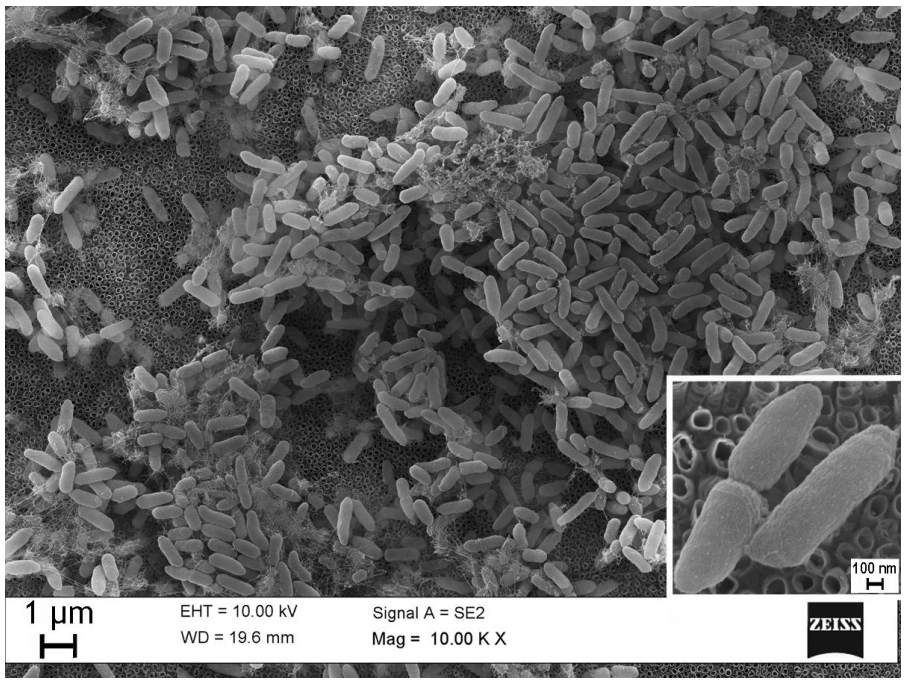
100 nm
1 µm
EHT = 10.00 kV
WD = 19.6 mm
Signal A = SE2
Mag = 10.00 K X
ZEISS

(b)

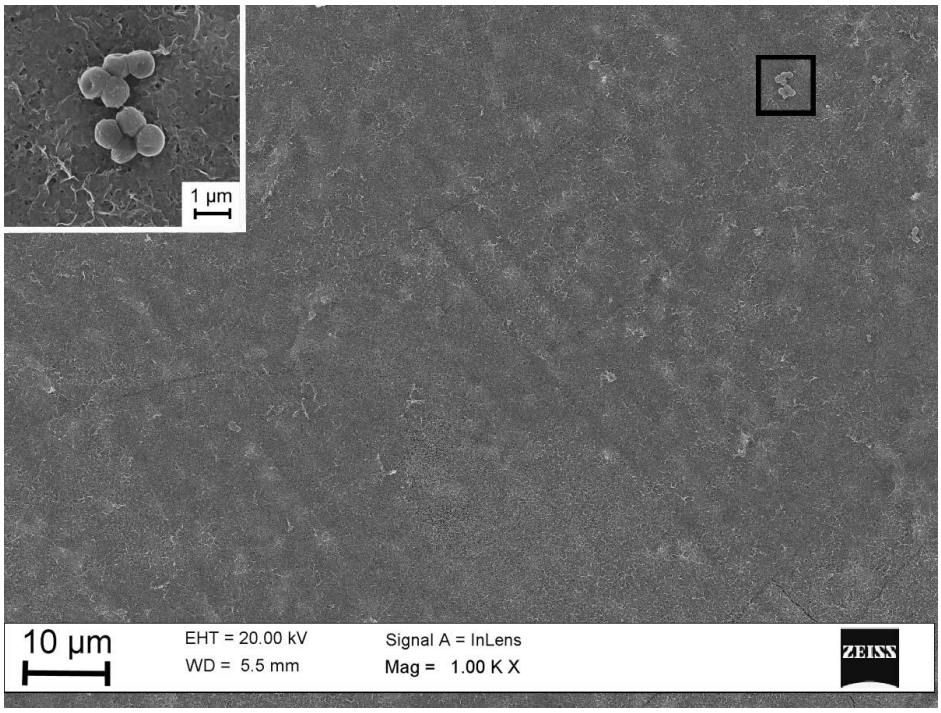

(c)

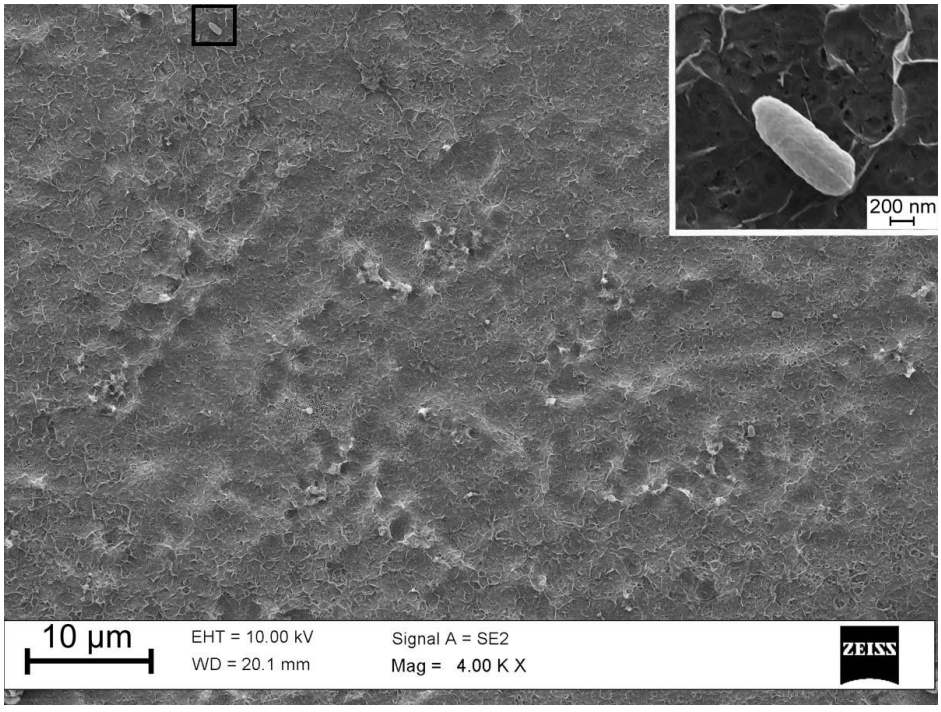

(d)

Figure 6.17. SEM micrographs of incubated bacteria over night with (a) *S. aureus*, and (b) *P. aeruginosa* on non-AMP treated NT control (c) *S. aureus*, and (d) *P. aeruginosa* on POPC-20. Very few bacteria were observed on POPC-20 samples.

6.3.7 Hemocompatibility

To verify hemocompatibility of the POPC-20, platelet activation and adhesion, and complement activation in human blood were tested. Figure 6.18 shows typical flow-cytometric plots for quantification of platelet activation status by analyzing P-selection expression, showing side scatter and positive labelling with the platelet-specific identifier (anti-CD62 antibodies). These plots illustrate the percentage of positive CD62 which reflect the proportion of activated platelets in the total population [325]. Figure 6.19 shows the expression of CD62-PE on the surface of platelets versus controls, and buffer. The POPC-20 showed the lowest platelet activation levels in the solution phase.

The same samples used in platelet activation test were qualitatively examined by FE-SEM analysis for platelet adhesion on POPC-20 samples. Signs of platelet activation appeared to be slightly less on POPC-20 than other samples as indicated by increased pseudopod formation and platelet spreading. Platelet aggregates of varying size were detectable on all samples. Figure 6.20 presents some typical SEM images of attached platelet after incubation with PRP for 2 h. As expected, adhesion and aggregation of platelets which is a well known functional aspect of platelet activation [326] was observed on all samples. Adhered platelets on all samples showed the presence of pseudopods which are typical for platelets in an activated state (Fig. 6.20c) [327].

From figure 6.21, it can be seen that the hemolytic activity for Ti, NT and POPCs significantly decreases in compare to positive control. No significant difference was observed between samples and buffer control. Figure 6.22 shows the interaction of RBC with POPC-20 coating surrounded by activated platelets. The presence of RBC together with activated platelets on Ti surface when exposed to platelet-rich plasma may indicate that the blood interface

comprised a fibrin film (which is the reaction product of thrombin and fibrinogen released into the site) and red blood cells [50].

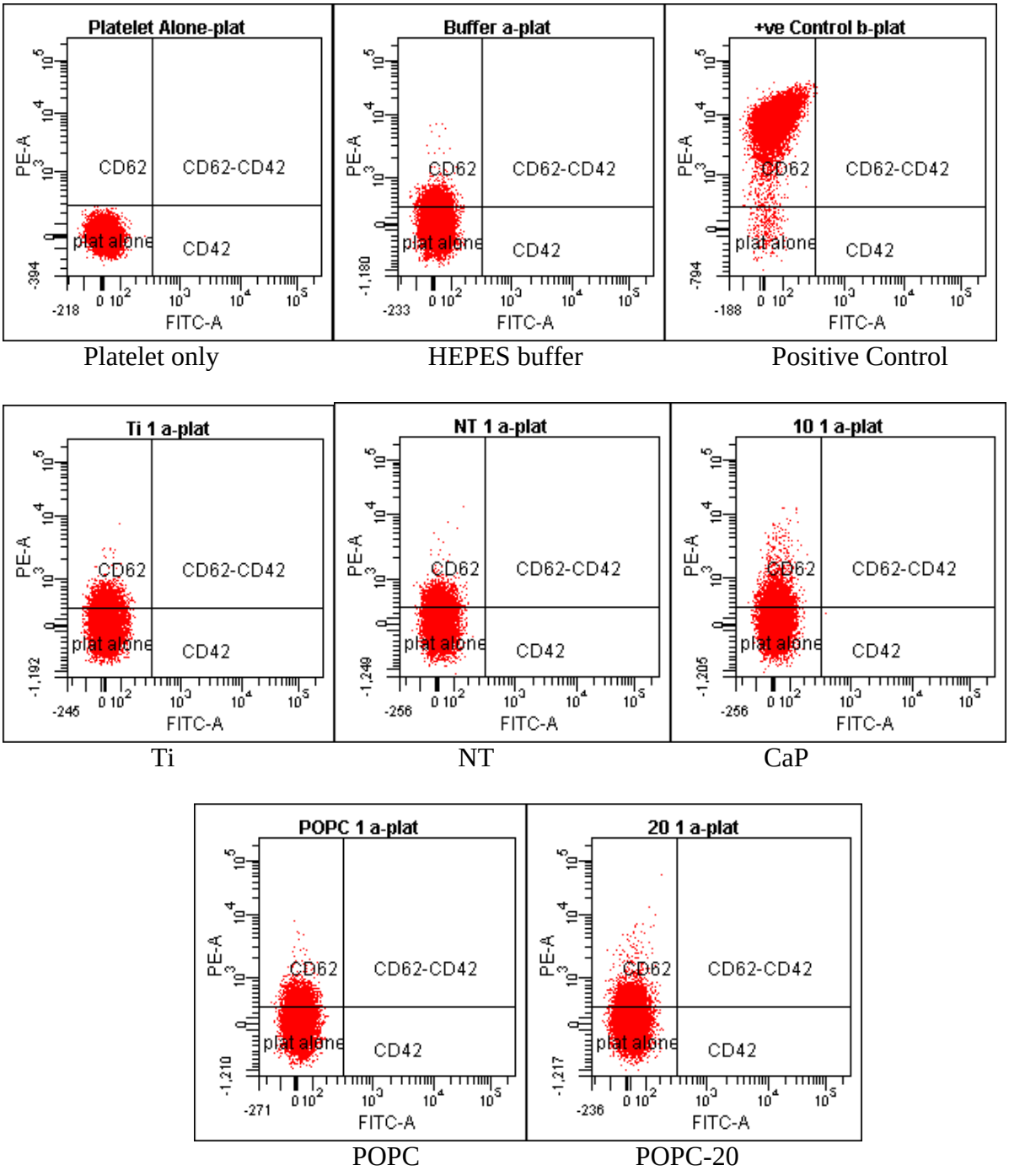

Figure 6.18. Flow-cytometric plots for platelet activation, showing side scatter and positive labelling with the platelet-specific identifier (anti-CD62P antibodies). Lowest platelet activation levels in the fluid phase were found for all samples.

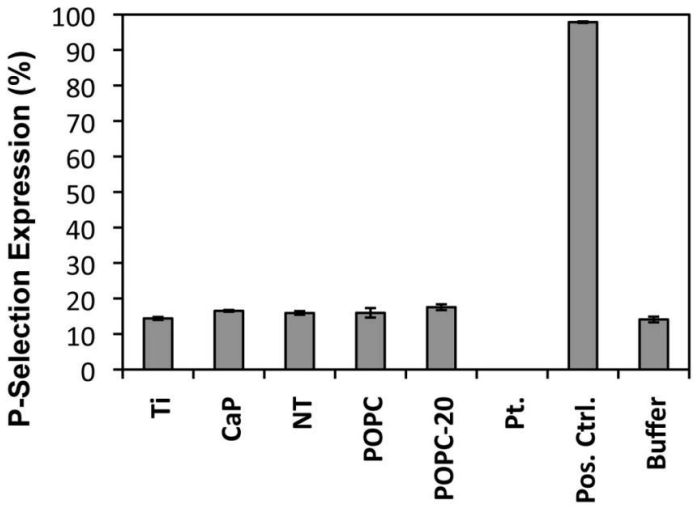

Figure 6.19. P-selection expression percentage in different samples, showed the lowest platelet activation levels in the fluid phase for all samples (n=3).

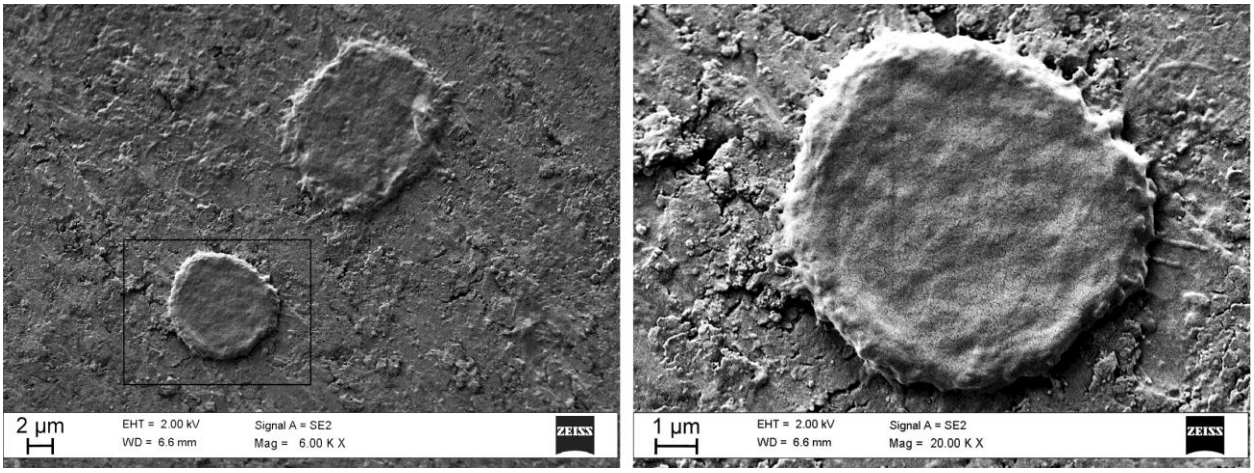

(a)

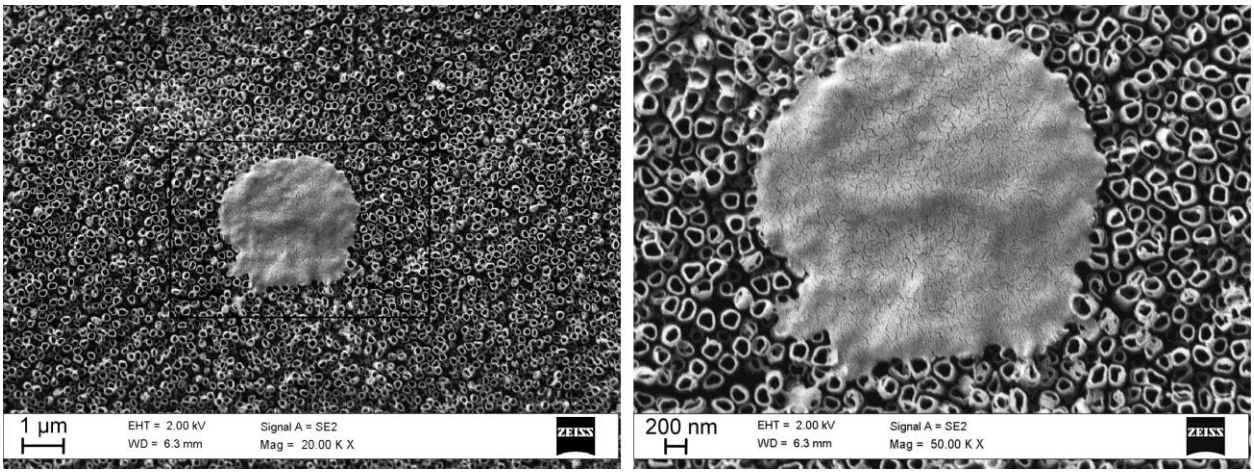

(b)

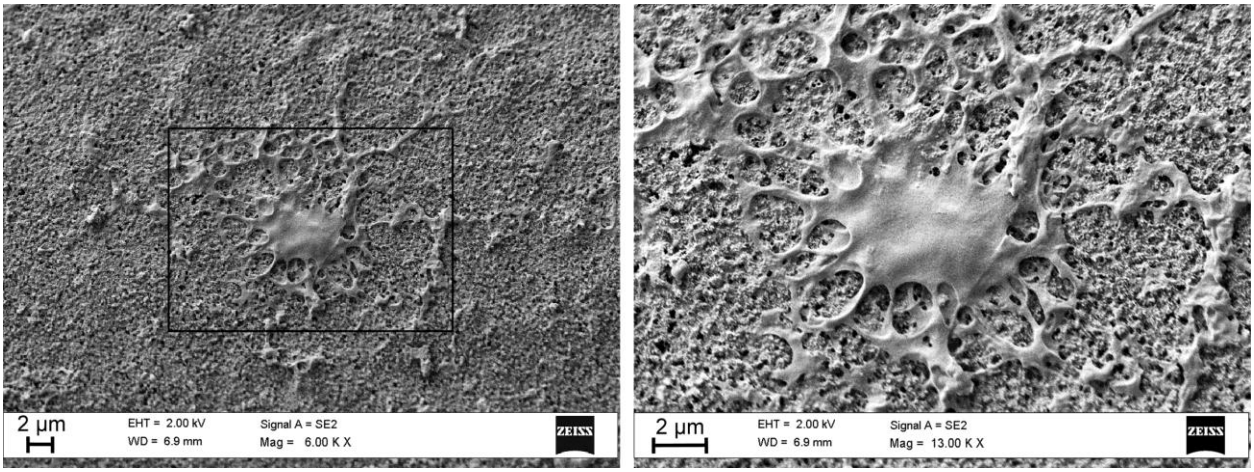

(c)

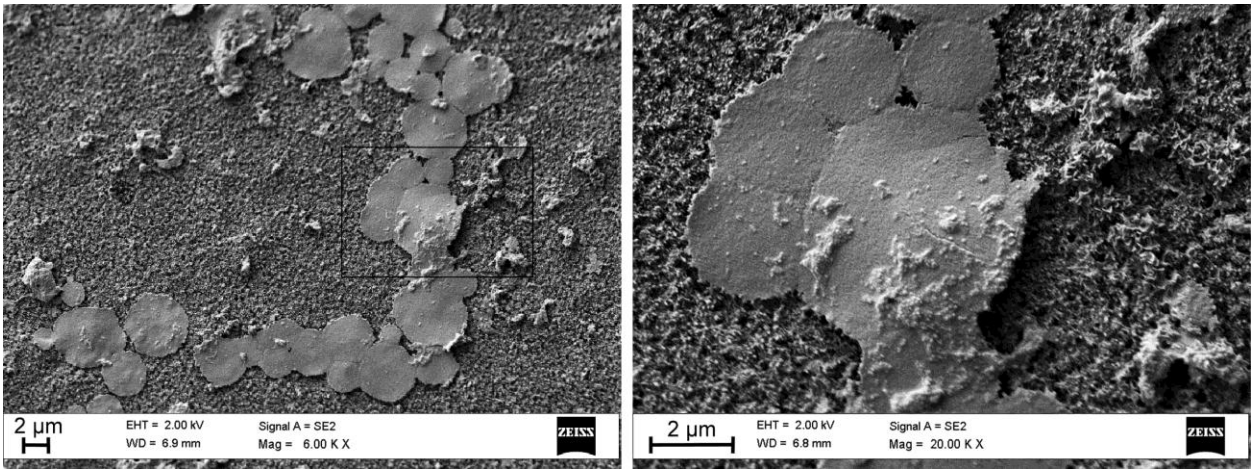

(d)

Figure 6.20. Platelet adhesion on different surfaces characterized by SEM. (a) Ti, (b) NT, (c) POPC-20 after 2h incubation with PRP. Activated platelets with pseudopods attached to the coating could be observed on the coating. (d) Slight aggregation of attached platelets was observed on POPC-20 samples.

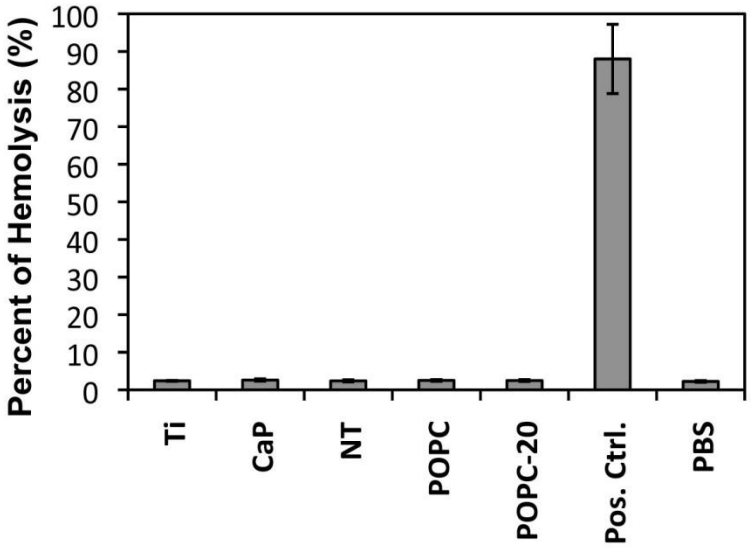

Figure 6.21. The haemolytic activity of implants after incubation with 10% hematocrit RBC suspension for 1 h at 37 °C. Very low hemolysis degree was observed for Ti, NT and POPCs in compare to positive control (n=3).

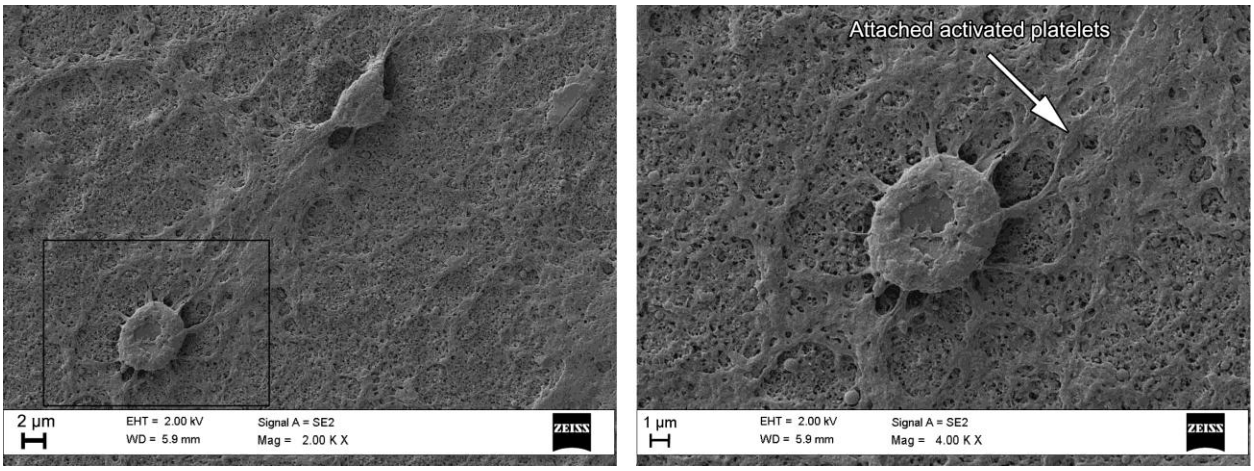

Figure 6.22. Image of an intact red blood cell attached on POPC-20 layer surrounded by activated platelets.

6.4 DISCUSSION

The layer-by-layer technique on flat surfaces is a simple but promising method for coating biological and non-biological substrates impregnated with drugs and other biological substances for controlled release [328]. Ideal design of multi-layered drug delivery systems as coatings on orthopaedic implants with respect to release antibiotics in a physiological environment, should meet a few requirements: (1) selection of proper antimicrobial agents which neither impair bone growth nor cause the development of multi-antibiotic-resistance, (2) incorporation of the antimicrobial agent, (3) a tailored kinetics of release, and (4) stable biomaterials with possibility to increase osteoconductivity without compromising biocompatibility.

To achieve this purpose, layer-by-layer coatings including nanotubes, calcium phosphate and phospholipid have been developed on Ti substrate in this chapter. In chapters four and five we fabricated OCP coatings on Ti implants using low temperature electrolytic deposition. Loading HHC36 AMP into OCP coatings created an antimicrobial coating that can effectively kill *S. aureus*, and *P. aeruginosa* bacteria in short time without negatively affecting MG-63 osteoblast like cells [236, 275]. The purpose of utilizing porous calcium phosphate coatings as antibiotic vector was to provide bone-implant integration [329-331]. Incorporation of HHC36 in OCP coatings could moderately enhanced bone growth *in vivo* [288]. Using ELD technique has also satisfied the need for application of low-temperature CaP coatings [11, 134, 156]. One concern however regarding this system was that the AMP could not be included in electrolyte during ELD process due to the expensive procedure, so the AMP was loaded using simple soaking technique afterward. Moreover, the electrostatic interactions between Arg, Lys in HHC36 and phosphate groups in OCP are not strong enough to delay the release of AMP. In

addition, mechanical strength of the interface between OCP coatings and Ti implants was not robust enough [275].

Our new proposed drop-and-dry technique in this chapter, took advantages of producing different thickness of uniform CaP coatings from a few nanometres to few microns based on the repetitions of coating cycles in low temperature. Unlike the ELD, this technique allows us to incorporate the AMP into the CaP coating process. The suggested mechanism for CaP film formation in drop-and-dry technique is evaporation-induced surface crystallization [317]. A gradual evaporation of a drop of super-saturated calcium phosphate on NT would increase the saturation level of CaP and raise the CaP ion concentrations. This would initiate the nucleation of CaP crystals on the surface. The completely dried film would be like a "crust" layer of CaP, and salt crystals (e.g. NaCl, Tris, etc.). By repeating the cycles and rinsing the coating with PBS, the salts would dissolve, and CaP crystals would grow in size and thickness [317].

To further control the burst release of the AMP, we developed a technique to control both the quantity of loaded AMP, and the release profile in antimicrobial level for longer period. In this work, thin film of hydrophilic POPC was applied as a barrier layer to control the release kinetics. Mass spectrometry analysis shows much higher signal intensity for POPC in comparison to conjugated POPC-HHC36 peak at 1125 which indicates a weak interaction between two molecules. This interaction is most likely hydrogen bonds between tryptophan residues and POPC based on Grossfield *et al.* [332]. Loading POPC with HHC36 including four Try in its sequence may play a role in the observed interaction. The prominent parameters of CaP coating thickness, NT diameters, POPC concentrations, and the AMP content loaded in each layer play significant role in controlling the kinetics of release (see the appendix C). One of the major advantages to Layer-by-layer assembly of multilayer thin film systems is that the thickness

of the films can be tuned according to anodization time of NT, processing drop-and-dry cycles of CaP, and amount and concentration of deposited POPC. Since AMP can be cyclically incorporated throughout each layer, the total drug loading scales is therefore also tunable (but not independently). Yamamura *et al.* reported that application of a hydrophobic lipid layer which serves as a barrier can retard the drug release from the calcium phosphate surfaces, but only up to 72 h *in vitro* [134, 156]. Santin *et al.* studied the ability of phospholipids to bind calcium. He reported that the calcium-binding phospholipid functional groups appear to act as both crystal nucleation centers and phospholipid cross-linking domains [333].

To find the best fitting model for the release kinetics of multilayered coated Ti (POPC-20), the profile was compared to several known models such as zero-order, first-order, Higuchi, Korsmeyer-Peppas etc. (see appendix C). It was found out that the first-order ($Q_t = Q_0\, e^{-kt}$), model is the closest fits for our release kinetics. This relationship can be used to describe the drug dissolution of water-soluble drugs in porous matrices or barrier membrane coatings (Fig. 6.23).

This means that the system is concentration dependent and we expect the release of AMP follows the degradation diffusion phenomenon [334]. Upon contact with the PBS, the POPC structure can undergo swelling with consequent drug dissolution. The outermost hydrophilic POPC layer (diffusion zone) is supposed to contribute most to the initial burst release behaviour of AMP. The heterogeneous degradation pattern of the coatings in figure 6.11 suggest that POPC layer would swell due to the accumulation of PBS during initial stage which eventually leads to the mechanical failure of the coating, however further studies need to be done on the mechanism of release or details of transition [334, 335].

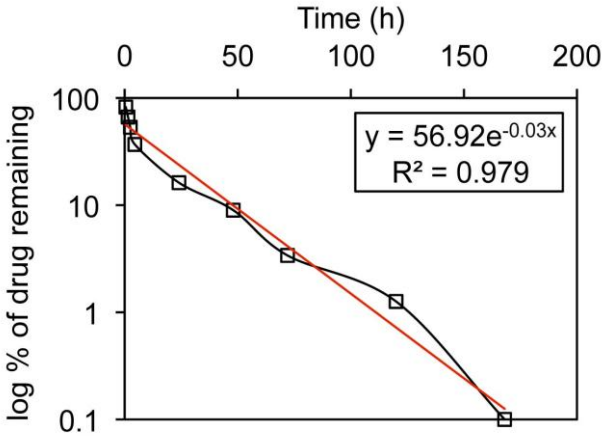

(a)

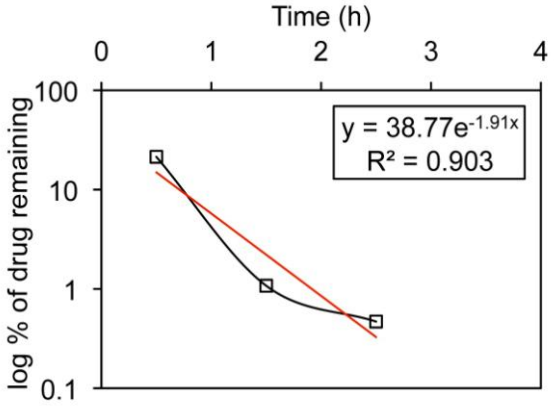

(b)

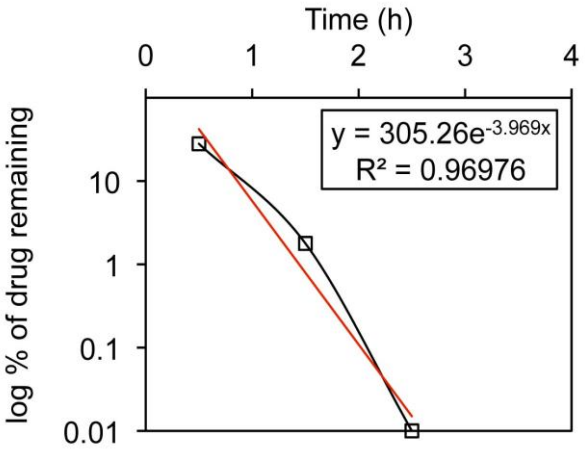

(c)

Figure 6.23. First order model fits best the release profiles (a) POPC-20 (b) CaP (c) nanotubes.

This release profile will sterilize the implant site in early stage and will effectively prevent any surviving bacteria from multiplying and re-colonizing the surface of the implant. Exposed implants to high concentration of bacteria overnight indicated the potency of eradicating infection *in vitro* for both Gram-positive and Gram-negative bacteria (Fig. 6.16,17). Cytocompatible release level of HHC36 (less than 200 μM), along with low MIC of HHC36 enable the implants to provide an antimicrobial substrate over a week while maintaining the osteointegration.

The moderate platelet activation on hydrophilic (Fig. 6.20) implant surface, and lowest platelet activation levels in the fluid phase were observed in the present study (Fig. 6.18-19). In vitro studies show favourable cell responses to charged, hydrophilic surfaces, corresponding to superior adsorption and bioactivity of adhesion proteins [336, 337]. As it is known, the initial stage of osteoconduction is the migration of osteogenic cells through a provisional fibrin matrix. Therefore at the first stage of the peri-implant bone healing, both the formation of a fibrin and the activation of blood cells entrapped at the implant interface are essential [48].

Park *et al.* reported that the implant/blood interface is composed of a fibrin film containing platelets and red blood cells [50]. Upon contact platelets should undergo the morphological and biochemical changes typical of their responses to foreign surfaces. Some of the changes that have been also observed in these *in vitro* platelet studies include adhesion, spreading and aggregation [338-340]. Yun *et al.* introduced the hemocompatibility of Ti alloys based on moderate activation of the intrinsic coagulation pathway [341]. Beside platelets, the major cells in blood which will initially come into contact with the implant surface are the RBCs. Cherkasov *et al.* Showed that HHC36 caused minimal red blood cell lysis for concentrations up to 251 μM [177]. This is confirmed by our hemolytic test. Very low hemolytic assay results

mean insignificant extent of both the dissolution of erythrocyte and the dissociation of hemoglobin. It is well known that the larger the hemolysis degree is, the poorer the biocompatibility is [342-344].

6.5 CONCLUSIONS

Thin hydrophilic films impregnated with antimicrobial peptide were constructed in layer-by-layer films on titanium implants by creating titania nanotubes, coated with calcium phosphate crystals, and topped with a thin layer of phospholipid. Antimicrobial peptide was loaded into each layer. Phopholipid layer as a barrier film successfully hindered the release of AMP. The coatings were degraded heterogeneously. First-order model is the closest fit for the release kinetics. This means that the system is concentration dependent and possibly more than one type of release mechanism could be involved. The films were effective in eradicating the *in vitro* growth of *S. aureus* and *P. Aeruginosa.* MG-63 osteoblast-like cells attached to the implants and no cytotoxicity observed after five days. The multi-layer assembly caused moderate platelet activation on implant surface with minimal activation in solution. Very low red blood cell lysis was observed on all implants, which is an indication of high biocompatibility.

CHAPTER 7 CONCLUSIONS AND PERSPECTIVES

7.1 CONCLUSIONS

This dissertation studied the processing and characteristics of two antimicrobial-containing coatings on Ti implants. *In vitro* evaluations, and *in vivo* performances in an animal model were conducted on implants and the following conclusions were made:

- Electrolytic deposition was used to prepare microporous CaP coatings on Ti implants. The XRD, and FTIR investigations indicated the coating mainly consisted of plate-like crystals of OCP with the possible inclusion of apatitic phase. The cross-sectional image of the coating showed an average thickness of ~7μm, with increased pore and crystal sizes from the bottom to the surface. The coating adhered to the Ti substrate without cracks. AMP was loaded into the coating through simple soaking technique, and using fluorometry technique the amount of loaded AMP into micro-porous CaP was determined to be as high as 9 $\mu g/cm^2$. MTT assessment of the peptide-loaded CaP coating on titanium surface showed no cytotoxicity to osteoblast-like cells. It could kill both *S. aureus* and *P. aeruginosa* bacteria within 30 min *in vitro*. When examined over longer periods (4 and 24 h), using the *lux* assay *P. aeruginosa* bacteria were still efficiently inhibited by 92% and 77% respectively. It is concluded that cationic antimicrobial peptides can be successfully loaded to the CaP-coated Ti substrates. The results indicated an interaction between the studied peptide (Tet213) and CaP coating. Although burst release of AMP was observed, the developed local delivery of antimicrobial peptides through CaP coated implant surfaces could be a potential solution for early stage peri-implant infection.

- In the second study cytotoxicity levels of tethered peptides and HHC36 (KRWWKWWRR) noncysteinylated form of Tet213 (KRWWKWWRRC) were evaluated against MG-63 osteoblast-like cells. The results showed that tethered peptides exhibit more cytotoxicity than HHC36, while the anitimicrobial activity of both peptide were almost the same when loaded on CaP coating. For the two potent antimicrobial peptides compared in this study, HHC36 and Tet213, despite their shared peptide sequence, the addition of one cysteine in Tet213 substantially lowered the minimal osteoblast toxicity concentrations from 300 to 75 μg/mL. In this work, the substantial amount of HHC36 (34.7± 4.2 $\mu g/cm^2$) loaded on CaP coating can be attributed to the affinity between the positively charged side groups of HHC36 and negatively charged phosphate groups in the CaP and the porous structure of the coating. The main goal of this study was to investigate the effect of AMP-CaP on *in vivo* bone growth. *In vitro* tests demonstrated that HHC36-CaP coating can effectively kill *S. aureus,* and *P. aeruginosa* bacteria without negatively affecting MG-63 osteoblast like cells. Study showed that osteoconductive OCP coating loaded with HHC36 AMP has the potential to serve as an antimicrobial coating while maintaining osteointegration. Loading of AMP HHC36 did not impair *in vivo* bone growth onto the implants. There was a significant bone on-growth on CaP-AMP as compared with the negative control. The ELD calcium phosphate coating and the simplicity of AMP loading provide substantial advantages for this antimicrobial coating.
- The main objective of third study was to develop Layer-by-layer assembly of multilayer thin films in order to control the prolonged AMP release on Ti implant. The multi-layers included a layer of titania nanotubes with thickness of 2 μm, with the approximately 120

nm NT diameter, and a thin layer of CaP coating topped with a POPC phospholipid barrier film. The NT was formed on Ti through anodization technique, and a new proposed drop-and-dry technique in this work, was used to produce uniform CaP coatings with the potential of creating different coating thickness from a few nanometres to few microns based on the repetitions of coating cycles. After four times treatment with super saturated calcium phosphate and washing the surface with PBS, the nanotubes were completely covered with CaP flakes that were about 1 μm long and less than 100 nm thick. The selected AMP (HHC36) was integrated into each layer using different methods and concentration. Antimicrobial peptide could be loaded into each film, with potential of altering the total amount of loaded AMP. The coatings were degraded heterogeneously when placed into aqueous environment and released their loaded AMP through diffusion. First-order model was the closest fit for the release kinetics. This means that the system is concentration dependent and possibly more than one type of release mechanism could be involved. The hydrophilic films were effective in eradicating the *in vitro* growth of *S. aureus* and *P. Aeruginosa,* without showing any cytotoxicity against MG63 osteoblast-like cells. The multi-layer assembly caused moderate platelet activation on implant surface with minimal activation in solution. Very low red blood cell lysis was observed on all implants, which is an indication of high biocompatibility.

7.2 LIMITATIONS

There are a few limitations to be addressed in order to reach antimicrobial coated implants.

- Cytotoxicity of antibacterial coatings: a key limitation for applying antimicrobial agents is the question of cytotoxicity. Many of the agents used for antibacterial coatings are toxic to mammalian cells, and this needs to be investigated more thoroughly as it might confine the range of applications for some coatings to specific medical devices. Therefore a lack of firm cytotoxicity data of different therapeutics for various cell lines is a major limitation.

- The antimicrobial coating approaches used in this thesis have been designed for the prevention of early onset infection which may occur within days to weeks after the implantation versus delayed infections which may occur months to years after surgery.

- Obtaining meaningful measurement for the strength of cell attachment to the surface is a difficult issue. A number of methods such as micromanipulation, flow cells, jet impingement and centrifugation [345] have been used which were not available in our lab facility.

- Multi drug resistant organisms are still serious limitations. It is unknown that even novel antimicrobial agents like antimicrobial peptides may cause bacteria resistance if AMP being widely used or not!

- Mechanical properties of coatings: orthopaedic implants go through aggressive insertion during surgery procedure. This may put high stress on ideal coating design, like rubbing off some parts of the coating. Hence, the bonding strength of coating to substrate is a

limitation which most of time conflicts with the degradable nature of smart coatings. For example in this thesis, microporous CaP coatings possess high osteoconductivity while carrying the AMP, but in contrast it has a low interfacial mechanical strength. Therefore developing surfaces with excellent tissue-integration ability and good antibacterial properties that have suitable mechanical strength is challenging.

- Antimicrobial agent release kinetics: there have been various ideas regarding the duration over which antibiotic release is needed. What is the ideal release profile time for the local antimicrobial delivery to inhibit bacterial adsorption and colonization? Opinions range from several hours to years and vary from device to device. The exact answer (if there is one) to this question will be useful for designing more efficient antibacterial coatings.

7.3 RECOMMENDATIONS

The following may be recommended for future studies.

- Different combinations of AMP content in layers have not been studied in this thesis (e.g. using anti-biofilm AMP and antimicrobial AMP). Altering the AMP contents will give a better impression on tuning parameters, and threshold of maximum loading within cytocompatibility range. By changing the AMP concentration in each layer, CaP coating thickness, and POPC content, it will be possible to demonstrate a pattern for AMP release kinetics.
- Another proposal is to prepare a mixture of POPC and AMP in ethanol as a ready to use spray that can be applied on CaP coated Ti at the time of surgery. This practical process will take a few minutes to set on Ti coating.
- The future antimicrobial coatings will be possibly the development and design of smart coatings that offer triggered release of antibiotics when demand is indicated by a signal,

such as a bacterial metabolite or enzyme. Design of smart coatings for triggered release may be a solution for the problems of limited release times and cell cytotoxicity.

REFRENCES

[1] Cook SD, Thomas KA, Kay JF, Jarcho M. Hydroxyapatite-coated titanium for orthopaedic implant applications. Clinical Orthopaedics and Related Research. 1988:225-43.

[2] Geetha M, Singh AK, Asokamani R, Gogia AK. Ti based biomaterials, the ultimate choice for orthopaedic implants - A review. Progress in Materials Science. 2009;54:397-425.

[3] Darouiche RO. Treatment of infections associated with surgical implants. New England Journal of Medicine. 2004;350:1422-9.

[4] Lowy FD. Medical progress - Staphylococcus aureus infections. New England Journal of Medicine.1998;339:520-32.

[5] Costerton JW, Montanaro L, Arciola CR. Biofilm in implant infections: Its production and regulation. Int J Artif Organs. 2005;28:1062-8.

[6] Schierholz JM, Beuth J. Implant infections: a haven for opportunistic bacteria. Journal of Hospital Infection. 2001;49:87-93.

[7] Costerton JW, Stewart PS, Greenberg EP. Bacterial biofilms: A common cause of persistent infections. Science. 1999;284:1318-22.

[8] Rogers SS, van der Walle C, Waigh TA. Microrheology of bacterial biofilms *in vitro*: Staphylococcus aureus and Pseudomonas aeruginosa. Langmuir. 2008;24:13549-55.

[9] Renvert S, Roos-Jansåker A-M, Lindahl C, Renvert H, Rutger Persson G. Infection at titanium implants with or without a clinical diagnosis of inflammation. Clinical Oral Implants Research. 2007;18:509-16.

[10] Sia IG, Berbari EF, Karchmer AW. Prosthetic joint infections. Infectious Disease Clinics of North America. 2005;19:885-914.

[11] Zhao L, Chu PK, Zhang Y, Wu Z. Antibacterial coatings on titanium implants. Journal of Biomedical Materials Research Part B: Applied Biomaterials. 2009;91B:470-80.

[12] Stewart PS, Costerton JW. Antibiotic resistance of bacteria in biofilms. Lancet. 2001;358:135-8.

[13] Shukla A, Fleming KE, Chuang HF, Chau TM, Loose CR, Stephanopoulos GN, et al. Controlling the release of peptide antimicrobial agents from surfaces. Biomaterials. 2010;31:2348-57.

[14] Zilberman M, Elsner JJ. Antibiotic-eluting medical devices for various applications. J Control Release. 2008;130:202-15.

[15] Vasilev K, Cook J, Griesser HJ. Antibacterial surfaces for biomedical devices. Expert Review of Medical Devices. 2009;6:553-67.

[16] Hetrick EM, Schoenfisch MH. Reducing implant-related infections: active release strategies. Chem Soc Rev. 2006;35:780-9.

[17] Gold HS, Moellering RC. Antimicrobial-Drug Resistance. New England Journal of Medicine. 1996;335:1445-53.

[18] Amyes SGB, Gemmell CG. Antibiotic resistance. Journal of Medical Microbiology. 1997;46:436-70.

[19] Kanellakopoulou K, Giamarellos-Bourboulis EJ. Carrier systems for the local delivery of antibiotics in bone infections. Drugs. 2000;59:1223-32.

[20] Price JS, Tencer AF, Arm DM, Bohach GA. Controlled release of antibiotics from coated orthopedic implants. Journal of Biomedical Materials Research. 1996;30:281-6.

[21] Stigter M, Bezemer J, de Groot K, Layrolle P. Incorporation of different antibiotics into carbonated hydroxyapatite coatings on titanium implants, release and antibiotic efficacy. J Control Release. 2004;99:127-37.

[22] Brown K, Li B, Guda T, Guelcher S, Wenke J. Local antibiotics do not inhibit bone growth when administered with growth factor. J Bone Joint Surg Br. 2011;93-B:100.

[23] Rathbone CR, Cross JD, Brown KV, Murray CK, Wenke JC. Effect of various concentrations of antibiotics on osteogenic cell viability and activity. Journal of Orthopaedic Research. 2011;29:1070-4.

[24] Brogden KA. Antimicrobial peptides: Pore formers or metabolic inhibitors in bacteria? Nature Reviews Microbiology. 2005;3:238-50.
[25] Pasupuleti M, Schmidtchen A, Malmsten M. Antimicrobial peptides: key components of the innate immune system. Critical Reviews in Biotechnology. 2012;32:143-71.
[26] Hancock REW, Lehrer R. Cationic peptides: a new source of antibiotics. Trends in Biotechnology. 1998;16:82-8.
[27] Hilpert K, Elliott M, Jenssen H, Kindrachuk J, Fjell CD, Korner J, et al. Screening and characterization of surface-tethered cationic peptides for antimicrobial activity. Chem Biol. 2009;16:58-69.
[28] Singh PK, Parsek MR, Greenberg EP, Welsh MJ. A component of innate immunity prevents bacterial biofilm development. Nature. 2002;417:552-5.
[29] Jenssen H, Hamill P, Hancock REW. Peptide antimicrobial agents. Clin Microbiol Rev. 2006;19:491-511.
[30] Hancock REW, Diamond G. The role of cationic antimicrobial peptides in innate host defences. Trends in Microbiology. 2000;8:402-10.
[31] Ganz T. The role of antimicrobial peptides in innate immunity. Integrative and Comparative Biology. 2003;43:300-4.
[32] Weiner S, Traub W, Wagner HD. Lamellar bone: Structure-function relations. Journal of Structural Biology. 1999;126:241-55.
[33] Weiner S, Wagner HD. The material bone: Structure mechanical function relations. Annual Review of Materials Science. 1998;28:271-98.
[34] Doblaré M, García JM, Gómez MJ. Modelling bone tissue fracture and healing: a review. Engineering Fracture Mechanics. 2004;71:1809-40.
[35] Miller SC. The bone lining cell – a distinct phenotype. Calcified Tissue International. 1987;41:1-5.
[36] Robling AG, Castillo AB, Turner CH. Biomechanical and molecular regulation of bone remodeling. Annual Review of Biomedical Engineering. 2006;8:455-98.
[37] Mitterhauser M, Toegel S. What to consider in the development of new bone seekers: mechanistic and tracer-related aspects. Nuclear Medicine and Biology. 2008;35:817-24.
[38] Murugan R, Ramakrishna S. Development of nanocomposites for bone grafting. Composites Science and Technology. 2005;65:2385-406.
[39] Schwarzenberg U. Lehrbuch der Anatomie des Menschen - Erster Band: Allgemeine Anatomie und Bewegungsapparat. Berlin-München, Germany1949.
[40] CD C. Clemente's anatomy dissector: : Lippincott Williams & Wilkins; 2006.
[41] St. Clair SF, Higuera C, Krebs V, Tadross NA, Dumpe J, Barsoum WK. Hip and knee arthroplasty in the geriatric population. Clinics in Geriatric Medicine. 2006;22:515-+.
[42] Jones CA, Beaupre LA, Johnston DWC, Suarez-Almazor ME. Total joint arthroplasties: Current concepts of patient outcomes after surgery. Rheumatic Disease Clinics of North America. 2007;33:71-+.
[43] Giannoudis P, Tzioupis C, Almalki T, Buckley R. Fracture heating in osteoporotic fractures: Is it really different? A basic science perspective. Injury-International Journal of the Care of the Injured. 2007;38:S90-S9.
[44] Siopack JS, Jergesen HE. Total hip-arthroplasty. Western Journal of Medicine. 1995;162:243-9.
[45] Holzwarth U. Total Hip Arthroplasty – State of the art, challenges and prospects. European Commission's Joint Research Centre Institution for Health and Consumer Protection; 2012.
[46] Gray H. Gray's Anatomy of the human body;1918.
[47] Park JY, Gemmelll CH, Davies JE. Platelet interactions with titanium: modulation of platelet activity by surface topography. Biomaterials. 2001;22:2671-82.
[48] Davies JE. Mechanisms of endosseous integration. International Journal of Prosthodontics. 1998;11:391-401.
[49] Gailit J, Clark RAF. Wound repair in the context of extracellular-matrix. Current Opinion in Cell Biology. 1994;6:717-25.

[50] Park JY, Davies JE. Red blood cell and platelet interactions with titanium implant surfaces. Clinical Oral Implants Research. 2000;11:530-9.
[51] Takagi J, Petre BM, Walz T, Springer TA. Global conformational rearrangements in integrin extracellular domains in outside-in and inside-out signaling. Cell. 2002;110:599-611.
[52] Variola F, Brunski JB, Orsini G, Tambasco de Oliveira P, Wazen R, Nanci A. Nanoscale surface modifications of medically relevant metals: state-of-the art and perspectives. Nanoscale. 2011;3:335-53.
[53] Siebers MC, ter Brugge PJ, Walboomers XF, Jansen JA. Integrins as linker proteins between osteoblasts and bone replacing materials. A critical review. Biomaterials. 2005;26:137-46.
[54] Biggs MJP, Richards RG, Dalby MJ. Nanotopographical modification: a regulator of cellular function through focal adhesions. Nanomedicine: Nanotechnology, Biology and Medicine. 2010;6:619-33.
[55] Girard PP, Cavalcanti-Adam EA, Kemkemer R, Spatz JP. Cellular chemomechanics at interfaces: sensing, integration and response. Soft Matter. 2007;3:307-26.
[56] Anselme K, Davidson P, Popa AM, Giazzon M, Liley M, Ploux L. The interaction of cells and bacteria with surfaces structured at the nanometre scale. Acta Biomaterialia. 2010;6:3824-46.
[57] Frame MC, Fincham VJ, Carragher NO, Wyke JA. V-SRC'S hold over actin and cell adhesions. Nat Rev Mol Cell Biol. 2002;3:233-45.
[58] Bustelo XR, Sauzeau V, Berenjeno IM. GTP-binding proteins of the Rho/Rac family: regulation, effectors and functions in vivo. BioEssays. 2007;29:356-70.
[59] McBeath R, Pirone DM, Nelson CM, Bhadriraju K, Chen CS. Cell Shape, cytoskeletal tension, and RhoA regulate stem cell lineage commitment. Developmental Cell. 2004;6:483-95.
[60] Dalton JE, Cook SD, Thomas KA, Kay JF. The effect of operative fit and hydroxyapatite coating on the mechanical and biological response to porous implants. Journal of Bone and Joint Surgery-American Volume. 1995;77A:97-110.
[61] Lang NP, Salvi GE, Huynh-Ba G, Ivanovski S, Donos N, Bosshardt DD. Early osseointegration to hydrophilic and hydrophobic implant surfaces in humans. Clinical Oral Implants Research. 2011;22:349-56.
[62] Puleo DA, Nanci A. Understanding and controlling the bone-implant interface. Biomaterials. 1999;20:2311-21.
[63] Friedl P, Brocker EB. The biology of cell locomotion within three-dimensional extracellular matrix. Cellular and Molecular Life Sciences. 2000;57:41-64.
[64] Terheyden H, Lang NP, Bierbaum S, Stadlinger B. Osseointegration - communication of cells. Clinical Oral Implants Research. 2012;23:1127-35.
[65] Berglundh T, Abrahamsson I, Lang NP, Lindhe J. De novo alveolar bone formation adjacent to endosseous implants - A model study in the dog. Clinical Oral Implants Research. 2003;14:251-62.
[66] Huber M, Reinisch G, Trettenhahn G, Zweymueller K, Lintner F. Presence of corrosion products and hypersensitivity-associated reactions in periprosthetic tissue after aseptic loosening of total hip replacements with metal bearing surfaces. Acta Biomaterialia. 2009;5:172-80.
[67] Iavicoli I, Gianluca F, Alessandrelli M, Rafaella C, De Santis V, Salvatori S, et al. The release of metals from metal-on-metal surface arthroplasty of the hip. Journal of Trace Elements in Medicine and Biology. 2006;20:25-31.
[68] Hennig FF, Raithel HJ, Schaller KH, Dohler JR. Nickel-concentrations, chrom-concentrations and cobalt-concentrations in human tissue and body-fluids of hip-prosthesis patients. Journal of Trace Elements and Electrolytes in Health and Disease. 1992;6:239-43.
[69] Dorr LD, Bloebaum R, Emmanual J, Meldrum R. Histologic, biochemical, and ion analysis of tissue and fluids retrieved during total hip-arthroplasty. Clinical Orthopaedics and Related Research. 1990:82-95.
[70] Thompson GJ, Puleo DA. Ti-6Al-4V ion solution inhibition of osteogenic cell phenotype as a function of differentiation timecourse in vitro. Biomaterials. 1996;17:1949-54.
[71] Thompson GJ, Puleo DA. Effects of sublethal metal-ion concentrations on osteogenic cells derived from bone-marrow stromal cells. Journal of Applied Biomaterials. 1995;6:249-58.

[72] Nichols KG, Puleo DA. Effect of metal ions on the formation and function of osteoclastic cells in vitro. Journal of Biomedical Materials Research. 1997;35:265-71.
[73] Jan Eirik Ellingsen SPL. Bio-Implant Interface: improving biomaterials and tissue reactions: CRC Press LLC; 2003.
[74] Puleo DA, Holleran LA, Doremus RH, Bizios R. Osteoblast responses to orthopedic implant materials *in vitro*. Journal of Biomedical Materials Research. 1991;25:711-23.
[75] Schwartz Z, Nasazky E, Boyan BD. Surface microtopography regulates osteointegration: the role of implant surface microtopography in osteointegration. The Alpha omegan. 2005;98:9-19.
[76] Grizon F, Aguado E, Hure G, Basle MF, Chappard D. Enhanced bone integration of implants with increased surface roughness: a long term study in the sheep. Journal of Dentistry. 2002;30:195-203.
[77] Gotman I. Characteristics of metals used in implants. Journal of Endourology. 1997;11:383-9.
[78] Head WC, Bauk DJ, Emerson RH. Titanium as the material of choice for cementless femoral components in total hip-arthroplasty. Clinical Orthopaedics and Related Research. 1995:85-90.
[79] Jinno T, Goldberg VM, Davy D, Stevenson S. Osseointegration of surface-blasted implants made of titanium alloy and cobalt-chromium alloy in a rabbit intramedullary model. Journal of Biomedical Materials Research. 1998;42:20-9.
[80] Lampin M, WarocquierClerout R, Legris C, Degrange M, SigotLuizard MF. Correlation between substratum roughness and wettability, cell adhesion, and cell migration. Journal of Biomedical Materials Research. 1997;36:99-108.
[81] Lim YJ, Oshida Y, Andres CJ, Barco MT. Surface characterizations of variously treated titanium materials. International Journal of Oral & Maxillofacial Implants. 2001;16:333-42.
[82] Lincks J, Boyan BD, Blanchard CR, Lohmann CH, Liu Y, Cochran DL, et al. Response of MG63 osteoblast-like cells to titanium and titanium alloy is dependent on surface roughness and composition. Biomaterials. 1998;19:2219-32.
[83] Boyan BD, Hummert TW, Dean DD, Schwartz Z. Role of material surfaces in regulating bone and cartilage cell response. Biomaterials. 1996;17:137-46.
[84] Junker R, Dimakis A, Thoneick M, Jansen JA. Effects of implant surface coatings and composition on bone integration: a systematic review. Clinical Oral Implants Research. 2009;20:185-206.
[85] Zhu X, Chen J, Scheideler L, Reichl R, Geis-Gerstorfer J. Effects of topography and composition of titanium surface oxides on osteoblast responses. Biomaterials. 2004;25:4087-103.
[86] Brunette DM. The effects of implant surface topography on the behavior of cells. The International journal of oral & maxillofacial implants. 1988;3:231-46.
[87] Bowers KT, Keller JC, Randolph BA, Wick DG, Michaels CM. Optimization of surface micromorphology for enhanced osteoblast responses in vitro. The International journal of oral & maxillofacial implants. 1992;7:302-10.
[88] Kieswetter K, Schwartz Z, Hummert TW, Cochran DL, Simpson J, Dean DD, et al. Surface roughness modulates the local production of growth factors and cytokines by osteoblast-like MG-63 cells. Journal of Biomedical Materials Research. 1996;32:55-63.
[89] Martin JY, Schwartz Z, Hummert TW, Schraub DM, Simpson J, Lankford J, et al. Effect of titanium surface-roughness on proliferation, differentiation, and protein-synthesis of human osteoblast-like cells (MG63). Journal of Biomedical Materials Research. 1995;29:389-401.
[90] Wiskott HWA, Belser UC. Lack of integration of smooth titanium surfaces: a working hypothesis based on strains generated in the surrounding bone. Clinical Oral Implants Research. 1999;10:429-44.
[91] Boyan BD, Batzer R, Kieswetter K, Liu Y, Cochran DL, Szmuckler-Moncler S, et al. Titanium surface roughness alters responsiveness of MG63 osteoblast-like cells to 1 alpha,25-(OH)(2)D3. Journal of Biomedical Materials Research. 1998;39:77-85.
[92] You MH, Kwak MK, Kim DH, Kim K, Levchenko A, Kim DY, et al. Synergistically enhanced osteogenic differentiation of human mesenchymal stem cells by culture on nanostructured surfaces with induction media. Biomacromolecules. 2010;11:1856-62.

[93] MacDonald DE, Deo N, Markovic B, Stranick M, Somasundaran P. Adsorption and dissolution behavior of human plasma fibronectin on thermally and chemically modified titanium dioxide particles. Biomaterials. 2002;23:1269-79.
[94] Liao HH, Andersson AS, Sutherland D, Petronis S, Kasemo B, Thomsen P. Response of rat osteoblast-like cells to microstructured model surfaces in vitro. Biomaterials. 2003;24:649-54.
[95] Webster TJ, Ergun C, Doremus RH, Siegel RW, Bizios R. Enhanced functions of osteoblasts on nanophase ceramics. Biomaterials. 2000;21:1803-10.
[96] Webster TJ, Ejiofor JU. Increased osteoblast adhesion on nanophase metals: Ti, Ti6Al4V, and CoCrMo. Biomaterials. 2004;25:4731-9.
[97] Kieswetter K, Schwartz Z, Dean DD, Boyan BD. The role of implant surface characteristics in the healing of bone. Critical Reviews in Oral Biology & Medicine. 1996;7:329-45.
[98] Kennedy SB, Washburn NR, Simon CG, Amis EJ. Combinatorial screen of the effect of surface energy on fibronectin-mediated osteoblast adhesion, spreading and proliferation. Biomaterials. 2006;27:3817-24.
[99] Barber TA, Golledge SL, Castner DG, Healy KE. Peptide-modified p(AAm-co-EG/AAc) IPNs grafted to bulk titanium modulate osteoblast behavior in vitro. J Biomed Mater Res Part A. 2003;64A:38-47.
[100] Lu X, Leng Y, Zhang XD, Xu JR, Qin L, Chan CW. Comparative study of osteoconduction on micromachined and alkali-treated titanium alloy surfaces in vitro and in vivo. Biomaterials. 2005;26:1793-801.
[101] Son WW, Zhu XL, Shin HI, Ong JL, Kim KH. In vivo histological response to anodized and anodized/hydrothermally treated titanium implants. J Biomed Mater Res Part B. 2003;66B:520-5.
[102] Basle MF, Chappard D, Grizon F, Filmon R, Delecrin J, Daculsi G, et al. Osteoclastic resorption of Ca-P biomaterials implanted in rabbit bone. Calcified Tissue International. 1993;53:348-56.
[103] Rashmirraven AM, Richardson DC, Aberman HM, Deyoung DJ. The response of cancellous and cortical canine bone to hydroxylapatite-coated and uncoated titanium rods. Journal of Applied Biomaterials. 1995;6:237-42.
[104] Gil FJ, Padros A, Manero JM, Aparicio C, Nilsson M, Planell JA. Growth of bioactive surfaces on titanium and its alloys for orthopaedic and dental implants. Materials Science & Engineering C-Biomimetic and Supramolecular Systems. 2002;22:53-60.
[105] Webster's medical dictionary.
[106] Larsen LH, Lange J, Xu Y, Schønheyder HC. Optimizing culture methods for diagnosis of prosthetic joint infections: a summary of modifications and improvements reported since 1995. Journal of Medical Microbiology. 2012;61:309-16.
[107] Hudetz D, Rod E, Radic A, Ivkovic A. Diagnosis and treatment of peri-prosthetic infections in total hip replacement. Med Glas. 2012;9:152-9.
[108] Rodriguez-Merchan EC. The infected knee prosthesis. Eur J Orthop Surg Traumatol. 2011;21:467-78.
[109] Roy M, Bandyopadhyay A, Bose S. *In vitro* antimicrobial and biological properties of laser assisted tricalcium phosphate coating on titanium for load bearing implant. Mater Sci Eng C-Mater Biol Appl. 2009;29:1965-8.
[110] Chen W, Liu Y, Courtney HS, Bettenga M, Agrawal CM, Bumgardner JD, et al. *In vitro* anti-bacterial and biological properties of magnetron co-sputtered silver-containing hydroxyapatite coating. Biomaterials. 2006;27:5512-7.
[111] Rohde H, Burandt EC, Siemssen N, Frommelt L, Burdelski C, Wurster S, et al. Polysaccharide intercellular adhesin or protein factors in biofilm accumulation of Staphylococcus epidermidis and Staphylococcus aureus isolated from prosthetic hip and knee joint infections. Biomaterials. 2007;28:1711-20.
[112] Ewald A, Gluckermann SK, Thull R, Gbureck U. Antimicrobial titanium/silver PVD coatings on titanium. Biomed Eng Online. 2006;5.
[113] Darouiche RO. Current concepts - Treatment of infections associated with surgical implants. N Engl J Med. 2004;350:1422-9.

[114] Total hip and total knee replacements in Canada. Canadian Institute for Health Information, Report; 2005.
[115] Sculco TP. The economic-impact of infected joint arthroplasty. Orthopedics. 1995;18:871-3.
[116] Bullough PG. Metallosis. Journal of Bone and Joint Surgery-British Volume. 1994;76B:687-8.
[117] Cobo J, Del Pozo JL. Prosthetic joint infection: diagnosis and management. Expert Rev Anti-Infect Ther. 2011;9:787-802.
[118] Masterson EL, Masri BA, Duncan CP. Instructional course lectures, The American Academy of Orthopaedic Surgeons - Treatment of infection at the site of total hip replacement. J Bone Joint Surg Am. 1997;79:1740-9.
[119] Antoci V, Adams CS, Parvizi J, Davidson HM, Composto RJ, Freeman TA, et al. The inhibition of Staphylococcus epidermidis biofilm formation by vancomycin-modified titanium alloy and implications for the treatment of periprosthetic infection. Biomaterials. 2008;29:4684-90.
[120] Toms AD, Davidson D, Masri BA, Duncan CP. The management of peri-prosthetic infection in total joint arthroplasty. J Bone Joint Surg-Br Vol. 2006;88B:149-55.
[121] Arica MY, Tuglu D, Basar MM, Kilic D, Bayramoglu G, Batislam E. Preparation and characterization of infection-resistant antibiotics-releasing hydrogels rods of poly hydroxyethyl methacrylate-co-(poly(ethylene glycol)-methacrylate : Biomedical application in a novel rabbit penile prosthesis model. J Biomed Mater Res Part B. 2008;86B:18-28.
[122] Campoccia D, Montanaro L, Arciola CR. The significance of infection related to orthopedic devices and issues of antibiotic resistance. Biomaterials. 2006;27:2331-9.
[123] Geipel U. Pathogenic organisms in hip joint infections. Int J Med Sci. 2009;6:234-40.
[124] Ceri H, Olson ME, Stremick C, Read RR, Morck D, Buret A. The calgary biofilm device: New technology for rapid determination of antibiotic susceptibilities of bacterial biofilms. J Clin Microbiol. 1999;37:1771-6.
[125] Montanaro L, Speziale P, Campoccia D, Ravaioli S, Cangini I, Pietrocola G, et al. Scenery of Staphylococcus implant infections in orthopedics. Future Microbiol. 2011;6:1329-49.
[126] van de Belt H, Neut D, Schenk W, van Horn JR, van der Mei HC, Busscher HJ. Infection of orthopedic implants and the use of antibiotic-loaded bone cements - A review. Acta Orthopaedica Scandinavica. 2001;72:557-71.
[127] Lombardi AV, Karnes JM, Berend KR. A motion maintaining antibiotic delivery system. J Arthroplast. 2007;22:50-5.
[128] Trampuz A, Zimmerli W. Antimicrobial agents in orthopaedic surgery - Prophylaxis and treatment. Drugs. 2006;66:1089-105.
[129] Engesaeter LB, Lie SA, Espehaug B, Furnes O, Vollset SE, Havelin LI. Antibiotic prophylaxis in total hip arthroplasty - Effects of antibiotic prophylaxis systemically and in bone cement on the revision rate of 22,170 primary hip replacements followed 0-14 years in the Norwegian Arthroplasty Register. Acta Orthopaedica Scandinavica. 2003;74:644-51.
[130] Nowinski RJ, Gillespie RJ, Shishani Y, Cohen B, Walch G, Gobezie R. Antibiotic-loaded bone cement reduces deep infection rates for primary reverse total shoulder arthroplasty: a retrospective, cohort study of 501 shoulders. Journal of Shoulder and Elbow Surgery. 2012;21:324-8.
[131] Tabutin J, D'Ollonne T, Cambas PM. Antibiotic addition to cement - is it beneficial? Hip Int. 2012;22:9-12.
[132] Pioletti DP, Gauthier O, Stadelmann VA, Bujoli B, Guicheux J, Zambelli P-Y, et al. Orthopedic implant used as drug delivery system: clinical situation and state of the research. Current Drug Delivery. 2008;5:59-63.
[133] Suh DY, Boden SD, Louis-Ugbo J, Mayr M, Murakami H, Kim HS, et al. Delivery of recombinant human bone morphogenetic protein-2 using a compression-resistant matrix in posterolateral spine fusion in the rabbit and in the non-human primate. Spine. 2002;27:353-60.
[134] Radin S, Campbell JT, Ducheyne P, Cuckler JM. Calcium phosphate ceramic coatings as carriers of vancomycin. Biomaterials. 1997;18:777-82.
[135] Walenkamp G, Kleijn LLA, de Leeuw M. Osteomyelitis treated with gentamicin-PMMA beads - 100 patients followed for 1-12 years. Acta Orthopaedica Scandinavica. 1998;69:518-22.

[136] Stabile DE, Jacobs AM. Local antibiotic-treatment of soft-tissue and bone-infections of the foot. Journal of the American Podiatric Medical Association. 1990;80:345-53.
[137] Lucke M, Schmidmaier G, Sadoni S, Wildemann B, Schiller R, Haas NP, et al. Gentamicin coating of metallic implants reduces implant-related osteomyelitis in rats. Bone. 2003;32:521-31.
[138] Harris LG, Mead L, Muller-Oberlander E, Richards RG. Bacteria and cell cytocompatibility studies on coated medical grade titanium surfaces. J Biomed Mater Res Part A. 2006;78A:50-8.
[139] Kim WH, Lee SB, Oh KT, Moon SK, Kim KM, Kim KN. The release behavior of CHX from polymer-coated titanium surfaces. Surface and Interface Analysis. 2008;40:202-4.
[140] Zhang F, Zhang ZB, Zhu XL, Kang ET, Neoh KG. Silk-functionalized titanium surfaces for enhancing osteoblast functions and reducing bacterial adhesion. Biomaterials. 2008;29:4751-9.
[141] Harris LG, Tosatti S, Wieland M, Textor M, Richards RG. Staphylococcus aureus adhesion to titanium oxide surfaces coated with non-functionalized and peptide-functionalized poly(L-lysine)-grafted-poly(ethylene glycol) copolymers. Biomaterials. 2004;25:4135-48.
[142] Chua PH, Neoh KG, Kang ET, Wang W. Surface functionalization of titanium with hyaluronic acid/chitosan polyelectrolyte multilayers and RGD for promoting osteoblast functions and inhibiting bacterial adhesion. Biomaterials. 2008;29:1412-21.
[143] Gao G, Lange D, Hilpert K, Kindrachuk J, Zou Y, Cheng JTJ, et al. The biocompatibility and biofilm resistance of implant coatings based on hydrophilic polymer brushes conjugated with antimicrobial peptides. Biomaterials. 2011;32:3899-909.
[144] Rai M, Yadav A, Gade A. Silver nanoparticles as a new generation of antimicrobials. Biotechnology Advances. 2009;27:76-83.
[145] Zhao LZ, Wang HR, Huo KF, Cui LY, Zhang WR, Ni HW, et al. Antibacterial nano-structured titania coating incorporated with silver nanoparticles. Biomaterials. 2011;32:5706-16.
[146] Srinivasan A, Karchmer T, Richards A, Song X, Perl TM. A prospective trial of a novel, silicone-based, silver-coated Foley catheter for the prevention of nosocomial urinary tract infections. Infection Control and Hospital Epidemiology. 2006;27:38-43.
[147] Hardes J, Ahrens H, Gebert C, Streitbuerger A, Buerger H, Erren M, et al. Lack of toxicological side-effects in silver-coated megaprostheses in humans. Biomaterials. 2007;28:2869-75.
[148] Schrand AM, Braydich-Stolle LK, Schlager JJ, Dai L, Hussain SM. Can silver nanoparticles be useful as potential biological labels? Nanotechnology. 2008;19.
[149] Trop M, Novak M, Rodl S, Hellbom B, Kroell W, Goessler W. Silver coated dressing Acticoat caused raised liver enzymes and argyria-like symptoms in burn patient. Journal of Trauma-Injury Infection and Critical Care. 2006;60:648-52.
[150] Jose B, Antoci Jr V, Zeiger AR, Wickstrom E, Hickok NJ. Vancomycin covalently bonded to titanium beads kills Staphylococcus aureus. Chem Biol. 2005;12:1041-8.
[151] Edupuganti OP, Antoci V, King SB, Jose B, Adams CS, Parvizi J, et al. Covalent bonding of vancomycin to Ti6Al4V alloy pins provides long-term inhibition of Staphylococcus aureus colonization. Bioorg Med Chem Lett. 2007;17:2692-6.
[152] Jose B, Antoci V, Zeiger AR, Wickstrom E, Hickok NJ. Vancomycin covalently bonded to titanium beads kills Staphylococcus aureus. Chem Biol. 2005;12:1041-8.
[153] Gollwitzer H, Ibrahim K, Meyer H, Mittelmeier W, Busch R, Stemberger A. Antibacterial poly(D,L-lactic acid) coating of medical implants using a biodegradable drug delivery technology. J Antimicrob Chemother. 2003;51:585-91.
[154] Alt V, Bitschnau A, Osterling J, Sewing A, Meyer C, Kraus R, et al. The effects of combined gentamicin-hydroxyapatite coating for cementless joint prostheses on the reduction of infection rates in a rabbit infection prophylaxis model. Biomaterials. 2006;27:4627-34.
[155] Campbell AA, Song L, Li XS, Nelson BJ, Bottoni C, Brooks DE, et al. Development, characterization, and anti-microbial efficacy of hydroxyapatite-chlorhexidine coatings produced by surface-induced mineralization. Journal of Biomedical Materials Research. 2000;53:400-7.
[156] Yamamura K, Iwata H, Yotsuyanagi T. Synthesis of antibiotic-loaded hydroxyapatite beads and in vitro drug release testing. Journal of Biomedical Materials Research. 1992;26:1053-64.

[157] Stigter M, de Groot K, Layrolle P. Incorporation of tobramycin into biomimetic hydroxyapatite coating on titanium. Biomaterials. 2002;23:4143-53.
[158] Tsuchiya H, Shirai T, Nishida H, Murakami H, Kabata T, Yamamoto N, et al. Innovative antimicrobial coating of titanium implants with iodine. Journal of orthopaedic science : official journal of the Japanese Orthopaedic Association. 2012;17:595-604.
[159] Statz AR, Park JP, Chongsiriwatana NP, Barron AE, Messersmith PB. Surface-immobilised antimicrobial peptoids. Biofouling. 2008;24:439-48.
[160] Popat KC, Eltgroth M, LaTempa TJ, Grimes CA, Desai TA. Decreased Staphylococcus epidermis adhesion and increased osteoblast functionality on antibiotic-loaded titania nanotubes. Biomaterials. 2007;28:4880-8.
[161] Wan YZ, Raman S, He F, Huang Y. Surface modification of medical metals by ion implantation of silver and copper. Vacuum. 2007;81:1114-8.
[162] Wan YZ, Xiong GY, Liang H, Raman S, He F, Huang Y. Modification of medical metals by ion implantation of copper. Appl Surf Sci. 2007;253:9426-9.
[163] Finke B, Polak M, Hempel F, Rebl H, Zietz C, Stranak V, et al. Antimicrobial potential of copper-containing titanium surfaces generated by ion implantation and dual high power impulse magnetron sputtering. Advanced Engineering Materials. 2012;14:B224-B30.
[164] Yoshinari M, Oda Y, Kato T, Okuda K. Influence of surface modifications to titanium on antibacterial activity in vitro. Biomaterials. 2001;22:2043-8.
[165] Gallardo-Moreno AM, Pacha-Olivenza MA, Saldana L, Perez-Giraldo C, Bruque JM, Vilaboa N, et al. *In vitro* biocompatibility and bacterial adhesion of physico-chemically modified Ti6Al4V surface by means of UV irradiation. Acta Biomaterialia. 2009;5:181-92.
[166] Ginebra MP, Traykova T, Planell JA. Calcium phosphate cements as bone drug delivery systems: A review. J Control Release. 2006;113:102-10.
[167] Josse S, Faucheux C, Soueidan A, Grimandi G, Massiot D, Alonso B, et al. Chemically modified calcium phosphates as novel materials for bisphosphonate delivery. Advanced Materials. 2004;16:1423-1427.
[168] Garbuz DS, Hu Y, Kim WY, Duan K, Masri BA, OxIand TR, et al. Enhanced gap filling and osteoconduction associated with alendronate-calcium phosphate-coated porous tantalum. Journal of Bone and Joint Surgery-American Volume. 2008;90A:1090-100.
[169] Wu P, Grainger DW. Drug/device combinations for local drug therapies and infection prophylaxis. Biomaterials. 2006;27:2450-67.
[170] Radin S, Ducheyne P. Controlled release of vancomycin from thin sol-gel films on titanium alloy fracture plate material. Biomaterials. 2007;28:1721-9.
[171] Darouiche RO, Green G, Mansouri MD. Antimicrobial activity of antiseptic-coated orthopaedic devices. Int J Antimicrob Agents. 1998;10:83-6.
[172] Rotem S, Mor A. Antimicrobial peptide mimics for improved therapeutic properties. Biochimica et Biophysica Acta (BBA) - Biomembranes. 2009;1788:1582-92.
[173] Hancock REW. Cationic peptides: effectors in innate immunity and novel antimicrobials. The Lancet Infectious Diseases. 2001;1:156-64.
[174] Brown KL, Hancock REW. Cationic host defense (antimicrobial) peptides. Innate immunity / Antigen processing and recognition. 2006;18:24-30.
[175] Hale JDF, Hancock REW. Alternative mechanisms of action of cationic antimicrobial peptides on bacteria. Expert Rev Anti-Infect Ther. 2007;5:951-9.
[176] Ingham AB, Moore RJ. Recombinant production of antimicrobial peptides in heterologous microbial systems. Biotechnology and applied biochemistry. 2007;47:1-9.
[177] Wu M, Hancock REW. Improved derivatives of bactenecin, a cyclic dodecameric antimicrobial cationic peptide. Antimicrob Agents Chemother. 1999;43:1274-6.
[178] Easton DM, Nijnik A, Mayer ML, Hancock REW. Potential of immunomodulatory host defense peptides as novel anti-infectives. Trends in Biotechnology. 2009;27:582-90.

[179] Cherkasov A, Hilpert K, Jenssen Hv, Fjell CD, Waldbrook M, Mullaly SC, et al. Use of artificial intelligence in the design of small peptide antibiotics effective against a broad spectrum of highly antibiotic-resistant superbugs. ACS Chemical Biology. 2008;4:65-74.
[180] Som A, Vemparala S, Ivanov I, Tew GN. Synthetic mimics of antimicrobial peptides. Biopolymers - Peptide Science Section. 2008;90:83-93.
[181] Hancock REW, Patrzykat A. Clinical development of cationic antimicrobial peptides: From Natural to Novel Antibiotics. Current Drug Targets - Infectious Disorsers. 2002;2:79-83.
[182] Hancock REW, Brown KL, Mookherjee N. Host defence peptides from invertebrates - emerging antimicrobial strategies. Immunobiology. 2006;211:315-22.
[183] Glukhov E, Stark M, Burrow LL, Deber CM. Basis for selectivity of cationic antimicrobial peptides for bacterial Versus mammalian membranes. American Society for Biochemistry and Molecular Biology; 2005.
[184] Mello Charlene M, Soares Jason W. Membrane selectivity of antimicrobial peptides. Microbial Surfaces: American Chemical Society; 2008. p. 52-62.
[185] Teixeira V, Feio MJ, Bastos M. Role of lipids in the interaction of antimicrobial peptides with membranes. Progress in Lipid Research. 2012;51:149-77.
[186] Zasloff M. Antimicrobial peptides of multicellular organisms. Nature. 2002;415:389-95.
[187] Han Y, Xu K, Lu J. Morphology and composition of hydroxyapatite coatings prepared by hydrothermal treatment on electrodeposited brushite coatings. Journal of Materials Science: Materials in Medicine. 1999;10:243-8.
[188] Betty Leon JAJ. Thin calcium phosphate coatings for medical implants: Springer Science; 2009.
[189] Suchanek W, Yoshimura M. Processing and properties of hydroxyapatite-based biomaterials for use as hard tissue replacement implants. J Mater Res. 1998;13:94-117.
[190] Bertazzo S, Zambuzzi WF, Campos DDP, Ogeda TL, Ferreira CV, Bertran CA. Hydroxyapatite surface solubility and effect on cell adhesion. Colloids and Surfaces B-Biointerfaces. 2010;78:177-84.
[191] Dorozhkin SV. Bioceramics of calcium orthophosphates. Biomaterials. 2010;31:1465-85.
[192] K D. Bisphosphonate-containing coatings for bone implants: University of British Columbia; 2007.
[193] Kuo MC, Yen SK. The process of electrochemical deposited hydroxyapatite coatings on biomedical titanium at room temperature. Materials Science & Engineering C-Biomimetic and Supramolecular Systems. 2002;20:153-60.
[194] Fan YW, Duan K, Wang RZ. A composite coating by electrolysis-induced collagen self-assembly and calcium phosphate mineralization. Biomaterials. 2005;26:1623-32.
[195] Tarasevich BJ, Howard CJ, Larson JL, Snead ML, Simmer JP, Paine M, et al. The nucleation and growth of calcium phosphate by amelogenin. Journal of Crystal Growth. 2007;304:407-15.
[196] Shujie L, Racquel ZL, John PL. Adherent octacalciumphosphate coating on titanium alloy using modulated electrochemical deposition method. J Biomed Mater Res Part A. 2003;66A:819-28.
[197] Rakngarm A, Mutoh Y. Electrochemical depositions of calcium phosphate film on commercial pure titanium and Ti-6Al-4V in two types of electrolyte at room temperature. Materials Science & Engineering C-Biomimetic and Supramolecular Systems. 2009;29:275-83.
[198] Lu X, Zhao Z, Leng Y. Calcium phosphate crystal growth under controlled atmosphere in electrochemical deposition. Journal of Crystal Growth. 2005;284:506-16.
[199] Peng P, Kumar S, Voelcker NH, Szili E, Smart RSC, Griesser HJ. Thin calcium phosphate coatings on titanium by electrochemical deposition in modified simulated body fluid. J Biomed Mater Res Part A. 2006;76A:347-55.
[200] Montero-Ocampo C, Villegas D, Veleva L. Electrochemical assisted deposition of calcium phosphate coatings for orthopaedic applications. Surface Engineering. 2008;24:18-22.
[201] Kawashita M, Itoh S, Miyamoto K, Takaoka GH. Apatite formation on titanium substrates by electrochemical deposition in metastable calcium phosphate solution. Journal of Materials Science: Materials in Medicine. 2008;19:137-42.
[202] Montero-Ocampo C, Villegas D, Veleva L. Controlled potential electrodeposition of calcium phosphate on Ti6Al4V. Journal of The Electrochemical Society. 2005;152:C692-C6.

[203] Miao SD, Weng WJ, Li ZL, Cheng K, Du PY, Shen G, et al. Electrolytic deposition of octacalcium phosphate/collagen composite coating on titanium alloy. Journal of Materials Science-Materials in Medicine. 2009;20:131-4.
[204] Duan K, Fan YW, Wang RZ. Electrolytic deposition of calcium etidronate drug coating on titanium substrate. J Biomed Mater Res Part B. 2005;72B:43-51.
[205] Miao S, Weng W, Li Z, Cheng K, Du P, Shen G, et al. Electrolytic deposition of octacalcium phosphate/collagen composite coating on titanium alloy. Journal of Materials Science-Materials in Medicine. 2009;20:131-4.
[206] Monma H. Electrolytic depositions of calcium phosphates on substrate. Journal of Materials Science. 1994;29:949-53.
[207] Wang J, Layrolle P, Stigter M, de Groot K. Biomimetic and electrolytic calcium phosphate coatings on titanium alloy: physicochemical characteristics and cell attachment. Biomaterials. 2004;25:583-92.
[208] Wang JW, van Apeldoorn A, de Groot K. Electrolytic deposition of calcium phosphate/chitosan coating on titanium alloy: Growth kinetics and influence of current density, acetic acid, and chitosan. J Biomed Mater Res Part A. 2006;76A:503-11.
[209] Wang SH, Shih WJ, Li WL, Hon MH, Wang MC. Morphology of calcium phosphate coatings deposited on a Ti-6Al-4V substrate by an electrolytic method under 80 Torr. Journal of the European Ceramic Society. 2005;25:3287-92.
[210] Roessler S, Born R, Scharnweber D, Worch H, Sewing A, Dard M. Biomimetic coatings functionalized with adhesion peptides for dental implants. Journal of Materials Science: Materials in Medicine. 2001;12:871-7.
[211] Koutsoukos P, Amjad Z, Tomson MB, Nancollas GH. Crystallization of calcium phosphates – constant composition study. Journal of the American Chemical Society. 1980;102:1553-7.
[212] Radin SR, Ducheyne P. The effect of calcium-phosphate ceramic composition and structure on in vitro behavior. II. precipitation. Journal of Biomedical Materials Research. 1993;27:1461-.
[213] Shi SL, Pan W, Fang MH, Fang ZY. Reinforcement of hydroxyapatite bioceramic by addition of Ti3SiC2. Journal of the American Ceramic Society. 2006;89:743-5.
[214] Chen ZF, Darvell BW, Leung VWH. Hydroxyapatite solubility in simple inorganic solutions. Archives of Oral Biology. 2004;49:359-67.
[215] Dorozhkin SV. Calcium Orthophosphates as bioceramics: State of the Art. Journal of Functional Biomaterials. 2010;1:22-107.
[216] Markovic M, Fowler BO, Tung MS. Preparation and comprehensive characterization of a calcium hydroxyapatite reference material. Journal of Research of the National Institute of Standards and Technology. 2004;109:553-68.
[217] Tas AC. Granules of brushite and octacalcium phosphate from marble. Journal of the American Ceramic Society. 2011;94:3722-6.
[218] Stayton PS, Drobny GP, Shaw WJ, Long JR, Gilbert M. Molecular recognition at the protein-hydroxyapatite interface. Critical Reviews in Oral Biology & Medicine. 2003;14:370-6.
[219] Luo QL, Andrade JD. Cooperative adsorption of proteins onto hydroxyapatite. Journal of Colloid and Interface Science. 1998;200:104-13.
[220] Glant TT, Jacobs JJ, Molnar G, Shanbhag AS, Valyon M, Galante JO. Bone-resorption activity of particulate-stimulated macrophages. Journal of Bone and Mineral Research. 1993;8:1071-9.
[221] Kay MI, and Young, R. A.. Crystal structure of hydroxyapatite. Nature. 1964;204.
[222] Kawasaki T. Theory of chromatography on hydroxyapatite columns with small loads : V. Determination of the adsorption energy of the [epsilon]-amino group of poly-l-lysine and the manner of adsorption of the molecule. Journal of Chromatography A. 1978;157:7-42.
[223] Harding IS, Rashid N, Hing KA. Surface charge and the effect of excess calcium ions on the hydroxyapatite surface. Biomaterials. 2005;26:6818-26.
[224] Janusz W, Skwarek E, Pasieczna-Patkowska S, Slosarczyk A, Paszkiewicz Z, Rapacz-Kmita A. A study of surface properties of calcium phosphate by means of photoacoustic spectroscopy (FT-

IR/PAS), potentiometric titration and electrophoretic measurements. European Physical Journal-Special Topics. 2008;154:329-33.
[225] Lee W-H, Zavgorodniy AV, Loo C-Y, Rohanizadeh R. Synthesis and characterization of hydroxyapatite with different crystallinity: Effects on protein adsorption and release. J Biomed Mater Res Part A. 2012;100A:1539-49.
[226] Weiger MC, Park JJ, Roy MD, Stafford CM, Karim A, Becker ML. Quantification of the binding affinity of a specific hydroxyapatite binding peptide. Biomaterials.31:2955-63.
[227] Gungormus M, Fong H, Kim IW, Evans JS, Tamerler C, Sarikaya M. Regulation of *in vitro* calcium phosphate mineralization by combinatorially selected hydroxyapatite-binding peptides. Biomacromolecules. 2008;9:966-73.
[228] Tamerler C, Sarikaya M. Genetically designed peptide-based molecular Materials. Acs Nano. 2009;3:1606-15.
[229] Tamerler C, Sarikaya M. Molecular biomimetics: nanotechnology and bionanotechnology using genetically engineered peptides. Philosophical Transactions of the Royal Society A: Mathematical, Physical and Engineering Sciences. 2009;367:1705-26.
[230] Candan T, Dmitriy K, Mustafa G, Turgay K, Oren EE, Marketa H, et al. Molecular biomimetics: GEPI-based biological routes to technology. Peptide Science.94:78-94.
[231] Sarikaya M, Tamerler C, Jen AKY, Schulten K, Baneyx F. Molecular biomimetics: nanotechnology through biology. Nature Materials. 2003;2:577-85.
[232] Khang D, Lu J, Yao C, Haberstroh KM, Webster TJ. The role of nanometer and sub-micron surface features on vascular and bone cell adhesion on titanium. Biomaterials. 2008;29:970-83.
[233] Divya Rani VV, Vinoth-Kumar L, Anitha VC, Manzoor K, Deepthy M, Shantikumar VN. Osteointegration of titanium implant is sensitive to specific nanostructure morphology. Acta Biomaterialia. 2012;8:1976-89.
[234] Brunette DM, Chehroudi B. The effects of the surface topography of micromachined titanium substrata on cell behavior in vitro and in vivo. Journal of Biomechanical Engineering-Transactions of the Asme. 1999;121:49-57.
[235] Roy P, Berger S, Schmuki P. TiO2 nanotubes: Synthesis and applications. Angewandte Chemie International Edition. 2011;50:2904-39.
[236] Ma MH, Kazemzadeh-Narbat M, Hui Y, Lu SS, Ding CF, Chen DDY, et al. Local delivery of antimicrobial peptides using self-organized TiO2 nanotube arrays for peri-implant infections. J Biomed Mater Res Part A. 2012;100A:278-85.
[237] Brammer KS, Oh S, Cobb CJ, Bjursten LM, Heyde Hvd, Jin S. Improved bone-forming functionality on diameter-controlled TiO2 nanotube surface. Acta Biomaterialia. 2009;5:3215-23.
[238] Lakshmi BB, Patrissi CJ, Martin CR. Sol-gel template synthesis of semiconductor oxide micro- and nanostructures. Chemistry of Materials. 1997;9:2544-50.
[239] Miao Z, Xu DS, Ouyang JH, Guo GL, Zhao XS, Tang YQ. Electrochemically induced sol-gel preparation of single-crystalline TiO2 nanowires. Nano Letters. 2002;2:717-20.
[240] Gong D, Grimes CA, Varghese OK, Hu WC, Singh RS, Chen Z, et al. Titanium oxide nanotube arrays prepared by anodic oxidation. J Mater Res. 2001;16:3331-4.
[241] Popat KC, Leoni L, Grimes CA, Desai TA. Influence of engineered titania nanotubular surfaces on bone cells. Biomaterials. 2007;28:3188-97.
[242] Kim SE, Lim JH, Lee SC, Nam S-C, Kang H-G, Choi J. Anodically nanostructured titanium oxides for implant applications. Electrochimica Acta. 2008;53:4846-51.
[243] Bauer S, Kleber S, Schmuki P. TiO2 nanotubes: Tailoring the geometry in H3PO4/HF electrolytes. Electrochem Commun. 2006;8:1321-5.
[244] von Wilmowsky C, Bauer S, Lutz R, Meisel M, Neukam FW, Toyoshima T, et al. *In vivo* evaluation of anodic TiO_2 nanotubes: An experimental study in the pig. J Biomed Mater Res Part B. 2009;89B:165-71.
[245] Albu SP, Ghicov A, Aldabergenova S, Drechsel P, LeClere D, Thompson GE, et al. Formation of Double-Walled TiO2 Nanotubes and Robust Anatase Membranes. Advanced Materials. 2008;20:4135-+.

[246] Li S, Zhang G, Guo D, Yu L, Zhang W. Anodization Fabrication of Highly Ordered TiO2 Nanotubes. The Journal of Physical Chemistry C. 2009;113:12759-65.
[247] Crawford GA, Chawla N. Porous hierarchical TiO2 nanostructures: Processing and microstructure relationships. Acta Materialia. 2009;57:854-67.
[248] Mor GK, Varghese OK, Paulose M, Shankar K, Grimes CA. A review on highly ordered, vertically oriented TiO2 nanotube arrays: Fabrication, material properties, and solar energy applications. Solar Energy Materials and Solar Cells. 2006;90:2011-75.
[249] Grimes CA. TiO2 nanotube arrays: Synthesis, properties, and applications: Springer Science; 2009.
[250] Rani S, Roy SC, Paulose M, Varghese OK, Mor GK, Kim S, et al. Synthesis and applications of electrochemically self-assembled titania nanotube arrays. Physical Chemistry Chemical Physics. 2010;12:2780-800.
[251] Losic D, Simovic S. Self-ordered nanopore and nanotube platforms for drug delivery applications. Expert Opinion on Drug Delivery. 2009;6:1363-81.
[252] Song Y-Y, Schmidt-Stein F, Bauer S, Schmuki P. Amphiphilic TiO_2 nanotube arrays: An actively controllable drug delivery system. Journal of the American Chemical Society. 2009;131:4230-4232.
[253] Aninwene HGE, Yao C, Webster TJ. Enhanced osteoblast adhesion to drug-coated anodized nanotubular titanium surfaces. International Journal of Nanomedicine. 2012;7:1573-.
[254] Eaninwene G, 2nd, Yao C, Webster TJ. Enhanced osteoblast adhesion to drug-coated anodized nanotubular titanium surfaces. International Journal of Nanomedicine. 2008;3:257-64.
[255] Shrestha NK, Macak JM, Schmidt-Stein F, Hahn R, Mierke CT, Fabry B, et al. Magnetically guided titania nanotubes for site-selective photocatalysis and drug release. Angewandte Chemie. 2009;121:987-90.
[256] Bae IH, Yun KD, Kim HS, Jeong BC, Lim HP, Park SW, et al. Anodic oxidized nanotubular titanium implants enhance bone morphogenetic protein-2 delivery. J Biomed Mater Res Part B. 2010;93B:484-91.
[257] Gultepe E, Nagesha D, Casse BDF, Banyal R, Fitchorov T, Karma A, et al. Sustained drug release from non-eroding nanoporous templates. Small. 2010;6:213-6.
[258] Zimmerli W, Sendi P. Pathogenesis of implant-associated infection: the role of the host. Seminars in Immunopathology. 2011;33:295-306.
[259] Fan Y, Duan K, Wang R. A composite coating by electrolysis-induced collagen self-assembly and calcium phosphate mineralization. Biomaterials. 2005;26:1623-32.
[260] Garbuz DS, Hu Y, Kim WY, Duan K, Masri BA, Oxland TR, et al. Enhanced gap filling and osteoconduction associated with alendronate-calcium phosphate-coated porous tantalum. J Bone Joint Surg Am. 2008;90:1090-100.
[261] Fjell CD, Jenssen H, Hilpert K, Cheung WA, Pante N, Hancock REW, et al. Identification of novel antibacterial peptides by chemoinformatics and machine learning. Journal of Medicinal Chemistry. 2009;52:2006-15.
[262] Xiao SJ, Textor M, Spencer ND, Wieland M, Keller B, Sigrist H. Immobilization of the cell-adhesive peptide Arg–Gly–Asp–Cys (RGDC) on titanium surfaces by covalent chemical attachment. Journal of Materials Science: Materials in Medicine. 1997;8:867-72.
[263] Smith RE, MacQuarrie R. A sensitive fluorometric method for the determination of arginine using 9,10-phenanthrenequinone. Analytical Biochemistry. 1978;90:246-55.
[264] Arellano-Jiménez MJ, García-García R, Reyes-Gasga J. Synthesis and hydrolysis of octacalcium phosphate and its characterization by electron microscopy and X-ray diffraction. Journal of Physics and Chemistry of Solids. 2009;70:390-5.
[265] Wang RZ, Cui FZ, Lu HB, Wen HB, Ma CL, Li HD. Synthesis of nanophase hydroxyapatite/collagen composite. Journal of Materials Science Letters. 1995;14:490-2.
[266] Slósarczyk A, Paluszkiewicz C, Gawlicki M, Paszkiewicz Z. The FTIR spectroscopy and QXRD studies of calcium phosphate based materials produced from the powder precursors with different Ca/P ratios. Ceramics International. 1997;23:297-304.

[267] Jenssen H, Hancock REW. Therapeutic potential of HDPs as immunomodulatory agents. In: Giuliani A, Rinaldi AC, editors. Antimicrobial peptides: Methods and Protocols: Humana Press Inc. p. 329-47.
[268] Stallmann HP, de Roo R, Faber C, Amerongen AVN, Wuisman P. *In vivo* release of the antimicrobial peptide hLF1-11 from calcium phosphate cement. Journal of Orthopaedic Research. 2008;26:531-8.
[269] Stallmann HP, Faber C, Bronckers A, Amerongen AVN, Wuisman P. Osteomyelitis prevention in rabbits using antimicrobial peptide hLF1-11-or gentamicin-containing calcium phosphate cement. Journal of Antimicrobial Chemotherapy. 2004;54:472-6.
[270] Stallmann HP, Faber C, Slotema ET, Lyaruu DM, Bronckers ALJJ, Amerongen AVN, et al. Continuous-release or burst-release of the antimicrobial peptide human lactoferrin 1-11 (hLF1-11) from calcium phosphate bone substitutes. Journal of Antimicrobial Chemotherapy. 2003;52:853-5.
[271] Duan K, Wang R. Surface modifications of bone implants through wet chemistry. Journal of Materials Chemistry. 2006;16:2309-21.
[272] Woods AS, Ferre S. Amazing stability of the arginine-phosphate electrostatic interaction. Journal of Proteome Research. 2005;4:1397-402.
[273] Trampuz A, Widmer AF. Infections associated with orthopedic implants. Current Opinion in Infectious Diseases. 2006;19:349-56.
[274] Yeaman MR, Yount NY. Mechanisms of antimicrobial peptide action and resistance. Pharmacological Reviews. 2003;55:27-55.
[275] Kazemzadeh-Narbat M, Kindrachuk J, Duan K, Jenssen H, Hancock REW, Wang R. Antimicrobial peptides on calcium phosphate-coated titanium for the prevention of implant-associated infections. Biomaterials. 2010;31:9519-26.
[276] Pace CN, Vajdos F, Fee L, Grimsley G, Gray T. How to measure and predict the molar absorption coefficient of a protein. Protein Sci. 1995; 4:2411-23.
[277] Delhaye S, Landry J. High-performance liquid chromatography and ultraviolet spectrophotometry for quantitation of tryptophan in barytic hydrolysates. Analytical Biochemistry. 1986;159:175-8.
[278] Thomas W. Bauer DM. Handbook of histology methods for bone and cartilage. Totowa, New Jersey: Humana Press; 2003.
[279] Woods AS, Ferre S. Amazing stability of the arginine-phosphate electrostatic interaction. Journal of Proteome Research. 2005;4:1397-402.
[280] Gerhart TN, Roux RD, Horowitz G, Miller RL, Hanff P, Hayes WC. Antibiotic release from an experimental biodegradable bone-cement. Journal of Orthopaedic Research. 1988;6:585-92.
[281] Joosten U, Joist A, Gosheger G, Liljenqvist U, Brandt B, von Eiff C. Effectiveness of hydroxyapatite-vancomycin bone cement in the treatment of Staphylococcus aureus induced chronic osteomyelitis. Biomaterials. 2005;26:5251-8.
[282] Schnieders J, Gbureck U, Thull R, Kissel T. Controlled release of gentamicin from calcium phosphate - poly(lactic acid-co-glycolic acid) composite bone cement. Biomaterials. 2006;27:4239-49.
[283] Faber C, Stallmann HP, Lyaruu DM, Joosten U, von Eiff C, Amerongen AV, et al. Comparable efficacies of the antimicrobial peptide human lactoferrin 1-11 and gentamicin in a chronic methicillin-resistant Staphylococcus aureus osteomyelitis model. Antimicrobial Agents and Chemotherapy. 2005;49:2438-44.
[284] Gough M, Hancock R, Kelly N. Antiendotoxin activity of cationic peptide antimicrobial agents. Infect Immun. 1996;64:4922-7.
[285] Chang YL, Stanford CM, Wefel JS, Keller JC. Osteoblastic cell attachment to hydroxyapatite-coated implant surfaces in vitro. International Journal of Oral & Maxillofacial Implants. 1999;14:239-47.
[286] Deligianni DD, Katsala ND, Koutsoukos PG, Missirlis YF. Effect of surface roughness of hydroxyapatite on human bone marrow cell adhesion, proliferation, differentiation and detachment strength. Biomaterials. 2001;22:87-96.

[287] Hilpert K, Volkmer-Engert R, Walter T, Hancock REW. High-throughput generation of small antibacterial peptides with improved activity. Nat Biotech. 2005;23:1008-12.
[288] Kazemzadeh-Narbat M, Noordin S, Masri BA, Garbuz DS, Duncan CP, Hancock REW, et al. Drug release and bone growth studies of antimicrobial peptide-loaded calcium phosphate coating on titanium. Journal of Biomedical Materials Research Part B: Applied Biomaterials. 2012;100:1344-52.
[289] Larsson C, Thomsen P, Lausmaa J, Rodahl M, Kasemo B, Ericson LE. Bone response to surface-modified titanium implants – studies on electropolished implants with different oxide thickness and morphology. Biomaterials. 1994;15:1062-74.
[290] Liu XY, Chu PK, Ding CX. Surface modification of titanium, titanium alloys, and related materials for biomedical applications. Mater Sci Eng R-Rep. 2004;47:49-121.
[291] Hanawa T, Kon M, Ukai H, Murakami K, Miyamoto Y, Asaoka K. Surface modification of titanium in calcium-ion-containing solutions. Journal of Biomedical Materials Research. 1997;34:273-8.
[292] de Groot K, Wolke JGC, Jansen JA. Calcium phosphate coatings for medical implants. Proceedings of the Institution of Mechanical Engineers Part H-Journal of Engineering in Medicine. 1998;212:137-47.
[293] KC P, M E, TJ L, CA G, TA D. Decreased Staphylococcus epidermis adhesion and increased osteoblast functionality on antibiotic-loaded titania nanotubes. D - 8100316.T - ppublish.
[294] Popat KC, Eltgroth M, La Tempa TJ, Grimes CA, Desai TA. Titania nanotubes: A novel platform for drug-eluting coatings for medical implants? Small. 2007;3:1878-81.
[295] Peng L, Mendelsohn AD, LaTempa TJ, Yoriya S, Grimes CA, Desai TA. Long-term small molecule and protein elution from TiO_2 nanotubes. Nano Letters. 2009;9:1932-6.
[296] Moseke C, Hage F, Vorndran E, Gbureck U. TiO2 nanotube arrays deposited on Ti substrate by anodic oxidation and their potential as a long-term drug delivery system for antimicrobial agents. Appl Surf Sci. 2012;258:5399-404.
[297] Crawford GA, Chawla N, Houston JE. Nanomechanics of biocompatible TiO_2 nanotubes by interfacial Force Microscopy (IFM). J Mech Behav Biomed Mater. 2009;2:580-7.
[298] Zou JP, Wang RZ. Crack initiation, propagation and saturation of TiO_2 nanotube film. Trans Nonferrous Met Soc China. 2012;22:627-33.
[299] Moskowitz JS, Blaisse MR, Samuel RE, Hsu HP, Harris MB, Martin SD, et al. The effectiveness of the controlled release of gentamicin from polyelectrolyte multilayers in the treatment of Staphylococcus aureus infection in a rabbit bone model. Biomaterials. 2010;31:6019-30.
[300] Morra M, Cassinelli C, Cascardo G, Carpi A, Fini M, Giavaresi G, et al. Adsorption of cationic antibacterial on collagen-coated titanium implant devices. Biomed Pharmacother. 2004;58:418-22.
[301] Richter RP, Him JLK, Brisson A. Supported lipid membranes. Materials Today. 2003;6:32-7.
[302] Ishihara K, Oshida H, Endo Y, Ueda T, Watanabe A, Nakabayashi N. Hemocompatibility of human whole blood on polymers with a phospholipid polar group and its mechanism. Journal of Biomedical Materials Research. 1992;26:1543-52.
[303] Bosetti M, Santin M, Lloyd AW, Denyer SP, Sabbatini M, Cannas M. Cell behaviour on phospholipids-coated surfaces. Journal of Materials Science-Materials in Medicine. 2007;18:611-7.
[304] Satsangi A, Satsangi N, Glover R, Satsangi RK, Ong JL. Osteoblast response to phospholipid modified titanium surface. Biomaterials. 2003;24:4585-9.
[305] Ye SH, Johnson CA, Woolley JR, Oh HI, Gamble LJ, Ishihara K, et al. Surface modification of a titanium alloy with a phospholipid polymer prepared by a plasma-induced grafting technique to improve surface thromboresistance. Colloids and Surfaces B-Biointerfaces. 2009;74:96-102.
[306] Ye SH, Johnson CA, Woolley JR, Snyder TA, Gamble LJ, Wagner WR. Covalent surface modification of a titanium alloy with a phosphorylcholine-containing copolymer for reduced thrombogenicity in cardiovascular devices. J Biomed Mater Res Part A. 2009;91A:18-28.
[307] Choi J, Konno T, Takai M, Ishihara K. Regulation of cell proliferation by multi-layered phospholipid polymer hydrogel coatings through controlled release of paclitaxel. Biomaterials. 2012;33:954-61.

[308] Pressl D, Teichert C, Hlawacek G, Clemens H, Iliev PP, Schuster A, et al. Characterization of Phospholipid Bilayers on Ti-6Al-4V and Ti-6Al-7Nb. Advanced Engineering Materials. 2008;10:B47-B52.
[309] Willumeit R, Schuster A, Iliev P, Linser S, Feyerabend F. Phospholipids as implant coatings. Journal of Materials Science-Materials in Medicine. 2007;18:367-80.
[310] Susin C, Qahash M, Hall J, Sennerby L, Wikesjo UME. Histological and biomechanical evaluation of phosphorylcholine-coated titanium implants. Journal of Clinical Periodontology. 2008;35:270-5.
[311] Trojanowicz MT. Miniaturized biochemical sensing devices based on planar bilayer lipid membranes. Fresenius' Journal of Analytical Chemistry. 2001;371:246-60.
[312] Prinz C, Höök F, Malm J, Sjövall P. Structural Effects in the Analysis of Supported Lipid Bilayers by Time-of-Flight Secondary Ion Mass Spectrometry. Langmuir. 2007;23:8035-41.
[313] Jones MI, McColl IR, Grant DM, Parker KG, Parker TL. Protein adsorption and platelet attachment and activation, on TiN, TiC, and DLC coatings on titanium for cardiovascular applications. Journal of Biomedical Materials Research. 2000;52:413-21.
[314] Davies JE. In vitro modeling of the bone/implant interface. Anatomical Record. 1996;245:426-45.
[315] Lind M. Growth factor stimulation of bone healing. Effects on osteoblasts, osteomies, and implants fixation. Acta orthopaedica Scandinavica Supplementum. 1998;283:2-37.
[316] Macak JM, Schmuki P. Anodic growth of self-organized anodic TiO_2 nanotubes in viscous electrolytes. Electrochimica Acta. 2006;52:1258-64.
[317] Duan K, Tang A, Wang RZ. Accelerating calcium phosphate growth on NaOH-treated poly-(lactic-co-glycolic acid) by evaporation-induced surface crystallization. Appl Surf Sci. 2008;255:2442-8.
[318] Pace CN, Vajdos F, Fee L, Grimsley G, Gray T. How to measure and predict the molar absorption-coefficient of a protein. Protein Science. 1995;4:2411-23.
[319] Li SQ, Zhang GM, Guo DZ, Yu LG, Zhang W. Anodization fabrication of highly ordered TiO_2 Nanotubes. Journal of Physical Chemistry C. 2009;113:12759-65.
[320] Macak JM, Tsuchiya H, Ghicov A, Yasuda K, Hahn R, Bauer S, et al. TiO_2 nanotubes: Self-organized electrochemical formation, properties and applications. Current Opinion in Solid State & Materials Science. 2007;11:3-18.
[321] Zhao J, Tamm LK. FTIR and fluorescence studies of interactions of synaptic fusion proteins in polymer-supported bilayers. Langmuir. 2003;19:1838-46.
[322] Lohmann C, Schachmann E, Dandekar T, Villmann C, Becker CM. Developmental profiling by mass spectrometry of phosphocholine containing phospholipids in the rat nervous system reveals temporo-spatial gradients. Journal of Neurochemistry. 2010;114:1119-34.
[323] Davies JE, Causton B, Bovell Y, Davy K, Sturt CS. The migration of osteoblasts over substrata of discrete surface-charge. Biomaterials. 1986;7:231-3.
[324] Bohil AB, Robertson BW, Cheney RE. Myosin-X is a molecular motor that functions in filopodia formation. Proceedings of the National Academy of Sciences of the United States of America. 2006;103:12411-6.
[325] Leytin V, Mody M, Semple JW, Garvey B, Freedman J. Quantification of platelet activation status by analyzing P-selectin expression. Biochemical and Biophysical Research Communications. 2000;273:565-70.
[326] Mustard JF, Packham MA, Kinloughrathbone RL, Perry DW, Regoeczi E. Fibrinogen and ADP-induced platelet-aggregation. Blood. 1978;52:453-66.
[327] Barnhart MI, Walsh RT, Robinson JA. A three-dimensional view of platelet responses to chemical stimuli. Annals of the New York Academy of Sciences. 1972;201:360-90.
[328] Mansouri S, Winnik FM, Tabrizian M. Modulating the release kinetics through the control of the permeability of the layer-by-layer assembly: a review. Expert Opinion on Drug Delivery. 2009;6:585-97.
[329] Baro M, Sanchez E, Delgado A, Perera A, Evora C. *In vitro-in vivo* characterization of gentamicin bone implants. J Control Release. 2002;83:353-64.
[330] Soriano I, Evora C. Formulation of calcium phosphates/poly (d,l-lactide) blends containing gentamicin for bone implantation. J Control Release. 2000;68:121-34.

[331] Teller M, Gopp U, Neumann HG, Kuehn KD. Release of gentamicin from bone regenerative materials: An in vitro study. J Biomed Mater Res Part B. 2007;81B:23-9.
[332] Grossfield A, Woolf TB. Interaction of tryptophan analogs with POPC lipid bilayers investigated by molecular dynamics calculations. Langmuir. 2002;18:198-210.
[333] Santin M, Rhys-Williams W, O'Reilly J, Davies MC, Shakesheff K, Love WG, et al. Calcium-binding phospholipids as a coating material for implant osteointegration. Journal of the Royal Society Interface. 2006;3:277-81.
[334] Siepmann J, Siepmann F. Mathematical modeling of drug delivery. International Journal of Pharmaceutics. 2008;364:328-43.
[335] Kaunisto E, Marucci M, Borgquist P, Axelsson A. Mechanistic modelling of drug release from polymer-coated and swelling and dissolving polymer matrix systems. International Journal of Pharmaceutics. 2011;418:54-77.
[336] Wilson CJ, Clegg RE, Leavesley DI, Pearcy MJ. Mediation of biomaterial-cell interactions by adsorbed proteins: A review. Tissue Eng. 2005;11:1-18.
[337] Drinker CK, Drinker KR, Lund CC. The circulation in the mammalian bone-marrow - With especial reference to the factors concerned in the movement of red blood cells from the bone marrow into the circulating blood as disclosed by perfusion of the tibia of the dog and by injections of the bone-marrow in the rabbit and cat. American Journal of Physiology. 1922;62:1-92.
[338] Shattil SJ, Kashiwagi H, Pampori N. Integrin signaling: The platelet paradigm. Blood. 1998;91:2645-57.
[339] Body SC. Platelet activation and interactions with the microvasculature. Journal of Cardiovascular Pharmacology. 1996;27:S13-S25.
[340] JM G, WB T, CD M, TA H. The effect of adsorbed fibrinogen, fibronectin, von Willebrand factor and. Biomaterials 2000 ;21(22):2243-52.
[341] Yun YH, Turitto VT, Daigle KP, Davidson JA, Slack SM. Initial hemocompatibility studies of titanium and zirconium alloys: Prekallikrein activation, fibrinogen adsorption, and their correlation with surface electrochemical properties. Journal of Biomedical Materials Research . 1996;32:77-85.
[342] Fischer D, Li YX, Ahlemeyer B, Krieglstein J, Kissel T. *In vitro* cytotoxicity testing of polycations: influence of polymer structure on cell viability and hemolysis. Biomaterials. 2003;24:1121-31.
[343] Richardson RR, Miller JA, Reichert WM. Polyimides as biomaterials-preliminary biocompatibility testing. Biomaterials. 1993;14:627-35.
[344]Wang XD, Gu XS, Yuan CW, Chen SJ, Zhang PY, Zhang TY, et al. Evaluation of biocompatibility of polypyrrole in vitro and in vivo. J Biomed Mater Res Part A. 2004;68A:411-22.
[345] Brunette DM, Tengvall P, Textor M, Thomsen P. Titanium in medicine: material science, surface science, engineering, biological responses and medical applications. Springer 2001; ISBN 3-540-66936-1.

APPENDICES

The appendices (Appendices A-C) are included to give complementary information corresponding to each chapter.

APPENDIX A CHAPTER 4 – ADDITIONAL DATA[4]

Surface wettability plays a major role in protein adsorption and subsequent cell adhesion. Therefore, hydrophilic surfaces initiate better cell attachment and result in faster osteointegration [93, 94]. On the other hand hydrophilicity of biomaterial surface is important for bacteria attachment, hydrophobic bacterial cell surfaces adhere better to hydrophobic biomaterial surfaces due to a reduction in free surface energy [6]. Figure A.1 compares the hydrophilicity of calcium phosphate fabricated using ELD technique and pure titanium. The wettability of surfaces was characterized by contact angles measurements using 1 µL distilled water by sessile drop method at room temperature. Images were captured and analyzed using Northern Eclipse software at 10x magnification. The results indicate that CaP coating increases the Ti surface wettability.

Cytotoxicity concentration levels of different tethered peptides were evaluated by measuring the mitochondrial dehydrogenase activity using a modified MTT (3-(4,5-dimetyl-2-tiazolyl)-2,5-diphenyl-2H-tetrazolium bromide). To assess the cytotoxicity of specimens, 10^4 of cell dispersion were seeded on specimens for 24 hours (Fig. A.2).

To evaluate MG-63 cell attachment and proliferation on CaP coated titanium loaded with Tet213, 5×10^5 MG-63/sample were cultured on each sample, and incubated for 4 h and 2 days

[4] Some data in appendix A has been published. Gao, Guangzheng; Lange, Dirk; Hilpert, Kai; Kindrachuk, Jason; Zou, Yuquan; Cheng, John T. J.; **Kazemzadeh-Narbat, Mehdi**; Yu, Kai; Wang, Rizhi; Straus, Suzana K.; Brooks, Donald E.; Chew, Ben H.; Hancock, Robert E. W.; Kizhakkedathu, Jayachandran N. The biocompatibility and biofilm resistance of implant coatings based on hydrophilic polymer brushes conjugated with antimicrobial peptides. Biomaterials, 2011.

respectively. The samples were then washed with 0.1 m PBS for three times and incubated in 2.5% glutaraldehyde in PBS for 2 h at 4°C. After washing the samples for 3 times with 0.1 M PBS, specimens were dehydrated using graded ethanol (50, 70, 80, 90, 95, and 100%, 15 min each), and critically point dried. The samples were Au sputter coated, and viewed using a SEM (Fig. A.3).

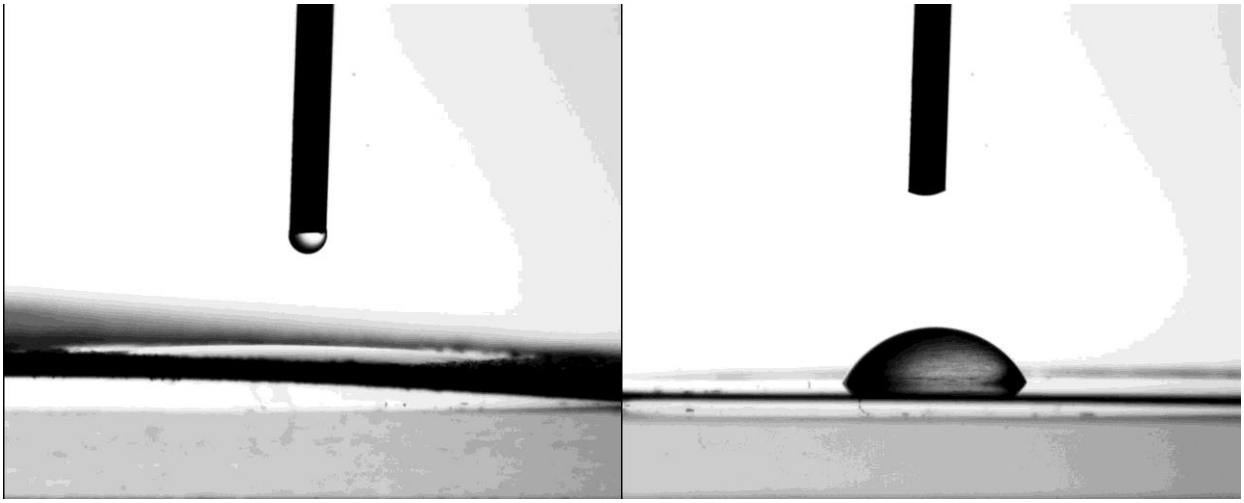

(a) (b)

Figure A.1. Images collected during contact angle measurements indicating the extensive spreading of water drop on (a) CaP coating with contact angle of ~7°, and (b) Ti with contact angle of ~ 67°.

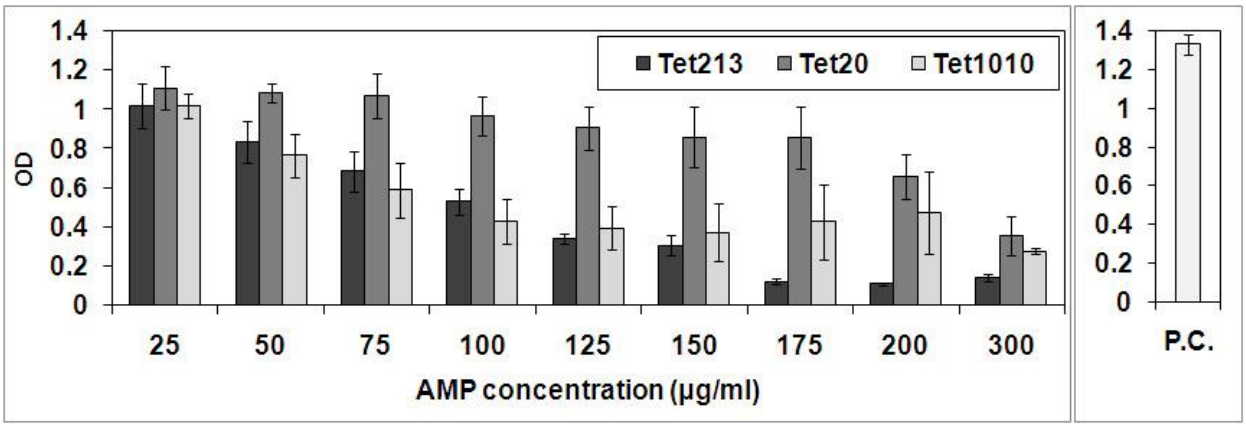

Figure A.2. Cytotoxicity levels of different concentrations of tethered peptides alone incubated with MG-63, in compare to positive control (cells alone). The diagram shows that tethered peptides exhibit cytotoxicity vs. MG-63 at high concetrations.

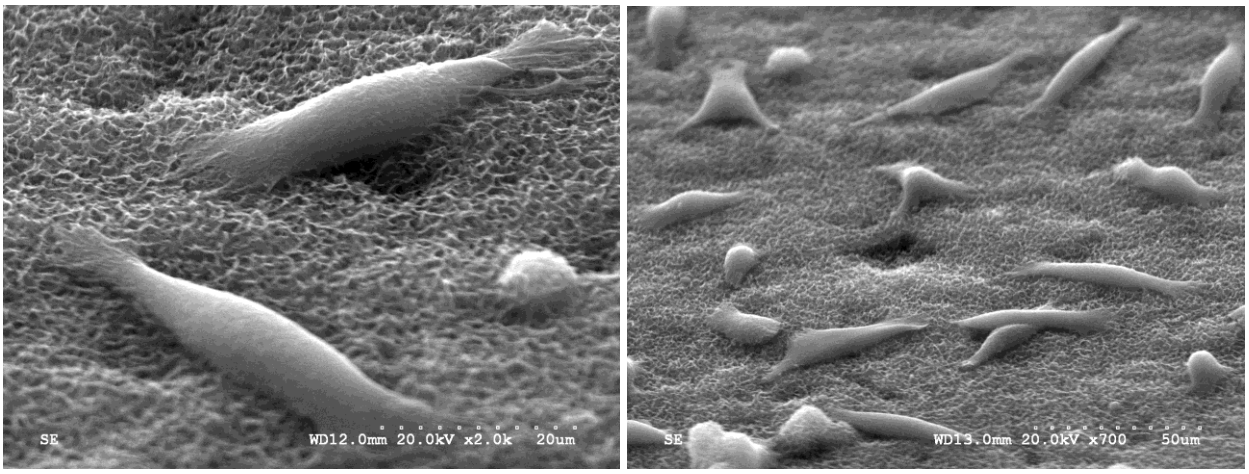

Figure A.3. Cell attachment CaP-AMP after seeding 5×10^5 MG-63/sample for 4 h.

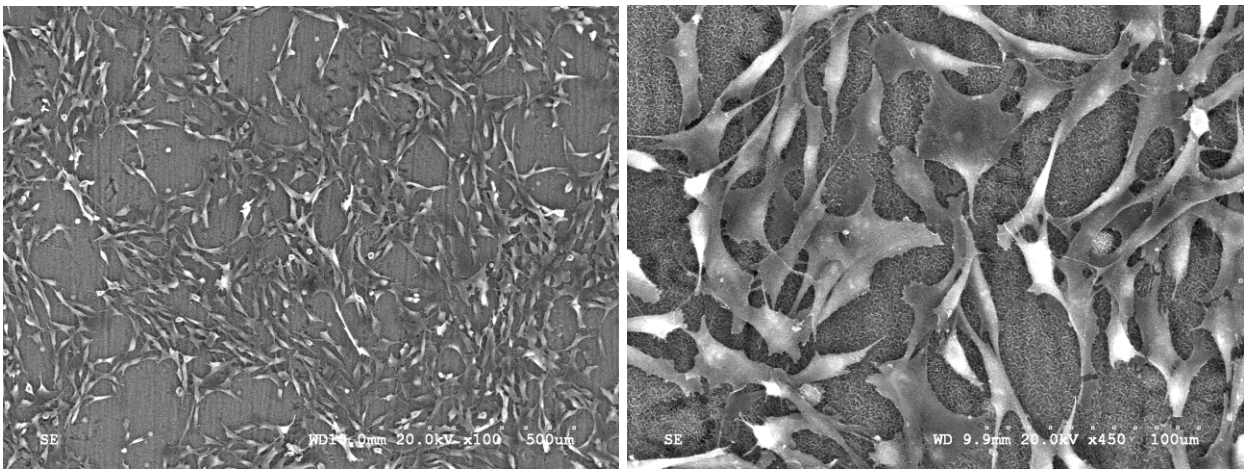

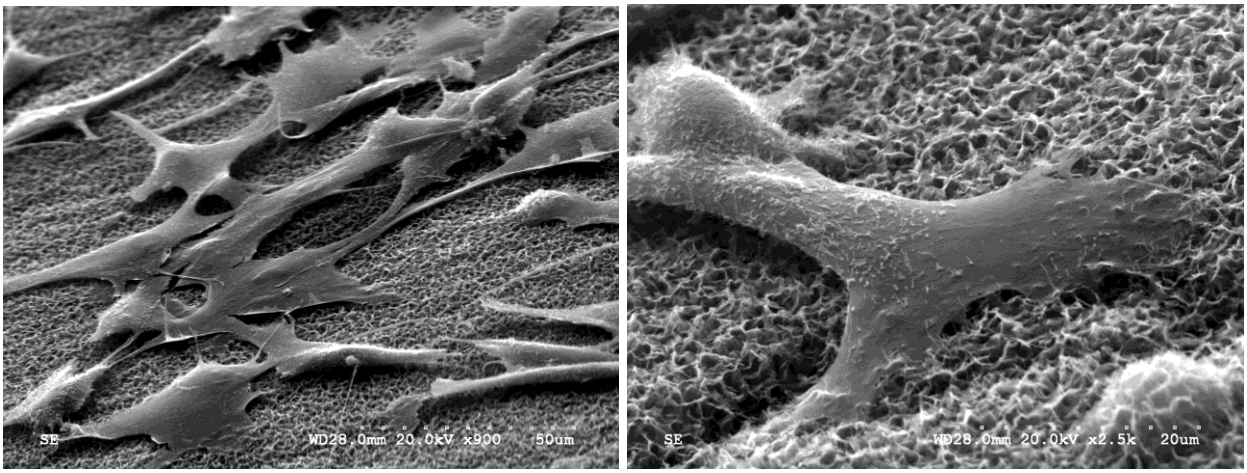

Figure A.4. Cell proliferation on CaP-AMP after seeding 5×10^5 MG-63/sample for 2 days.

APPENDIX B CHAPTER 5 – ADDITIONAL DATA

Histology process for sample preparation

The femur was cut parallel to the radius direction of the condyle arc. Figure B.1 shows some details of surgery procedure. The proper time of euthanization was determined by Micro-CT scan investigation after six weeks on one control rabbit (Fig B.4). The obtained samples were fixed, dehydrated, infiltrated, and then embedded in epoxy resin (SPURR, Canemco St. Laurent, QC, Canada) following a standard histological procedure according to table B-1 (Fig. B.5-6). After embedding the samples in SPURR, the examining surfaces were ground and polished (Fig. B.7). The image analysis was performed on the low magnification BSE images using image analysis software (Clemex Vision PE 3.5, Longueuil, QC, Canada). The quadrilateral defined by the four corners of caps was considered the sample area. Gray level discrimination was used to identify epoxy, new bone formation and implant. Figure B.8 shows how Clemex processes the images.

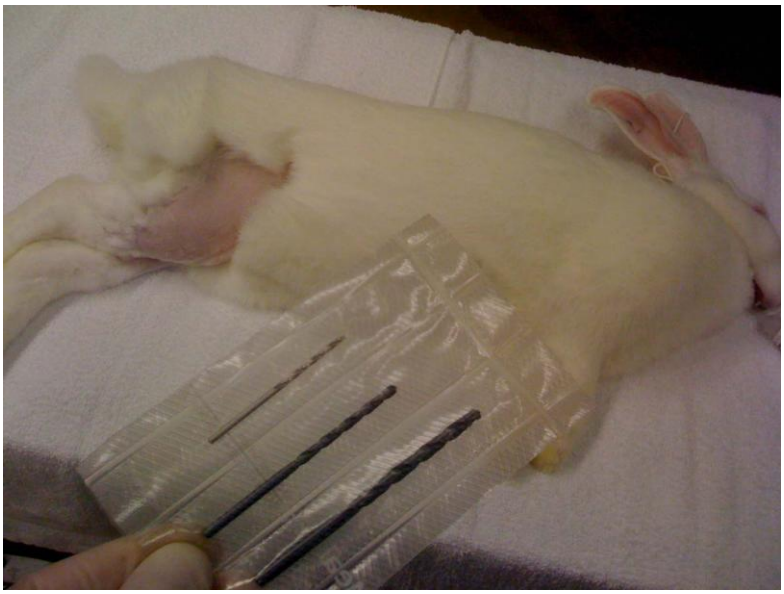

Figure B.1. To avoid thermal damage to bone, a 4.37-mm hole was created perpendicular to the distal femoral condyle bilaterally using sequential low speed drilling of growing diameter (1.95, 3.18, and 4.37 mm) with saline irrigation.

Table B-1. Processes and schedule for fixation, dehydration, and infiltration

Processes	Chemicals	Temperature	Duration	Processes
Fixation	10% buffered formalin	RT	2 days	Fixation
Dehydration	70% Ethanol/Water	RT	3 days	Dehydration
Dehydration	90% Ethanol/Water	RT	3 days	Dehydration
Dehydration	100% Ethanol	RT	3 days	Dehydration
Dehydration	100% Ethanol	RT	3 days	Dehydration
Infiltration	50% SPURR	RT	3 days	Infiltration
Infiltration	80% SPURR	4 °C	3 days	Infiltration
Infiltration	100% SPURR	4 °C	3 days	Infiltration
Infiltration	100% SPURR	4 °C	3 days	Infiltration

Figure B.2. Sterile implants were placed into Cryo-Tubes after preparation.

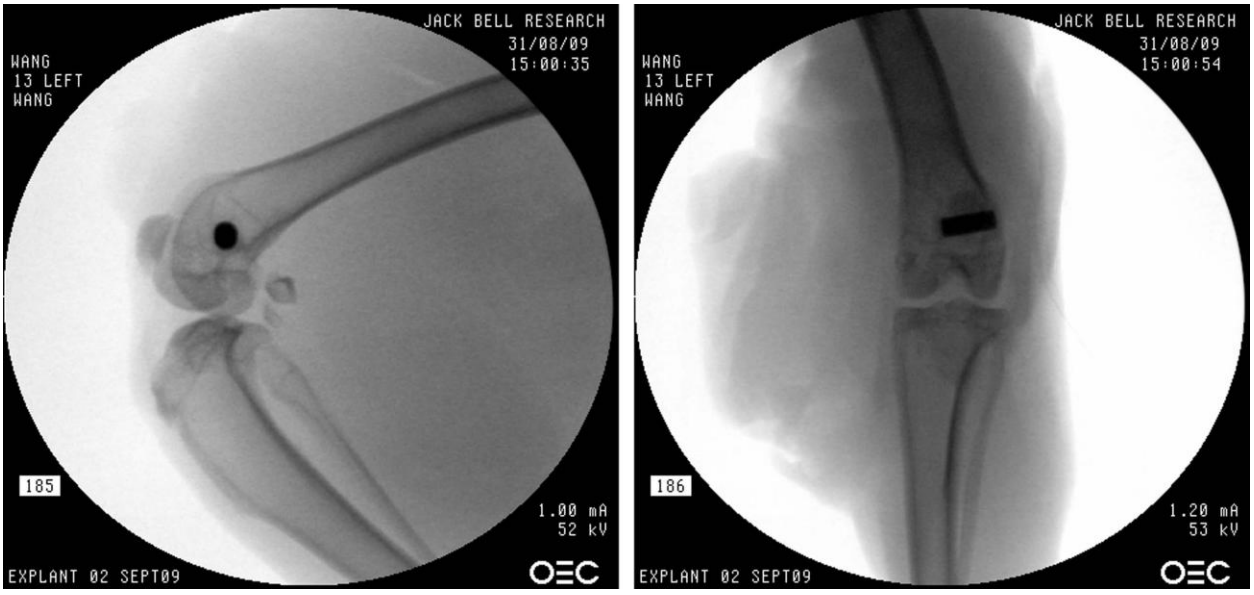

Figure B.3. Representative X-ray images of implant press-fitted in 4.37-mm hole at distal femur of rabbits.

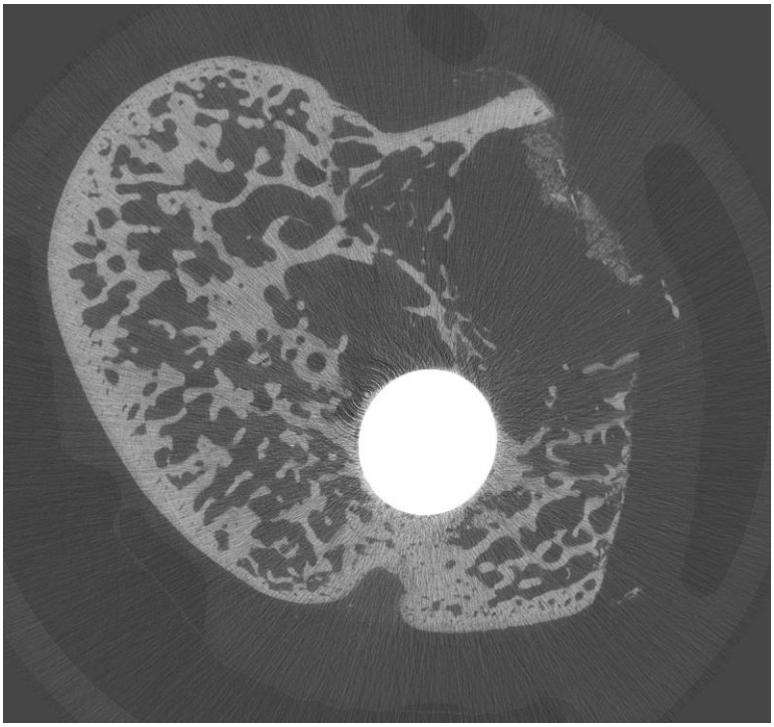

Figure B.4. µ-CT scan was carried out on one rabbit after 6 weeks for investigation of proper euthanization time. The image is a representative transverse (90°), section of implant located in left leg. The white circle is the implant, and the light gray is the bone growth.

Figure B.5.The samples were put into cassettes, and were labelled with pencil. All specimens were infiltrated under vacuum.

Figure B.6. Embedded samples in 100% SPURR.

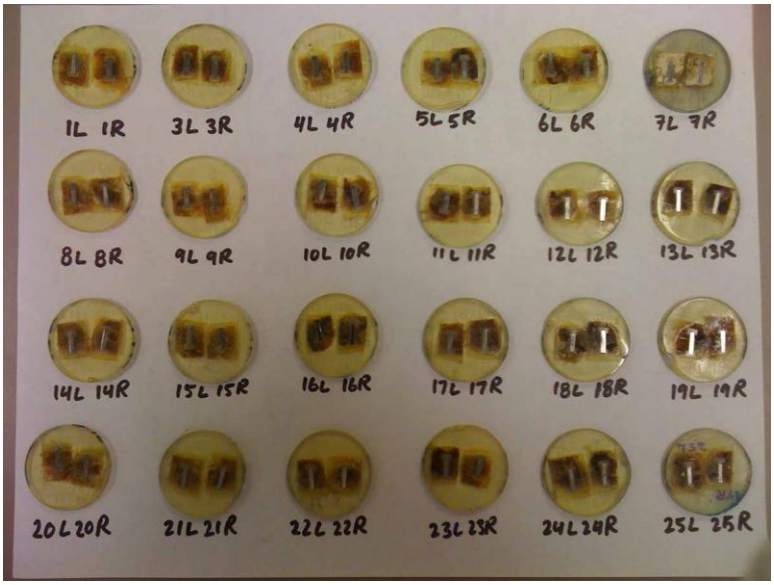

Figure B.7. Molded samples in epoxy-resin were ground and polished into three sections at 200, 850, and 1500 µm deep from tangent surface of the implant.

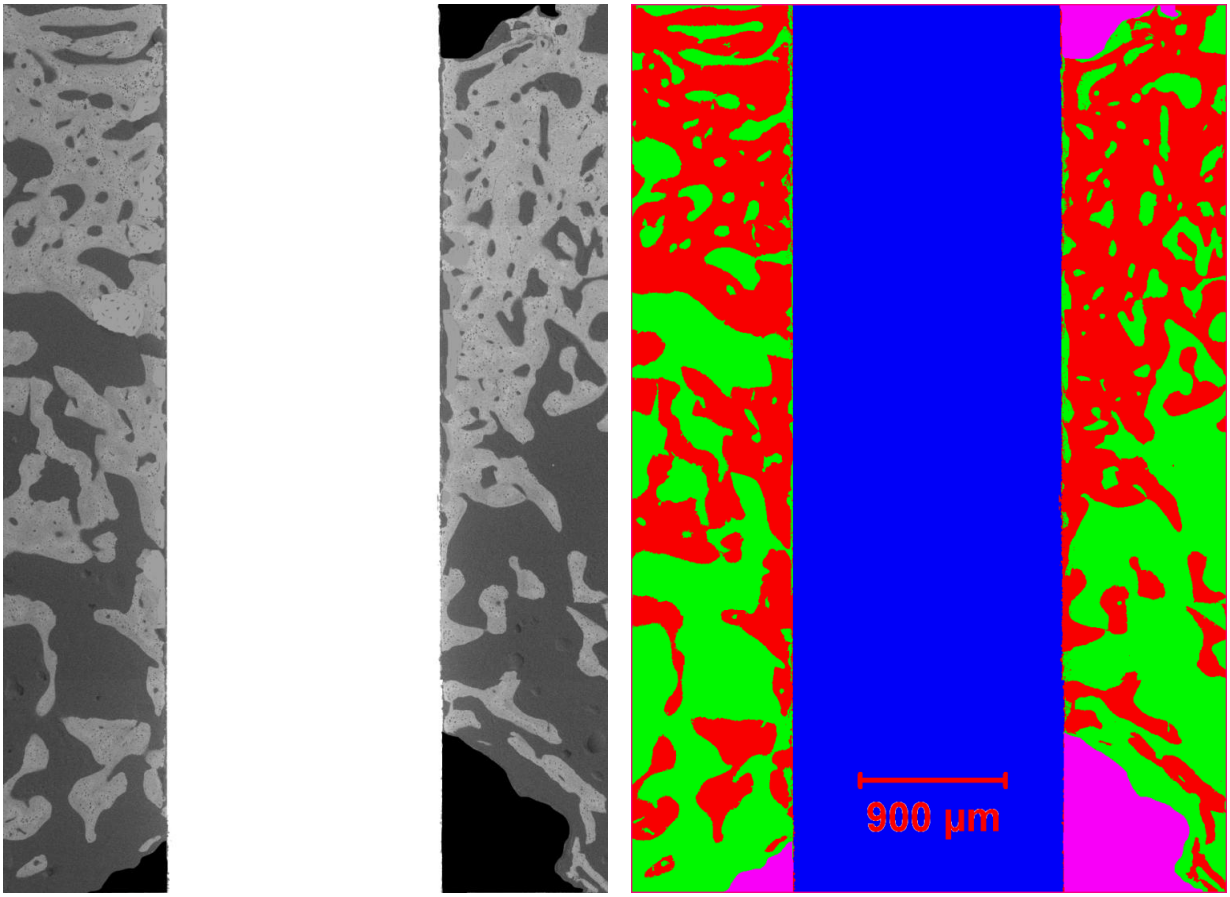

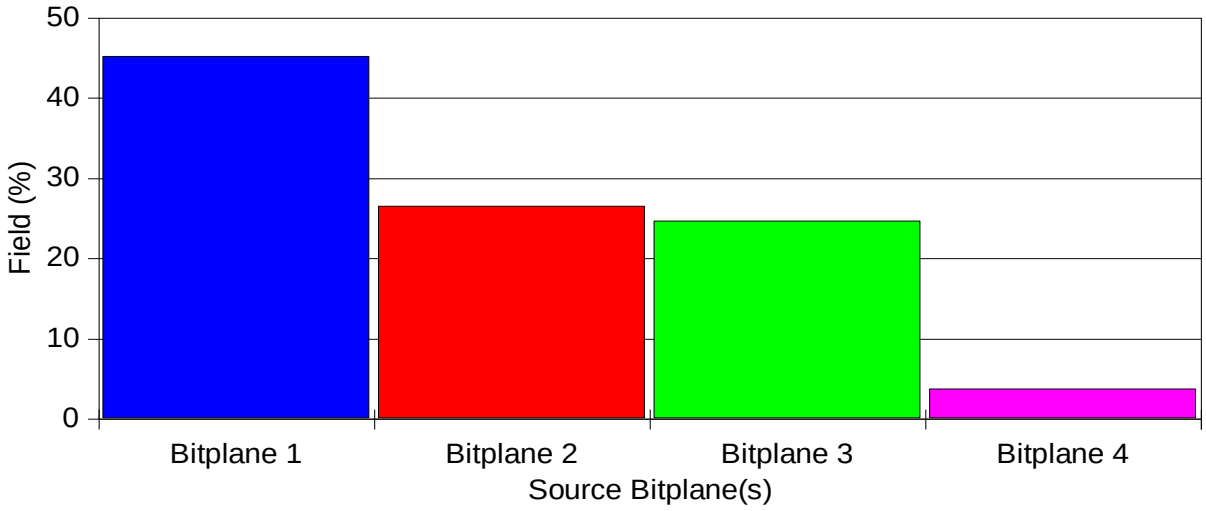

Figure B.8. Representative images for low magnification BSE, and histogram for image analysis, green, red and purple colors correspond to SPURR, bone and bone cement cap respectively.

Table B-2. Details of bone growth on different implants.

		% [Bone/(Bone+SPURR)]					
		First section		Second section		Third section	
Bunny No	Implant	Left	Right	Left	Right	Left	Right
1	CaP	30	40.24	31.72	40.96	36.19	22.59
2	(AMP) Failed	***	***	***	***	***	***
3	Ti	22.79	16.07	30.18	16.46	25.28	14.76
4	CaP	30.23	30.25	25	25.97	18.33	19.42
5	AMP	51.84	54.76	44.13	50.38	40.17	41.75
6	CaP	9.44	15.22	8.58	16.93	8.96	16.07
7	Ti	9.54	47.07	11.92	47.69	13.72	48.07
8	AMP	19.08	15.92	19.87	12.82	16.84	11.05
9	AMP	44.13	39.04	41.24	41.19	50.54	43.97
10	CaP	26.48	34.65	28.97	25.78	38.16	30.54
11	AMP	15.03	25.44	26.52	26.29	19.35	40.47
12	AMP	26.51	32.62	28.64	30.23	35.32	23.4
13	CaP	30.26	27.41	33.81	39.36	43.89	41.3
14	AMP	37	33.2	34.06	34.83	40.21	38.53
15	Ti	21.5	38	25.24	37.78	24.36	34.76
16	CaP	27.87	44.43	30.41	34.46	35.26	30.7
17	AMP	32.7	39.63	31.23	31.26	26.91	26.13
18	Ti	23.13	18.17	23.58	15.24	21.52	15.79
19	CaP	14.64	17.61	16.08	16.67	18.24	16.58
20	AMP	41.64	42.56	43.54	35.08	40.74	36.52
21	Ti	48	42.26	44.43	40.19	47.45	37.46
22	CaP	32.36	35.17	44.41	33.47	29.19	32.23
23	AMP	32.62	16.13	38.3	17.55	35.24	15.17
24	CaP	27.44	32.62	24.75	43.28	24.31	42.81
25	CaP	45.52	24.61	38.42	32.96	48.88	44.23

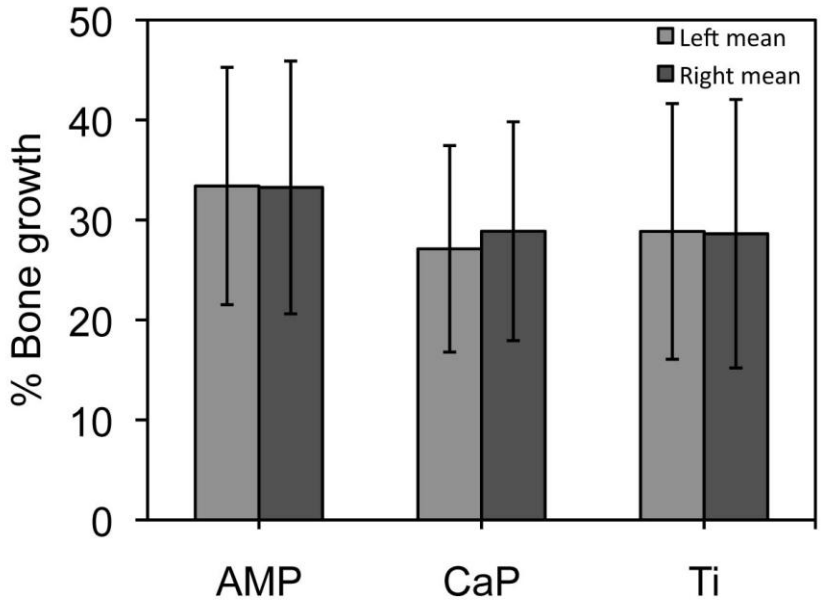
50
40
30
20
10
0
% Bone growth
Left mean
Right mean
AMP
CaP
Ti

(a)

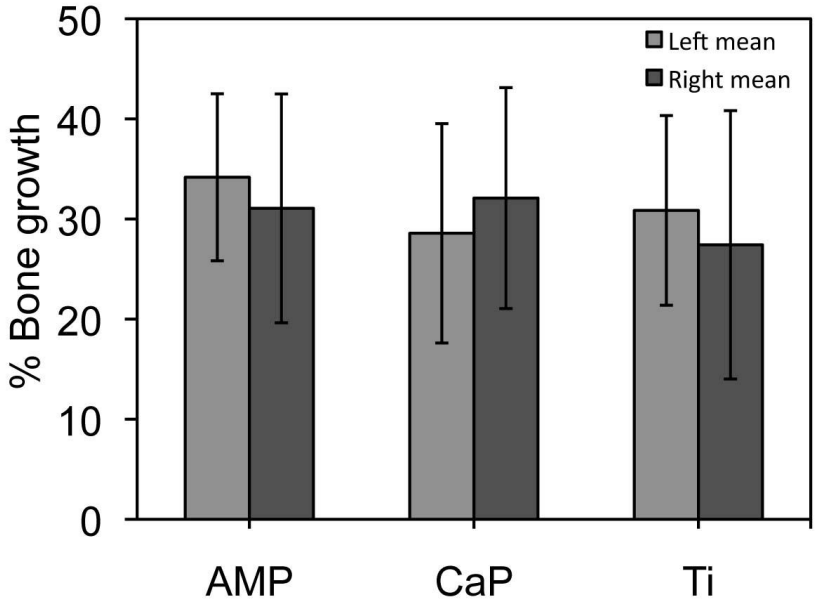
50
40
30
20
10
0
% Bone growth
Left mean
Right mean
AMP
CaP
Ti

(b)

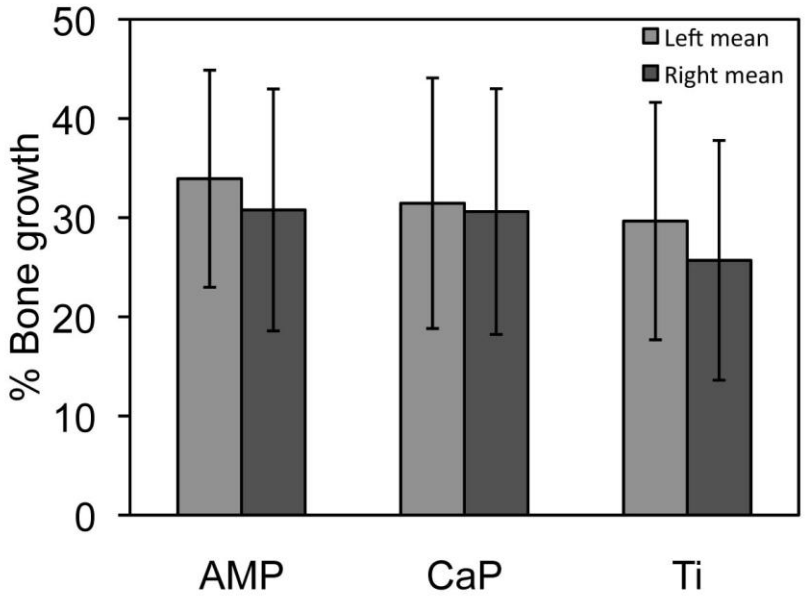

(c)

Figure B.9. Bone growth percentage on different samples implanted in left or right legs (a) first section, (b) second section, (c) third section

APPENDIX C CHAPTER 6 – ADDITIONAL DATA[5]

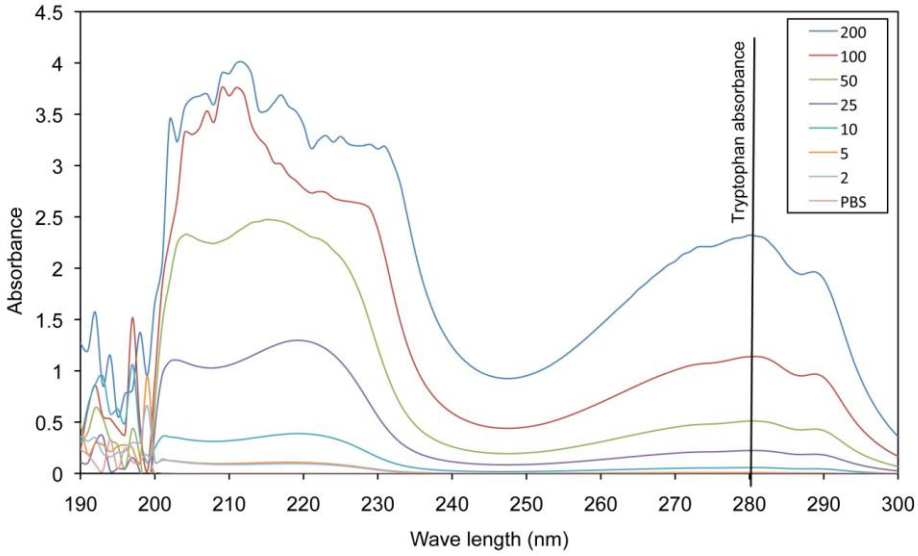

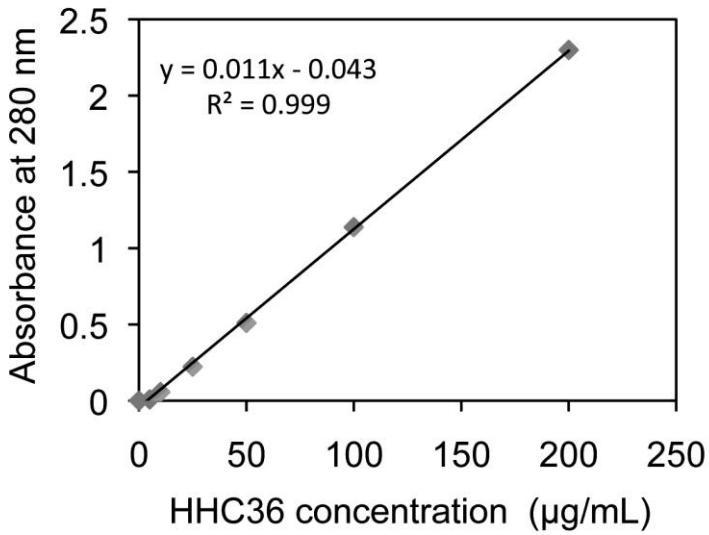

Figure C.1. Known HHC36 concentrations (2, 5, 10, 25, 50, 100, and 200 µg/mL) were measured using UV/Vis spectroscopy at 280 nm based on External Standard Method.

[5] Some data in appendix C has been published. Ma, Menghan; **Kazemzadeh-Narbat, Mehdi**; Hui, Yu; Lu, Shanshan; Ding, Chuanfan; Chen, David D. Y.; Hancock, Robert E. W.; Wang, Rizhi. Local delivery of antimicrobial peptides using self-organized TiO2 nanotube arrays for peri-implant infections. Journal of Biomedical Materials Research Part A, 2012.

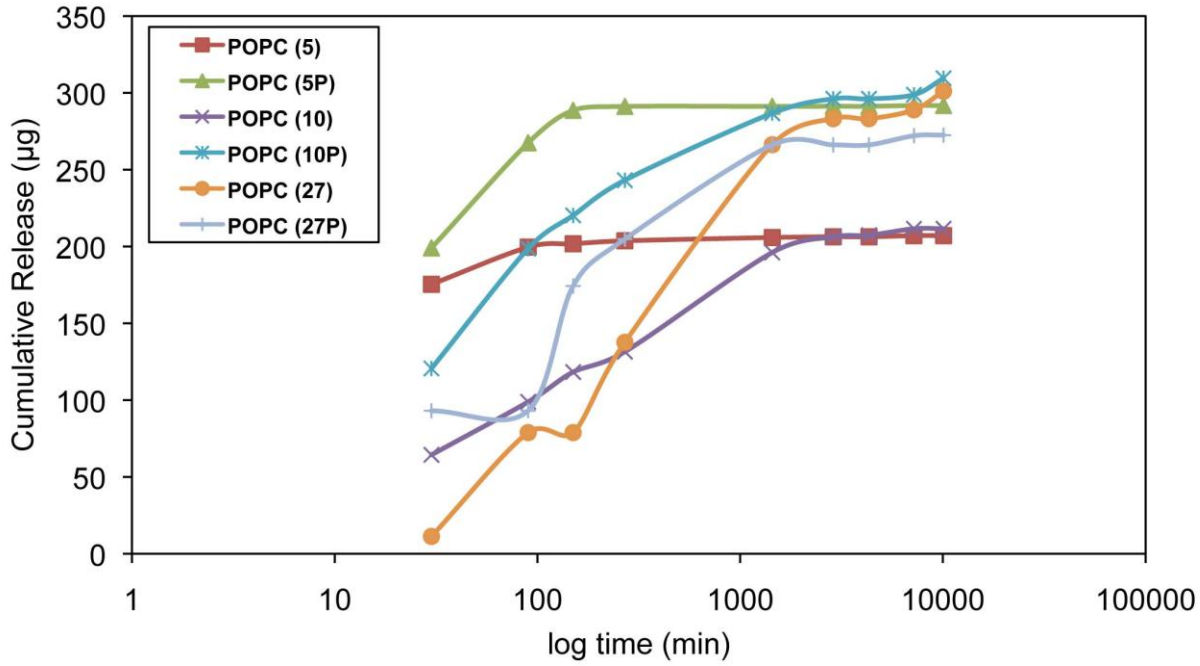

Figure C.2. Loading technique: One time AMP (250 µL of 2mg/mL AMP) deposition and drying under vacuum following one time POPC coating (1 mg/mL AMP was mixed with POPC alternatively).

No washing with PBS

POPC 5 = 5mg POPC in 1 mL Ethanol

POPC 5P = 5mg POPC and 1 mg AMP in 1 mL Ethanol

POPC 10 = 10mg POPC in 1 mL Ethanol

POPC 10P = 10mg POPC and 1 mg AMP in 1 mL Ethanol

POPC 27 = 27mg POPC in 1 mL Ethanol

POPC 27P = 27mg POPC and 1 mg AMP in 1 mL Ethanol

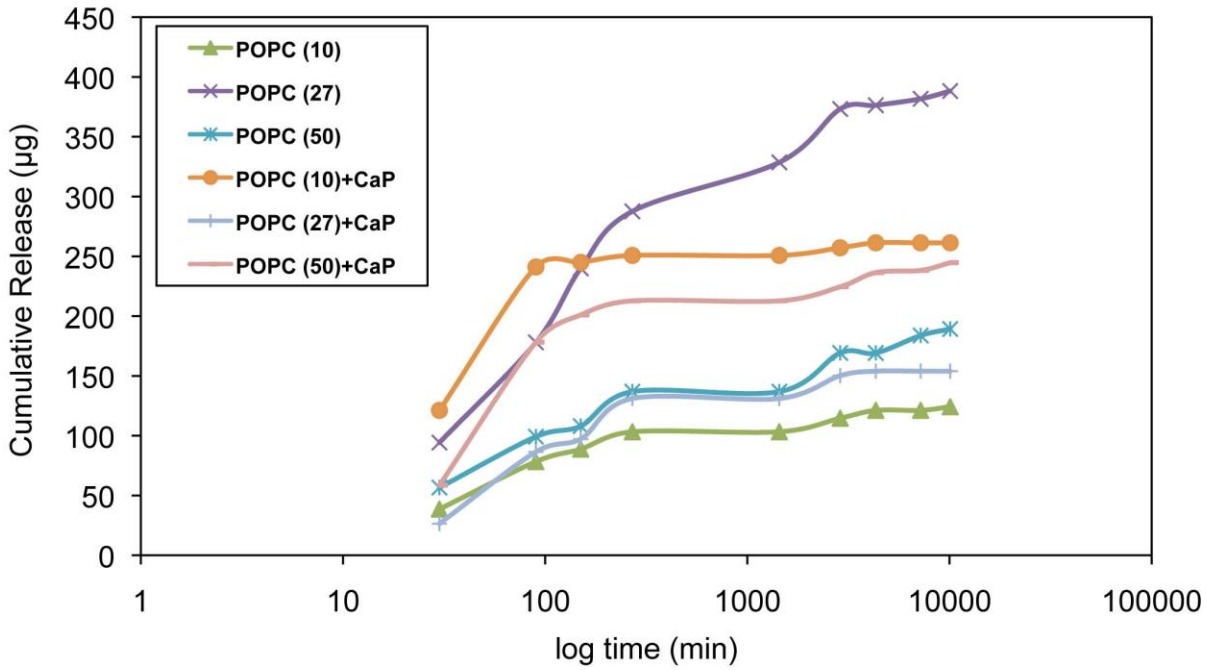

Figure C.3. Loading technique: 3 times AMP (250 µL of 1mg/mL AMP) deposition and drying under vacuum following one time POPC coating/ 8 times CaP coating.

POPC 10 = 10mg POPC in 1 mL Methanol

POPC 10+CaP = 10mg POPC in 1 mL Methanol coated 8 times with CaP after drying POPC

POPC 27 = 27mg POPC in 1 mL Methanol

POPC 27+CaP = 10mg POPC in 1mL Methanol coated 8 times with ACP after drying POPC

POPC 50 = 50mg POPC in 1 mL Methanol

POPC 10+CaP = 50mg POPC in 1mL Methanol coated 8 times with ACP after drying POPC

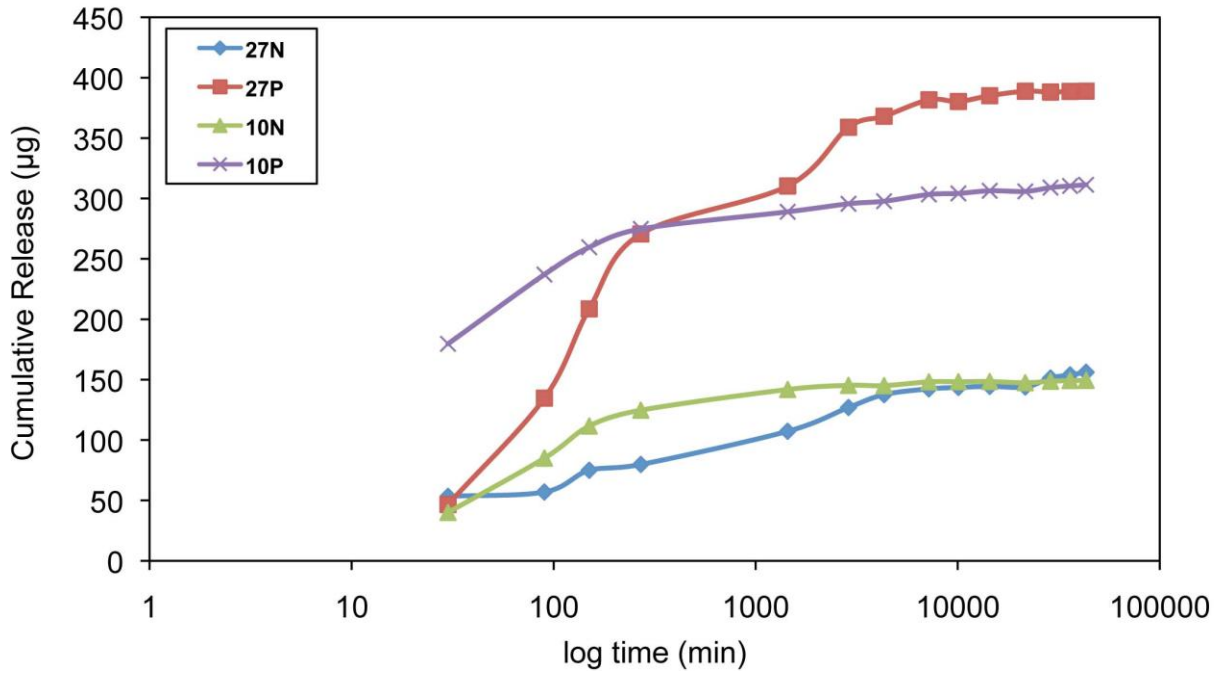

Figure C.4. Loading technique: Three time AMP (50 µL drop of 2mg/mL AMP on each sample) deposition and drying under vacuum following one time POPC coating.

Washing with PBS three times

10P = Loaded with peptide and coated with 10mg POPC in 1 mL Ethanol+2 mg AMP

10N = Not loaded with peptide but coated with 10mg POPC in 1 mL Ethanol+2 mg AMP

27P = Loaded with peptide and coated with 27mg POPC in 1 mL Ethanol+2 mg AMP

27N = Not loaded with peptide but coated with 27mg POPC in 1 mL Ethanol+2 mg AMP

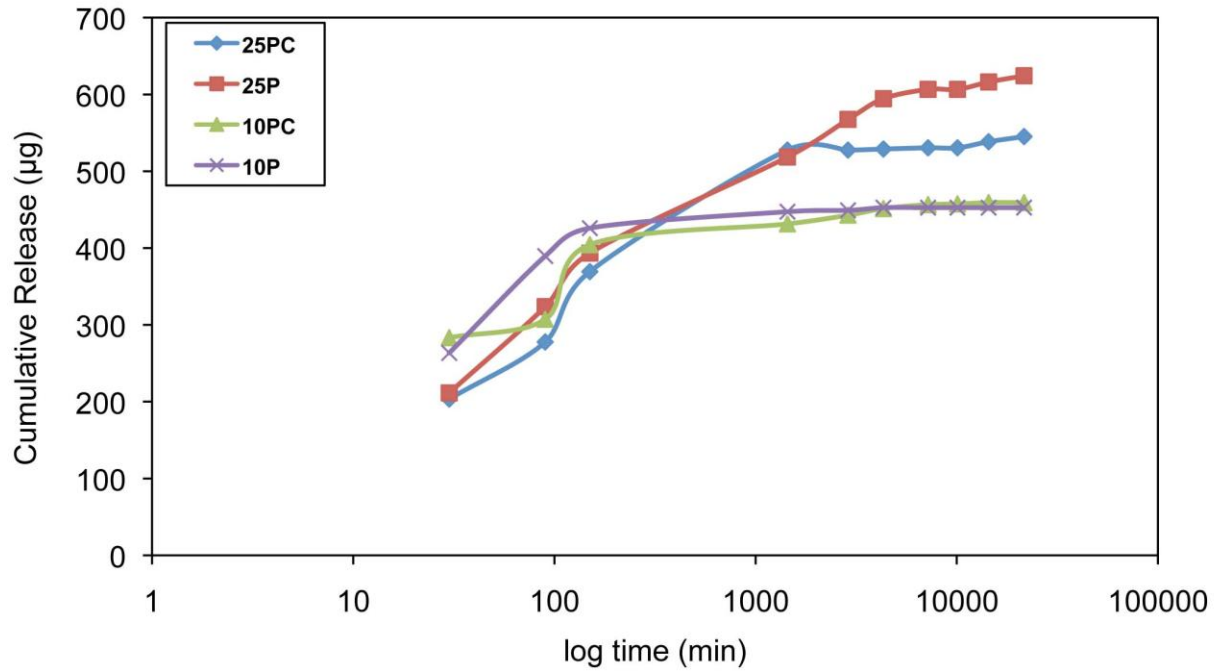

Figure C.5. Loading technique: Three time AMP (50 µL drop of 2mg/mL AMP on each sample) deposition and drying under vacuum following one time POPC (and cholestrol) coating.

Washing with PBS three times

10P = Loaded with peptide and coated with 10mg POPC in 1 mL Ethanol+2 mg AMP

10PC = Loaded with peptide and coated with 10mg POPC in 1 mL Ethanol+2 mg AMP +2.5 mg Cholesterol

25P = Loaded with peptide and coated with 25mg POPC in 1 mL Ethanol+2 mg AMP

25PC = Loaded with peptide and coated with 25mg POPC in 1 mL Ethanol+2 mg AMP +2.5 mg Cholesterol

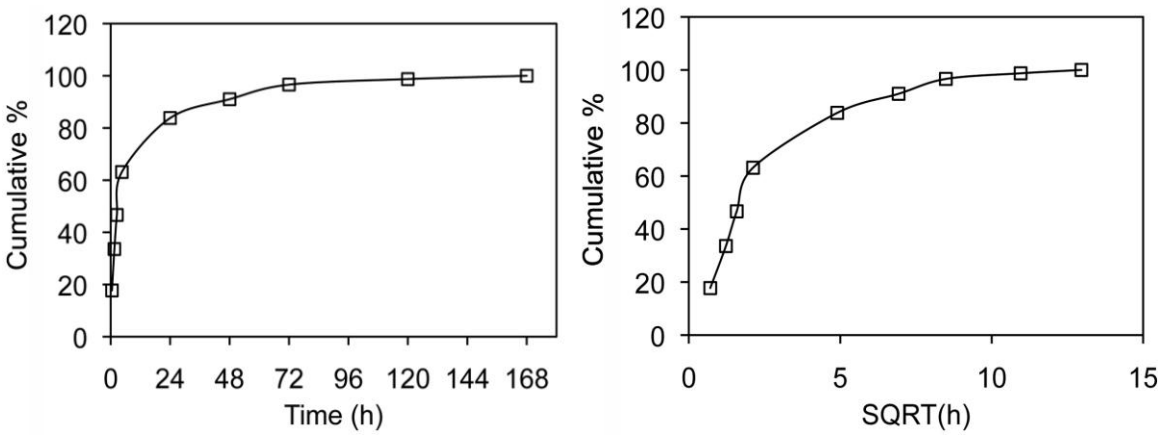

(a)

(b)

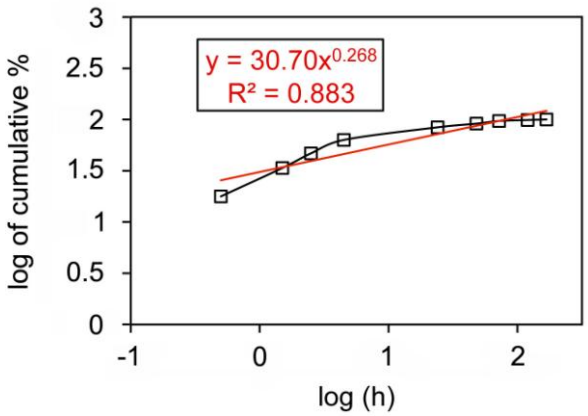

(c)

Figure C.6. Comparison between models best fitting to the POP-20 release profile (a) Zero order (b) Higuchi (c) Korsmeyer-Peppas models.